

**PROBABILISTIC SEISMIC DESIGN
AND ASSESSMENT METHODOLOGIES
FOR THE NEW GENERATION
OF DAMAGE RESISTANT STRUCTURES**

A thesis submitted in partial fulfilment of the requirements for the
Degree of Master of Engineering in Civil Engineering
at the University of Canterbury

by

Kathryn Louise Robertson

Supervised by

Professor John B. Mander

Dr Athol J. Carr

Department of Civil Engineering

University of Canterbury

Christchurch, New Zealand

2005

ABSTRACT

Following the evolution of a damage avoidance design (DAD) frame system, with rocking beam-column joints, at the University of Canterbury, analytical studies are carried out to evaluate the performance of proposed structures, and verify the proposed design methodology. A probabilistic seismic risk assessment methodology is proposed, from which the expected annualised financial loss (EAL) of a structure can be calculated. EAL provides a consistent basis for comparison of DAD frame systems with state-of-practice ductile monolithic construction. Such comparison illustrates the superior performance of DAD frame systems.

The proposed probabilistic seismic assessment methodology requires the response of the structure to be evaluated over a range of seismic intensities. This can be achieved by carrying out an incremental dynamic analysis, explicitly considering seismic randomness and uncertainty; or from a pushover analysis, and assuming an appropriate value of the dispersion. By combining this information with the seismic hazard, probabilistic response curves can be derived, which when combined with information about damage states for the particular structure, can be transformed into 'resilience curves'. Integration of information regarding the financial loss occurring due to each of the damage states, results in an estimate of EAL.

ACKNOWLEDGEMENTS

The research presented in this thesis was carried out in the Department of Civil Engineering at the University of Canterbury, under the supervision of Prof. John Mander. I would like to convey sincere gratitude to John for his guidance, suggestions and inspiration throughout my studies. Additionally, I would like to thank Dr Athol Carr and Dr Rajesh Dhakal for their help and suggestions with the computational modelling probabilistic risk assessment aspects of this research.

Thanks to the Future Building Systems research program, the University of Canterbury and New Zealand Concrete Society for providing financial assistance.

Thanks to my fellow postgraduate students, particularly Luoman Li, Kevin Solberg, Keryn Goble, Tonny Rahardjo and Naoto Mashiko, for their lively discussions, sharing of information and suggestions.

Thanks to my friends and family for their support and encouragement during this time. Lastly, I'd like to thank my fiancée Wilfrid Robinson for helping me endure the seemingly endless process of completing this tome.

CONTENTS

Abstract	iii
Acknowledgements	v
List of Tables	xi
List of Figures	xiii
Nomenclature	xv
Introduction	1
Chapter One: Seismic Vulnerability Analysis of Buildings and Financial Loss Estimation. I: Methodology	5
1.1 Introduction	6
1.2 Existing Loss Estimation Methodologies	7
1.3 Existing Tools from which Methodology is Developed	10
<i>1.3.1 Developments and Applications of Incremental Dynamic Analysis</i>	<i>10</i>
<i>1.3.2 Fragility Curve Theory</i>	<i>12</i>
1.4 Quantitative Seismic Vulnerability Analysis and Financial Loss Estimation Methodology	14
<i>1.4.1 Step by Step Procedure to Calculate the Expected Annualised Seismic Loss</i>	<i>14</i>
<i>1.4.2 Present Worth and Time Value of Money</i>	<i>25</i>
1.5 Sensitivity Analysis	26
<i>1.5.1 Sensitivity Parameter</i>	<i>26</i>
<i>1.5.2 Swing Analysis</i>	<i>27</i>
<i>1.5.3 Extreme Values of the Input Parameters</i>	<i>28</i>
<i>1.5.4 Observed Trends</i>	<i>29</i>
1.6 Discussion of Applications	31
1.7 Conclusions	32
1.8 References	33

Chapter Two: Seismic Vulnerability Analysis of Buildings and Financial Loss Estimation. II: Application	45
2.1 Introduction	46
2.2 Findings from Previous Research	47
2.2.1 <i>Damage Avoidance Design Background</i>	49
2.2.2 <i>Theoretical Moment-Rotation Response of DAD Beam-Column Connection</i>	53
2.2.3 <i>Modelling of Rocking Systems</i>	55
2.3 Description of Frames for Analysis	57
2.3.1 <i>Red Book Frame</i>	57
2.3.2 <i>DAD Arnold Gravity Frame</i>	59
2.3.3 <i>DAD Davies Seismic Frame</i>	61
2.3.4 <i>Modelling of DAD Beam-Column Connections</i>	63
2.4 Probabilistic Seismic Vulnerability Methodology Application	65
2.4.1 <i>Red Book Results</i>	66
2.4.2 <i>DAD Gravity Frame Results</i>	67
2.4.3 <i>DAD Seismic Frame Results</i>	68
2.5 Economic Comparison	69
2.6 Sensitivity Analysis	70
2.6.1 <i>Sensitivity Parameter</i>	71
2.6.2 <i>Swing Analysis</i>	72
2.7 Conclusions	73
2.8 References	74
Chapter Three: Damage Avoidance Design and Evaluation of a Six Storey Precast Concrete Building	93
3.1 Introduction	94
3.2 Rapid-IDA to EAL Methodology	95
3.3 Proposed Six Storey Building Design	102
3.3.1 <i>Gravity Frame Design</i>	103
3.3.2 <i>Seismic Only Frame Design</i>	105
3.3.3 <i>Design of Columns</i>	106
3.4 Application of Rapid-IDA to EAL Methodology	106
3.5 Incremental Dynamic Analysis Based Assessment Methodology	109
3.5.1 <i>East-West Gravity Frame</i>	110
3.5.2 <i>North-South Seismic Frame</i>	111

3.6 Discussion of Results	112
3.6.1 Sensitivity of Methodologies	112
3.6.2 Differences Between the Two Methodologies	113
3.7 Conclusions	115
3.8 References	116
Conclusions	131
References	135
Appendix A: Mathematical Derivation of Fragility and Resilience Curves	143
Appendix B: Details of Rapid Pushover Method	149
Appendix C: Some Observations on the Dynamic Behaviour of the Ten Storey Conventional and Damage Avoidance Design Frames	155
C.1 Mode Shapes and Periods of Vibration	155
C.2 Identification of Critical Earthquake Ground Motions	156
C.3 Time-History Displacement Profiles	156
C.4 Validity of Modelling Assumptions	157
Appendix D: Design of a Six Storey Damage Avoidance Design Apartment Building	171
D.1 Loadings	171
D.2 Design of Gravity Frames	172
D.2.1 Internal Gravity Frames (Grids B to E)	172
D.2.2 External Gravity Frames (Grids A and F)	181
D.3 Design of Seismic Frame	185
D.4 Design of Columns	189
D.5 Shear Design	191
Appendix E: Some Observations on the Dynamic Behaviour of the Proposed Six Storey Damage Avoidance Design Apartment Building	195
E.1 Mode Shapes and Periods of Vibration	195
E.2 Time-History Displacement Profiles	195
E.3 Validity of Modelling Assumptions	196

LIST OF TABLES

Table 1-1: Details of 20 ground motion records used	38
Table 1-2: Definition of damage states	38
Table 2-1: Definition of damage states for conventional structure	78
Table 2-2: Definition of damage states for DAD frames	78
Table 2-3: Summary of Ramberg-Osgood statistical analysis for θ_{MAX}	79
Table 2-4: Parameter sensitivity: Percentage change in EAL to a +1.0% change in each parameter	80
Table 2-5: Extreme values of parameters for swing analysis	81
Table 3-1: Definition of damage states for rapid-IDA to EAL evaluation	119
Table 3-2: Calculation of \tilde{IM}_{DSi} for E-W gravity frame	119
Table 3-3: Calculation of \tilde{IM}_{DSi} for N-S seismic frame	119
Table 3-4: Summary of Ramberg-Osgood statistical analysis for θ_{MAX}	120
Table 3-5: Definition of damage states for IDA-based method	121
Table 3-6: Sensitivity parameters for rapid-IDA evaluation	121
Table 3-7: Parameters defining resilience curves	122
Table D-1: Column hinge design and properties	193

LIST OF FIGURES

Figure 1-1: Seismic hazard curve and data obtained from NZS 4203:1992	39
Figure 1-2: 5% damped acceleration response spectra, dispersion, and displacement response spectra for the 20 selected ground motion records, normalised to $S_A(T = 1 s)$	40
Figure 1-3: Summary of steps in fitting R-O equation to IDA output	41
Figure 1-4: Summary of risk assessment of structure	42
Figure 1-5: Summary of annualised loss calculation	43
Figure 1-6: Normalised tornado diagram indicating variability of parameters	44
Figure 2-1: Details of the prototype DAD building for experimental investigations carried out at the University of Canterbury	82
Figure 2-2: General scheme of the Red Book building	83
Figure 2-3: Moment-rotation curves for the DAD beam-column joints	84
Figure 2-4: Incremental dynamic analysis output for Red Book frame	85
Figure 2-5: Summary of probabilistic seismic vulnerability assessment methodology applied to the Red Book frame	86
Figure 2-6: Incremental dynamic analysis output for E-W DAD gravity frame	87
Figure 2-7: Summary of probabilistic seismic vulnerability assessment methodology applied to E-W DAD gravity frame	88
Figure 2-8: Incremental dynamic analysis output for N-S DAD seismic frame	89
Figure 2-9: Summary of probabilistic seismic vulnerability assessment methodology applied to N-S DAD seismic frame	90
Figure 2-10: Results of swing analyses presented as tornado diagrams	91
Figure 3-1: Plan and elevation of proposed apartment building	123
Figure 3-2: Elastic 5% damped ADRS for design	124
Figure 3-3: Summary of rapid-IDA to EAL method applied to E-W gravity frame	124
Figure 3-4: Summary of rapid-IDA to EAL method applied to the N-S seismic frame	125
Figure 3-5: Incremental dynamic analysis output for E-W gravity frame	126
Figure 3-6: Summary of IDA-based probabilistic seismic vulnerability assessment of E-W gravity frame	127
Figure 3-7: Incremental dynamic analysis output for N-S seismic frame	128
Figure 3-8: Summary of IDA-based probabilistic seismic vulnerability assessment of N-S seismic frame	129
Figure 3-9: Observed differences between probabilistic seismic vulnerability assessment methodology and rapid-IDA methodology	130

Figure A-1: Ramberg-Osgood curve parameters	147
Figure B-1: General collapse mechanism of lateral resisting frame	154
Figure B-2: Base shear force evaluation from plastic mechanism analysis	154
Figure C-1: Mode shapes and periods of vibration for the ten storey frames	159
Figure C-2: Red Book displacement time histories and selected vertical snapshots for earthquakes representative of the 50 th percentile DBE	160
Figure C-3: Red Book displacement time histories and selected vertical snapshots for earthquakes representative of the 90 th percentile DBE	161
Figure C-4: Red Book displacement time histories and selected vertical snapshots for earthquakes representative of the 50 th percentile MCE	162
Figure C-5: DAD E-W gravity frame displacement time histories and vertical snapshots for earthquakes representative of the 50 th percentile DBE	163
Figure C-6: DAD E-W gravity frame displacement time histories and vertical snapshots for earthquakes representative of the 90 th percentile DBE	164
Figure C-7: DAD E-W gravity frame displacement time histories and vertical snapshots for earthquakes representative of the 50 th percentile MCE	165
Figure C-8: DAD N-S seismic frame displacement time histories and vertical snapshots for earthquakes representative of the 50 th percentile DBE	166
Figure C-9: DAD N-S seismic frame displacement time histories and vertical snapshots for earthquakes representative of the 90 th percentile DBE	167
Figure C-10: DAD N-S seismic frame displacement time histories and vertical snapshots for earthquakes representative of the 50 th percentile MCE	168
Figure C-11: Vertical drift profiles at DBE and MCE	169
Figure C-12: Maximum beam moments occurring during selected analyses	169
Figure D-1: Plan and elevation of proposed building	194
Figure E-1: Mode shapes and periods of vibration for the proposed six storey apartment building	197
Figure E-2: E-W gravity DAD frame displacement time histories and vertical snapshots for earthquakes representative of the 50 th percentile DBE	198
Figure E-3: E-W gravity DAD frame displacement time histories and vertical snapshots for earthquakes representative of the 50 th percentile DBE	199
Figure E-4: E-W gravity DAD frame displacement time histories and vertical snapshots for earthquakes representative of the 50 th percentile DBE	200
Figure E-5: N-S seismic DAD frame displacement time histories and vertical snapshots for earthquakes representative of the 50 th percentile DBE	201
Figure E-6: N-S seismic DAD frame displacement time histories and vertical snapshots for earthquakes representative of the 90 th percentile DBE	202
Figure E-7: N-S seismic DAD frame displacement time histories and vertical snapshots for earthquakes representative of the 50 th percentile MCE	203
Figure E-8: Vertical drift profiles at DBE and MCE	204
Figure E-9: Maximum beam moments occurring during selected analyses	204

NOMENTCLATURE

ABV	Assembly-Based Vulnerability
A_g	Gross cross-sectional area
A_i	Area enclosed between the $p_a = 0$ and the resilience curve corresponding to DSi
A_{PS}	Area of prestress tendon
$A_{PS \min}$	Minimum area of prestress reinforcement required
a	Power law parameter
B	Damping reduction factor (generalised)
b	Power law parameter
C_c	Acceleration capacity of the structure
C_c^*	Acceleration capacity of an equivalent SDOF system
C_h	Basic seismic hazard coefficient
DAD	Damage Avoidance Design
DBE	Design Basis Earthquake
DM	Damage Measure
DR	Damage Ratio
DS	Damage State
DSi	i^{th} damage state
d_b	Beam depth (overall)
d_c	Column depth (overall)
EAL	Expected Annualised Loss
EAL_{DAD}	Expected Annualised Loss of DAD frame
EAL_{RB}	Expected Annualised Loss of conventional Red Book frame
EDP	Engineering Demand Parameter
EDP_c	Critical EDP
EL	Expected Loss
E_{PS}	Modulus of elasticity of prestress material
E-W	East-West direction of the DAD buildings (gravity frame)

e_c	Eccentricity of draped prestress tendons, measured from the top of the beam
e_d	Eccentricity of dissipator from centreline of beam
e_{PS}	Eccentricity between centre of beam and prestress tendon
$F_v S_1$	Spectral acceleration at a period of 1 second
$(F_v S_1)_{DBE}^*$	Design spectral acceleration corresponding to the design basis earthquake
$(F_v S_1)_{DBE}^{cap}$	Spectral acceleration capacity evaluated for the design basis earthquake
f'_c	Design concrete strength
f_d	Yield strength of dissipators
f_i	Initial stress in prestress tendons
f_{PS}	Yield strength of prestress material
f_y	Yield strength of reinforcing
G	Gravity load
g	Acceleration due to gravity (taken as 9.81 m/s^2)
H	Column lateral force
H_i	Storey lateral force at level i
h_s	Inter-storey height
IDA	Incremental Dynamic Analysis
IM	Intensity Measure
$IM(T = 475)$	Intensity measure corresponding to 475 year return period earthquake
IM_c	Critical IM occurring at the onset of large EDP
i	Interest rate
K	Initial slope of IDA curve
L	Beam length, measured between column centrelines
L_d	Yielding length of tension-compression dissipator
L_{beam}	Length of drop in beam (or distance between beam hinges)
L_{PS}	Length of prestress tendon, between anchorages
M_b	Beam hinge moment
MCE	Maximum Considered Earthquake

$M_{col\ NS}^*$	Design column moment for the north-south frame
$M_{col\ WE}^*$	Design column moment for the west-east frame
M_d	Moment contribution from dissipators
$M_{elastic}$	Elastic flexural capacity of the beam
M_{open}	Moment required to cause opening of the joint
M_{pb}	Plastic moment capacity of the beams
M_{pc}	Plastic moment capacity of the columns
M_{PS}	Moment contribution from prestress
$M_{PS\ i}$	Initial prestress moment capacity (before the joint opens)
$M_{PS\ yield}$	Moment at which yield of the prestressing occurs
M_Q	Moment induced by live load
m_i	Mass associated with level i
n	Number of earthquake ground motion records used for IDA
N-S	North-South direction of DAD buildings (seismic only frame)
N	Period of interest (uniform series present worth factor)
$N_{average}$	Average column joint axial load
n_b	Number of bays in the frame
N_{bottom}	Axial load (due to gravity forces) applied over the bottom column joint
N_s	Number of storeys in the frame
n_{sp}	Number of storeys participating in the mechanism
N_{top}	Axial load applied over the top column joint
P_a	Annual frequency of earthquake occurrence
$P_{a(max)}$	Maximum considered annual frequency
$(P/A, i, N)$	Uniform series present worth factor
PBEE	Performance-Based Earthquake Engineering
P_d	Force in dissipator
PEER	Pacific Earthquake Engineering Research
PGA	Peak Ground Acceleration

P_{PS}	Force in prestress tendon
$P_{PS i}$	Initial prestress force
$P_{PS yield}$	Yield force in prestress tendons
PRESSS	Precast Seismic Structural Systems
Q	Live load
q	Exponent based on local seismic hazard-recurrence relations
R-O	Ramberg-Osgood
r	Exponential constant (R-O equation)
S_A	Spectral acceleration at a period of 1 second
$S_A(T = 1 s)$	Spectral acceleration at a period of 1 second
$S_A(T_1)$	Spectral acceleration at the fundamental period of the structure
S_x	Elastic section moment
T	Return period (earthquake), years
T	Period of vibration
T_1	First mode period of vibration
Tr	Specified return period
t_d	Thickness of dissipator
V	Construction and replacement value of structure of interest
V_{base}	Base shear capacity
V_{DAD}	Value of the DAD building
$V_{j des}$	Design shear of rocking joint
V_{RB}	Value of the Red Book building
W	Seismic weight of structure
w_d	Width of dissipator
w_G	Gravity load applied to beam
w_Q	Live load applied to beam (udl)
\tilde{x}	Median value of parameter x
$x_{10\%}$	10 th percentile value of x
$x_{90\%}$	90 th percentile value of x

y	Model output (EAL)
α	Factor to account for elastic tension stress of concrete
α	Beam joint rotation corresponding to design drift
α_A	Acceleration transformation factor
α_D	Displacement transformation factor
β	Lognormal dispersion
β	Factor to account for elastic compression limit stress of concrete
$\bar{\beta}$	Best estimate of dispersion based on IDA analysis
β_C	Dispersion associated with the structural capacity
β_{Comp}	Composite dispersion (accounting for all sources of randomness and uncertainty)
β_D	Dispersion corresponding to the earthquake demand
β_{Pa}	Dispersion of the resilience curves
β_U	Dispersion parameter accounting for epistemic modelling uncertainties
β_x	Dispersion associated with parameter x
γ_{conc}	Concrete density
γ_i	Sensitivity parameter
Δ^*	Displacement of equivalent SDOF system
$\Delta_{d\ yield}$	Yield displacement of dissipator
Δ_i	Lateral displacement at ith level.
Δ_{top}	Displacement of the top storey of the mechanism
$\epsilon_{d\ allow}$	Allowable strain in dissipator at design rotation
$\epsilon_{d\ yield}$	Yield strain of dissipator
$\epsilon_{PS\ \alpha}$	Allowable strain in prestress at design rotation
$\epsilon_{PS\ yield}$	Yield strain of prestress tendons
η	Energy absorption factor
θ	Design drift
θ_b	Beam hinge rotation
θ_c	Column hinge rotation

θ_{ce}	Column drift due to elastic flexure
$\theta_{c (PS \text{ yield})}$	Column drift when yield of beam prestressing occurs
$\theta_{d \text{ yield}}$	Beam joint rotation corresponding to yield of dissipator
θ_j	Beam-column joint connection rotation
θ_{MAX}	Maximum inter-storey drift
$\theta_{PS \text{ yield}}$	Connection rotation at which yield of prestressing occurs
$\theta_{PS \text{ slack}}$	Connection rotation at which prestress tendons become slack
θ_{RBR}	Rigid body rotation of the frame
$\theta_{RBR (PS \text{ yield})}$	Rigid body rotation of frame corresponding to yield of beam prestressing
κ	Factor relating base shear to beam moment capacity
λ_{col}	Column overstrength factor
λ_d	Dissipator overstrength factor
λ_T	Return period scale factor
μ	Ductility
ξ_{eff}	Total effective damping
ξ_{hyst}	Hysteretic damping
ξ_{int}	Intrinsic damping
ξ_{rad}	Radiation damping
ϕ	Capacity reduction factor
ϕ_{PS}	Prestress undercapacity factor

INTRODUCTION

Motivational Background

Recent earthquakes, such as Northridge, 1994 and Hyogoken-Nanbu 1995, have demonstrated that even though structures performed as designed, that is collapse prevention to ensure life safety, significant damage none the less occurs to many structures. The economic cost of damage due to smaller, more frequent earthquakes is still significant. Following these earthquakes there has been significant research effort into the seismic design of buildings explicitly considering damage (so called performance-based earthquake engineering, PBEE), loss estimation methodologies, and building systems which reduce or eliminate damage due to small more frequent earthquakes.

A damage avoidance design (DAD) philosophy was proposed by Mander and Cheng (1997) for rocking bridge piers whereby the piers are designed such that damage occurs in specially designed and easily replaceable components, with no damage occurring to the remainder of the structure. Compared to current design philosophies, where structures are designed using the principles of '*capacity design*' to remain standing following an earthquake and ensure no loss of life, DAD further confines damage to replaceable components of the structure and represents a significant step forward in reducing the economic impacts of earthquakes.

DAD concepts have recently been extended to a modular frame system with post-tensioned rocking beam-column joints by Arnold (2004) and Davies (2003) at the University of Canterbury. Innovative features of this proposed system include the ability to carry out post-tensioning offsite, and then construct the building by bolting together a number of precast and post-tensioned components. Following on from their experimental investigations, Arnold (2004) and Davies (2003) both present design examples of DAD

frame buildings using a design methodology based on the rapid pushover method proposed by Martínez (2002). This design methodology for the DAD frames requires validation through a number of computational non-linear time-history analyses.

To accurately illustrate the advantages of a DAD frame with rocking beam-column joints when compared to the current state-of-practice of ductile cast in place emulation reinforced concrete frames, a consistent approach, incorporating damage, is needed. For this purpose, a probabilistic risk assessment methodology is developed, the output of which is an estimate of the annualised cost of structural damage due to earthquakes, and this can be used to demonstrate superior performance of DAD systems.

Therefore, the purpose of the current research has been to propose, develop and validate a design and assessment procedure for frames utilising a DAD philosophy. Furthermore, it is desirable to illustrate superior performance of the DAD philosophy when compared to conventional ductile monolithic frames. To this end, a probabilistic seismic vulnerability assessment methodology is proposed, based on incremental dynamic analysis (IDA). This methodology is then applied to a conventional ductile monolithic frame, and the DAD frames designed by Arnold (2004) and Davies (2003), to illustrate superior performance of the frames designed using the DAD philosophy. Inconsistencies in the design methodologies presented by Arnold (2004) and Davies (2003) are reduced and a rapid evaluation methodology is proposed, which is more suitable for application in an engineering design office situation.

Format of this Thesis

Following this introductory section, this thesis consists of three main chapters which are outlined as follows:

- A discussion of earthquake loss estimation is presented in Chapter One. A probabilistic seismic vulnerability assessment methodology which determines an estimate of the expected annualised seismic loss (EAL) is proposed, based on IDA, and fragility curve theory. The sensitivity and applications of the proposed methodology are discussed.
- Further details of the DAD philosophy and performance of rocking beam-column joints are discussed in Chapter Two. The probabilistic seismic vulnerability assessment methodology is then applied to produce estimates of EAL for a conventional ductile monolithic reinforced concrete frame, and the DAD frames designed by Arnold (2004) and Davies (2003). Discussion of sensitivity of the results and limitations of the proposed methodology are made. Favourable performance of the DAD frames is observed.
- Chapter Three presents the theoretical basis for a rapid evaluation methodology similar to the computationally based IDA methodology presented in Chapter One. This so-called rapid-IDA assessment methodology is then applied to a new six storey DAD apartment building, and results consistent with the IDA based probabilistic seismic vulnerability assessment methodology are obtained.

What is Particularly New in this Thesis

A probabilistic seismic vulnerability assessment methodology is proposed, based on IDA and fragility curve theory. This methodology is presented in a transparent step by step manner, providing clarity and demonstrating to users all steps in the process. ‘*Resilience curves*’, which illustrate the probability of occurrence each damage state for earthquakes of all annual frequencies are a useful contribution and clarify the process of calculating EAL. They clearly illustrate the probability of damage for earthquakes of all annual frequencies, and furthermore are useful for evaluating whether the structure achieves desirable performance targets.

Refinements have been made to the design methodologies proposed by Arnold (2004) and Davies (2003) to provide a more consistent approach to the design of both gravity and non-gravity load carrying DAD frames. A rapid evaluation methodology, based on a pushover analysis, has been proposed for multi-degree of freedom (MDOF) systems to evaluate the performance of these DAD frames. While this so-called rapid-IDA assessment methodology can be applied to any structure providing a lateral force-displacement relationship exists, it is somewhat simplified for the DAD frames by use of the rapid pushover methodology proposed by Martínez (2002).

The rapid-IDA assessment methodology can be validated by comparing outcomes with those obtained from the IDA based methodology, and vice versa. Good agreement between the two methodologies is found when applied to the DAD frames, thus providing verification for both of these methodologies.

Superior performance of DAD frame systems is illustrated by comparing the EAL of a conventional monolithic ductile reinforced concrete building to the EAL of two DAD frames. Results from the non-linear time-history analyses of the DAD frames illustrate the displacements occurring during the earthquake conform to the design mixed mechanism.

CHAPTER ONE

SEISMIC VULNERABILITY OF BUILDINGS AND FINANCIAL LOSS ESTIMATION. I: METHODOLOGY

Chapter Summary

A probabilistic seismic risk assessment methodology is proposed, from which the expected annualised financial loss of a structure can be calculated. This risk assessment methodology uses incremental dynamic analysis to determine the seismic response of the structure over a range of seismic intensities, explicitly considering seismic randomness and uncertainty. By combining this information with the seismic hazard, probabilistic response curves are derived, which when combined with information about the damage states, can be transformed into '*resilience curves*'. Together with information of the loss due to each of the damage states, the expected annualised loss (EAL) can be calculated. EAL for different structures can then be compared to show which structure has superior performance, in terms of financial loss.

1.1 INTRODUCTION

Recently, damage avoidance design (DAD) moment resisting beam-column joints have been tested at the University of Canterbury by Arnold (2004) and Davies (2003) in the gravity and non-gravity load carrying directions, respectively. These beam-column joints were post-tensioned and possess self-centring capabilities. Outstanding performance of these DAD beam-column joints was observed, and damage was confined to replaceable mechanical energy dissipators mounted across the rocking beam-column joint interfaces at drifts up to 4%.

It has been observed during computational non-linear time-history studies of single degree of freedom (SDOF) oscillators with varying hysteretic properties, that those with a flag-shaped hysteresis show similar results when compared to those with an elasto-plastic hysteresis in terms of displacement; however they have the advantage that they do not incur any residual drift (Christopoulos et al. (2002; 2003)). Christopoulos et al. (2003) state that the performance of such flag-shaped hysteresis systems, therefore, can correctly be compared to more traditional systems when residual deformations are considered. However consideration of both maximum deformations and residual displacements without explicitly considering the cost of reparation of any damage occurring to the structure, may also lead to erroneous conclusions.

To compare distinctly different systems, such as the DAD frames tested by Arnold (2004) and Davies (2003) with more conventional reinforced concrete buildings, financial loss estimation is required. Existing earthquake loss estimation methods and studies are reviewed. A new transparent seismic vulnerability analysis including financial loss estimation is proposed. The output of this process is the expected annualised loss (EAL). The proposed methodology builds on incremental dynamic analysis (IDA) and fragility

curve theory. Applications of the proposed method are discussed, incorporating the time value of money, and approaches to determining the sensitivity of EAL are presented.

1.2 EXISTING LOSS ESTIMATION METHODOLOGIES

Geographic information system (GIS) based software, such as HAZUS (Whitman et al., 1997) is available for estimating economic impacts of a scenario earthquake over a large region. A major component of the methodology estimates the probability of various building structural and non-structural damage states by combining a pushover curve with appropriate fragility curves. Built into the software are a number of generic building damage functions that are applicable to the majority of building types (Kircher et al., 1997). Advances to HAZUS since its introduction include the ability to predict casualties, indirect losses caused by loss of use of various structures (Bendimerad, 2001), and development of building-specific damage functions for structures not included in the range of built-in functions. (FEMA, 2003).

Porter et al. (2001) describe a technique named assembly-based vulnerability (ABV). ABV is a time-consuming, highly detailed method to produce a probabilistic seismic vulnerability function. The analysis proceeds as follows: A given building, with known contents at a specified location, is analytically modelled under a given ground motion with specified intensity. All the components, both structural and non-structural, are categorised into assemblies prior to the analysis and damage to all the assemblies, as a result of the time-history analysis in the building are determined. Then given the damage states for each component the repair cost and repair schedule can be simulated. Hence, the total loss from that earthquake is determined by considering both damage to the structure, and downtime while the structure is being repaired. By performing similar analyses using a number of earthquake ground motions, incorporating both randomness and uncertainty in

both the structure properties and the repair costs, over a range of intensity levels, the probabilistic seismic vulnerability function is determined. Porter et al. (2002) carried out a sensitivity study which showed that the most significant contributors to the overall damage factor were the capacity of the building assemblies and the spectral acceleration of the site. Their analysis shows that uncertainty and randomness associated with mass, damping and hysteresis behaviour of the structure are comparatively minor contributions to the overall uncertainty.

Lang and Bachmann (2004) developed vulnerability functions suitable for different classes of residential wall buildings in the city of Basel, Switzerland. These functions were developed by performing non-linear static analysis on 87 specific residential buildings, then aggregating the results into the various structure classes. The results were aggregated as it was felt that the non-linear static analysis procedure used would be too time-consuming to use on each individual building, and the purpose of the study was to estimate damage across the city due to a scenario event.

Smyth et al. (2004) consider the benefits of three possible retrofit schemes for a typical five storey apartment building in Istanbul, Turkey. Fragility curves, considering four damage levels were constructed, based on the results of 400 synthetic spectrum compatible earthquake records, using the maximum likelihood method (Shinozuka et al., 2000). The expected damage cost associated with each of these damage states was expressed as a percentage of the value of the building. Seismic hazard information derived specifically for the site, assuming the hazard is constant, is combined with the fragility and expected loss information, to calculate the present value of the total loss in T^* years, assuming the structure will only be repaired or rebuilt once during this period. This estimate represents a lower bound of the total loss, and randomness and uncertainty in either the structure or the ground motion capacity are not explicitly considered.

Porter et al (2004) develop mathematical relationships that show that the expected annual loss is a function of the probable frequent loss (mean loss caused by an earthquake with 10% probability of exceedance in a 5 year period). The probable frequent loss can then be calculated using a simplified linear ABV technique, as, assuming the equal displacement theorem, the structural response is not expected to deviate significantly from the linear response.

Ongoing research at the Pacific Earthquake Engineering Research (PEER) Centre aims to generate a clear generic approach to performance-based earthquake engineering (PBEE). A significant development is the so-called PEER framework formula (Krawinkler and Miranda, 2004):

$$\lambda(DV) = \iiint G(DV|DM) |dG(DM|EDP)| |dG(EDP|IM)| |d\lambda(IM) \quad (1-1)$$

in which $\lambda(DV)$ is the mean annual frequency of exceeding the decision variable, DV (i.e. repair cost, downtime); IM is the intensity measure (i.e. peak ground acceleration, spectral acceleration); EDP is the engineering demand parameter (i.e. maximum inter-storey drift); DM is the damage measure (i.e. maximum drift without damage); and $G(X|Y) = P(X \geq x|Y = y)$, the complementary cumulative distribution function. Equation (1-1) deconstructs assessment of a structure into four basic elements, being hazard analysis, demand prediction, modelling damage, and failure or loss estimation. This formula has widely been accepted as a generic foundation for PBEE which decouples analysis into four subtasks: (1) assessment of seismic hazard; (2) structural fragility; (3) damage; and (4) loss. These subtasks are recoupled via integration over all levels of the intermediate variables IM, EDP and DM. Implicit in the formula is a probabilistic analysis, incorporating a number of uncertainties and combining those uncertainties in accordance with the total probability theorem. The manner in which this formula is solved,

its limitations, and its potential expansion, have been the subject of rigorous research, both within and outside PEER. A good overview of such developments can be found in Porter (2003) or Krawinkler and Miranda (2004).

These existing methodologies generally fall between two extremes, being category based methods, such as HAZUS, and structure specific methods, eg. ABV. To compare the response of traditional and DAD systems, a method more specific than a generalised category based method is required. At the other extreme, ABV requires highly detailed structure-specific information, which in general is unavailable at the design stage, and is felt to be too time consuming to be useful in a design situation. More generalised work, such as Smyth et al. (2004) omit the steps between fragility curves and hazard information and arrive at an estimate of the total loss. The aim of this work, therefore, is to elucidate certain aspects of loss estimation and to make it more amenable for implementation in engineering design practice.

1.3 EXISTING TOOLS FROM WHICH METHODOLOGY IS DEVELOPED

Later in this chapter, a financial loss estimation methodology is proposed, which is based on incremental dynamic analysis (IDA) and fragility curve theory. These are discussed in detail.

1.3.1 DEVELOPMENT AND APPLICATIONS OF INCREMENTAL DYNAMIC ANALYSIS

The concept of conducting a series of non-linear time-history analyses for a specified structure and earthquake ground motion under progressively increasing seismic intensities was first proposed by Bertero (1980). He was particularly interested in identifying the

dynamic characteristics of earthquake ground motions that lead to minimum strength of a given structure.

Luco and Cornell (1998) introduced '*dynamic pushover*' analysis (analogous to IDA) as a method for determining the median and dispersion of the maximum drift capacity of a given structure. Through performing non-linear time-history analyses for a structural model and a specific earthquake ground motion, with incrementally increasing intensity, an estimate of the maximum drift capacity for that given earthquake is found from the point where the structural drift increases dramatically for small increases in seismic intensity.

The IDA procedure has recently gained popularity, as the computational cost of carrying out large numbers of non-linear time-history analyses has significantly decreased. Vamvatsikos and Cornell (2002) present a consistent terminology for IDA, and further developed this by carrying out a practical example of IDA, using a suite of 20 earthquake ground motions, on a nine-storey steel moment-resisting frame (Vamvatsikos and Cornell, 2004). Further study of IDA curves by Vamvatsikos and Cornell (2002; 2005) have exploited the observed relationship between IDA curves and used the results from a static pushover analysis to generate summarised IDA curves.

Independently from the above analyses, Mwafy and Elnashai (2001) created dynamic pushover envelopes for 12 reinforced concrete structures, based on IDA using eight EC8 spectrum compatible earthquake ground motions. These results were compared to results of static pushover analyses. From this analysis, they were able to show the static pushover analysis results match well with the dynamic pushover curves, particularly for low rise, short period structures.

1.3.2 FRAGILITY CURVE THEORY

Fragility curves graphically illustrate the relationship between the probability of structural damage and earthquake intensity (IM). Fragility curves are typically modelled by a lognormal cumulative distribution function, and express the probability of reaching or exceeding a particular damage state (DS), for a given IM. A variety of methods of formulating fragility curves occur in the literature, and there appears to be no accepted consistent approach (Erberik and Elnashai, 2004). However, these methods fall into three broad categories, being; (1) Monte-Carlo simulation approach where analytical fragility curves are defined via large numbers of non-linear time-history analysis; (2) empirical fragility curves based on observed earthquake damage data; and (3) a deterministic approach where the fragility curve is described by median response and dispersion of the lognormal cumulative probability distribution function. These three methods are described briefly below.

Analytical Simulation

An analytical model of the structure is constructed, typically allowing for variation in properties of the structure due to randomness and uncertainty. A number of earthquake ground motion records are obtained (either natural or synthetically generated), to represent the region of interest, and these are scaled to or grouped in a number of discrete IMs over the range for which the curves are required. Non-linear time-history analysis is carried out, and structural damage during each analysis determined. The probability of exceeding each damage state at each IM is found, either directly from the data (Karim and Yamazaki, 2001), or by fitting a lognormal distribution to the EDP at each IM from which the probability of exceeding each damage state is calculated (Singhal and Kiremidjian, 1996; Erberik and Elnashai, 2004). This data is plotted, and a cumulative lognormal distribution

fitted, using least-squares regression or similar approach, to these points. An alternative approach exists using the maximum likelihood method (Shinozuka et al., 2000).

Empirical Data

A technique similar to above is used, except observed earthquake damage, rather than analytically generated data is used. Fragility curves for highway bridges based on empirical data have been determined for the 1994 Northridge (Kiremidjian and Basöz, 1997), and 1995 Hyogoken-Nanbu (Yamazaki et al., 2000) earthquakes. Mander and Basöz (1999) compared and found good agreement between analytical fragility curves with empirically derived fragility curves for highway bridges damaged during the 1989 Loma Prieta and 1994 Northridge earthquakes. Karim and Yamazaki (2001) have shown that the empirical curves match well with analytical curves employing earthquake ground motion records obtained during the 1995 Hyogoken-Nanbu earthquake.

The difference between the empirical data and analytical simulation approaches is that the data is being observed from an actual earthquake in the case of empirical data, rather than simulated data, in the case of analytical simulation. Since empirical earthquake data is not readily available, fragility curves are often based on simulated data.

Deterministic Approach

Martínez (2002) defines a deterministic fragility based analysis approach, for the performance based assessment of multi-storey reinforced concrete buildings. The median seismic intensity level required to cause a certain level of damage is determined using deterministic analysis and an estimate of the composite dispersion (slope of the lognormal fragility curves) is obtained through statistical analysis and engineering judgement. Mander and Basöz (1999) and Mander (2004) show that the composite dispersion for fragility curves is approximately 0.6. A similar method has independently been proposed by Rosowsky and Ellingwood (2002).

1.4 QUANTITATIVE SEISMIC VULNERABILITY ANALYSIS AND FINANCIAL LOSS ESTIMATION METHODOLOGY

IDA is a somewhat sophisticated and highly refined analytical procedure used to obtain the relationship between the seismic capacity and demand of a particular structure. It is used as the basis for the seismic vulnerability analysis and financial loss estimation. The IDA results are further manipulated by incorporating the probability of an event of given IM occurring and assigning damage states to present the outcomes of the IDA in the format of a resilience curves. From these results, it is possible to calculate the expected annualised seismic loss (EAL) resulting from earthquake damage. EAL can be thought of as equivalent to an annual insurance payment for the particular loss considered, and gives an indication of the total lifetime cost of the structure, which is useful for cost/benefit analysis of the structure.

1.4.1 STEP BY STEP PROCEDURE TO CALCULATE THE EXPECTED ANNUALISED SEISMIC LOSS

The seismic vulnerability analysis method to calculate EAL is presented in a step-by-step format to allow easy application and so the theoretical aspects are clearly presented.

Step One: Site-Dependent Hazard Recurrence Relation

The annual frequency of an earthquake depends on its magnitude. According to the New Zealand loadings standard (NZS 4203:1992) the design basis earthquake (DBE) is an earthquake with 10% probability of occurrence in 50 years (475 year return period). Similarly, the maximum considered earthquake (MCE) is defined as an earthquake with 2% probability of occurrence in 50 years (2450 year return period). A return period dependent scale factor λ_T is required to scale a given response spectra to different annual frequencies (or return periods). Values for the return period factor are derived by drawing

a representative line through the hazard curves (spectral acceleration as a function of annual frequency). For average seismicity this curve is given by:

$$\lambda_T = \frac{IM(T = Tr)}{IM(T = 475)} = \left(\frac{Tr}{475}\right)^q = (475 p_a)^{-q} \quad (I-2)$$

in which $IM(T = Tr) = IM$ at the relevant return period; $IM(T = 475) = IM$ at the reference return period of 475 years (10% probability in 50 years); Tr = return period; $p_a = 1/Tr$ = annual frequency; and q = an exponent based on local seismic hazard-recurrence relations. Based on average New Zealand seismicity, where the data points were taken from information provided in the New Zealand loadings standard (NZS 4203:1992), $q = 0.333$ (Martínez, 2002), as illustrated in Figure 1-1.

Step Two: Select Suitable Earthquake Ground Motions

A suite of earthquake ground motions is required for the IDA analysis. It has been shown that for mid-rise structures, 10 to 20 earthquake ground motions can provide reasonable accuracy in the estimation of seismic demands (Shome et al., 1998). The selected earthquake ground motions need to be scaled to a suitable IM. Typical IMs used for IDA include peak ground acceleration, PGA, and spectral acceleration at the fundamental period of the structure, $S_A(T_1)$, although other IMs can be used. The IM selected depends on the properties of the structure and the purpose of the IDA.

A suite of 20 earthquake ground motions, presented in Table 1-1, have been selected for all IDA carried out in this research. These ground motions were obtained from earthquakes with magnitudes in the range of 6.5 to 6.9, recorded on firm soil, with moderate epi-central distances ranging from 16 to 32 km. This suite of earthquake ground motions has been used by others in previous IDA studies (Vamvatsikos and Cornell, 2004;

Rahardjo, 2004; Dhakal and Mander, 2005), and have been shown to provide adequate results for mid-rise structures (Vamvatsikos and Cornell, 2004).

Each earthquake ground motion has been scaled such that spectral acceleration at a period of one second, $S_A(T = 1s) = 1.0 g$. The spectral acceleration for these records is presented in Figure 1-2(a). It can be seen that there is significant variability in the input data. It can be shown that the distribution of the spectral accelerations, for a given period T , is well represented by a lognormal distribution (Martínez, 2002). Hence the median, rather than the mean, spectral acceleration is plotted on the graph. This is compared with the appropriately scaled elastic design spectra from the New Zealand loadings code (NZS 4203:1992) for intermediate soil types, and the ‘*design*’ spectrum used for rapid derivation of EAL. It can be seen that the median spectral acceleration is similar to these spectra. The dispersion β_D of this suite of earthquakes is plotted in Figure 1-2(b), and the spectral displacement of this suite of earthquake ground motions is plotted in Figure 1-2(c).

Step Three: Analytical Model of the Structure of Interest

A numerical model for the structure of interest is required for analysis with any non-linear time-history analysis software programme. The model needs to be sufficiently detailed so as to adequately describe the behaviour of the structure over the complete range of elastic and inelastic deformations, through to collapse due to global instability, and have realistic hysteretic properties.

Step Four: Carry Out Non-linear Time-history Analysis

Once the numerical model for the structure is prepared, and the earthquake ground motions are selected, IDA can be performed. Each of the earthquake records is scaled to increasing levels of IM until collapse of the structure occurs. It is possible to run analyses at progressively increasing increments of IM, or use an advanced algorithm, eg. ‘*hunt & fill*’

(Vamvatsikos and Cornell, 2002). For each analysis, the EDP of interest can be recorded (eg. maximum deflections and inter-storey drifts, maximum member forces and deformations).

Each non-linear time-history analysis gives one point in the IM versus EDP domain. As shown in Figure 1-3(a), connecting these points, for a specific earthquake ground motion, creates an IDA curve. Additionally, similar curves can be plotted for all other earthquake ground motions, once all the analyses are completed.

Step Five: Ramberg-Osgood Curve Fitting

In order to carry out more advanced analysis, it is essential to be able to predict the EDP for all levels of IM. In their previous study, Vamvatsikos and Cornell (2004) used cubic spline interpolation to obtain estimates of EDP for all levels of IM. However, piecewise cubic polynomial equations are too complex to be useful for further analysis.

It is convenient to be able to express each IDA curve in terms of a parametric equation for EDP given IM, where the parameters are fitted separately for each individual IDA curve. This method is powerful as the process provides a set of parameter values, on which statistical analysis can be performed. Vamvatsikos and Cornell (2002) give the power law model:

$$EDP = a[IM]^b \quad (1-3)$$

where a and b are power law parameters, calculated by regression analysis, as an example of such a parametric equation. Equation (1-3) was proposed by Luco and Cornell (1998) for obtaining the median relationship between spectral acceleration and drift.

In a similar fashion to Rahardjo (2004) and Dhakal and Mander (2005), Ramberg-Osgood (R-O) functions are selected as parametric equations to approximate the IDA curves.

The R-O equation is given as:

$$EDP = \frac{IM}{K} \left[1 + \left| \frac{IM}{IM_c} \right|^{r-1} \right] \quad (1-4)$$

where K = slope of IDA curve in initial range; IM_c = ‘critical’ IM occurring at the onset of large EDP consequently leading to collapse; and r = an exponential constant.

Alternatively, equation (1-4) can be expressed as:

$$\frac{EDP}{EDP_c} = \frac{IM}{IM_c} + \left[\frac{IM}{IM_c} \right]^r \quad (1-5)$$

where EDP_c is the ‘critical’ EDP, defined as:

$$EDP_c = \frac{IM_c}{K} \quad (1-6)$$

The significance of the three R-O parameters (IM_c , r , and K or EDP_c) can be examined in Figure 1-3(b). It can be seen that as parameter $r \rightarrow \infty$, the curve tends towards a bi-linear curve. If the input is greater than the ‘critical’ value ($IM > IM_c$) then the response will be such that $EDP > 2EDP_c$, and structural instability is imminent.

The R-O equation parameters are estimated for the IDA curves produced from each earthquake ground motion using non-linear least squares analysis. An example is presented in Figure 1-3(c). Statistical analysis is then performed on the R-O parameters, assuming they are lognormally distributed, to find the median (50th percentile) and lognormal dispersion, β , of each of the parameters. Due to the relationship, between EDP_c , IM_c and K , defined by equation (1-6), only two of these parameters are statistically independent, so the median and dispersion of the third can be derived from the other two.

In subsequent analysis, it was found that EDP_c and K are statistically independent. Therefore the median and dispersion of IM_c can be found, from well-known work by Kennedy et al. (1980), as:

$$I\tilde{M}_c = E\tilde{D}P_c \tilde{K} \quad (1-7)$$

and logarithmic standard deviation given by

$$\beta_{IM_c} = \sqrt{\beta_{EDP_c}^2 + \beta_K^2} \quad (1-8)$$

Using the results from this statistical analysis, upper and lower bound (10th and 90th percentiles, respectively) R-O parameters can be determined, from which upper and lower bound R-O curves are plotted to completely summarise the IDA output. These curves are illustrated in Figure 1-3(d).

Step Six: Definition of Damage States

Once these summary IDA curves have been generated, it is possible to determine the expected EDP for an earthquake with a certain IM. Furthermore, it is possible to determine the median IM required to induce a certain EDP. Correlating EDP with damage, it is possible to estimate the median IM required to cause a particular level of damage. For further analysis, discrete damage states are introduced to describe the post-earthquake state of the structure, which are defined in terms of EDP.

Similar to HAZUS, (FEMA, 2003) five damage states can be defined as: No Damage (DS1); Minor Damage allowing immediate occupancy of the structure following an earthquake (DS2); Repairable Damage (DS3); Irreparable Damage (DS4); and Partial or Total Collapse (DS5). It is possible to define, using engineering judgement and experience, damage states as a function of EDP, for any structure. An example of the definition of such damage states is presented in Table 1-2. The median threshold EDP

values defining the damage states are also identified on the summarised IDA curves, illustrated in Figure 1-4(b).

Step Seven: Demand Hazard Curves

Using the summarized R-O IDA curves previously developed, the output can be presented in the form of ‘demand hazard curves’, by substituting equation (1-2) into equation (1-4), as given by:

$$EDP = \frac{IM(T = 475)}{K(475 p_a)^q} \left[1 + \left| \frac{IM(T = 475)}{IM_C(475 p_a)^q} \right|^{r-1} \right] \quad (1-9)$$

where parameters IM_C , K , and r depend on the level of confidence which is being modelled.

It is important to note, that in all the preceding steps, variation in EDP is due only to randomness displayed in the input earthquake ground motions. This is because the non-linear time-history analysis is carried out using data which explicitly incorporates earthquake ground motion randomness. However, it is noted that structural resistance, in terms of strength and displacement capacity is inherently variable, and additionally the computational modelling is imprecise, therefore there is an additional measure of variability that occurs between the predicted and observed responses.

To allow for the randomness of seismic demand, as well as the inherent randomness of structural capacity and uncertainty due to inexactness of the computational modelling, it is necessary to use an integrated approach to encompass all sources of variability. Kennedy et al. (1980), suggests that the composite value of the dispersion be found by:

$$\beta_{Comp} = \sqrt{\beta_C^2 + \beta_D^2 + \beta_U^2} \quad (1-10)$$

where β_{Comp} is the composite dispersion; β_C is the dispersion associated with the structural capacity; β_D is the dispersion corresponding to the earthquake demand; and β_U is the dispersion parameter accounting for epistemic modelling uncertainties. The dispersion in each R-O parameter corresponding to the earthquake demand is calculated above. For this analysis, β_C is taken as 0.2 (Dutta, 1999) and β_U is taken as 0.2.

Equation (1-10) is used to determine the R-O parameters for the 10th and 90th percentile responses accounting for all randomness and uncertainty. This composite demand hazard curve is plotted in Figure 1-4(d) at the 90% confidence level accounting for all sources of randomness and uncertainty.

Step Eight: Fragility Analysis

Utilising the information presented in Figure 1-4(b), fragility curves can be simply and elegantly determined. A fragility curve can be graphically constructed as follows: The IM at which the median (50th percentile) IDA curve intersects the vertical line defining the boundary between two adjacent damage states can plotted in the cumulative probability - IM domain (fragility plot) of Figure 1-4(a), at a cumulative probability of 0.5; the IM at which the 10th percentile intersects this vertical line is plotted at a cumulative probability of 0.9; and the IM at which the 90th percentile intersects this vertical line is plotted at a cumulative probability of 0.1; and finally, these three points are connected with a lognormal curve. This method of plotting fragility curves is analogous to the method used by Karim and Yamazaki (2001).

Since the R-O parameters are lognormally distributed, fragility curves can be defined from these parameters, where the median and dispersion associated with each curve are defined as follows:

For the fragility curves defining DS2, DS3 and DS4:

$$I\tilde{M}_{DSi} = E\tilde{D}P_{DSi} \tilde{K} \quad (1-11)$$

and for the fragility curve defining DS5:

$$I\tilde{M}_{DS5} = IM_C \quad (1-12)$$

where the dispersion is given as the larger of:

$$\begin{aligned} \beta_{IM} &= \sqrt{\beta_{EDP_{DSi}}^2 + \beta_K^2} \\ \beta_{IM} &= \beta_{IM_C} \end{aligned} \quad (1-13)$$

to prevent overlapping of fragility curves at the extremes. The derivation of these equations, based on a bi-linear approximation to the R-O curves, is presented in Appendix A.

Step Nine: Resilience Curves

In a similar fashion to construction of fragility curves above, where information from the summarised IDA curves together with five defined damage state regions (Figure 1-4(b)) were incorporated together and expressed as fragility curves (Figure 1-4(a)), the information presented in the hazard curve of Figure 1-4(d) can be extracted and presented as a ‘*resilience curve*’. This resilience curve provides easily interpretable information regarding the expected damage to the structure due to a seismic event with a given annual frequency.

Using Figure 1-4(d), the annual probability of the median demand hazard curve where EDP corresponds to the onset of DS2, is plotted (in Figure 1-4(c)) at the 50% confidence level. Similarly, the annual probability of the 90% percentile demand hazard curve where EDP corresponds to the onset of DS2, is plotted at the 90% confidence level, and a third point, corresponding to the 10% percentile demand hazard curve where EDP corresponds to the onset of DS2, is plotted at the 10% confidence level. It is assumed, due

to the underlying assumed lognormal distribution of the response of the structure, that these three points can be joined to form a lognormal cumulative distribution curve. As they are already plotted on a log scale; the curve shape is that of a normal cumulative probability distribution. Additionally, similar information can be extracted in a similar manner to plot curves in Figure 1-4(c) corresponding to the onset of further damage states. Again, these curves can be derived mathematically, as explained in Appendix A, with the equations given as follows:

For the resilience curves defining DS2, DS3 and DS4:

$$\tilde{P}_{a(DSi)} = \frac{1}{475} \left[\frac{IM(Tr = 475)}{EDP_{DSi} \tilde{K}} \right]^{1/q} \quad (1-14)$$

and the resilience curve defining DS5:

$$\tilde{P}_{a(DS5)} = \frac{1}{475} \left[\frac{IM(Tr = 475)}{I\tilde{M}_c} \right]^{1/q} \quad (1-15)$$

where the dispersion is given as the larger of:

$$\begin{aligned} \beta_{Pa} &= \sqrt{\left(\frac{1}{q}\right)^2 \beta_{EDP_{DSi}}^2 + \left(\frac{1}{q}\right)^2 \beta_K^2} \\ \beta_{Pa} &= \sqrt{\left(\frac{1}{q}\right)^2 \beta_{IM_c}^2} = \frac{\beta_{IM_c}}{q} \end{aligned} \quad (1-16)$$

Resilience curves graphically illustrate the expected seismic performance of a structure taking into consideration variation in seismic response due to all randomness and uncertainty. They illustrate the complete range of outcomes of a seismic event with a given probability, and can be used to estimate the likelihood, or confidence level associated with exceeding of each of these outcomes for seismic events with specified annual frequencies (or return periods). For these reasons, they are a powerful measure of a structure's seismic performance.

Step Ten: Definition of Damage Ratios

Resilience curves illustrate the probability of attaining discrete damage states for a particular earthquake frequency. In order to estimate financial losses, median damage ratios (DR) need to be assigned, through engineering judgement and rational reasoning, to each of the damage states. Damage ratios are defined for each damage state as the fraction of the total replacement cost of the structure. For the five damage states defined in Table 1-2, $DR(DS1) = 0$, as no damage occurs; and $DR(DS5) = 1$, as the structure needs to be completely replaced. These values, along with typical damage ratios for structural damage to reinforced concrete buildings for DS2, DS3 and DS4 are included in Table 1-2.

Step Eleven: Expected Annualised Financial Loss

The expected loss due to a seismic event with any given frequency can be calculated by summing the probability of each damage states multiplied by its respective damage ratio. Mathematically this is expressed as:

$$EL(p_a) = \sum_{i=1}^n P[DS_i | p_a] \cdot DR(DS_i) \quad (1-17)$$

where $EL(p_a)$ is the expected repair cost as a function of annual frequency, p_a , $P[DS_i | p_a]$ is the probability of damage belonging to DS_i for the given p_a , and $DR(DS_i)$ is the DR associated with DS_i . $EL(p_a)$ can be calculated for all p_a , and is plotted in Figure 1-5(b). The expected annualised loss (EAL) is estimated by integrating the shaded area beneath this curve, using a numerical integration method.

Alternatively, EAL can be calculated by multiplying the area enclosed between the appropriate resilience curves by the damage ratio for that damage state, and summing over all damage states. This can be calculated from the generalised expression:

$$EAL = DR_{DS1} + \sum_{i=2}^n (DR_{DS_i} - DR_{DS_{(i-1)}}) A_i \quad (1-18)$$

where A_i is the area enclosed between the $p_a = 0$ and the resilience curve corresponding to DS_i . Graphically this is represented by Figure 1-5(c).

For the purposes of financial loss estimation, resilience curves are truncated at a maximum considered annual frequency, $p_{a(\max)}$. This annual frequency, $p_{a(\max)}$, is chosen such that we are 90% confident that damage will not occur to the structure (DS2 or greater). This can be calculated as:

$$p_{a(\max)} = \frac{1}{475} \left[\frac{IM(T = 475)}{EDP_{DS2} K_{90\%}} \right]^{1/q} \quad (1-19)$$

where EDP_{DS2} is the EDP corresponding to the onset of DS2, and $K_{90\%}$ is the 90th percentile estimate of R-O parameter K . This means the effect of highly frequent small magnitude earthquakes, which dominate EAL, is somewhat minimised.

1.4.2 PRESENT WORTH AND TIME VALUE OF MONEY

Once EAL is known, direct comparison of the cost of the structure, using the principles of engineering economics, can be made with that of an alternative structure. If the value and economic lifetime of the two structures is the same, the two EAL can be directly compared. Otherwise, the annualised losses over the lifetime of the structure need to be converted to their present value, before they can be directly compared, as follows:

$$PW = V[1 + EAL (P/A, i, N)] \quad (1-20)$$

where V is construction/replacement cost of the structure, EAL is the expected annualised loss, and $(P/A, i, N)$ is the uniform series present worth factor for a given interest rate i and period of interest N .

The uniform series present worth factor is calculated as:

$$(P/A, i, N) = \frac{(1+i)^N - 1}{i(1+i)^N} \quad (1-21)$$

and as $i \rightarrow 0$, $(P/A, i, N) = N$.

1.5 SENSITIVITY ANALYSIS

There are many interrelationships involved in estimating EAL. The hazard recurrence relationship is developed based on historical data, and is extrapolated beyond the range of data presented in NZS 4203:1992. Furthermore, the seismic hazard is characterised by $IM(T = 475)$, which is determined from NZS 4203:1992 based on the geographic location and one of three soil types. The IM-EDP relationship is based on curve-fitting of results derived from IDA, the threshold EDP for each damage state are determined based on assumptions and engineering judgement, and additionally damage ratio are assumed based on engineering judgement.

Therefore EAL is calculated as a function of a number of uncertain inputs, which although are estimated through rigorous analysis and engineering judgement, are not known with certainty. In this section, two approaches to determining the sensitivity of EAL to the various inputs are described.

1.5.1 SENSITIVITY PARAMETER

Elms (1985), among others, has pointed out the futility of a highly detailed model with a number of uncertain inputs, when the output of the model is highly dependent on the value of one or more the input values used. Elms (1985) formalised this concept as '*The Principle of Consistent Crudeness*'.

The sensitivity factor of a model to a parameter can be expressed as:

$$\gamma_i = \frac{x_i}{y} \frac{\partial y}{\partial x_i} \quad (1-22)$$

where γ_i is the percentage change in the model output, y , due to a one percent change in input parameter x_i (Elms, 1985). Equation (1-22) can be used to calculate the ‘*sensitivity parameter*’ for each of the input variables.

The sensitivity parameter provides little information about the magnitude of the uncertainty associated with each parameter, and its total effect on the model output. Therefore a second method of calculating the sensitivity of the solution for each input is presented, this is similar to that adopted by Porter et al. (2002).

1.5.2 SWING ANALYSIS

In decision analysis, a figure called a ‘*tornado diagram*’ illustrates the sensitivity of an uncertain output value to the more-basic input variables that contribute to it (Eschenbach, 1992). EAL is a known deterministic function of a number of input variables, for which the extreme values or the probability distribution of each is known.

EAL is studied using a series of deterministic tests. First, each input variable is set to its median value, and the output is measured. This establishes a baseline output, represented in the tornado diagram by the vertical line. One by one, each input parameter is set to both high and low extreme values, and the outputs are measured. The absolute value of the difference between these two outputs, called the ‘*swing*’, is a measure of the sensitivity of EAL to that input parameter. The parameter is returned to its median value, and the process continues for all parameters. The input parameters can then be ranked according to their swing. The larger the swing the more significant the input uncertainty.

1.5.3 EXTREME VALUES OF THE INPUT PARAMETERS

The seismic hazard, represented by parameter $IM(T = 475)$ is determined from the New Zealand loadings code (NZS 4203:1992) based on one of three soil types. In the subsequent analysis, buildings that are assumed to be located on an intermediate soil type are analysed. Due to the limited number of soil categories, extreme values of $IM(T = 475)$ are taken as the averages of the values representing the intermediate soil and the neighbouring categories, being rock and soft soil. The slope of the hazard curve, q , is estimated by fitting a power curve to the data provided in NZS 4203:1992, as illustrated in Figure 1-1, where extreme values of 0.33 and 0.35 are found by fitting the curve to different regions of data.

The 10th and 90th percentile estimates of the median of parameters IM_C , K , and EDP_C are obtained, assuming they are lognormally distributed:

$$x_{10\%} = \frac{\tilde{x}}{e^{t_{0.1}\left(\frac{\beta_x}{\sqrt{n}}\right)}} \quad (1-23)$$

$$x_{90\%} = \tilde{x} e^{t_{0.1}\left(\frac{\beta_x}{\sqrt{n}}\right)} \quad (1-24)$$

where \tilde{x} is the median value, β_x is the dispersion of the parameter, n is the sample size (number of earthquake ground motions used to estimate \tilde{x} and β_x), $t_{0.1}$ is the value of the t-statistic based on $(n - 1)$ degrees of freedom, which is obtainable from statistical tables.

The 10th and 90th percentile estimates of the dispersion of parameters IM_C , K , and EDP_C are obtained, assuming these parameters are lognormally distributed:

$$\beta_{10\%} = \sqrt{\frac{(n-1)\bar{\beta}^2}{\chi_{0.9}^2}} \quad (1-25)$$

$$\beta_{90\%} = \sqrt{\frac{(n-1)\bar{\beta}^2}{\chi_{0.1}^2}} \quad (1-26)$$

where $\bar{\beta}$ is the estimated dispersion, and χ_{α}^2 is the value of the χ^2 -statistic based on $(n-1)$ degrees of freedom, again, obtainable from statistical tables.

Extreme values of threshold EDP to define the damage states and damage ratios are based on engineering judgement, as explained in subsequent chapters.

1.5.4 OBSERVED TRENDS

A normalised tornado diagram is presented in Figure 1-6 for a conventional reinforced concrete frame. It can be seen from this figure that EAL is sensitive to the majority of parameters, however the best estimate of EAL is of the correct order of magnitude. The three parameters contributing most to the uncertainty are $IM(T = 475)$, β_K , and \tilde{K} . These are discussed below.

$IM(T = 475)$ defines the earthquake ground motion intensity, and this is selected given the location of the structure and its soil type, from the loadings code (NZS 4203:1992). This result shows the assumptions made when selecting $IM(T = 475)$ for the analysis will significantly affect the EAL calculated. Therefore careful seismological assessment of the ground conditions and seismic hazard at each site would be advantageous. Furthermore, further seismological research into definition of the seismic hazard, particularly with a higher level of complexity when considering the response of different soil types would be advantageous.

Indirectly, \tilde{K} defines the resistance of the structure to the earthquake hazard, since $IM_c = K EDP_c$. The high degree of variability associated with \tilde{K} shows the median resistance of the structure is an important parameter, and reducing the number of

earthquake ground records used for the IDA will only increase the uncertainty associated with this parameter. Associated with \tilde{K} is its dispersion, β_K , which is a function of the suite of earthquake ground motion records used for the IDA. While the capacity of the structure is inherently random, these results also show that the seismic resistance depends, to a certain extent, on the variability of the seismic demand, which is represented by variability in the suite of earthquake ground motions used for the IDA.

Effect of Seismic Hazard Definition

The seismic hazard curve has been defined by fitting a smooth power law curve to data obtained from the New Zealand loadings code (NZS 4203:1992). The data obtained from NZS 4203:1992 is presented for return periods of 30 years to 2 000 years, and the curve fitted is extrapolated to cover the complete spectrum of data points. This is illustrated in Figure 1-1. It can be seen from Figure 1-1 that the seismic hazard relationship defined by equation (1-2) is not a perfect fit to the data, and extrapolation for frequent earthquakes appears to return higher seismic intensities than is necessary. Indeed the seismic intensities obtained for more frequent earthquakes are higher than suggested by experience.

As EAL is estimated by integrating over a complete range of annual frequencies, more frequent earthquakes will dominate the estimate. As it was observed that the seismic intensities for more frequent earthquakes are being over-estimated, the corresponding estimates of EAL are probably conservative. Further research is required to gain a greater understanding of the seismic hazard and implement a better model into the proposed probabilistic seismic vulnerability assessment methodology.

1.6 DISCUSSION OF APPLICATIONS

In Chapter Two, the probabilistic seismic vulnerability assessment methodology is applied to calculate EAL of three frame structures, considering structural damage to the frame, determined on the basis of maximum inter-storey drift. These three structures are a traditional ten storey reinforced concrete frame (CCANZ, 1998), and the companion ten storey DAD frames designed by Arnold (2004) and Davies (2003). The results are compared using principles of engineering economics, and EAL calculated for the DAD frames is significantly lower than EAL calculated for the traditional reinforced concrete frame.

The comparisons made in Chapter Two are limited to structural damage, which is determined on the basis of maximum inter-storey drift. However the methodology presented in this chapter is sufficiently general that it could additionally be used to determine non-structural losses, based on either maximum inter-storey drift or floor acceleration. In addition, other expenses incurred during the buildings' lifetime, such as maintenance could also be included in cost-benefit analyses.

The design of both gravity and non-gravity load carrying DAD frames for a six storey apartment building is presented in Chapter Three. Prior to the rigorous analysis presented in this chapter, a more simplified rapid methodology for estimating EAL is presented, based on a pushover analysis. These results are compared with EAL calculated from the more rigorous IDA based probabilistic seismic vulnerability assessment methodology presented in this chapter.

1.7 CONCLUSIONS

A probabilistic seismic vulnerability assessment methodology, whose output is the expected annualised loss (EAL), was proposed in this chapter. This proposed methodology, while based on well established incremental dynamic analysis (IDA) and fragility curve theory, includes several advances which make earthquake loss estimation more clear to users. An estimate of EAL is obtained, which can directly be used on cost-benefit analysis by considering principles on engineering economics. In the development of EAL, resilience curves were introduced. Resilience curves graphically illustrate the probability of attaining particular damage states for an earthquake with given annual frequency. By assigning damage ratios to each of the damage states and integrating over the resilience curve plot, EAL is easily obtained.

Unlike many existing loss estimation methodologies, this method is general and transparent, and although a large number of non-linear time-history analyses are required as part of the IDA, it is suitable for use in engineering practice. It can be used for any structure, for both structural and non-structural losses, and incorporates all sources of randomness and uncertainty. This methodology is particularly suitable for comparative purposes where structure types have distinctively different design approaches and response characteristics, as earthquake damage is taken into consideration.

The basis for formal sensitivity analysis was presented. Two techniques were employed to evaluate the sensitivity of the various inputs of EAL, being determination of a sensitivity parameter and swing analysis. General trends show EAL is most sensitive to parameters defining the seismic hazard, the median seismic resistance of the structure and the suite of ground motion records used for the IDA.

1.8 REFERENCES

- Arnold, D.M. (2004) Development and Experimental Testing of a Seismic Damage Avoidance Designed Beam to Column Connection Utilising Draped Unbonded Post-Tensioning. ME Thesis, Department of Civil Engineering, University of Canterbury, Christchurch, New Zealand.
- Bendimerad, F. (2001) Loss estimation: a powerful tool for risk assessment and mitigation. *Soil Dynamics and Earthquake Engineering*, **21**(5), 467-472.
- Bertero, V.V. (1980) 'Strength and Deformation Capacities of Buildings Under Extreme Environments'. In: *Structural Engineering and Structural Mechanics: A Volume Honouring Egor P. Popov*. Ed: K.S. Pister. Prentice Hall, Englewood Cliffs, NJ. pp 188-237.
- Cement and Concrete Association of New Zealand (CCANZ) (1998) *Examples of Concrete Structural Design to NZS 3101:1995 – "Red Book"*. Cement and Concrete Association of New Zealand, Wellington.
- Christopoulos, C., Filiatrault, A. and Folz, B. (2002) Seismic response of self-centring hysteretic SDOF systems. *Earthquake Engineering and Structural Dynamics*, **31**(5), 1131-1150.
- Christopoulos, C., Pampanin, S. and Priestley, M.J.N. (2003) Performance-Based Seismic Response of Frame Structures Including Residual Deformations. Part I: Single-Degree of Freedom Systems. *Journal of Earthquake Engineering*, **7**(1), 97-118.
- Davies, M.N. (2003) Seismic Damage Avoidance Design on Beam-Column Joints Using Unbonded Post-Tensioning: Theory, Experiments and Design Example. ME Thesis, Department of Civil Engineering, University of Canterbury, Christchurch, New Zealand.
- Dhakal, R.P. and Mander, J.B. (2005) Probabilistic Risk Assessment Methodology Framework for Natural Hazards. Final Report submitted to Institute of Geological and Nuclear Science.

- Dutta, A. (1999) On Energy-Based Seismic Analysis and Design on Highway Bridges. PhD Dissertation, Department of Civil, Structural and Environmental Engineering, State University of New York at Buffalo, Buffalo, NY, USA.
- Elms, D.G. (1985) 'The Principle of Consistent Crudeness'. In: *Proceedings of NSF Workshop on Civil Engineering Applications of Fuzzy Sets*. Eds: C.B. Brown, J.-L. Chameau, R.N. Palmer and J.T.P. Yao. Purdue University, West Lafayette, IN. pp 35-44.
- Erberik, M.A. and Elnashai, A.S. (2004) Fragility analysis of flat-slab structures. *Engineering Structures*, **26**(7), 937-948.
- Eschenbach, T.G. (1992) Spiderplots versus Tornado Diagrams for Sensitivity Analysis. *Interfaces*, **22**(6) 40-46.
- Federal Emergency Management Agency (FEMA) (2003) HAZUS-MH MR1 Advanced Engineering Building Module: Technical and User's Manual. FEMA.
- Karim, K.R. and Yamazaki, F. (2001) Effect of earthquake ground motions on fragility curves of highway bridge piers based on numerical simulation. *Earthquake Engineering and Structural Dynamics*, **30**(12), 1839-1856.
- Kennedy, R.P., Cornell, C.A., Campbell, R.D., Kaplan, S. and Perla, H.F. (1980) Probabilistic Seismic Safety Study of an Existing Nuclear Power Plant. *Nuclear Engineering and Design*, **59**(2), 315-338.
- Kircher, C.A., Nassar, A.A., Kustu, O. and Holmes, W.T. (1997) Development of Building Damage Functions for Earthquake Loss Estimation. *Earthquake Spectra*, **13**(4), 663-682.
- Kiremidjian, A.A. and Bazöz, N. (1997) Evaluation of Bridge Damage Data from Recent Earthquakes. *NCEER Bulletin*, **11**(2), 1-7.
- Krawinkler, H. and Miranda, E. (2004) 'Performance-Based Earthquake Engineering'. In: *Earthquake Engineering: From Engineering Seismology to Performance-Based Engineering*. Eds: Y. Bozorgnia and V.V Bertero. CRC Press, Boca Raton, FL. Chapter 9.

- Lang, K. and Bachmann, H. (2004) On the Seismic Vulnerability of Existing Buildings: A Case Study of the City of Basel. *Earthquake Spectra*, **20**(1), 43-66.
- Luco, N. and Cornell, C.A. (1998) Effects of Random Connection Fractures on the Demands and Reliability for a 3-Story Pre-Northridge SMRF Structure. Proceedings Sixth US Conference on Earthquake Engineering (Seattle, WA) 31 May – 4 June. Paper 224.
- Mander, J.B. (2004) Beyond Ductility: The Quest Goes On. *Bulletin of the New Zealand Society of Earthquake Engineering*, **37**(1), 35-44.
- Mander J.B., and Basöz N. (1999) ‘Seismic Fragility Curve Theory for Highway Bridges in Transportation Lifeline Loss Estimation’. In: *Optimizing Post-Earthquake Lifeline System Reliability*, Eds: Elliot and McDonough. TCLEE Monograph No. 16, ASCE. pp 31-40.
- Martínez, M.E. (2002) Performance-Based Seismic Design and Probabilistic Assessment of Reinforced Concrete Moment Resisting Frame Structures. ME Thesis, Department of Civil Engineering, University of Canterbury, Christchurch, New Zealand.
- Mwafy, A.M., and Elnashai, A.S. (2001) Static pushover versus dynamic collapse analysis of RC buildings. *Engineering Structures*, **23**(5), 407-424.
- Porter, K.A. (2003) ‘Seismic Vulnerability’. In: *Earthquake Engineering Handbook*. Eds: W.-F. Chen and C. Scawthorn. CRC Press, Boca Raton, FL. Chapter 21.
- Porter, K.A., Beck, J.L and Shaikhutdinov, R.V. (2004) Simplified Estimation of Economic Seismic Risk for Buildings. *Earthquake Spectra*, **20**(4), 1239-1263.
- Porter, K.A., Beck, J.L. and Shaikhutdinov, R.V. (2002) Sensitivity of Building Loss Estimates to Major Uncertain Variables. *Earthquake Spectra*, **18**(4), 719-743.
- Porter, K.A., Kiremidjian, A.S. and LeGrue, J.S. (2001) Assembly-Based Vulnerability of Buildings and Its Use in Performance Evaluation. *Earthquake Spectra*, **17**(2), 291-312.

- Rahardjo, T. (2004) Experiments and stochastic modelling of New Zealand grown *Pinus radiata* timber and timber piles under seismic loading. ME Thesis, Department of Civil Engineering, University of Canterbury, Christchurch, New Zealand.
- Rosowsky, D.V. and Ellingwood, B.R. (2002) Performance-Based Engineering of Wood Frame Housing: Fragility Analysis Methodology. *Journal of Structural Engineering*, **128**(1), 32-38.
- Shinozuka, M., Feng, M.Q., Lee, J. and Naganuma, T. (2000) Statistical Analysis of Fragility Curves. *Journal of Engineering Mechanics*, **126**(12), 1224-1231.
- Shome, N., Cornell, C.A., Bazzurro, P. and Carballo, J.E. (1998) Earthquakes, Records, and Nonlinear Responses. *Earthquake Spectra*, **14**(3), 469-500.
- Singhal, A. and Kiremidjian, A.S. (1996) Method for Probabilistic Evaluation of Seismic Structural Damage. *Journal of Structural Engineering*, **122**(12), 1459-1467.
- Smyth, A.W., Altay, G., Deodatis, G., Erdik, M., Franco, G., Gülkan, P., Kunreuther, H., Luş, H., Mete, E., Seeber, N. and Yüzügüllü, Ö. (2004) Probabilistic Benefit-Cost Analysis for Earthquake Damage Mitigation: Evaluating Measures for Apartment Houses in Turkey. *Earthquake Spectra*, **20**(1), 171-203.
- Standards New Zealand (1992) Code of Practice for General Structural Design and Design Loadings for Buildings, known as the loadings standard, NZS 4203:1992, Volumes 1 and 2. Standards New Zealand, Wellington, New Zealand.
- Vamvatsikos, D. and Cornell, C.A. (2002) Incremental dynamic analysis. *Earthquake Engineering and Structural Dynamics*, **31**(3), 491-514.
- Vamvatsikos, D. and Cornell, C.A. (2004) Applied Incremental Dynamic Analysis. *Earthquake Spectra*, **20**(2), 523-553.
- Vamvatsikos, D. and Cornell, C.A. (2005) Direct Estimation of Seismic Demand and Capacity of Multidegree-of-Freedom Systems through Incremental Dynamic Analysis of Single Degree of Freedom Approximation. *Journal of Structural Engineering*, **131**(4), 589-599.

Whitman, R.V., Anagnos, T., Kircher, C.A., Lagorio, H.J., Lawson, R.C. and Schneider, P. (1997) Development of a National Earthquake Loss Estimation Methodology. *Earthquake Spectra*, **13**(4), 643-661.

Yamazaki, F., Motomura, H. and Hamada, T. (2000) Damage Assessment of Expressway Networks in Japan based on Seismic Monitoring. Proceedings 12th World Conference on Earthquake Engineering (Auckland, New Zealand), 30 January – 4 February. Paper 0551.

Table 1-1: Details of 20 ground motion records used

No	Event	Station	Φ^{*1}	M^{*2}	R^{*3} (km)	PGA (g)
1	Loma Prieta	1989 Agnews State Hospital	90	6.9	28.2	0.159
2	Imperial Valley	1979 Plaster City	135	6.5	31.7	0.057
3	Loma Prieta	1989 Hollister Diff. Array	255	6.9	25.8	0.279
4	Loma Prieta	1989 Anderson Dam	270	6.9	21.4	0.244
5	Loma Prieta	1989 Coyote Lake Dam	285	6.5	22.3	0.179
6	Imperial Valley	1979 Cucapah	85	6.9	23.6	0.309
7	Loma Prieta	1989 Sunnyvale Colton Ave	270	6.9	28.8	0.207
8	Imperial Valley	1979 El Centro Array #13	140	6.5	21.9	0.117
9	Imperial Valley	1979 Westmoreland Fire Sta.	90	6.5	15.1	0.074
10	Loma Prieta	1989 Hollister South & Pine	0	6.9	28.8	0.371
11	Loma Prieta	1989 Sunnyvale Colton Ave	360	6.9	28.8	0.209
12	Superstition Hills	1987 Wildlife Liquefaction Array	90	6.7	24.4	0.180
13	Imperial Valley	1979 Chihuahua	282	6.5	28.7	0.254
14	Imperial Valley	1979 El Centro Array #13	230	6.5	21.9	0.139
15	Imperial Valley	1979 Westmoreland Fire Sta.	180	6.5	15.1	0.110
16	Loma Prieta	1989 WAHO	0	6.9	16.9	0.370
17	Superstition Hills	1987 Wildlife Liquefaction Array	360	6.7	24.4	0.200
18	Imperial Valley	1979 Plaster City	45	6.5	31.7	0.042
19	Loma Prieta	1989 Hollister Diff. Array	165	6.9	25.8	0.269
20	Loma Prieta	1989 WAHO	90	6.9	16.9	0.638

¹ Component² Moment Magnitude³ Closest Distance to Fault RuptureSource: PEER Strong Motion Database, <http://peer.berkeley.edu/smcat/>**Table 1-2: Definition of damage states**

Damage State	Failure Mechanism	Repair Required	Outage	Damage Ratio
DS1	No Damage	Pre-yield	None	0
DS2	Minor Damage	Post-yield Minor cracking & spalling	Inspect, Patch	< 3 days 2.5%
DS3	Repairable Damage	Post-yield Significant spalling	Repair components	< 3 weeks 20%
DS4	Irreparable Damage	Strength degradation Bar buckling & hoop fracture	Demolish and rebuild structure	> 3 months 75%
DS5	Partial/Total Collapse	Partial/Total Collapse	Remove rubble and rebuild structure	> 3 months 100%

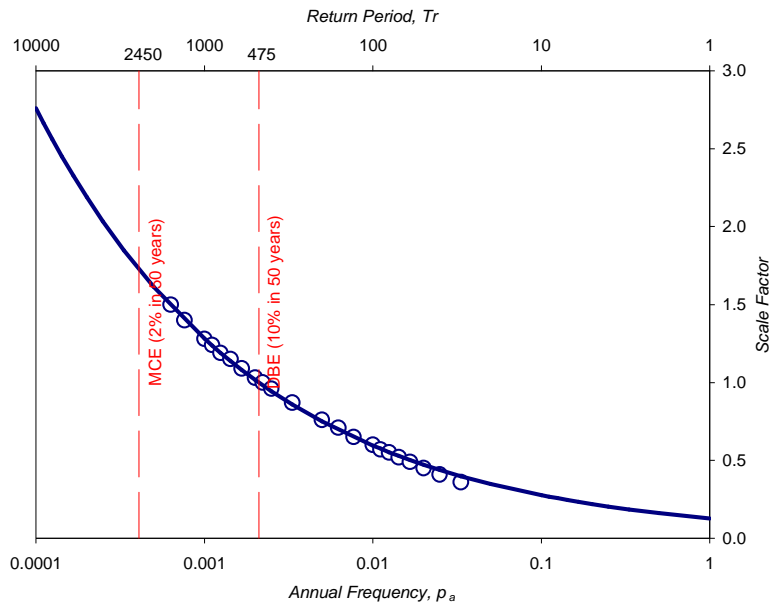
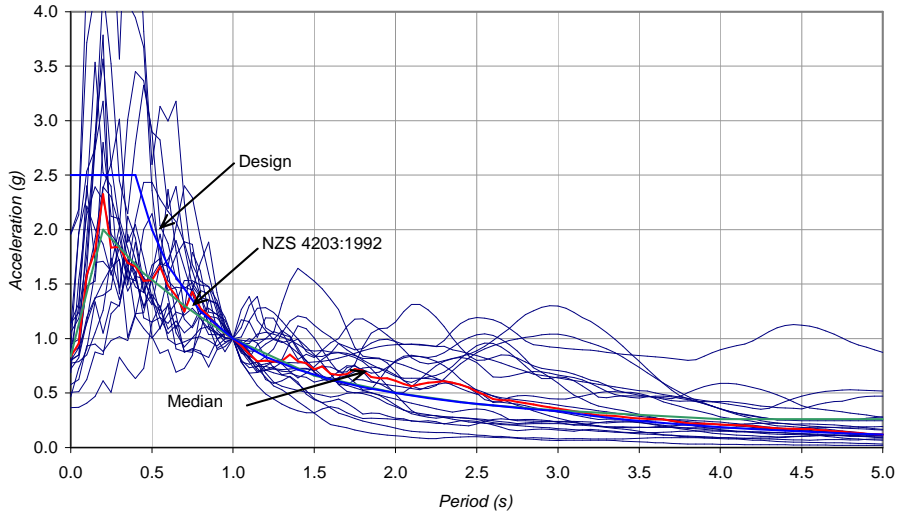
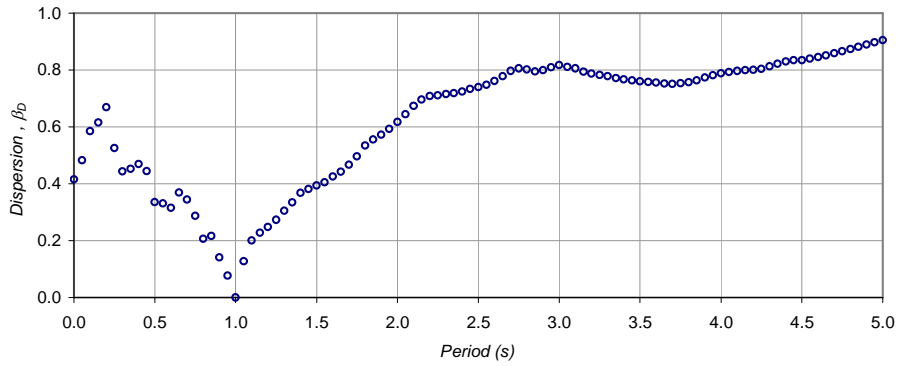


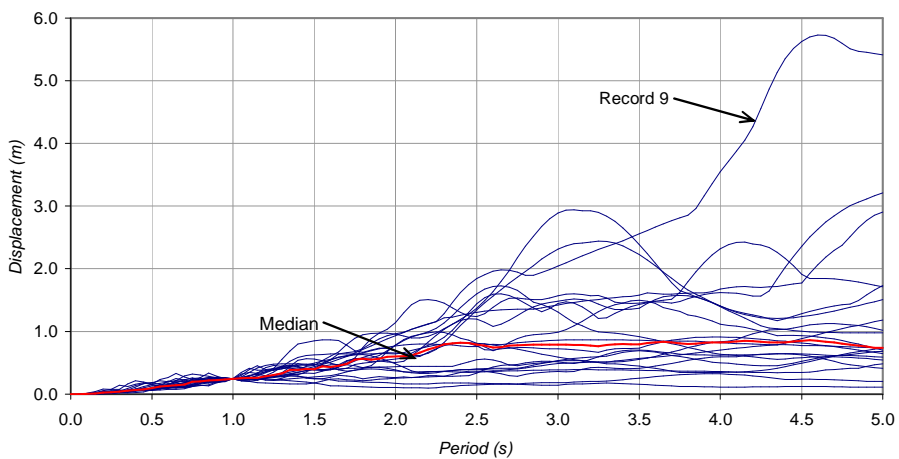
Figure 1-1: Seismic hazard curve and data obtained from NZS 4203:1992



(a) Response acceleration spectra for the suite of 20 selected earthquakes

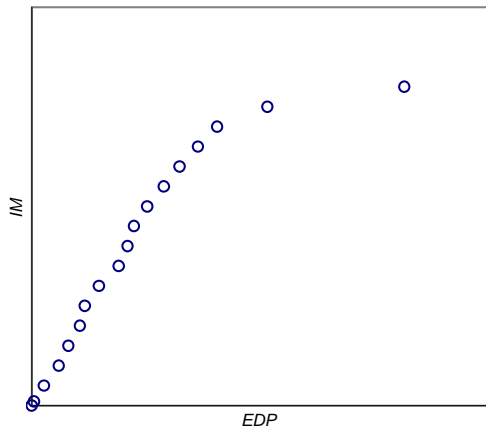


(b) Dispersion β_D of the seismic demand

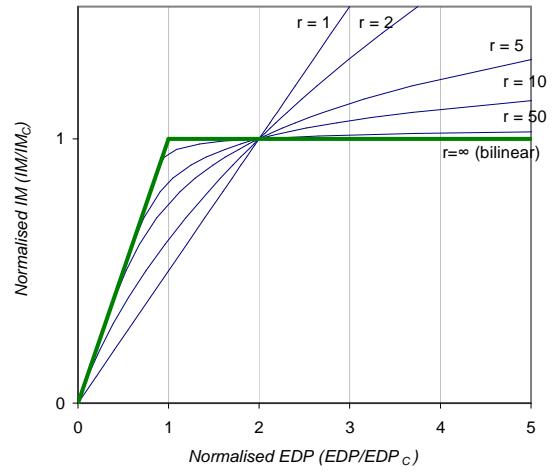


(c) Displacement Response Spectra for the suite of 20 selected earthquakes

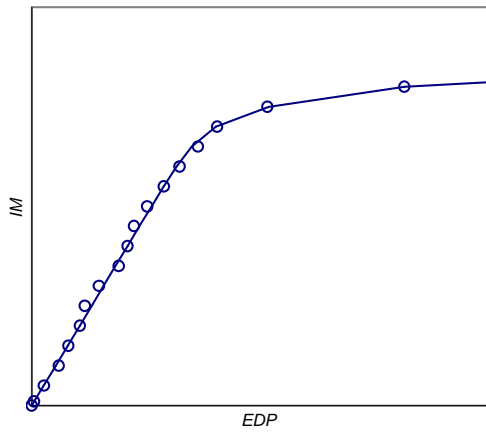
Figure 1-2: 5% damped acceleration response spectra, dispersion, and displacement response spectra for the 20 selected ground motion records, normalised to $S_A(T = 1s)$



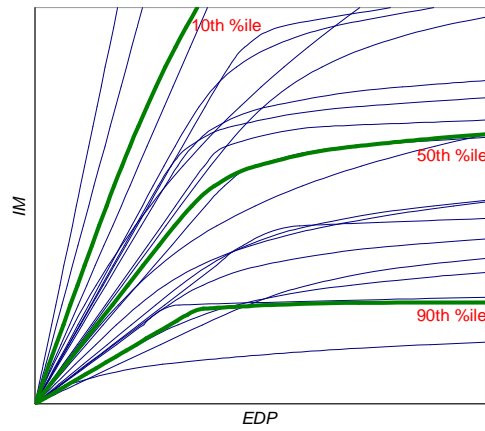
(a) IDA data points



(b) R-O curve parameters

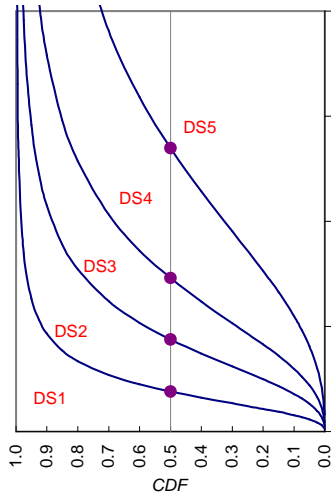


(c) Fitting of R-O curve

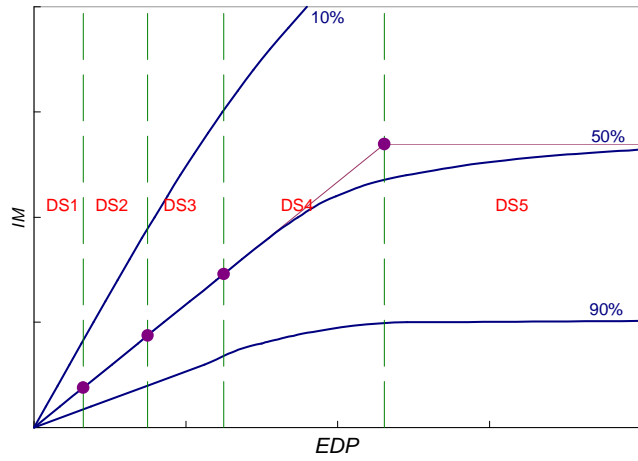


(d) R-O IDA curves summarised by 10th, 50th and 90th percentiles

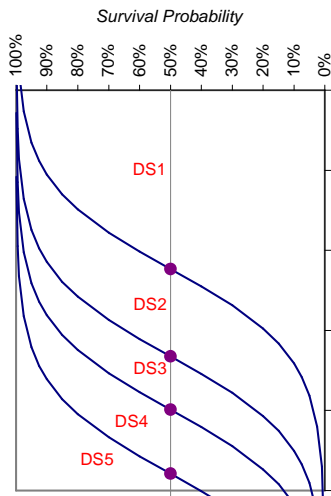
Figure 1-3: Summary of steps in fitting R-O equation to IDA output



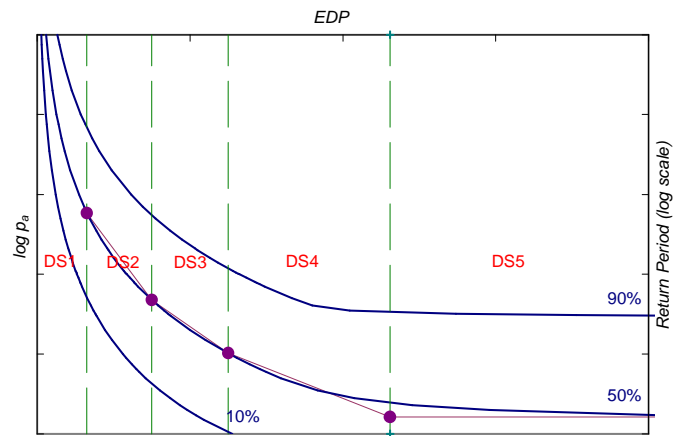
(a) Fragility curves



(b) Summarised R-O IDA output

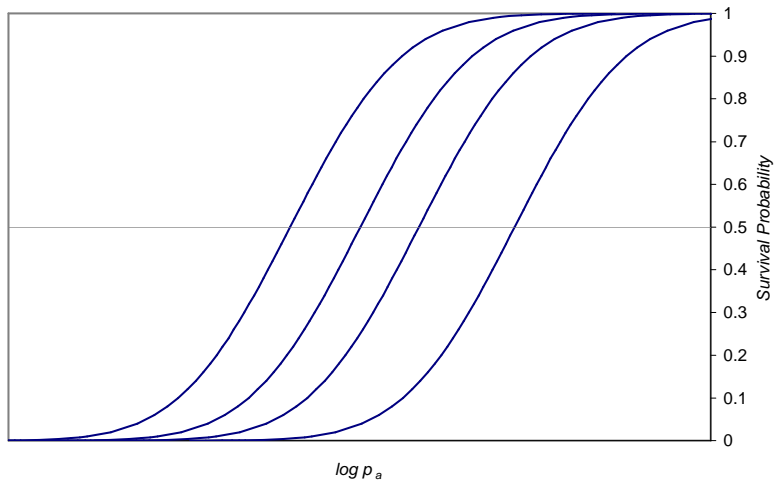


(c) Resilience Curves

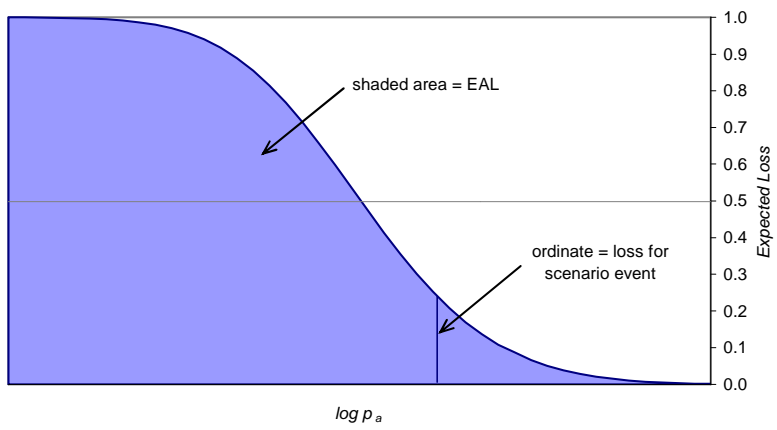


(d) Hazard Curves

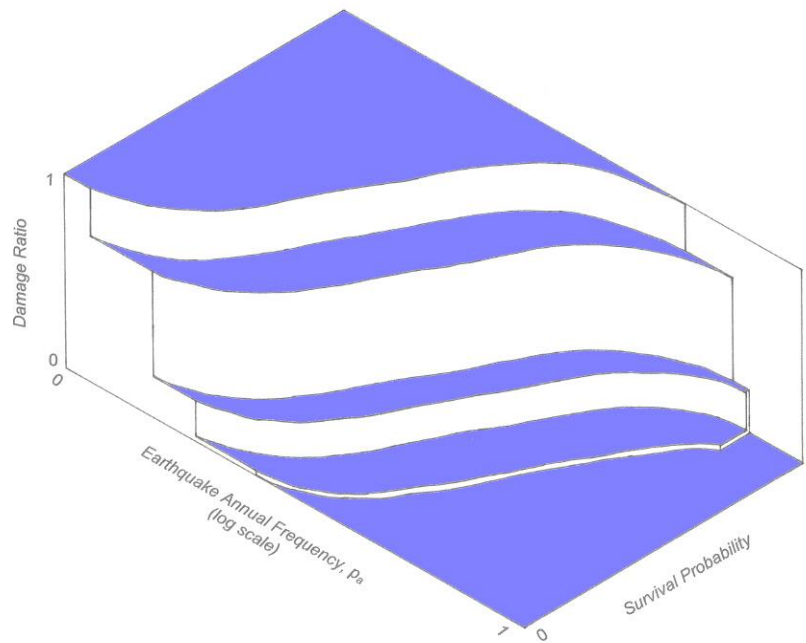
Figure 1-4: Summary of risk assessment of structure



(a) Resilience Curves



(b) Expected Loss Ratio



(c) 3D representation of volume calculation

Figure 1-5: Summary of annualised loss calculation

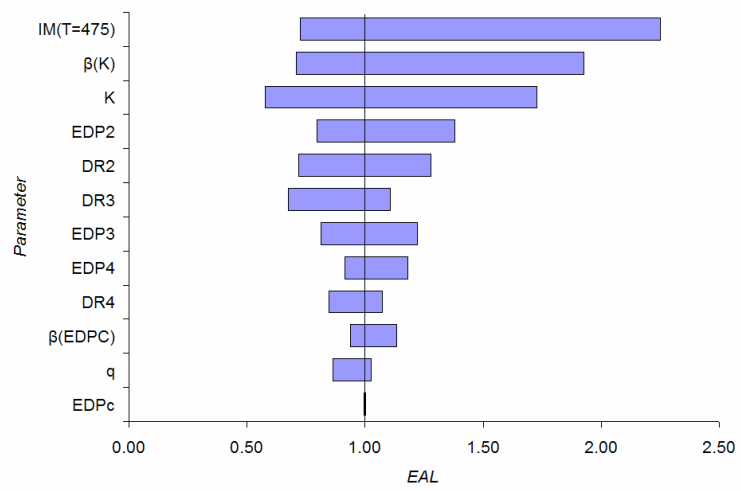


Figure 1-6: Normalised tornado diagram indicating variability of parameters

CHAPTER TWO

SEISMIC VULNERABILITY OF BUILDINGS AND FINANCIAL LOSS ESTIMATION. II: APPLICATION

Chapter Summary

The probabilistic seismic vulnerability assessment methodology is applied to three different types of ten storey moment resisting concrete frame, to determine the expected annualised seismic loss (EAL). The first of these frames is a typical reinforced concrete frame, designed and detailed for ductility in accordance with the principles of capacity design; this benchmark structure represents the current state-of-practice. The second and third of these frames are state-of-the-art structures designed and detailed in accordance with the principles of damage avoidance design (DAD). The DAD detailing of the beam-column joints consists of steel armouring to the rocking interfaces and supplemental energy dissipators bolted across the connections. The EAL calculated for the DAD frames is significantly lower than that calculated for the benchmark structure, indicating superior performance of these frames in terms of economic loss. Further, discussion of the sensitivity of the methodology shows the EAL is somewhat sensitive to the definition of the seismic hazard and the suite of earthquake ground motions used for incremental dynamic analysis.

2.1 INTRODUCTION

Recent earthquakes, such as Northridge, 1994, and Hyogoken-Nanbu, 1995, have illustrated that even though buildings have performed satisfactorily, in terms of life safety, significant damage to the structure, and the building contents have occurred, resulting in severe economic losses. Since these earthquakes there has been significant research effort into developing alternative building systems that minimise the damage incurred to structures and building contents. One such alternative system involves the use of post-tensioned beam-column connections detailed according to a damage avoidance design (DAD) philosophy with steel armouring at the rocking interfaces to prevent damage. Experimental testing of such frame systems has recently been carried out at the University of Canterbury (Davies, 2003; Arnold, 2004; Murahidy, 2004). These beam-column connections have been designed such that earthquake damage only occurs to replaceable components, thereby significantly reducing the economic cost of damage to buildings during earthquakes.

The probabilistic seismic vulnerability assessment methodology, developed in Chapter One can be used to calculate the expected annualised seismic loss (EAL) for any given structure. This methodology accounts for all earthquake intensities and frequencies, and incorporates the various sources of randomness and uncertainty. By explicitly considering damage in terms of financial loss, the proposed methodology is particularly suitable for comparing the seismic response of different types of structure.

The purpose of this chapter is to demonstrate superior performance of a DAD structure when compared with a more conventional structure. The performance of precast concrete structures with post-tensioned rocking connections has previously been investigated through a number of analytical and experimental investigations. Such studies

indicate better performance of post-tensioned rocking structures when compared to monolithic construction. In this chapter, the proposed probabilistic seismic vulnerability assessment methodology is used to determine EAL, considering only structural losses, for three ten-storey frames. Initially a conventional ductile monolithic reinforced concrete office building is considered as a state-of-practice benchmark structure. The second structure is a frame designed using the DAD philosophy to resist both gravity and seismic loads, and the third is a DAD frame designed to resist predominantly seismic loads. The results of these analyses are compared to illustrate superior performance of the DAD frames. A complete description of the analytical modelling is provided below. First, the DAD philosophy and development of rocking systems is discussed.

2.2 FINDINGS FROM PREVIOUS RESEARCH

From the early nineties there has been increasing research interest in the performance of structures constructed from precast concrete elements connected with unbonded post-tensioned prestress tendons. In particular significant advances were made as part of the precast seismic structural systems (PRESSSS) research programme. Priestley and Tao (1993) carried out a number of computational non-linear time-history analyses of structural systems with partially unbonded post-tensioned tendons (bi-linear elastic hysteresis). Their results indicated that the peak displacements of this system were not significantly different to those of a monolithic prestressed structure. An observed advantage of jointed precast frames is that design of the beam-column joint is simplified due to a large proportion of joint shear being transferred through formation of a concrete compression strut within the joint.

Priestley and MacRae (1996) report on an experimental investigation of two large-scale ungrouted post-tensioned frame subassemblies representing an internal and external

beam-column connection. Significantly less damage was observed than that which would have been expected for an equivalent monolithic frame. Some cover concrete spalling occurred in the rocking zones, however negligible residual drifts remained after removal of lateral loads. The outcomes of this research validated the findings of Priestley and Tao (1993).

The National Institute of Standards and Technology (NIST) in the United States executed a multi-year programme aimed at creating recommended guidelines for precast beam-column connections in regions of high seismicity. One outcome of this programme was the development of a '*hybrid*' moment resisting connection that uses both unbonded post-tensioned reinforcement and bonded mild steel reinforcement (Stanton et al., 1997). The force-displacement response of frame subassemblies built with these hybrid beam-column connections exhibited the same minimal residual drift characteristics of the joints tested by Priestley and MacRae (1996) but also possessed significant levels of hysteretic damping.

A 60% scale five-storey precast concrete building consisting four different precast frame systems in one direction and a jointed structural wall system in the other, summarised by Priestley et al. (1999), was tested at the conclusion of the PRESSS research programme. Damage to the frame systems under seismic loading was minimal, with minor spalling of concrete at the beam ends and some crushing of fibre-reinforced grout at the beam-column interface observed. In addition, some problems with slip and torsion of the beam interface were experienced due to inadequate clamping forces and torsional load from the flooring system.

The hybrid post-tensioned beam-column connection has been successfully applied in the construction of a 39 storey apartment building, "The Paramount", in San Francisco, completed in 2001 (Englekirk, 2002). An added advantage of using post-tensioned beam-

column connections for this building was the reduction of maintenance costs of caulked waterproof slip joints.

Recently these concepts have been extended to post-tensioned steel beam-column connections, where energy dissipation is provided either through bolted angle plates (Ricles et al., 2001; Garlock et al., 2005) friction damping devices (Rojas et al., 2002) or energy dissipation bars placed across the joint (Christopoulos et al., 2002).

2.2.1 DAMAGE AVOIDANCE DESIGN BACKGROUND

Mander and Cheng (1997) applied the concept of jointed precast construction using unbonded prestressing tendons to the design of a modular bridge pier system. They proposed a damage avoidance design (DAD) philosophy whereby damage to the rocking piers was avoided by special detailing of the rocking interfaces. Testing of a prototype pier substructure showed that it possessed a bi-linear force-displacement response and it had the potential to survive seismic excitations undamaged. Little or no degradation in the strength or stiffness of the pier was observed.

Experimental studies into the performance of post-tensioned beam-column connections designed and detailed according to a DAD philosophy were recently carried out at the University of Canterbury by Davies (2003) and Arnold (2004). Following on from their experimental investigations, both Davies (2003) and Arnold (2004) present a design example of a ten storey moment resisting frame employing similar beam-column connections as tested in their experimental investigations. Both the experimental investigations and design example were developed from a prototype building, illustrated in Figure 2-1, similar to the ten storey three bay by three bay “Red Book” building (CCANZ, 1998). The prototype building has a one-way floor slab, therefore the connections tested in the north-south (N-S) direction by Davies (2003) were designed to resist predominantly

seismic forces, while those tested in the east-west (E-W) direction by Arnold (2004) were designed to resist both gravity and seismic loading. Here, both experimental investigations and frame designs are described.

Experimental Investigations: Davies Seismic Frame

Davies (2003) carried out quasi-static reversed cyclic tests on an 80% scale interior beam-column subassembly designed to resist seismic (lateral) loads only. The particularly innovative feature of this beam-column connection was the use of a steel armoured endplate assembly which allows for off-site post-tensioning of the beams. Therefore the rocking interface was shifted by the length of the steel end plate away from the column face into the beam. It was proposed that once the beams are cast and post-tensioned off site, they will be transported to the site and bolted to the column using threaded rods.

Tests were carried out on the specimen with prestress only, and two types of energy dissipation devices, being (1) ‘*dog-bone*’ tension-compression energy dissipators cut from mild steel plate bolted across the top and bottom of the rocking interface with high strength bolts; and (2) ‘*boomerang*’ flexural energy dissipators bolted to each side of the rocking interface with high strength bolts. Due to a 0.5 mm tolerance in the bolt holes and the flexibility of the bolts in single shear, significant pinching was observed in the hysteresis loop. To eliminate this slop, the bolt heads were welded to the dissipators, and this provided a much better response. No damage occurred to the system up to 3% drift, and the tension-compression ‘*dog-bone*’ dissipators provided the best energy dissipation. It was found that the moment-rotation response of the connection could accurately be predicted by equations developed assuming rigid body rotation about the rocking interfaces.

Experimental Investigations: Arnold Gravity Frame

Arnold (2004) conducted an experimental study on an 80% scale interior beam-column subassembly from a frame designed to resist gravity and seismic loads. The subassembly used a DAD philosophy; hence the rocking interfaces were protected with steel armouring to prevent damage. A draped post-tensioned tendon was provided to balance the gravity load. The connection was located approximately one member depth into the beam span – as this was the location of the point of inflection of bending moment due to gravity load. The beams were cast and prestressed off-site, and then lowered into position. Threaded prestressing bolt bars were inserted through column and beam stubs to a coupler at the beam end where they were tightened, to complete on-site erection of the structure.

Tests were carried out with prestress only, and three different types of energy dissipation, being (1) ‘*dog-bone*’ tension-compression dissipator, bolted across the connection, both with and without the bolt head welded to the dissipator; (2) ‘*boomerang*’ flexural yielding dissipator bolted to the connection; and (3) threaded rod tension-compression dissipator, both snug tightened and pretensioned to yield. These dissipators were all located on the sides of the beam. Similar to Davies (2003), Arnold (2004) found that even with tolerances in the order of 0.2 mm, there was significant slop causing the bolted ‘*dog-bone*’ and ‘*boomerang*’ dissipators to be ineffective. The welded ‘*dog-bone*’ dissipators and pretensioned threaded rod dissipators performed best.

Further testing was carried out to yield the bolt bars (which were milled down to ensure yielding of the draped tendons did not occur), and the results showed limited yielding of the bolt-bar is allowable under extreme loading, as full design performance was regained by restressing to the original prestress levels. The yielding of the bolt-bars provided extra energy dissipation.

Design Example: Davies Seismic Frame

Davies (2003) presented a design example for a ten storey post-tensioned precast moment resisting frame, designed to resist seismic loads only. The design of this frame was based on a ten storey prototype building from which his experimental studies were developed. The design method is briefly summarised as follows:

The rapid pushover method proposed by Martínez (2002) is used to determine the correct number of storeys participating in a generalised mixed collapse mechanism, from which the corresponding base shear can be found. The acceleration capacity and displacement of the equivalent single degree of freedom (SDOF) system are then found (for further details, see Appendix B), so the seismic demand for the given structure location is directly equated with the acceleration capacity to give the required beam moment capacity for the frame.

Design Example: Arnold Gravity Frame

Arnold (2004) presented a design example for a ten storey post-tensioned precast moment resisting frame, designed so gravity loads are balanced by draped tendons in the beams, and also to resist seismic loads. The design of this frame was based on a ten storey prototype building, illustrated in Figure 2-1, from which his experimental studies were developed. The design method is briefly summarised as follows:

First, the initial prestress force in the beams is calculated by balancing the dead and probable live loads, and then the area of prestressing tendons can be determined. The rapid pushover method proposed by Martínez (2002) is used to determine the number of storeys participating in a generalised mixed collapse mechanism, and corresponding base shear. Thus the acceleration capacity and displacement of the equivalent SDOF system can be found at both the design basis earthquake (DBE) and maximum considered event (MCE), from which the spectral acceleration capacity is found. This is then compared with

the spectral acceleration demand, using a capacity reduction factor, $\phi = 0.7$. Since insufficient capacity was provided, additional energy dissipation was provided.

It is observed that while both the design approaches are fundamentally the same, Arnold (2004) incorporates the use of a capacity reduction factor, whereas Davies (2003) does not. As a consequence the frame designed by Arnold (2004) is stronger, and has slightly larger members than that designed by Davies (2003).

2.2.2 THEORETICAL MOMENT-ROTATION RESPONSE OF DAD BEAM-COLUMN CONNECTION

Prior to joint opening, normal flexural elastic behaviour of the members will occur. Following opening of the rocking connection, the prestress tendons will elongate, resulting in an increase in the prestress force, and energy dissipators will yield and begin to strain harden. The rocking connection moment resisted, M_b , can thus be separated into contributions from the prestress and energy dissipators, and expressed as:

$$M_b = M_{PS} + M_d \quad (2-1)$$

where M_{PS} is the moment contribution provided by the prestress and M_d is the moment contribution provided by the dissipators.

As the connection opens, a small compression zone will form at the rocking interface. An iterative methodology to determine the moment-rotation behaviour of ‘*hybrid*’ beam-column joints, considering the depth of the compression zone, was formulated by Pampanin et al. (2001). However, due to the high strength and stiffness of the steel armouring, the moment-rotation response of these joints can be approximated by assuming rocking occurs about the extreme edges of the connection. Arnold (2004) and Davies (2003) both found good agreement between their experimental results and

theoretical moment-rotation curves derived using this approximation. Therefore M_{PS} and M_d can be evaluated as:

$$M_{PS}^{\pm} = P_{PS} \left(\frac{d_b}{2} \mp e_{PS} \right) \quad (2-2)$$

$$M_d^{\pm} = P_d \left(\frac{d_b}{2} \mp e_d \right) \quad (2-3)$$

where P_{PS} and P_d are the prestress and dissipator forces, respectively, d_b is the overall beam depth and e_{PS} and e_d are the eccentricity of the prestress and dissipator lines of action from the centreline of the beam-column connection.

Where no gravity load is present, the connections at each end will open the same amount. When gravity loads are present this will not be the case. However, for predicting the moment-rotation response for design purposes, the connection rotations can be assumed to be equal in magnitude. Therefore the prestress force can be calculated in terms of the connection rotation:

$$P_{PS} = P_{PSi} + \frac{A_{PS} E_{PS}}{L_{PS}} d_b |\theta_j| \quad (2-4)$$

where P_{PSi} is the initial prestress force, A_{PS} is the area of the prestressing tendon, E_{PS} is the modulus of elasticity of the prestressing material, L_{PS} is the length of the tendon, and θ_j is the connection rotation.

The moment contribution from the prestress and rotation of the connection when yield of the tendon occurs, $M_{PS\ yield}$ and $\theta_{PS\ yield}$ can be calculated as:

$$M_{PS\ yield} = f_{PS} A_{PS} \left(\frac{d_b}{2} \mp e_{PS} \right) \quad (2-5)$$

$$\theta_{PS \text{ yield}} = \left(1 - \frac{P_{PS i}}{f_{PS} A_{PS}}\right) \frac{f_{PS}}{E_{PS}} \frac{L_{PS}}{d_b} \quad (2-6)$$

where f_{PS} is the yield stress of the tendon. Once the prestress tendons have yielded, there is a reduced clamping force available to re-centre the connections. The connection rotation required for the tendons to become slack is:

$$\theta_{PS \text{ slack}} = \frac{f_{PS}}{E_{PS}} \frac{L_{PS}}{d_b} \quad (2-7)$$

which is independent of the initial prestress force in the tendons.

2.2.3 MODELLING OF ROCKING SYSTEMS

El-Sheikh et al (1999) proposed two analytical methods for modelling unbonded post-tensioned beam-column connections using the computer program *DRAIN-2DX* (Prakash et al., 1993). The first was a more complicated fibre model, where the individual components of the system were modelled using fibre elements, and the overall behaviour was derived from the contribution of the components. The second was a simpler spring model, where the beams and columns were modelled with elastic members and the non-linear behaviour was lumped at the beam-column interface using a zero-length inelastic spring. It was expected that the latter approach would be less accurate; however it was convenient as the behaviour of the joints could be expressed in terms of a single parameter.

Pampanin et al. (2001) proposed modelling the hybrid connection with two moment-rotation springs in parallel. The hysteresis of these springs were chosen to represent the non-linear moment-rotation response of the unbonded tendons and yielding reinforcing bars, being non-linear elastic and modified Takeda respectively. The resulting hysteresis loop was flag-shaped, while the beam elements remain elastic. This approach

was satisfactorily used to predict the response of the five-storey PRESS building (Priestley et al., 1999).

A multispring element for the non-linear time-history analysis programme *RUAUMOKO* (Carr, 2005) has been developed. This element has been used to accurately predict the experimental response of the beam-column subassemblies tested by Arnold (2004) and Davies (2003), both with (Spieth et al., 2004a) and without energy dissipation devices (Spieth et al., 2004b).

Results of non-linear time-history analyses carried out on four frames by El-Sheikh et al. (1999) showed that while the maximum deformations of unbonded post-tensioned seismic frames are larger under seismic loading when compared with monolithic frames, due to low energy dissipation, the residual drift is expected to be much smaller.

Christopoulos et al. (2003) carried out an investigation into the seismic response of single degree of freedom (SDOF) systems with flag-shaped hysteretic behaviour, and compared their response to SDOF systems with elasto-plastic and Takeda hysteretic behaviour. Their results showed flag-shaped systems have similar results in terms of displacement ductility, however possess the advantage that they do not incur any residual drift. The performance of such systems, therefore, can correctly be compared to traditional systems when residual deformations are considered. Furthermore, Christopoulos et al. (2003) observed that self-centring systems appear to be less vulnerable to $P-\Delta$ effects, even those with negative post-yield stiffness.

2.3 DESCRIPTION OF FRAMES FOR ANALYSIS

Three three bay, ten storey concrete frames are analysed using the probabilistic seismic vulnerability methodology proposed in Chapter One. These three frames are:

- A state-of-practice reinforced concrete frame building, whose design is presented in “*Example of Concrete Structural Design to New Zealand Standard NZS 3101:1995*”, popularly known as the “*Red Book*” (CCANZ, 1998). This frame is referred to as “Red Book” throughout the rest of this chapter.
- A ten storey, three bay DAD frame, designed to resist both gravity and seismic loads in the E-W direction from the prototype DAD building, as presented by Arnold (2004).
- A ten storey, three bay DAD frame from the prototype DAD building, designed to carry seismic loads in the N-S direction, as presented by Davies (2003).

Further description of these three buildings, and their respective analytical models, can be found below.

2.3.1 RED BOOK FRAME

The Red Book building is a square ten-storey reinforced concrete office building, with a plan area of approximately 900 m^2 . The Red Book building was chosen for analysis as it is representative of the current state-of-practice for the design of buildings in New Zealand. It was designed in accordance with principles of capacity design, as dictated by the New Zealand Loadings Standard (NZS 4203:1992) and the New Zealand Concrete Code (NZS 3101:1995), ensuring formation of a ductile mechanism capable of sustaining deformation in the post-yield range.

Moment-resisting perimeter frames act as the primary lateral load resisting system for the building, and the absence of corner columns means the frames are designed to act in one direction only. The general scheme of a frame is illustrated in Figure 2-2. Internal (or gravity) frames, within the building, are assumed to only carry gravity load, however they are detailed to sustain deformation imposed by the perimeter frames. The floor slabs are one-way precast hollow core units with an in-situ topping, and specified design concrete strength, $f'_c = 30 \text{ MPa}$.

CCANZ (1998) concentrates on the design of the level two beams, which are shown to be the worst case. For this analysis it is assumed that the beam reinforcing details throughout the structure are the same, and the column reinforcing is also the same throughout the structure. The frame is modelled using the non-linear time-history analysis program *RUAUMOKO-2D* (Carr, 2005), with Giberson beam elements for the beams, and concrete beam-column elements for the columns. As in the design of the structure (CCANZ, 1998), rigid beam-column joints were assumed. Plastic hinge regions, assumed to be half the section depth, are modelled using the modified Takeda hysteresis rule (Carr, 2005). The floor slabs are assumed to act as rigid diaphragms, so no allowance for beam-elongation effects is made, and P- Δ effects are included through the use of a ‘*gravity only*’ column. Initial stiffness Rayleigh damping, of 5% specified in modes 1 and 9 is used for the analysis, which is carried out at a time step of $1 / 1000^{\text{th}}$ of a second. The fundamental period of the frame, $T_1 = 2.14 \text{ s}$ (refer to Appendix C for details).

Five damage states have been defined for the Red Book frame as follows: No Damage (DS1); Minor Damage, allowing immediate occupancy of the structure following the earthquake (DS2); Repairable Damage (DS3); Irreparable Damage (DS4); and Partial or Total Collapse (DS5). The damage states are defined in terms of the maximum absolute

inter-storey drift which occurs over the height of the building, θ_{MAX} , and are presented in Table 2-1. These damage states are similar to the four damage states defined by HAZUS (FEMA, 2003). Damage ratios (DR) have been assigned to each of these damage states, as presented in Table 2-1. These damage ratios are conservative estimates of damage, selected from within the range of possible loss ratios defined by the HAZUS Manual (FEMA, 2003).

2.3.2 DAD ARNOLD GRAVITY FRAME

The frame designed by Arnold (2004) in the E-W direction of the DAD building is a three bay, ten storey frame, with inter-storey height, h_s , of 3.6 m, bay length, L , of 9.6 m, and supporting a tributary width of 10 m. The beam dimensions are 400 mm by 750 mm, and the column dimensions are 850 mm by 850 mm. The drop-in beams, 7.2 m in length, and armoured at each end, are post-tensioned off-site with two draped 32 mm prestressing threadbars ($f_{PS} = 1000 \text{ MPa}$ and $P_{PS i} = 835 \text{ kN}$). Design concrete strength f'_c is taken as 45 MPa and 60 MPa for the drop-in beams and columns respectively. Two ‘dog-bone’ tension-compression mild-steel energy dissipators, with cross-section dimensions of 20 mm by 35 mm, and yield strength, $f_d = 300 \text{ MPa}$ are mounted on both sides of the beam across the connection at the level of the tendons. It is assumed the method of construction is the same throughout the frame.

The beam prestressing has been designed so the gravity loads are balanced. Therefore, the seismic resistance of frames within a building will depend on the tributary width of the frame, and because of this the internal and external frames of the prototype building will have different strengths. For simplicity, it is assumed that the internal prototype building frame designed by Arnold (2004) is part of a ‘long’ building, and the frame resists its tributary seismic weight.

The number of storeys participating in the plastic mechanism, n_{sp} , was found using the rapid pushover method described in Appendix B. Arnold (2004) found six storeys participating in the plastic mechanism, and as such rocking column hinges, with bi-linear elastic hysteresis, were provided at the base of the structure, and the underside of the beams at level six to allow for this desired mechanism. The columns, between rocking hinges are post-tensioned with two 32 mm tendons stressed to an initial prestress force of 1126 kN ($0.7 f_{PS}$).

Arnold (2004) provides adequate details on the reinforcement of both the beams and columns. Due to load-balancing requirements, it is assumed that the upper levels of the structure have the same beam prestressing and reinforcing configuration.

The frame is modelled with *RUAUMOKO-2D* using elastic Giberson beam elements for the beams and columns, and four moment-rotation springs in parallel to describe the behaviour of the rocking joints. A description of the hysteresis loop (moment-rotation response) provided by these springs is in Section 2.3.4. Beam-elongation effects are neglected through the use of rigid diaphragms at each level. This approximation was made to simplify the analyses and for consistency with the Red Book frame. Constant 5% damping is assumed.

Difficulties were encountered when choosing a suitable time-step for the analysis, as rapid and significant changes of stiffness occur throughout the structure when the rocking joints open and close. The sudden, and substantial, increase in stiffness, which occurs when the joints close, introduces a ‘ringing effect’ causing the analysis results become numerically unstable if the time step is too large. The majority of analyses were carried out at a time step of $1 / 8\,000^{\text{th}}$ of a second, and for higher intensity earthquakes,

where the analyses became numerically unstable, this time step was further decreased, to as small as $1 / 20\,000^{\text{th}}$ of a second.

2.3.3 DAD DAVIES SEISMIC FRAME

The frame designed by Davies (2003) is a three bay, ten storey frame, with a bay width of 10 m , and provides seismic resistance for a tributary width of 9.6 m from the DAD building in the N-S direction. The beam dimensions are 350 mm by 600 mm , and the column dimensions are 700 mm by 700 mm . The design concrete strength, $f'_c = 40\text{ MPa}$. The drop-in beams, 8.9 m in length, and armoured at each end, are post-tensioned off-site with two 26.5 mm prestressing threadbars ($f_{ps} = 950\text{ MPa}$ and initial prestress force = 461 kN) into specially fabricated steel end plate assemblies, 200 mm long, at each end of the beam. ‘Dog-bone’ tension-compression mild-steel energy dissipators, with cross-section dimensions of 20 mm by 23 mm are mounted across the top and bottom of the connection. Similar to Arnold’s frame, the same construction is assumed throughout the frame and Davies frame is assumed to be from a ‘long’ building.

The frame was designed using the rapid pushover method, as described briefly in Section 2.2.1. Davies (2003) found six storeys participating in the mechanism, accordingly, rocking column hinges have been detailed in the analytical model at the base and the underside of the beams at level six. These rocking joints have a bi-linear elastic hysteretic behaviour.

Davies (2003) pays attention to the details of the rocking beam connection, however omits other details of the frame. Therefore, assumptions are made about the beam and column reinforcement, beams in the upper levels of the structure, and the rocking column connections, to generate an analytical model of the structure. The beam reinforcing was designed to ensure the beams remain in a cracked elastic state up to yield

of the prestress bars, and have additional reinforcing at each end to help distribute high contact stresses developed in the rocking process. For simplicity, it is assumed the beams in the upper levels of the structure, have the same properties as those of lower levels of the structure.

The columns are assumed to be reinforced with 12 D25 ($f_y = 300 \text{ MPa}$) longitudinal reinforcing bars throughout the height of the structure. Between the rocking joints, the columns are post-tensioned with four 26.5 mm bars, with initial prestress forces of 755 kN and 63 kN for the outer and inner columns respectively. The difference between these initial prestress levels is due to the difference in gravity (axial) loads on the columns, and an attempt to have the column hinge capacity the same for all columns.

A *RUAUMOKO-2D* model of this frame was created, using elastic Giberson beam elements for the beams and columns, and two moment-rotation springs in parallel to describe the behaviour of each of the rocking joints. The properties of these springs are described in Section 2.3.4. Again, rigid diaphragms preclude beam-elongation effects, and constant 5% damping is assumed. Difficulties were again encountered when choosing a suitable time step for the analysis. These difficulties are explained in Section 2.3.2. The majority of analyses were carried out at a time step of $1 / 8\,000^{\text{th}}$ of a second, and for higher intensity earthquakes, where the analyses became numerically unstable, this time step was further decreased, to as small as $1 / 40\,000^{\text{th}}$ of a second.

It was previously observed that, while the gravity frame was designed by Arnold (2004) including the effects of an undercapacity factor, Davies seismic frame was not. Therefore these two frames are not directly comparable.

The DAD frames respond to seismic loading through opening and closing of the post-tensioned beam-column joints. Because of armouring to the rocking interfaces, no

damage is expected to occur to the precast concrete elements. The dissipators, placed across the rocking interface are expected to yield in tension and compression as the joint opens and closes. After a number of large inelastic cycles, the dissipators should be replaced to ensure sufficient capacity for future earthquake events. Additionally, when very large displacements are induced, yielding of the post-tensioned tendons may occur. Following the earthquake these will need to be re-tensioned.

Damage states for the DAD frames are defined as follows: No Damage, as the rocking joints remained closed, or if the rocking joints open, insignificant yielding of energy dissipators occurs (DS1); Minor damage, where replacement of the energy dissipators is required due to extensive yielding resulting in reduction of fatigue life or fracture of energy dissipators (DS2); Repairable damage, where yield of the prestress tendons occurs, caused by significantly large joint rotations (DS3); and toppling, where sufficient prestress has been lost and P- Δ effects cause collapse of the structure (DS5). For a DAD frame, DS4, that is irreparable damage, is not expected to occur. The damage state regions are defined in terms of θ_{MAX} , as presented in Table 2-2. Differences in the geometry and dynamic behaviour of the two DAD frames cause the thresholds defining each of the damage states to be slightly different.

Although the building will not suffer any serious damage, there is a cost associated with replacing the dissipators and re-tensioning the prestress tendons. These costs are expressed in terms of damage ratios and presented in Table 2-2.

2.3.4 MODELLING OF DAD BEAM-COLUMN CONNECTIONS

The theoretical moment-rotation behaviour of the beam-column joints has been developed by Arnold (2004) and Davies (2003), and has been described in Section 2.2.2. The moment-rotation behaviour of the E-W frame rocking beam joints is illustrated in Figure 2-

3. The response of the N-S frame rocking joints is similar. To model this behaviour, a number of moment-rotation springs were used in parallel. A combination of flag-shape and bi-linear elastic hysteresis models were used. The springs were infinite axial and shear stiffnesses, and their moment-rotation properties were determined so that the desired theoretical behaviour would be obtained.

Energy dissipation, is provided by tension-compression ‘*dog-bone*’ dissipators. During lateral loading, the dissipators will yield in tension and compression. After the first cycle of loading the dissipators will commence subsequent joint opening cycles in compression, reducing the opening moment of the joint (Figure 2-3(a)). For analytical modelling, it was assumed the dissipators had previously yielded, and a probable strength factor of 1.12 was applied to the dissipators. Strain hardening of the dissipators was not considered. Furthermore, a simplified approach was taken to model the opening of the joints and yield of the dissipators as illustrated in Figure 2-3(b).

Additional energy dissipation is provided from yield of the tendons. It is assumed the tendons have reasonable elasto-plastic behaviour, and the resulting moment-rotation response is illustrated in Figure 2-3(c). Once yield of the tendons occurs, there is a reduction in the prestress force for subsequent cycles. For simplicity, this effect has been excluded from the model. This exclusion is justified because the response is still accurate at levels of drift up to yield of the prestress, and it is found EAL is less sensitive to higher levels of damage. The effect of carrying out IDA on a model which does not include strength deterioration has been discussed by Krawinkler et al. (2003).

2.4 PROBABILISTIC SEISMIC VULNERABILITY METHODOLOGY APPLICATION

The intensity measure (IM) selected for these analyses is the 5% damped spectral acceleration at a period of one second, $S_A(T = 1s)$, denoted from here as S_A . Although not considered a typical IM (Fülöp and Dubina, 2004), it is felt that S_A is a better descriptor of the seismic input than peak ground acceleration (PGA) for multi-storey buildings, as the periods of these structures are reasonably long. Because the results of such analyses are to be compared, the spectral acceleration at the fundamental period of the structure, $S_A(T_1)$, is deemed not a suitable IM. Furthermore, S_A is used as the principal design parameter for design in the United States, thus S_A is considered a reasonable IM for comparative design purposes.

IDA is carried out using the non-linear time-history analysis program *RUAUMOKO-2D*. A suite of 20 earthquake ground motion records was selected, as presented in Chapter One. Each of the earthquakes was scaled such that $S_A = 0.1 g$, and then increased in 0.1 g increments until results indicating the onset of DS5 (representative of total damage), were obtained. For each analysis the absolute maximum inter-storey drift at each level of the structure was recorded, and the engineering demand parameter (EDP) chosen for further analysis is the maximum absolute inter-storey drift occurring over the height of the structure, θ_{MAX} . The analysis then proceeds as described in Chapter One.

2.4.1 RED BOOK RESULTS

The IDA curves for this building are presented in Figure 2-4(a). This figure shows structural collapse occurs between $S_A = 0.2 g$ and $0.3 g$ for one earthquake record. This response is unexpected, as it is assumed the building should withstand this ground motion intensity. However, upon further examination, it was discovered that the earthquake ground motion responsible for this result is record 9. This ground motion is highlighted in the spectral displacement plot, Figure 1-2(c), where it can be seen that the spectral displacement for this structure is significantly greater than other earthquakes at periods greater than one second, causing larger displacement demands to be imposed on the structure when it softens due to plastic hinging. These large displacements are exacerbated by P- Δ effects combine to cause total damage to this structure under this earthquake at low S_A .

The IDA curves in Figure 2-4(a) are summarised by 10th, 50th and 90th percentile curves. These percentile levels are calculated as the average of the 2nd and 3rd, 10th and 11th and 18th and 19th ranked data points, respectively, for each S_A level. Of interest for probabilistic analysis is the dispersion of θ_{MAX} for each S_A , which is plotted in Figure 2-4(b). Since Martínez (2002) showed θ_{MAX} is lognormally distributed at each S_A , the dispersion is found by fitting a lognormal distribution to θ_{MAX} for each S_A . It is expected that the dispersion associated with θ_{MAX} be greater than the dispersion of the earthquake input. Ramberg-Osgood (R-O) curves are fitted to each of the IDA curves, and the parameters are presented in Table 2-3, and the curves are plotted and summarised in Figure 2-4(c). Selected time-history analysis output for ‘critical’ earthquakes is presented in Appendix C.

A summary of the probabilistic seismic vulnerability assessment methodology steps to calculate EAL are presented in Figure 2-5. EAL is found to be 0.0029, which can alternatively be expressed as \$2900 per million dollars of building value.

Implicit in NZS 4203:1992 is the notion that irreparable damage should be prevented for DBE (return period 475 years) and collapse of the structure should be prevented for MCE (return period 2450 years). The resilience curves, illustrated in Figure 2-5(d), provide a convenient format for evaluating the probability of exceeding a particular DS for a desired annual frequency earthquake. From Figure 2-5(d), it can be found that there is a 90% survival probability that irreparable damage will not occur to this structure during an earthquake with a return period of 486 years. Similarly there is a 90% survival probability of no collapse of the building for an earthquake with return period 3050 years. These results indicate this frame meets the desirable performance limits defined above.

2.4.2 DAD GRAVITY FRAME RESULTS

A summary of the IDA results for the E-W gravity frame designed by Arnold (2004) are presented in Figure 2-6. The R-O parameters obtained for the IDA curves for this frame are presented in Table 2-3. Selected time-history analysis results for ‘*critical*’ earthquakes are included in Appendix C.

The idealised moment-rotation response of the beam-column connections is presented in Section 2.2.2, where it is observed that once the tendons have yielded, there is a reduced clamping force available to ensure re-centring of the connections. Conservatively, the joint rotation required to cause the tendons to become slack, $\theta_{PS\ slack}$, has been used as a limiting maximum in the IDA analysis. This value has been assumed as strength degradation to account for yielding of the post-tensioned tendons has not been

considered, and it was felt that after this point, results from the non-linear time-history analysis become dubious.

A summary of the probabilistic seismic vulnerability assessment methodology steps to calculate EAL are presented in Figure 2-7. EAL is found to be 0.000063, which can alternatively be expressed as \$63 per million dollars of building value. From the resilience curves it can be found that there is a 90% survival probability that dissipator replacement (DS2) will not be required following an earthquake with a return period of 150 years. Similarly there is a 90% survival probability that the tendons will not require restressing (DS3) following an earthquake with return period of 1200 years, and there is a 90% survival probability of no collapse (DS5) of the building for an earthquake with return period 12 000 years.

2.4.3 DAD SEISMIC FRAME RESULTS

A summary of the IDA results for the N-S DAD seismic frame designed by Davies (2003) are presented in Figure 2-8. R-O parameters for this analysis are presented in Table 2-3. Selected time-history analysis results are presented in Appendix C.

A summary of the probabilistic seismic vulnerability assessment methodology steps to calculate EAL are presented in Figure 2-7. EAL is found to be 0.00011, which can alternatively be expressed as \$110 per million dollars of building value. From the resilience curves it can be found that there is a 90% survival probability that dissipator replacement (DS2) will not be required following an earthquake with a return period of 84 years. Similarly there is a 90% survival probability that the tendons will not require restressing (DS3) following an earthquake with return period of 1900 years, and there is a 90% survival probability of no collapse (DS5) of the building for an earthquake with return period 6600 years.

It is observed that EAL for the DAD N-S seismic frame is higher than that for the DAD E-W gravity frame. This is because the DAD E-W gravity frame is stronger than the DAD N-S seismic frame, due to the presence of the undercapacity factor used in its design. The effect of exclusion of the undercapacity factor in the design phase can also be observed when comparing the survival probabilities of each of the damage states from the resilience curves. It is observed that the DAD E-W gravity frame has larger return period earthquakes corresponding to 90% survival probability of DS2 and DS5, compared with the DAD N-S seismic frame. The difference in the 90th percentile survival probability for DS3 is due to a significant difference in the onset of yield of the tendons. However, it is also observed that the DAD N-S seismic frame, designed without the undercapacity factor, satisfies the desirable performance objective of collapse prevention for the MCE event. These results indicate the undercapacity factor of $\phi = 0.7$ may be unduly conservative, as the larger, stronger and hence more expensive DAD E-W gravity frame does not have a significantly lower EAL. Furthermore, the DAD N-S seismic frame, designed without an undercapacity factor, still meets desirable performance standards. For economic comparison of results between the benchmark ductile monolithic and DAD structures, the EAL for the DAD N-S seismic frame, being the worst case of the two DAD frames, is taken as being representative of the DAD system.

2.5 ECONOMIC COMPARISON

Principles of engineering economics are used to find the present cost of each type of frame, assuming the initial and replacement costs of the frame are \$1 000 000, including construction cost and EAL over a typical 50 year expected life time. Assuming a modest interest rate of 3%, the present worth value of the benchmark ductile monolithic frame is \$1 074 600, and the present worth value of the DAD frame is \$1 002 900. Comparison of

these values shows the superior performance of DAD frames, with respect to conventional reinforced concrete structures.

To calculate how much more can initially be spent on a DAD building, the present cost of both the Red Book and DAD frames are equated as follows:

$$PW = V_{RB} [1 + EAL_{RB}(P/A, i, N)] = V_{DAD} [1 + EAL_{DAD}(P/A, i, N)] \quad (2-8)$$

where V_{RB} is construction/replacement cost of a the conventional building, V_{DAD} is the construction/replacement cost of a DAD building, and $(P/A, i, N)$ is the uniform series present worth factor, from which:

$$\frac{V_{DAD}}{V_{RB}} = \frac{1 + EAL_{RB}(P/A, i, N)}{1 + EAL_{DAD}(P/A, i, N)} \quad (2-9)$$

For $i = 3\%$ and $N = 50$ years, $\frac{V_{DAD}}{V_{RB}} = 1.07$.

This result can be viewed in two ways. First it shows that it could be worthwhile initially investing some 7% more in a DAD structure, as over the 50-year life-span of the structure the total costs would work out to be about the same. Alternatively, it could be viewed that there is approximately a 7% overall saving in performance costs that should also be added to any other savings associated with construction.

2.6 SENSITIVITY ANALYSIS

In the above calculations the inputs to the expected annualised repair cost are not known with certainty. In this section, the sensitivity of EAL to the various input parameters is calculated. Two approaches, described in Chapter One, are used to investigate the sensitivity of the solution, these being the calculation of a '*sensitivity parameter*' and calculation of the '*swing*' of each of the parameters.

The purpose of carrying out this sensitivity analysis is to gain an understanding of the uncertainty or variability of EAL, and which variables significantly affect it. As pointed out by Elms (1985), among others, there is no point in having a highly detailed model with a number of uncertain inputs, when the output of the model is highly dependent on the value of one or more the input values used.

2.6.1 SENSITIVITY PARAMETER

The sensitivity factor of a model to a parameter can be expressed as:

$$\gamma_i = \frac{x_i}{y} \frac{\partial y}{\partial x_i} \quad (2-10)$$

where γ_i is the percentage change in the model output, y , due to a one percent change in input parameter x_i (Elms, 1985). Equation (2-10) is used to calculate the so called sensitivity parameter for each of the input variables for each of the three building models described above. These factors are presented in Table 2-4.

The results in Table 2-4 show similar trends in γ_i for each of the three buildings. EAL is consistently most sensitive to the value of $S_A(T = 475)$ which defines the seismic hazard. EAL is also particularly sensitive to the capacity of the structure, represented by \tilde{K} , and its dispersion β_K , and the slope of the seismic hazard curve q . Together q and β_K define the slope of the resilience curves, and it is observed that the slope of these curves significantly affects the results. Additionally, the definition of the seismic hazard effects the results, represented by $S_A(T = 475)$ and q . This indicates the importance of adequately defining the seismic hazard for a particular site. Further discussion of these parameters is made in Chapter One.

An interesting phenomenon observed in Table 2-4 is that the influence of the lower damage states (specifically DS3) on the estimate of EAL is more significant for the Red Book frame, while the influence of DS5 is minimal. However, the DAD frames are more sensitive to DS5, rather than the lower damage states. This is because there is higher damage ratios associated with the lower damage states for the Red Book frame, and the majority of the EAL is due to DS3 and DS4. However, the major component of loss for the DAD frames is DS5.

2.6.2 SWING ANALYSIS

The swing analysis procedure, developed from the method presented by Porter et al. (2002) is described in Chapter One. Extreme values of each of the parameters are tabulated in Table 2-5.

Tornado diagrams are presented in Figure 2-10 for all three frames, where the vertical lines represent the median response. The tornado diagram indicates the possible variability in EAL due to extreme values of the individual parameters affecting the outcome. These graphs indicate that the DAD frames are sensitive to similar inputs, and these are similar to those of the Red Book. The three parameters contributing most to the uncertainty are $S_A(T = 475)$, β_K , and \tilde{K} . These are discussed in Chapter One.

It can be seen, in all three swing graphs, that the seismic hazard definition, $S_A(T = 475)$ is a factor that significantly contributes to variation in EAL. Seismic hazard is determined from the New Zealand loadings code, NZS 4203:1992, based design spectra given for three different soil types. The significant changes in EAL based on $S_A(T = 475)$ are not significant when using this methodology for comparing two different structures for the same site, however if EAL is to be used as a basis for earthquake insurance, then care

needs to be taken to accurately determine the seismic hazard for the particular site considered.

2.7 CONCLUSIONS

The probabilistic seismic vulnerability assessment methodology presented in Chapter One was successfully applied to a conventional state-of-practice reinforced concrete frame and two frames designed and detailed in accordance with a damage avoidance design (DAD) philosophy for comparative purposes. The following conclusions can be drawn from the results:

- Superior performance of the DAD frames, when compared to the state-of-practice ductile monolithic frame, was illustrated by a significantly lower expected annualised loss (EAL). For the ductile monolithic frame, the EAL was estimated as \$2900 per million dollars building value, whereas EAL for the DAD frames was estimated as approximately \$100 per million dollars building value.
- Economic comparison of the results shows construction of a DAD structure results in approximately a 7% saving over a 50 year period, assuming an interest rate of 3%.
- Formal sensitivity analysis shows EAL is particularly sensitive to the seismic hazard, the median seismic resistance of the structure and the variability associated with the suite of earthquake ground motions used for analysis.

2.8 REFERENCES

- Arnold, D.M. (2004) Development and Experimental Testing of a Seismic Damage Avoidance Designed Beam to Column Connection Utilising Draped Unbonded Post-Tensioning. ME Thesis, Department of Civil Engineering, University of Canterbury, Christchurch, New Zealand.
- Carr, A.J. (2005) *Ruaumoko Computer Programme Manual*. Department of Civil Engineering, University of Canterbury, Christchurch, New Zealand.
- Cement and Concrete Association of New Zealand (CCANZ) (1998) *Examples of Concrete Structural Design to NZS 3101:1995 – “Red Book”*. Cement and Concrete Association of New Zealand, Wellington.
- Christopoulos, C., Filiatrault, A., Uang, C.-M. and Folz, B. (2002) Post-tensioned Energy Dissipating Connections for Moment-Resisting Steel Frames. *Journal of Structural Engineering*, **128**(9), 1111-1120.
- Christopoulos, C., Pampanin, S. and Priestley, M.J.N. (2003) Performance-Based Seismic Response of Frame Structures Including Residual Deformations. Part I: Single-Degree of Freedom Systems. *Journal of Earthquake Engineering*, **7**(1), 97-118.
- Davies, M.N. (2003) Seismic Damage Avoidance Design on Beam-Column Joints Using Unbonded Post-Tensioning: Theory, Experiments and Design Example. ME Thesis, Department of Civil Engineering, University of Canterbury, Christchurch, New Zealand.
- Elms, D.G. (1985) ‘The Principle of Consistent Crudeness’. In: *Proceedings of NSF Workshop on Civil Engineering Applications of Fuzzy Sets*. Eds: C.B. Brown, J.-L. Chameau, R.N. Palmer and J.T.P. Yao. Purdue University, West Lafayette, IN. pp 35-44.
- El-Sheikh, M.T., Sause, R., Pessiki, S. and Lu, L.-W. (1999) Seismic Behaviour and Design of unbonded Post-Tensioned Precast Concrete Frames. *PCI Journal*, **44**(3), 54-71.

- Englekirk, R.E. (2002) Design-Construction of The Paramount – A 39-Story Precast Prestressed Concrete Apartment Building. *PCI Journal*, **47**(4), 56-71.
- Federal Emergency Management Agency (FEMA) (2003) HAZUS-MH MR1 Advanced Engineering Building Module: Technical and User's Manual. FEMA.
- Fülöp, L.A., and Dubina, D. (2004) Performance of wall-stud cold-formed shear panels under monotonic and cyclic loading. Part II: Numerical modelling and performance analysis. *Thin-Walled Structures*, **42**(2), 339-349.
- Garlock, M.M., Ricles, J.M. and Sause, R. (2005) Experimental Studies of Full-Scale Posttensioned Steel Connections. *Journal of Structural Engineering*, **131**(3), 438-448.
- Krawinkler, H., Medina, R. and Alavi, B. (2003) Seismic drift and ductility demands and their dependence on ground motions. *Engineering Structures*, **25**(5), 637-653.
- Mander, J.B. and Cheng, C.-T. (1997) *Seismic Resistance of Bridge Piers Based on Damage Avoidance Design*. Technical Report NCEER-97-0014, Department of Civil, Structural and Environmental Engineering, State University of New York at Buffalo, Buffalo, NY, USA.
- Martínez, M.E. (2002) Performance-Based Seismic Design and Probabilistic Assessment of Reinforced Concrete Moment Resisting Frame Structures. ME Thesis, Department of Civil Engineering, University of Canterbury, Christchurch, New Zealand.
- Murahidy, A.G. (2004) Design, Construction, Dynamic Testing and Computer Modelling of a Precast Prestressed Reinforced Concrete Frame Building with Rocking Beam-Column Connections and ADAS Elements. ME Thesis, Department of Civil Engineering, University of Canterbury, Christchurch, New Zealand.
- Pampanin, S., Priestley, M.J.N. and Sritharan, S. (2001) Analytical Modelling of the Seismic Behaviour of Precast Concrete Frames Designed with Ductile Connections. *Journal of Earthquake Engineering*, **5**(3), 329-367.

- Porter, K.A., Beck, J.L. and Shaikhutdinov, R.V. (2002) Sensitivity of Building Loss Estimates to Major Uncertain Variables. *Earthquake Spectra*, **18**(4), 719-743.
- Prakash, V., Powell, G. and Campbell, S. (1993) *DRAIN-2DX Base Program Description and User Guide; Version 1.10*. Report No. UCB/SEMM-93/17 & 18, Structural Engineering Mechanics and Materials, Department of Civil Engineering, University of California, Berkeley, CA.
- Priestley, M.J.N. and MacRae, G.A. (1996) Seismic Tests of Precast Beam-to-Column Connections With Unbonded Tendons. *PCI Journal*, **41**(1), 64-81.
- Priestley, M.J.N. and Tao, J.R. (1993) Seismic Response of Precast Prestressed Concrete Frames With Partially Unbonded Tendons. *PCI Journal*, **38**(1), 58-69.
- Priestley, M.J.N., Sritharan, S., Conley, J.R. and Pampanin, S. (1999) Preliminary Results and Conclusions from the PRESSS Five-Story Precast Concrete Test Building. *PCI Journal*, **44**(6), 42-67.
- Ricles, J.M., Sause, R., Garlock, M.M. and Zhao, C. (2001) Posttensioned Seismic-Resistant Connections for Steel Frames. *Journal of Structural Engineering*, **127**(2), 113-121.
- Rojas, P., Garlock, M.M., Ricles, J.M. and Sause, R. (2002) Reducing Seismic Damage in Steel Frames Using Post-Tensioning. Proceedings Seventh U.S. National Conference on Earthquake Engineering (Boston, MA), July 21-25. pp 4115-4124.
- Spieth, H.A., Arnold, D., Davies, M., Mander, J.B. and Carr, A.J. (2004a) Seismic Performance of Post-Tensioned Precast Concrete Beam to Column Connections with Supplementary Energy Dissipation. Proceedings New Zealand Society for Earthquake Engineering Conference (Rotorua), 19-21 March. Paper 15.
- Spieth, H.A., Carr, A.J., Murahidy, A.G., Arnold, D., Davies, M. and Mander, J.B. (2004b) Modelling of Post-Tensioned Precast Reinforced Concrete Frame Structures with Rocking Beam-Column Connections. Proceedings New Zealand Society for Earthquake Engineering Conference (Rotorua), 19-21 March. Paper 32.

Standards New Zealand (1992) *Code of Practice for General Structural Design and Design Loadings for Buildings, known as the Loadings Code, NZS 4203:1992*, Volumes 1 and 2. Standards New Zealand, Wellington, New Zealand.

Standards New Zealand (1995) *Concrete Structures Standard, known as the Concrete Code standard, NZS 3101:1995*, Volumes 1 and 2. Standards New Zealand, Wellington, New Zealand.

Stanton, J., Stone, W.C. and Cheok, G.S. (1997) A Hybrid Reinforced Precast Frame for Seismic Regions. *PCI Journal*, **42**(2), 20-32.

Table 2-1: Definition of damage states for conventional structure

Damage State		Drift Range	Maximum Drifts	Brief Description	Damage Ratio
DS1	No Damage	$< \theta_y$	$< 0.6\%$	Pre-yield of structure	0
DS2	Minor Damage	$1.25 \theta_y - 2.5 \theta_y$	0.5 – 1.2%	Cracking of concrete. Building is essentially undamaged, does not require repairs	2.5%
DS3	Reparable Damage	$2.5 \theta_y - 5 \theta_y$	1.2 – 2.5%	Spalling of concrete. Requires patching, etc.	20%
DS4	Irreparable Damage	$5 \theta_y - \theta_C$	2.5 – 4.6%	Reinforcing buckling, hoop fracture. Large residual displacements.	75%
DS5	Partial or Total Collapse	$> \theta_C$	$> 4.6\%$	Partial or Total Collapse	100%

Table 2-2: Definition of damage states for DAD frames

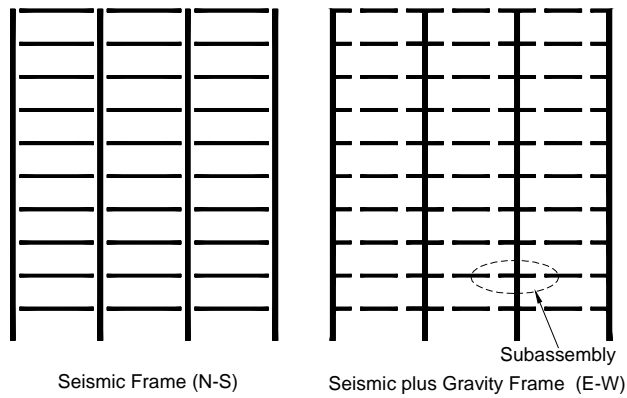
Damage State		Drift Range	Gravity Arnold	Seismic Davies	Repair Required	Damage Ratio
DS1	No Damage	$< \theta_d$	$< 0.4\%$	$< 0.4\%$	nil	0
DS2	Minor Damage	$\theta_d - \theta_{PS\ yield}$	1.6 – 3.3%	1.6 – 4.5%	Replace energy dissipators	2%
DS3	Reparable Damage	$\theta_{PS\ yield} - \theta_C$	3.3 – 7.1%	6.5 – 6.9%	Retensioning of tendons and replace energy dissipators	4%
DS4	Irreparable Damage					
DS5	Toppling	$> \theta_C$	$> 7.1\%$	$> 6.9\%$	Replacement of structure	100%

Table 2-3: Summary of Ramberg-Osgood statistical analysis for θ_{MAX}

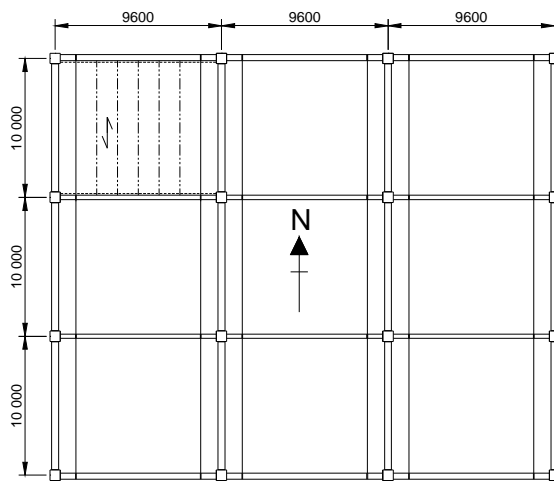
Eq. No	"Red Book"				DAD E-W (Arnold)				DAD N-S (Davies)			
	S_C	θ_C (%)	r	K	S_C	θ_C (%)	r	K	S_C	θ_C (%)	r	K
1	1.35	5.1	23	26.5	1.75	7.4	81	23.8	2.00	7.7	264	25.9
2	1.92	4.8	139	39.7	2.17	5.2	7	41.9	2.40	8.1	291	29.6
3	2.00	5.8	33	34.7	2.55	6.7	42	37.8	2.40	7.1	418	33.6
4	1.51	3.7	20	40.3	2.60	6.7	154	38.8	1.15	5.1	33	22.3
5	1.20	4.8	10	24.9	1.73	7.5	39	23.1	1.00	5.1	6	19.5
6	1.61	4.2	22	38.0	3.00	7.4	163	40.4	2.60	7.2	85	36.0
7	0.96	5.5	31	17.4	1.09	7.1	164	15.2	1.10	7.2	161	15.3
8	1.44	4.5	33	32.0	2.60	8.2	170	31.8	1.70	6.9	235	24.8
9	0.21	1.5	5	14.1	0.41	4.7	60	8.6	0.46	6.9	86	6.7
10	2.00	5.1	22	39.0	3.00	7.2	173	41.8	2.40	6.4	249	37.3
11	0.93	5.5	37	17.0	1.09	8.1	153	13.5	1.40	7.9	152	17.7
12	0.60	5.3	63	11.2	0.88	7.3	148	12.2	0.53	5.0	22	10.4
13	2.27	4.3	33	52.3	3.20	7.2	202	44.6	3.00	6.5	103	46.4
14	0.56	3.4	27	16.6	0.89	5.0	12	17.7	0.85	6.7	48	12.8
15	0.60	4.9	77	12.3	1.10	7.9	203	13.9	0.89	7.6	135	11.7
16	6.60	6.1	115	108.7	6.00	8.0	500	75.3	6.00	7.3	57	82.3
17	1.90	6.2	17	30.6	2.60	8.1	222	32.2	1.16	5.8	60	20.2
18	0.79	4.5	10	17.5	1.10	6.9	209	16.0	0.98	7.3	33	13.4
19	1.00	5.4	13	18.5	2.00	8.4	162	23.8	1.90	7.8	204	24.3
20	4.09	4.7	28	86.5	5.40	8.0	440	64.4	4.59	7.8	75	58.7
10%	3.38	6.8	10	61.3	4.31	8.7	29	56.0	3.65	8.2	24	50.3
50%	1.28	4.6	27	27.9	1.86	7.1	113	26.3	1.56	6.8	91	22.9
90%	0.49	3.1	78	12.9	0.80	5.7	450	12.4	0.60	5.6	347	10.4
β	0.75	0.31	0.82	0.61	0.66	0.17	1.08	0.59	0.67	0.15	1.04	0.61

Table 2-4: Parameter sensitivity: Percentage change in EAL to a +1.0% change in each parameter

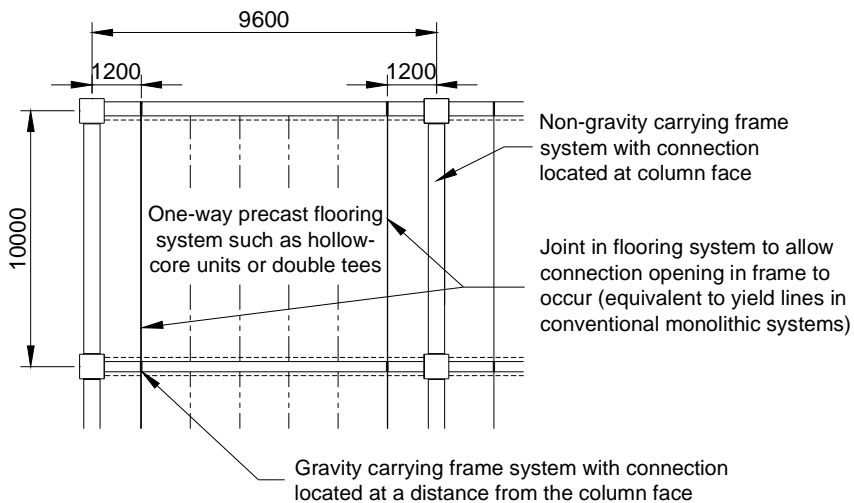
Parameter	Red Book	DAD E-W	DAD N-S
$S_A(T = 475)$	3.03	3.03	3.03
q	-2.56	1.36	1.95
K	-2.94	-2.94	-2.94
β_K	2.23	2.41	3.88
θ_C	-0.05	-1.96	-1.93
β_{θ_C}	0.40	0.16	0.10
θ_{DS2}	-1.17	-0.87	0.35
θ_{DS3}	-1.05	-0.13	-0.06
θ_{DS4}	-0.86		
DR2	0.18	0.18	0.22
DR3	0.46	0.10	0.04
DR4	0.28		
DR5	0.07	0.72	0.74
$p_{a(\max)}$	0.27	0.16	0.17



(a) Elevation of Prototype Structure



(b) Plan View of Prototype Structure



(c) Detail of One-Way flooring System

Figure 2-1: Details of the prototype DAD building for experimental investigations carried out at the University of Canterbury (adapted from Davies, 2003 and Arnold, 2004)

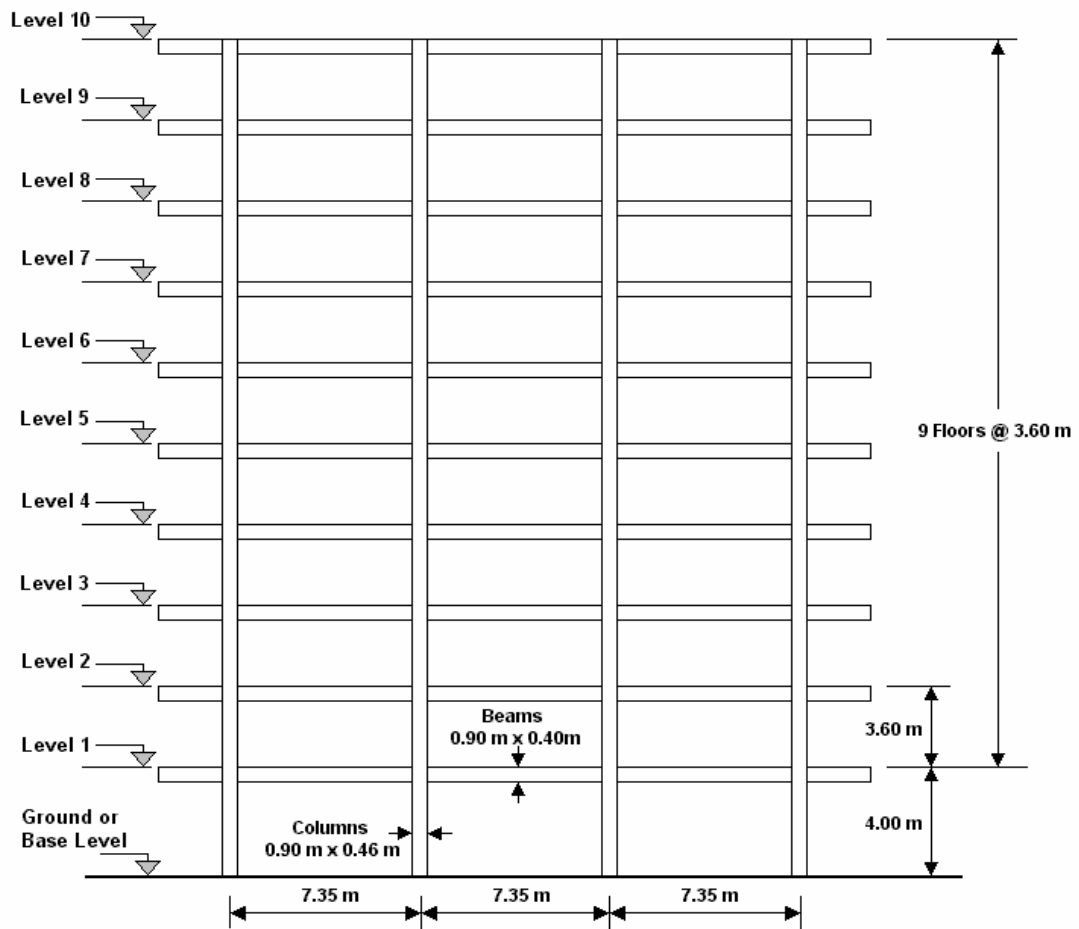
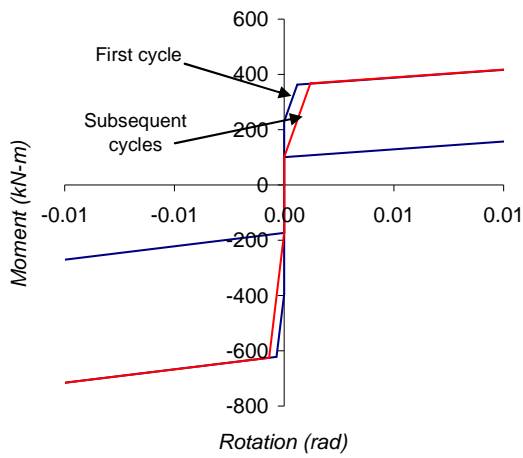
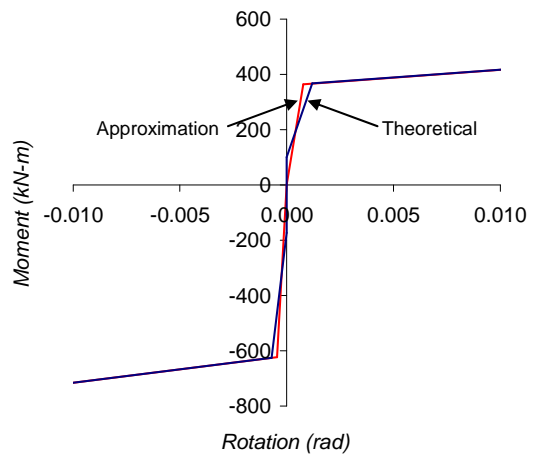


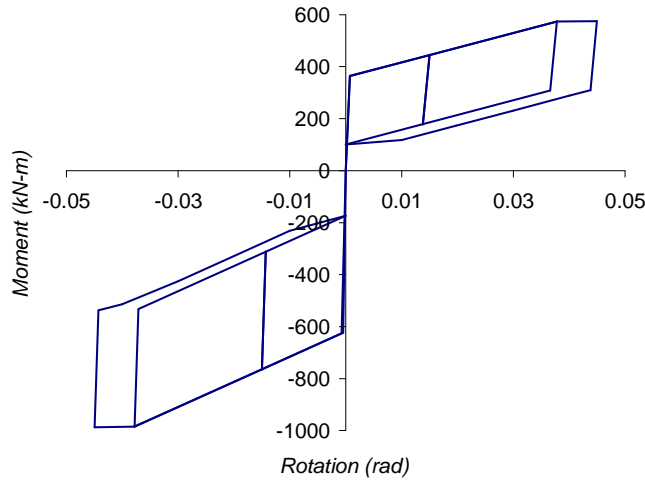
Figure 2-2: General scheme of the Red Book building (adapted from Martínez, 2002)



(a) Theoretical Moment-Rotation showing effect of yield of dissipator.

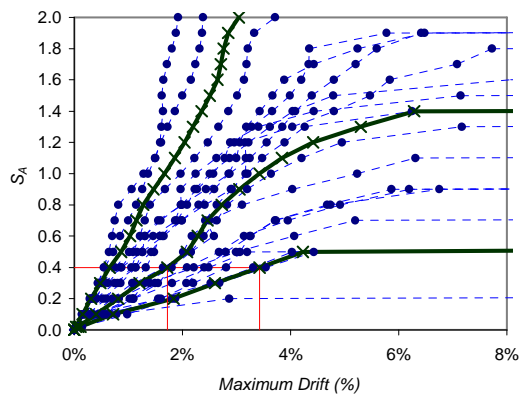


(b) Yield of dissipator approximation for analytical modelling.

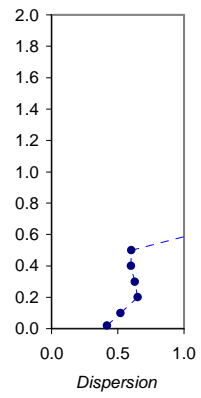


(c) Moment-Rotation curves showing the shape of the hysteresis once the tendons have yielded

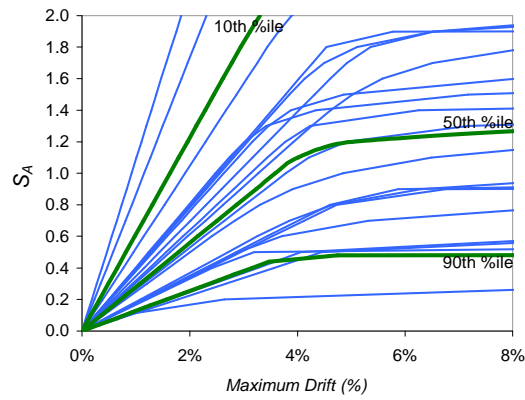
Figure 2-3: Moment-rotation curves for the DAD beam-column joints. Illustrated are those from the E-W gravity frame. N-S seismic are similar but symmetric.



(a) IDA curves for all earthquakes



(b) Dispersion β



(c) R-O curves fitted to data and summarised by 10th, 50th and 90th percentile curves

Figure 2-4: Incremental dynamic analysis output for Red Book frame

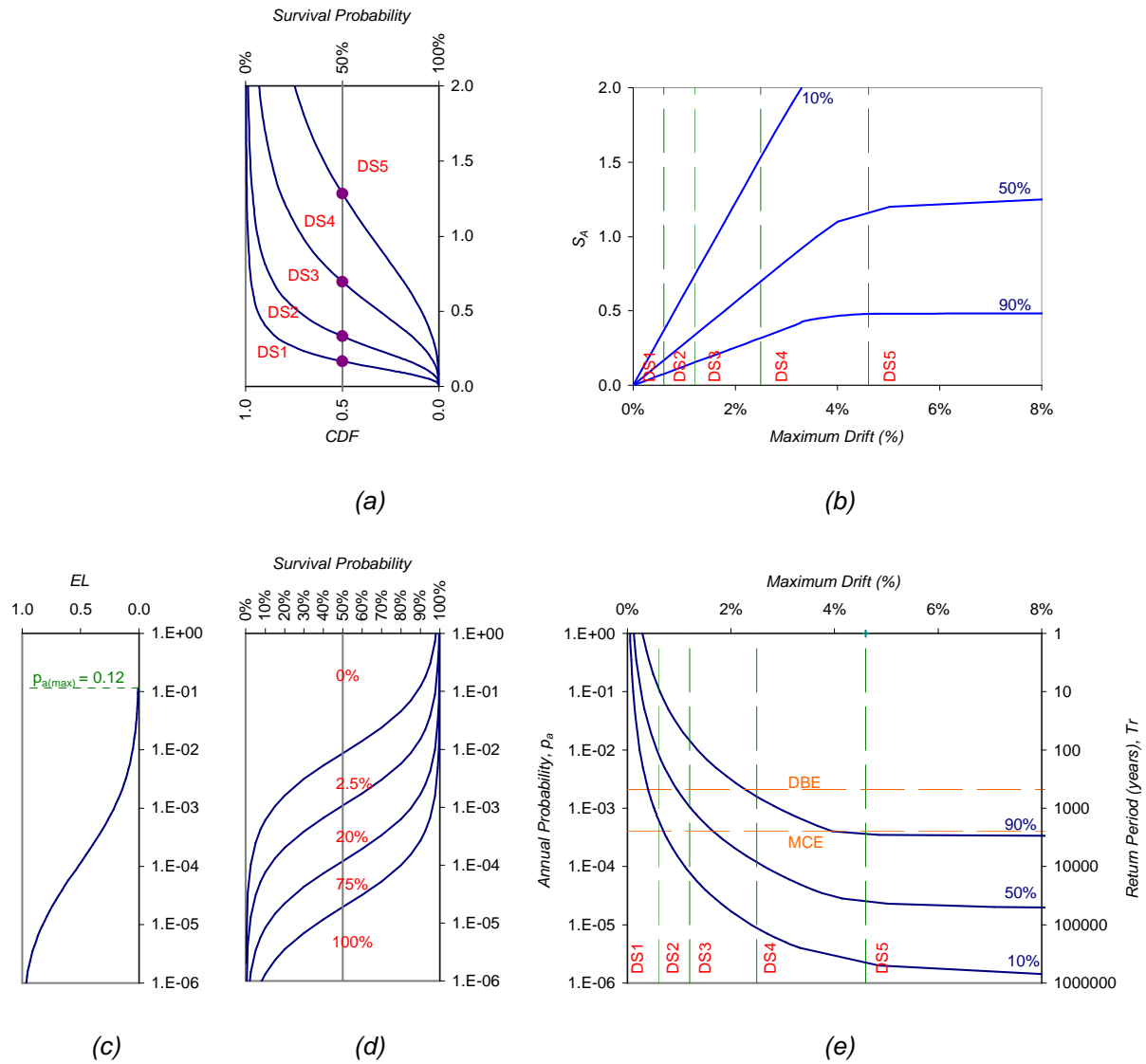
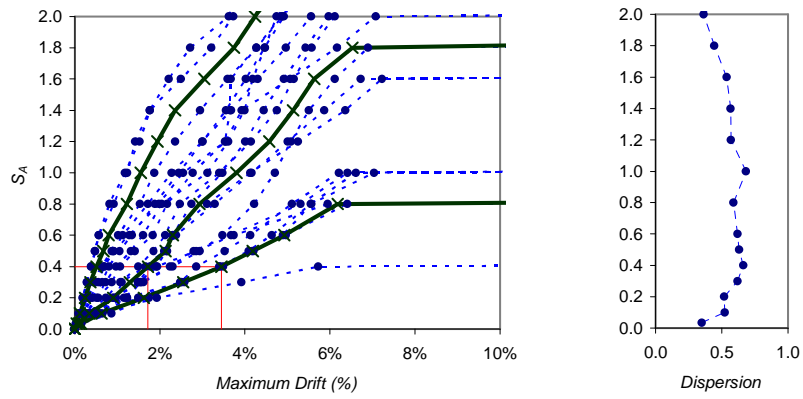
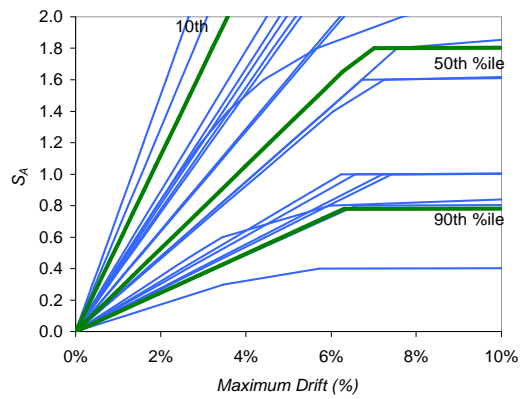


Figure 2-5: Summary of probabilistic seismic vulnerability assessment methodology applied to the Red Book frame



(a) IDA curves for all earthquakes

(b) Dispersion β



(c) R-O curves fitted to data and summarised by 10th, 50th and 90th percentile curves

Figure 2-6: Incremental dynamic analysis output for E-W DAD gravity frame

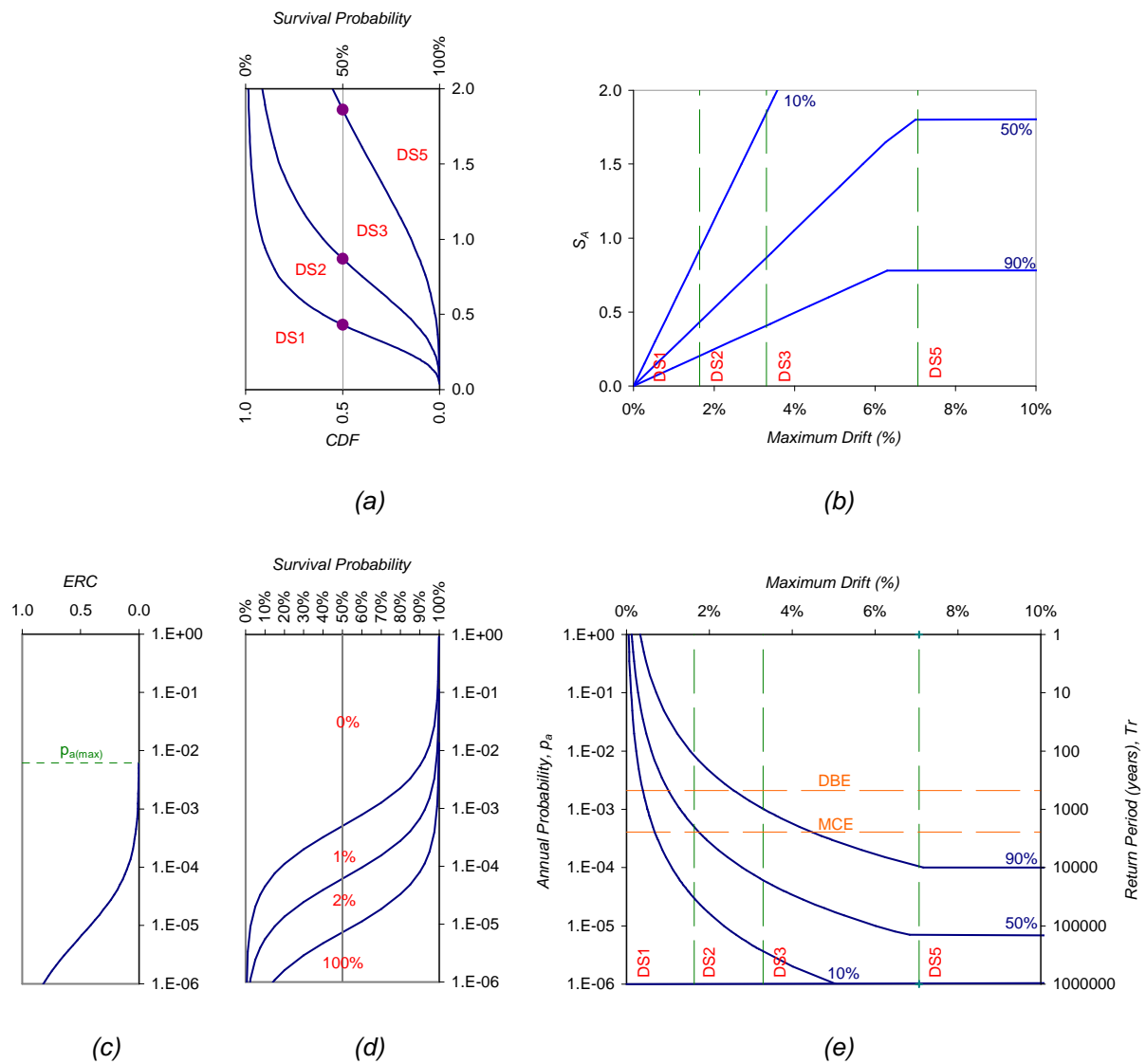
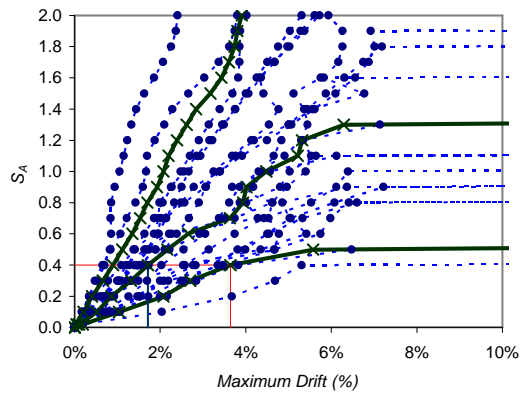
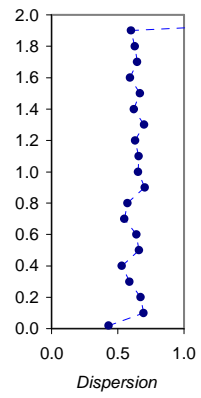


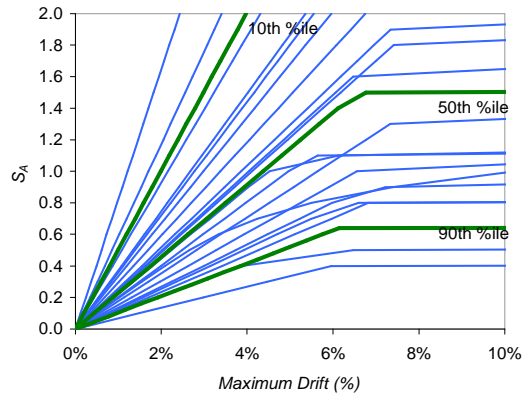
Figure 2-7: Summary of probabilistic seismic vulnerability assessment methodology applied to E-W DAD gravity frame



(a) IDA curves for all earthquakes



(b) Dispersion β



(c) R-O curves fitted to data and summarised by 10th, 50th and 90th percentile curves

Figure 2-8: Incremental dynamic analysis output for N-S DAD seismic frame

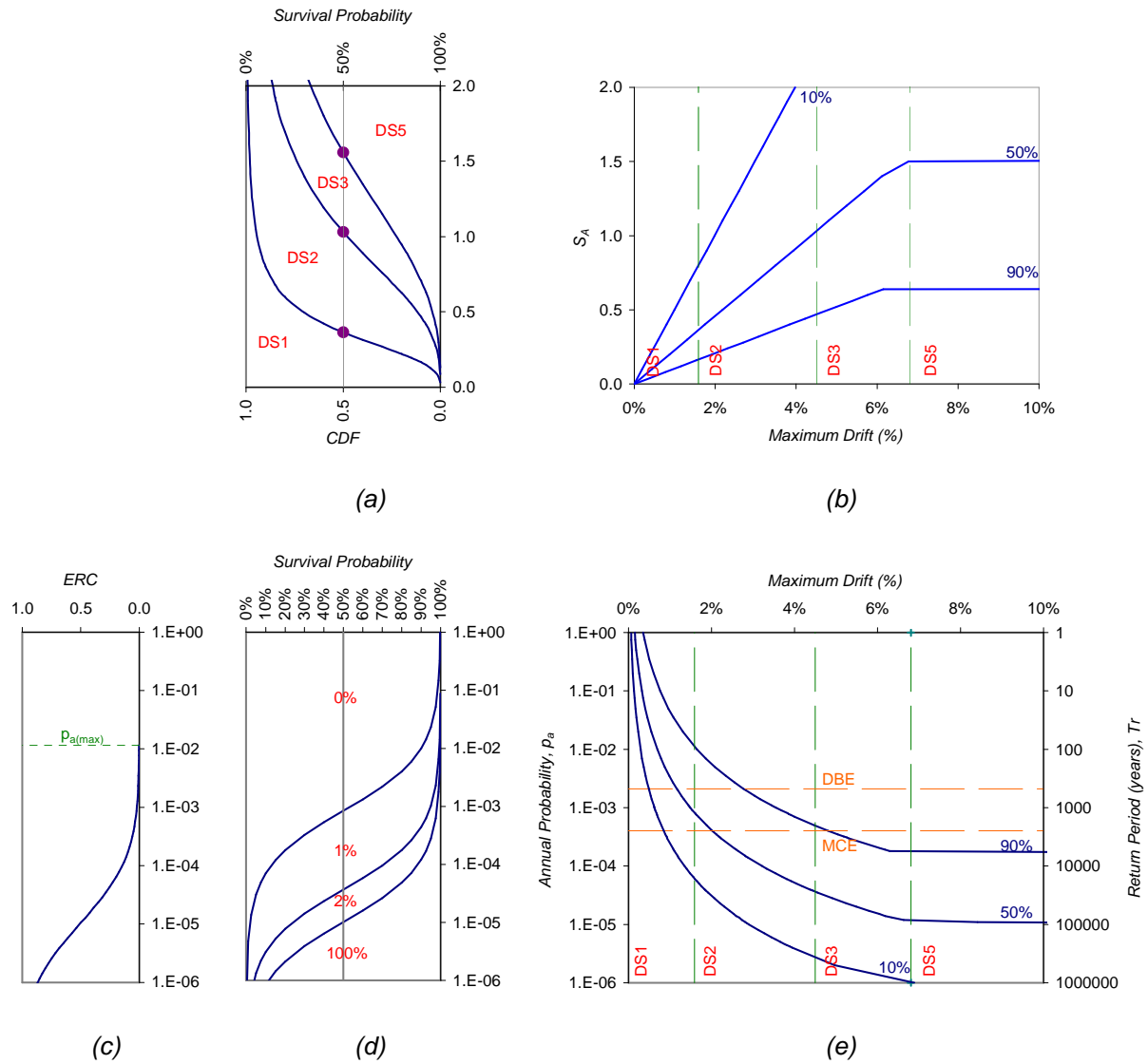
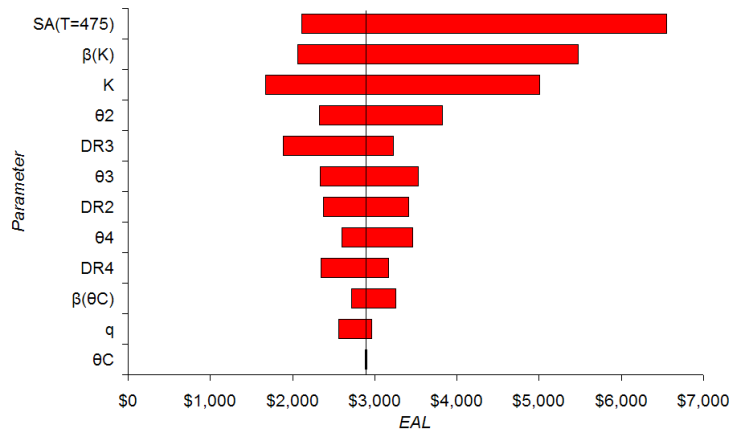
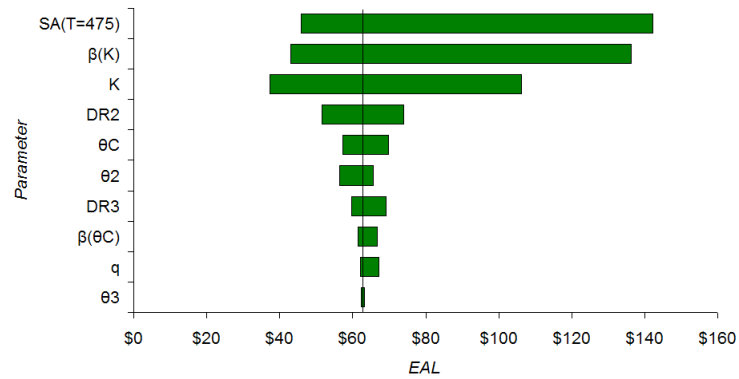


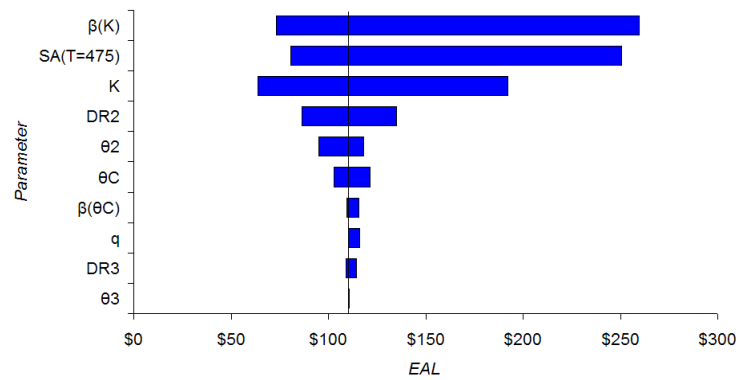
Figure 2-9: Summary of probabilistic seismic vulnerability assessment methodology applied to N-S DAD seismic frame



(a) Red Book frame



(b) DAD E-W gravity frame



(c) DAD N-S seismic frame

Figure 2-10: Results of swing analysis presented as tornado diagrams. These diagrams show how EAL is affected by setting all input parameters to their median value except for one which is set to its low (10th percentile) and then high (90th percentile) values. The resulting EAL are represented by the ends of the horizontal bars. Parameters are shown in decreasing order of their influence on EAL. The vertical lines represent EAL when all parameters are taken at their median values.

CHAPTER THREE

DAMAGE AVOIDANCE DESIGN AND EVALUATION OF A SIX STOREY PRECAST CONCRETE BUILDING

Chapter Summary

A rapid evaluation technique to estimate the expected annualised seismic loss (EAL) is presented. This evaluation technique can be applied to any structure, providing a pushover curve defining the relationship between acceleration capacity and displacement can be obtained. The technique makes use of a capacity spectrum method to determine the median spectral acceleration capacity, from which fragility curves and resilience curves are plotted, assuming an appropriate dispersion. EAL can be found by assigning damage ratios to each of the damage states and integrating. This technique is then applied to a proposed six storey post-tensioned precast concrete apartment building. The results compare favourably to those obtained using the probabilistic seismic vulnerability methodology presented in Chapter One.

3.1 INTRODUCTION

The seismic design and performance evaluation of a proposed six storey precast concrete apartment building with post-tensioned beam-column connections and rocking columns, detailed in accordance with the principles of damage avoidance design (DAD), is presented in this chapter. The beam-column connections are located adjacent to the column face where plastic hinging occurs in conventional monolithic cast-in-place or precast emulation frame systems, and rocking column joints located at the base of the columns and the top of the highest storey participating in a general mechanism. The beam-column connection and rocking column connection are detailed with steel armouring of the connection to prevent damage to the frame system.

The proposed building consists of a two-way moment-resisting frame as illustrated in Figure 3-1. The flooring system is a one-way precast system such as precast hollowcore units, as typically used in multistorey buildings throughout New Zealand. Hence the frames running north-south (N-S) on grids 1 through 5 resist seismic loads only, while the perpendicular east-west (E-W) frames on grids A through F resist both gravity and seismic loads. These frames are similar to those designed by Arnold (2004) and Davies (2003), however the design methodologies presented by these two are inconsistent. Therefore, the design of the proposed building is based on the design methodologies used by Arnold (2004) and Davies (2003), but modified for consistency between the orthogonal frames.

The performance of the structure is evaluated by estimating the expected annualised seismic loss (EAL) due to structural damage. This can be evaluated using the probabilistic seismic vulnerability assessment methodology based on incremental dynamic analysis (IDA) presented in Chapter One. However, as this methodology requires a large number of non-linear time-history analyses, which are impractical in most practical

engineering applications, a simplified rapid evaluation technique is proposed. This new rapid evaluation technique (hereinafter rapid-IDA) is based on a modified capacity spectrum method, and proceeds in a similar manner to the methodology presented in Chapter One. The rapid-IDA technique is used to produce estimates of EAL for the proposed building, then these estimates are compared to those obtained using the IDA based methodology presented in Chapter One.

3.2 RAPID-IDA TO EAL METHODOLOGY

It is observed that deriving an estimate of EAL, via the IDA based probabilistic seismic vulnerability assessment methodology presented in Chapter One, is time consuming since a highly refined numerical model of the structure needs to be developed, and a large number of time-history analyses carried out. Furthermore, computational time-history analysis requires significant details that are unlikely to be available at an early design stage. Therefore this methodology is unlikely to be regularly used in engineering design practice.

For any structure under lateral loading, it is possible to define a relationship between the total lateral force (base shear) applied to the structure and its displacement, commonly known as a pushover curve. The pushover curve is unique for a single degree of freedom (SDOF) structure, however for a multi degree of freedom (MDOF) structure (eg. a multi-storey building) the shape of the pushover curve depends on both the lateral load profile and which displacement is recorded.

Vamvatsikos and Cornell (2002; 2005) observed a relationship between IDA curves and pushover curves, so exploited this relationship to generate summarised IDA curves for the structure from a pushover curve. This process is carried out using *SPO2IDA* software, which incorporates empirical relationships between a quadrilinear backbone pushover and portions of the summarised IDA curves, developed by Vamvatsikos (2002).

By using expected (median) values for material properties, a similar relationship can also be observed between the structural capacity curve, derived directly using a capacity spectrum method, to give a ‘median IDA’ curve. This is the so-called ‘*rapid-IDA*’ part of the procedure. From this, together with assumptions regarding aleatoric and epistemic uncertainties¹, customary fragility curves can be derived (Martínez, 2002). Therefore it follows that an approximate value of EAL can be estimated. The entire procedure can be conducted without the need for using non-linear time-history analysis.

The latter part of this methodology proceeds in a similar manner to the probabilistic seismic vulnerability assessment methodology proposed in Chapter One, where a number of damage states (DS), and their associated damage ratios (DR) are required. However, the first part of this methodology involves estimation of the median IDA curve, or in particular median intensity measures, \tilde{IM}_{DSi} , corresponding to the onset of each of the damage states, defined by median engineering demand parameters \tilde{EDP}_{DSi} , via a rapid-IDA methodology for the onset of each damage state.

Step One: Determination of Structural Capacity

Typically, design spectra are defined by three spectral regions, as illustrated in the acceleration-displacement response spectra (ADRS) given in Figure 3-2. Note that there are three distinct performance regions for short, medium and long period structures which are respectively associated with constant acceleration, constant velocity and constant displacement. The entire damped capacity-spectrum is therefore defined by the greater of:

$$F_v S_1 = T_v B_a C_c^* \quad (3-1)$$

¹ Aleatoric uncertainties arise from the inherent randomness of materials and processes and can be defined in terms of probability distributions. For example, uncertainty in reinforcing strength is an example of aleatoric uncertainty. Epistemic uncertainties occur due to assumptions and simplifications made in the modelling process. Usually this cannot be described in terms of probability distributions, but can be allowed for, for example by comparing experimental tests with model outcomes. A third category of uncertainty exists, that is ontological uncertainty, which arises from the unknown, unexpected and unconsidered. (Elms, 2004). Ontological uncertainty must be considered separately and is not explicitly considered in this thesis.

$$F_v S_1 = 2\pi B_v \sqrt{\frac{C_c^* \Delta^*}{g}} \quad (3-2)$$

$$F_v S_1 = 4\pi^2 B_d \frac{\Delta^*}{T_d g} \quad (3-3)$$

where $F_v S_1$ is the 5% damped design spectral acceleration at a period of 1 s; B_a , B_v , and B_d are damping reduction factors, applied to the constant acceleration, velocity and displacement regions of the spectrum, respectively; and T_v and T_d are the periods at the commencement of the velocity and displacement portions of the spectra, taken as 0.4 s and 3.0 s, respectively.

Applying the rapid pushover method (Martínez, 2002) described in Appendix B, the base shear capacity of a regular frame, V_{base} , can be determined for each $E\tilde{D}P_{DSi}$, as:

$$V_{base} = \kappa M_b \quad (3-4)$$

where $M_b = f(E\tilde{D}P_{DSi})$, as determined by the moment-rotation relationship for the beam plastic hinges. Alternatively, V_{base} may be identified from the appropriate pushover curve for each $E\tilde{D}P_{DSi}$. As the purpose of the pushover analysis is to determine the median response of the structure, expected (median) values rather than nominal values (specified strengths) for the structural properties should be adopted.

In order to evaluate the spectral acceleration corresponding to $E\tilde{D}P_{DSi}$, V_{base} and $E\tilde{D}P_{DSi}$, must be converted to their equivalent SDOF acceleration capacity and displacement, through the use of appropriate transformation factors, presented in Appendix B for regular frames participating in a mixed mechanism. To determine which portion of the spectra governs the behaviour, the effective period is determined:

$$T_{DS_i} = 2\pi \sqrt{\frac{\Delta^*}{C_c^* g}} \quad (3-5)$$

where C_c^* and Δ^* are the equivalent SDOF acceleration capacity and displacement factors evaluated at $E\tilde{D}P_{DS_i}$. If $T_{DS_i} < T_v$, the constant acceleration portion of the spectra governs; if $T_v < T_{DS_i} < T_d$, the constant velocity portion of the spectra governs; and if $T_{DS_i} > T_d$, the constant displacement portion of the spectra governs. Now, $F_v S_1$ can be evaluated after using equation (3-1), (3-2), or (3-3) as appropriate. The damping reduction factors are described in the next section. This can then be converted to another IM if appropriate. These values shall be denoted as $I\tilde{M}_{DS_i}$.

Consideration of Structural Damping

The total effective damping, ξ_{eff} , may be evaluated by adding the contributions of any intrinsic damping ξ_{int} ; radiation damping due to rocking, ξ_{rad} ; and hysteretic damping, ξ_{hyst} :

$$\xi_{eff} = \xi_{int} + \xi_{rad} + \xi_{hyst} \quad (3-6)$$

It is assumed that ξ_{rad} is small compared with ξ_{int} and ξ_{hyst} , so shall be ignored. Typically ξ_{int} is taken as 5% for reinforced concrete structures, and ξ_{hyst} can be approximated by (Pekcan et al., 1999):

$$\xi_{hyst} = \frac{2}{\pi} \eta \left[1 - \frac{1}{\mu} \right] \quad (3-7)$$

where η is an experimentally calibrated energy efficiency absorption factor and μ is the ductility.

A number of models exist whereby the damping reduction factors in equations (3-1), (3-2) and (3-3) can be evaluated based on the total effective damping ξ_{eff} . Herein, the damping reduction factors based on the formulation of Lin and Chang (2004) are adopted. These damping reduction factors were also adopted by Abul Hamid (2006). At the time of writing, the work of Lin and Chang (2004) is most comprehensive, and it has been shown (Lin et al., 2005) that this model provides the best estimation of elastic displacement and viscous damping when compared to other models. Therefore, for evaluation of the proposed buildings in the present work, the following damping reduction factors shall be adopted.

The damping reduction factors for the constant acceleration and constant displacement portions of the spectra, B_a and B_d , are given as:

$$B_a = \sqrt{\frac{0.02 + \xi_{eff}}{0.07}} \quad (3-8)$$

$$B_d = \sqrt{\frac{0.08 + \xi_{eff}}{0.13}} \quad (3-9)$$

where ξ_{eff} is the total effective damping. The damping reduction factor for the constant velocity portion of the spectrum is linearly interpolated between these two values:

$$B_v = \frac{(B_d - B_a)(T - T_v)}{T_d - T_v} + B_a \quad (3-10)$$

where T is the period of the structure.

The total effective damping, ξ_{eff} , is evaluated from equation (3-6). Intrinsic damping is typically taken as 5% for reinforced concrete or 2% for steel and prestressed concrete.

Step Two: Fragility and Resilience curves

In the first part of this rapid-IDA methodology, the results of a pushover analysis were coupled with capacity spectrum approach to generate values of $IM_{DSi}^{\tilde{}}$, which correspond to $EDP_{DSi}^{\tilde{}}$, the median EDP threshold for each of the damage states considered. Since fragility curves have the shape of a lognormal cumulative distribution (Martínez, 2002), they can now be plotted for the structure, assuming an appropriate value for the dispersion. The cumulative lognormal density function is defined by:

$$CPF = \Phi \left[\frac{1}{\beta_{Comp}} \ln \left(\frac{x}{\tilde{x}} \right) \right] \quad (3-11)$$

where x is the lognormally distributed random variable, \tilde{x} is the median of the lognormally distributed values, β_{Comp} is the normalised lognormal standard deviation, accounting for all sources of randomness and uncertainty, otherwise known as the dispersion; and Φ is the standard lognormal cumulative distribution function. This can also be approximated by (Martínez, 2002):

$$CPF = \frac{1}{1 + \left(\frac{x}{\tilde{x}} \right)^{1.8/\beta_{Comp}}} \quad (3-12)$$

Evaluation of equation (3-11) or equation (3-12) requires an estimate of the composite dispersion, β_{Comp} . Martínez (2002) determines β_{Comp} to be in the range of 0.50-0.61 by using the central limit theorem to combine all sources of uncertainty. Composite values of dispersion obtained based on IDA results for the ten storey frames analysed in Chapter Two ranged from 0.67 to 0.74. Also, β_{Comp} has been assessed by Pekcan (1998), Dutta and Mander (1998) and validated by Mander and Basöz (1999) against fragility curves derived from data obtained in 1994 Northridge, and 1989 Loma Prieta earthquakes,

who recommended $\beta_{Comp} = 0.60$ for US highway bridges. Based on these previous analytical and experiential observations, along with the present study, it is proposed that a composite value of dispersion, which incorporates aspects of uncertainty and randomness for both capacity and demand, β_{Comp} be taken as approximately 0.60.

By applying an equivalent argument, resilience curves, which also have the shape of a lognormal cumulative distribution, can be derived for the structure, where the median annual frequencies, $\tilde{P}_{a,DSi}$, corresponding to each damage state, calculated as:

$$\tilde{P}_{a,DSi} = \frac{1}{475} \left[\frac{IM(T=475)}{IM_{DSi}} \right]^{1/q} \quad (3-13)$$

where q is an exponent based on local seismic hazard-recurrence relations. The dispersion associated with $\tilde{P}_{a,DSi}$ is calculated as:

$$\beta_{P_{a,i}} = \frac{\beta_{Comp}}{q} \quad (3-14)$$

where β_{Comp} is the composite dispersion, which is determined based on assumptions about the randomness and uncertainty associated with the structural capacity, earthquake demand, and epistemic uncertainties.

Step Three: Expected Annualised Seismic Loss

Now, EAL is calculated by multiplying the area enclosed between the appropriate resilience curves by the damage ratio for that damage state, and summing over all damage states. This can be calculated from the generalised expression:

$$EAL = DR_{DS1} + \sum_{i=2}^n (DR_{DSi} - DR_{DS(i-1)}) A_i \quad (3-15)$$

where A_i is the area enclosed between the $p_a = 0$ and the resilience curve corresponding to DS_i , and has an upper bound of $p_{a(\max)}$. Evaluation of equation (3-15) typically requires numerical integration, as described in Chapter One. $p_{a(\max)}$ is chosen as the annual frequency where we are 90% confident damage ($>DS_2$) will not occur. Here, this can be evaluated as:

$$p_{a(\max)} = \frac{1}{475} \left[\frac{e^{1.28\beta_{p_a,i}} IM(T=475)}{IM_{DS_2}} \right]^{1/q} \quad (3-16)$$

3.3 PROPOSED SIX STOREY BUILDING DESIGN

The proposed six storey apartment building, illustrated in Figure 3-1 is five-bays 10 m long by four-bays 7.3 m wide. A one-way floor slab spans north-south (N-S) along the building, supported by gravity beams with draped tendons in the east-west (E-W) direction. In the N-S direction, frames resisting predominantly seismic loads are formed by beams with straight tendons. Specially designed beam-column joints are detailed according to a damage avoidance design philosophy such that rocking of these joints occurs and damage only occurs in easily replaceable components. In addition, rocking column hinges are detailed.

The proposed building is located on intermediate soil in Christchurch. The spectral acceleration $F_v S_1$ is obtained from the acceleration response spectra given by the New Zealand loadings code (NZS 4203:1992) as 0.4 g. Therefore the design basis earthquake (DBE) spectral acceleration demand is expressed as:

$$(F_v S_1)_{DBE}^* = 0.4 \text{ g} \quad (3-17)$$

The corresponding design drift is taken as 2%. The spectral acceleration capacity is determined, and compared to the design spectral acceleration demand to determine if the lateral strength capacity is adequate, where ϕ is taken as 0.7 (Shama and Mander, 2003):

$$(F_v S_1)_{DBE}^* \leq \phi (F_v S_1)_{DBE}^{cap} \quad (3-18)$$

Complete design of the complete building is described in Appendix D, and the key details are summarised below.

3.3.1 GRAVITY FRAME DESIGN

The design of the gravity frames are carried out in a similar fashion to the method presented by Arnold (2004). A summary of the key findings for the internal frames on grids B to E are presented herein.

The force in the draped prestress tendons is determined to be $P_{PS\ i} = 645\ kN$, by balancing lateral loads. Service load stresses are checked to ensure the beams remain in an elastic state when live load is applied. The cross-sectional prestress area is determined by considering the required rigid body rotation capacity when yield of the tendons occurs. By assuming a rigid body rotation capacity of 3%, the required prestress area is chosen to be $A_{PS\ min} = 1890\ mm^2$, from which two 36 mm bars are chosen, giving $A_{PS} = 2040\ mm^2$.

Once the prestress design is determined, a check of the capacity of the structure is required for the design basis earthquake. The spectral acceleration capacity of the frame can be evaluated from:

$$(F_v S_1)_{cap} = 2\pi B \sqrt{\frac{C_c^* \Delta^*}{g}} \quad (3-19)$$

where B is the reduction factor to allow for system damping, and C_c^* and Δ^* are the acceleration capacity and displacement of an equivalent SDOF system, described in Appendix B. The base shear capacity of the structure is established by performing a plastic mechanism analysis as described in Appendix B. The base shear can be expressed as:

$$V_{base} = 4.25 M_b \quad (3-20)$$

The acceleration and displacement transformation factors are evaluated from equations (B-13) and (B-14) as $\alpha_A = 0.871$ and $\alpha_D = 1.161$.

A check of the capacity of the structure shows that supplemental energy dissipators are required so that the design criteria is satisfied. To ensure re-centring of the connection, the connection moment provided by the dissipators should satisfy:

$$\lambda_d M_d \leq \phi_{PS} M_{PS} \quad (3-21)$$

where λ_d is an overstrength factor to account for strain-hardening of the dissipator material, ϕ_{PS} is a prestress undercapacity factor, and M_d and M_{PS} are the moment contributions of the dissipators and prestress, respectively. Given mild steel tension-compression ‘dog-bone’ dissipators mounted on either side of the beam at the depth of the prestress, the maximum force in the dissipators is calculated as $P_d = 387 \text{ kN}$, which is provided by two dissipators with a cross-sectional area of 20 by 29 mm. The equivalent SDOF acceleration capacity is recalculated as $C_c^* = 0.212$.

Assuming $\eta = 0.15$ (Arnold, 2004), and conservatively assuming opening of the rocking joints occurs at an elastic column drift of $\theta_{ce} = 0.5\%$, the additional hysteretic damping provided by supplemental energy dissipators, is calculated as 7.2% from equation (3-7), and the damping reduction factor evaluated as 1.31, therefore the spectral acceleration capacity is evaluated as 0.60 which satisfies equation (3-18).

As a final check, the displacement capacity of the frame when yield of the prestress occurs is calculated as 3.7%. This is considered acceptable.

3.3.2 SEISMIC ONLY FRAME DESIGN

The design of the non-gravity load carrying frames is carried out using a similar method to that presented by Davies (2003). The biggest change is that a capacity reduction factor is incorporated in the design process. The base shear capacity of the structure is established by performing a plastic mechanism analysis described by Appendix B, where four storeys are found to be participating in the mechanism and the base shear can be expressed as:

$$V_{base} = 5.06 M_b \quad (3-22)$$

The required beam connection capacity at the design drift can be evaluated directly from:

$$M_{b\ des} = \frac{W\alpha_A\alpha_D g}{h_s n_{sp} \kappa\theta_c} \left(\frac{F_v S_1}{2\pi\phi B} \right)^2 \quad (3-23)$$

where equation (3-23) is derived in Appendix D. The total effective damping is estimated as 13% from which B is approximated as 1.33, and equation (3-23) is evaluated as 427 kN-m. The required prestress moment at the design drift is evaluated by considering overstrength of the dissipators and the allowable strain in the tendons, and evaluated as 317 kN-m.

Two 32 mm diameter prestressing threadbars are chosen, based on the tendon strain at the design drift, giving a total area of 1608 mm². The required initial prestress force is calculated as 463 kN, and for simplicity, it was decided to take the initial prestress force as 32% of the yield prestress force. The initial prestress moment is therefore

171 *kN-m*. Tension-compression dog-bone energy dissipators, 20 *mm* by 22 *mm*, are to be mounted on the top and bottom of the connection to give a dissipator moment of 103 *kN-m*.

3.3.3 DESIGN OF COLUMNS

The column dimensions were selected as 750 *mm* by 750 *mm*, with four ducts for 36 *mm* post-tensioned tendons running the full height of the column. Additionally, the columns are reinforced with 12-D25 reinforcing bars. Appendix D describes how the column prestressing was determined.

3.4 APPLICATION OF RAPID-IDA TO EAL METHODOLOGY

The rapid-IDA evaluation methodology proposed above is applied to both the N-S and E-W frames to evaluate EAL for the proposed apartment building and determine the structural performance. Five damage states are defined for the proposed apartment building as follows: No Damage, as the rocking joints remained closed, or if the rocking joints open, insignificant yielding of energy dissipators occurs (DS1); Minor damage, where replacement of the energy dissipators is required due to extensive yielding resulting in reduction of fatigue life or fracture of energy dissipators (DS2); Repairable damage, where yield of the prestress tendons occurs, caused by significantly large joint rotations (DS3); and toppling, where sufficient prestress has been lost and P- Δ effects cause collapse of the structure (DS5). These damage states qualitatively represent the same response as the damage states defined for the ten storey DAD frames designed by Arnold (2004) and Davies (2003) presented in Chapter Two. The damage state regions are defined in terms of the beam-column joint rotations, θ_j , as presented in Table 3-1. Differences in the geometry and cause the thresholds defining the damage states in orthogonal directions to be slightly different.

In the first part of the rapid-IDA evaluation method, the capacity spectrum method is used to determine the median S_A corresponding to each threshold EDP. For this rapid analysis, damage states are defined in terms of rotation of the beam-column joints, θ_j (where θ_j is the EDP), and these values are tabulated in Table 3-1. Derivation of the spectral acceleration proceeds quickly, once the properties of the frame are known, as follows. Here, calculations are presented for the E-W frame at the onset of DS2. The joint rotation corresponding to the low cycle fatigue limit of the energy dissipators has been calculated as 1.5%, which corresponds to the onset of DS2. The prestress force in the tendons is calculated as:

$$P_{PS} = P_{PSi} + \frac{A_{PS} E_{PS}}{L_{PS}} d_b |\theta_j| = 645 + \frac{2040 \times 205}{8.23} \times 0.7 \times 1.5\% = 1170 \text{ kN} \quad (3-24)$$

The moment capacity of the connection is evaluated as:

$$M_b = \frac{(P_{PS} + P_d) d_b}{2} = \frac{(1170 + 383) \times 0.7}{2} = 543 \text{ kN-m} \quad (3-25)$$

hence, the base shear capacity is found from equation (3-20), as 2310 kN, and the equivalent SDOF acceleration capacity is calculated as:

$$C_c^* = \frac{V_{base}}{W \alpha_A} = \frac{2310}{13450 \times 0.871} = 0.20 \quad (3-26)$$

The elastic contribution to the column drift, θ_{ce} , is evaluated using:

$$\theta_{ce} = \frac{H}{12 h_s} \left[\frac{(h_s - d_b)^3}{EI_{col}^*} + \frac{h_s^2 (L - d_c)^3}{L^2 EI_{beam}^*} \right] \quad (3-27)$$

where H is the column lateral force, evaluated as:

$$H = \frac{2M_b}{h_s} \frac{L}{L_{beam}} \quad (3-28)$$

Equation (3-27) is evaluated as 0.3%, where the column lateral force is 361 kN. The elastic contribution to the drift is added to the contribution due to rigid body rotation of the beam-column connections, giving:

$$\theta_c = \theta_j \frac{L_{beam}}{L} + \theta_{ce} = 1.5 \times \frac{6.1}{7.3} + 0.3 = 1.5 \% \quad (3-29)$$

from which the equivalent SDOF displacement is calculated as:

$$\Delta^* = \frac{n_{sp} \theta_c h_s}{\alpha_D} = \frac{4 \times 0.015 \times 3.6}{1.161} = 0.19 \text{ m} \quad (3-30)$$

The effective period, T_{eff} is calculated as

$$T_{eff} = 2\pi \sqrt{\frac{\Delta^*}{C_c^* g}} = 2\pi \sqrt{\frac{0.19}{0.20 \times 9.81}} = 2.0 \text{ s} \quad (3-31)$$

indicating that the velocity portion of the spectra governs. The hysteretic damping is evaluated, assuming $\eta = 0.15$ as:

$$\xi_{hyst} = \frac{2}{\pi} \eta \left(1 - \frac{1}{\mu}\right) = \frac{2}{\pi} \times 0.15 \times \left(1 - \frac{1}{5}\right) = 0.08 \quad (3-32)$$

from which the total effective damping is calculated using equation (3-6) as $\xi_{eff} = 0.13$, where the intrinsic damping ξ_{int} is assumed to be 5%. Using equations (3-8), (3-9), and (3-10), the damping reduction factor B_v is calculated as 1.33. Therefore equation (3-2) can be used to determine the spectral acceleration capacity:

$$F_v S_1 = 2\pi B_v \sqrt{\frac{C_c^* \Delta^*}{g}} = 2\pi \times 1.33 \times \sqrt{\frac{0.20 \times 0.19}{9.81}} = 0.52 \quad (3-33)$$

The same calculations are presented in Table 3-2 for the remaining damage states, from which fragility curves, and resilience curves can be plotted, as illustrated in Figure 3-3. The EAL for the gravity E-W frame is found to be 0.000132, which can alternatively be expressed as \$132 per million dollars of building value.

Similarly, the rapid evaluation method can be applied to the seismic N-S frame, where the calculations are presented in Table 3-3, and fragility and resilience curves illustrated in Figure 3-4. The EAL for this frame is found to be 0.000111, which can alternatively be expressed as \$111 per million dollars of building value.

Evaluation of the return period earthquakes for which there is a 90% survival probability of a given damage state, is possible by rearranging equation (3-16):

$$Tr_{P(DS < DSi)=0.9} = 475 \left[\frac{IM_{DSi}}{e^{1.28\beta_c} IM(T=475)} \right]^{1/q} \quad (3-34)$$

where Tr is the return period, and IM_{DSi} is the median intensity measure corresponding to the onset of DSi . Using equation (3-34), it is found that there is a 90% probability that restressing of the tendons will not be required in a 2470 and 2270 year return-period event for the N-S and E-W frames, respectively. Additionally, there is a 90% probability of surviving frame toppling in 5000 and 3600 year earthquake events, for the N-S and E-W frames respectively.

3.5 INCREMENTAL DYNAMIC ANALYSIS BASED ASSESSMENT METHODOLOGY

A rapid-IDA evaluation procedure has been presented and applied to a proposed six storey building to calculate EAL. Now, the IDA based probabilistic seismic vulnerability assessment methodology proposed in Chapter One shall be applied to calculate EAL for

the proposed building. Performing this analysis will give a further estimate of EAL, so the proposed rapid-IDA methodology can be verified.

3.5.1 EAST-WEST GRAVITY FRAME

A frame from the proposed building, typical of grids B to E, in the east-west (E-W) gravity direction is modelled using *RUAUMOKO-2D* (Carr, 2005). This model consists of elastic Giberson frame elements to represent the beams and columns. The non-linear behaviour of the rocking beam joints is represented by four parallel rotational springs, whose properties are assigned to represent the designed tri-linear moment-rotation response and energy dissipation of the joints. The rocking column hinges are also represented by two parallel springs. The floor slab is assumed to act as a rigid diaphragm, eliminating beam-elongation effects from the analysis and 2240 kN weight is associated with each of the six floors (this is the tributary weight on the frame). Constant 5% damping is assumed. The fundamental period of the model structure prior to rocking is $T_1 = 1.04$ s. Further details on the mode shapes of the frame both prior to and during rocking can be found in Appendix E.

A summary of the IDA results for this frame are presented in Figure 3-5. It is observed in Figure 3-5(a) and (b) that at low S_A the dispersion is low, and as the intensity increases, the dispersion observed in the results increases. It is observed that the dispersion is increasing due to increasing amounts of non-linear behaviour. The Ramberg-Osgood (R-O) parameters obtained for the IDA curves for this building are presented in Table 3-4. Five damage states, as described in Section 3.4, are again used to describe the non-linear behaviour of the structure. Here, these have been redefined in terms of the maximum

absolute inter-storey drift occurring over all levels of the frame, and their associated damage ratios are defined in Table 3-5.

A summary of the probabilistic seismic vulnerability methodology steps to calculate EAL are presented in Figure 3-6. EAL is found to be 0.000077, which can alternatively be expressed as \$77 per million dollars of building value. From the resilience curves it can be seen that we are 90% confident of surviving DS2 in a 650 year event, 90% confident of surviving DS3 in a 4600 year event, and 90% confident of surviving DS5 in a 5900 year event.

3.5.2 NORTH-SOUTH SEISMIC FRAME

An interior frame from the proposed building in the north-south (N-S) seismic direction is modelled using *RUAUMOKO-2D*. This model consists of elastic Giberson frame elements to represent the beams and columns, designated to remain elastic throughout the earthquake analysis. The non-linear behaviour of the rocking beam-column connections is represented by two rotational springs in parallel, whose properties are assigned to represent the designed tri-linear moment-rotation response and energy dissipation of the joints. The rocking column hinges are also represented by two rotational springs in parallel. The floor slab is assumed to act as a rigid diaphragm, precluding elongation of the beams with due to rocking behavior, 2240 kN weight is associated with each of the six floors (it is assumed each of the five frames in this direction resist the same seismic mass) and P- Δ effects are included though a ‘gravity-only’ column whose displacements are slaved to the frame. Constant 5% damping is assumed.

A summary of the IDA results for this frame are presented in Figure 3-7 and selected time-history analysis results are presented in Appendix E. Five damage states, previously

defined, are used to describe the non-linear behaviour of the structure. These and their associated damage ratios are defined in Table 3-5. A summary of the probabilistic seismic vulnerability methodology steps to calculate EAL are presented in Figure 3-8. EAL is found to be 0.000097, which can alternatively be expressed as \$97 per million dollars of building value. From the resilience curves it can be seen that we are 90% confident of surviving DS2 in a 260 year event, 90% confident of surviving DS3 in a 4600 year event, and 90% confident of surviving DS5 in a 5500 year event.

3.6 DISCUSSION OF RESULTS

The expected annualised seismic loss (EAL) has been estimated in the preceding sections for two orthogonal frames of a proposed building by a rapid-IDA evaluation method proposed in this chapter and an incremental dynamic analysis (IDA) based methodology presented in Chapter One. The two different methods have produced different results for both the frames, however the results are comparable.

3.6.1 SENSITIVITY OF METHODOLOGIES

The sensitivity parameter (Elms, 1985) of a model to a parameter is expressed as:

$$\gamma_i = \frac{x_i}{y} \frac{\partial y}{\partial x_i} \quad (3-35)$$

where γ_i is the percentage change in the model output, y , due to a one percent change in input parameter x_i . The sensitivity parameter is determined for each of the input parameters to the rapid-IDA evaluation methodology, and the results are presented in Table 3-6.

It can be seen from Table 3-6 that the parameters that most significantly effecting EAL are those defining seismic hazard, $S_A(T = 475)$ and q , the dispersion factor, β_{Comp} , the structural capacity, represented by M_b , the definition of DS5 and its damage ratio, $\theta_{j_{DS5}}$ and DR5, and the hysteretic damping energy adsorption parameter η . Of this list of parameters, it is observed that β_{Comp} and η are assumed, based on experience and understanding of the structure of interest, $\theta_{j_{DS5}}$ is calculated based on an assumption of when collapse of the structure will occur. Therefore it can be seen that these assumptions made about β_{Comp} , η and the definition of total damage will significantly affect EAL.

3.6.2 DIFFERENCES BETWEEN THE TWO METHODOLOGIES

It is observed when comparing the EAL values, that for N-S seismic frame, the two methodologies produce similar estimates, being \$111 and \$97 per million dollars building value for the rapid-IDA evaluation and IDA based probabilistic seismic vulnerability assessment methodology respectively. This would suggest the rapid-IDA methodology produces similar results to the IDA based method, however, there is a larger difference between the two values calculated for E-W gravity frame. These values are \$132 and \$77 per million dollars building value, for the rapid-IDA and IDA based methods, respectively.

Significant variability was observed in the estimates of EAL in Chapter Two. Assuming that EAL is lognormally distributed, a 90% confidence interval for the real annualised loss can be obtained for the IDA based method as:

$$\left(\frac{\tilde{x}}{e^{t_{0.05}\left(\frac{\beta_{pa}}{\sqrt{n}}\right)}}, \tilde{x} e^{t_{0.05}\left(\frac{\beta_{pa}}{\sqrt{n}}\right)} \right) \quad (3-36)$$

where $t_{0.05}$ is the t-statistic based on $(n-1)$ degrees of freedom, obtainable from statistical tables and n is the number of earthquake ground motions used in the IDA to estimate EAL.

Evaluation of equation (3-36) gives a confidence interval of (\$39, \$153) for the E-W gravity frame and (\$47, \$200) for the N-S seismic frame per million dollars building value. As illustrated in Figure 3-9(a) and (b), it is observed that the estimates of EAL obtained by the rapid-IDA methodology fall within these 90% confidence intervals. This confirms the validity of the rapid-IDA methodology.

While a number of the input parameters between the two models, such as $S_A(T=475)$, q , and the damage ratios have been kept constant between the two methodologies, there are differences in the maximum drifts that define the damage states, in the dispersion. As far as practical, the structural properties for non-linear time-history analysis were the same as for the rapid-IDA evaluation methodology. However, there are some differences between the non-linear time-history model and the rapid-IDA evaluation model. In particular, the beam-column joint hysteresis was approximated for the time-history at small rotations, and the base shear capacity in the rapid evaluation was evaluated assuming κ is constant. For the IDA-based methodology, approximations were made since a suite of only 20 earthquakes are used for the IDA, and the output IDA curves are approximated by R-O functions. These curves were then statistically summarised and estimation of the median response is finally made from a bi-linear curve.

A comparison of the median IDA values obtained via the R-O approximation used in the probabilistic seismic vulnerability assessment methodology, the rapid-IDA points, and a distributionless IDA median taken as the average of the 10th and 11th ranked earthquake responses (out of a total of 20 earthquakes) is made in Figures 3-9(c) and (d)

for the E-W and N-S frames respectively. The latter are the subject of investigations by Solberg (2006) for their suitability of determining EAL for SDOF systems.

It is observed these differences and approximations are causing the differences in the median and dispersions of the resilience curves, as illustrated in Table 3-7. It is observed in Table 3-7, that the rapid-IDA evaluation methodology has consistently larger $\tilde{p}_{a,DSi}$ for all damage states and both frames. This observation is particular to these frames and may not be the general rule. However, it is likely that the higher $\tilde{p}_{a,DSi}$ are causing the rapid evaluation estimates of EAL to be larger than the IDA based estimates of EAL. Additionally, it can be seen in Table 3-7, that the dispersion of the IDA based resilience curves is smaller than that of the rapid-IDA evaluation derived resilience curves, hence contributing to the lower EAL estimated by the IDA based method.

3.7 CONCLUSIONS

A rapid-IDA evaluation method to estimate the expected annualised seismic loss (EAL) has been presented. This method is comparable to the probabilistic seismic vulnerability assessment methodology presented in Chapter One, however does not require non-linear time-history analyses. It can be applied to any structure, providing a pushover curve defining the relationship between acceleration capacity and displacement can be obtained. The method makes use of a capacity spectrum method to determine the median spectral acceleration capacity, from which fragility curves and resilience curves can be plotted, by assuming an appropriate value of the dispersion. Similar to the probabilistic seismic vulnerability methodology presented in Chapter One, EAL can be found by assigning damage ratios to each of the damage states and integrating.

The rapid-IDA evaluation methodology was applied two orthogonal frames from a proposed six storey DAD apartment building to calculate EAL. Additionally, EAL was calculated for both these frames using the incremental dynamic analysis based probabilistic seismic vulnerability methodology presented in Chapter One. It was observed EAL is rather sensitive to a number of the input parameters. Although the EAL calculated by both methods was not the same for either frame, the rapid-IDA estimates fell within the 90% confidence intervals for EAL based on the IDA-based methodology. Additionally, the results for both frames were of the same order of magnitude, indicating that EAL for the proposed DAD apartment building is approximately \$100 per million dollars of building value.

3.8 REFERENCES

- Abul Hamid, N.Y. (2006) ?. PhD Thesis, Department of Civil Engineering, University of Canterbury, Christchurch, New Zealand. *in preparation*.
- Arnold, D.M. (2004) Development and Experimental Testing of a Seismic Damage Avoidance Designed Beam to Column Connection Utilising Draped Unbonded Post-Tensioning. ME Thesis, Department of Civil Engineering, University of Canterbury, Christchurch, New Zealand.
- Carr, A.J. (2005) *Ruaumoko Computer Programme Manual*. Department of Civil Engineering, University of Canterbury, Christchurch, New Zealand.
- Davies, M.N. (2003) Seismic Damage Avoidance Design on Beam-Column Joints Using Unbonded Post-Tensioning: Theory, Experiments and Design Example. ME Thesis, Department of Civil Engineering, University of Canterbury, Christchurch, New Zealand.
- Dutta A. and Mander J. B. (1998) *Capacity design and fatigue analysis of confined concrete columns*. Tech. Rep. MCEER-98-0007, Multidisciplinary Center for Earthquake Engineering. State University of New York at Buffalo, Buffalo, NY.

- Elms, D.G. (1985) ‘The Principle of Consistent Crudeness’. In: *Proceedings of NSF Workshop on Civil Engineering Applications of Fuzzy Sets*. Eds: C.B. Brown, J.-L. Chameau, R.N. Palmer and J.T.P. Yao. Purdue University, West Lafayette, IN. pp 35-44.
- Elms, D.G. (2004) Structural safety – issues and progress. *Progress in Structural Engineering and Materials*, **6**(2), 116-126.
- Lin, Y.-Y. and Chang, K.-C. (2004) Effects of Site Classes on Damping Reduction Factors. *Journal of Structural Engineering*, **130**(11), 1667-1675.
- Lin, Y.-Y., Miranda, E. and Chang, K.-C. (2005) Evaluation of damping reduction factors for estimating elastic response of structures with high damping. *Earthquake Engineering and Structural Dynamics*, **34**(11), 1427-1443.
- Mander J.B., and Basöz N. (1999) ‘Seismic Fragility Curve Theory for Highway Bridges in Transportation Lifeline Loss Estimation’. In: *Optimizing Post-Earthquake Lifeline System Reliability*, Eds: Elliot and McDonough. TCLEE Monograph No. 16, ASCE. pp 31-40.
- Mander, J.B. (2004) Beyond Ductility: The Quest Goes On. *Bulletin of the New Zealand Society of Earthquake Engineering*, **37**(1), 35-44.
- Martínez, M.E. (2002) Performance-Based Seismic Design and Probabilistic Assessment of Reinforced Concrete Moment Resisting Frame Structures. ME Thesis, Department of Civil Engineering, University of Canterbury, Christchurch, New Zealand.
- Newmark, N.M. and Hall, W.J. (1982) *Earthquake Spectra and Design*. EERI Monograph Series. Earthquake Engineering Research Institute, Oakland, CA.
- Pekcan, G., Mander, J.B. and Chen, S.S. (1999) Fundamental considerations for the design of non-linear viscous dampers. *Earthquake Engineering and Structural Dynamics*, **28**(11), 1405-1425.
- Pekcan, G. (1998) Design of Seismic Energy Dissipation Systems for Reinforced Concrete and Steel Structures. PhD Dissertation, Department of Civil, Structural and

Environmental Engineering, State University of New York at Buffalo, Buffalo, NY.

Shama, A.A. and Mander, J.B. (2003) The seismic performance of braced timber pile bents. *Earthquake Engineering and Structural Dynamics*, **32**(3), 463-482.

Solberg, K. (2006) ?. ME Thesis, Department of Civil Engineering, University of Canterbury, Christchurch, New Zealand. *in preparation*.

Standards New Zealand (1992) *Code of Practice for General Structural Design and Design Loadings for Buildings, known as the Loadings Code*, NZS 4203:1992, Volumes 1 and 2. Standards New Zealand, Wellington, New Zealand.

Vamvatsikos, D. (2002) Seismic Performance, Capacity and Reliability of Structures as seen through Incremental Dynamic Analysis. PhD Dissertation, Department of Civil and Environmental Engineering, Stanford University, CA.

Vamvatsikos, D. and Cornell, C.A. (2002) Incremental dynamic analysis. *Earthquake Engineering and Structural Dynamics*, **31**(3), 491-514.

Vamvatsikos, D. and Cornell, C.A. (2005) Direct Estimation of Seismic Demand and Capacity of Multidegree-of-Freedom Systems through Incremental Dynamic Analysis of Single Degree of Freedom Approximation. *Journal of Structural Engineering*, **131**(4), 589-599.

Table 3-1: Definition of damage states for Rapid-IDA to EAL evaluation

	Damage State Description	Joint Rotation Range	E-W gravity frame joint rotations	N-S seismic frame joint rotations	Damage Ratio
DS1	Elastic Performance	$< \theta_d$	$< 1.5\%$	$< 1.1\%$	0%
DS2	Replace Energy Dissipators	$\theta_d - \theta_{PS\ yield}$	1.5 – 3.6%	1.1 – 4.0%	1%
DS3	Yield of Tendons	$\theta_{PS\ yield} - \theta_{PS\ slack}$	4.5 – 5.5%	4.0 – 5.9%	2%
DS4	Irreparable Damage				
DS5	Complete Damage	$> \theta_{PS\ slack}$	$> 5.5\%$	$> 5.9\%$	100%

Table 3-2: Calculation of \tilde{IM}_{DSi} for E-W gravity frame

	θ_j	P_{PS}	M_b	V_{base}	C_c^*	H	θ_{ce}	θ_c	Δ^*	T_{eff}	ξ_{hyst}	ξ_{eff}	B_a	B_d	B_v	$F_v S_1$
DS2	1.5%	1170	540	2300	0.20	361	0.31%	1.5%	0.19	2.0	0.082	0.132	1.47	1.28	1.35	0.53
DS3	3.6%	1940	810	3500	0.29	540	0.46%	3.5%	0.43	2.4	0.090	0.140	1.51	1.30	1.35	0.97
DS5	5.5%	1940	810	3500	0.29	540	0.46%	5.0%	0.62	2.9	0.092	0.142	1.52	1.10	1.31	1.13

Table 3-3: Calculation of \tilde{IM}_{DSi} for N-S seismic frame

	θ_j	P_{PS}	M_b	V_{base}	C_c^*	H	θ_{ce}	θ_c	Δ^*	T_{eff}	ξ_{hyst}	ξ_{eff}	B_a	B_d	B_v	$F_v S_1$
DS2	1.1%	780	380	1910	0.16	240	0.36%	1.3%	0.17	2.0	0.073	0.132	1.43	1.25	1.32	0.53
DS3	4.0%	1530	640	3230	0.28	400	0.61%	4.1%	0.51	2.7	0.089	0.139	1.51	1.30	1.32	0.97
DS5	5.9%	1530	640	3230	0.28	500	0.62%	5.8%	0.72	3.2	0.091	0.141		1.30		1.13

Table 3-4: Summary of Ramberg-Osgood statistical analysis for θ_{MAX}

Eq. No	E-W gravity frame				N-S seismic frame			
	S_c	θ_c (%)	r	K	S_c	θ_c (%)	r	K
1	0.71	2.2	5	32.0	1.20	6.8	142	17.6
2	2.08	5.1	96	40.7	2.00	5.7	43	35.2
3	2.31	4.6	500	50.0	2.30	4.4	15	52.1
4	1.67	5.0	60	36.6	1.70	5.5	33	30.7
5	1.00	4.8	19	20.7	1.07	6.4	45	16.8
6	1.70	5.6	242	30.1	1.90	6.4	89	29.5
7	0.73	2.9	6	24.9	0.57	2.5	5	22.7
8	1.30	3.7	9	35.0	1.50	6.2	33	24.3
9	0.62	2.4	5	26.2	0.53	2.6	5	19.9
10	2.30	4.6	36	50.3	2.08	4.2	14	49.9
11	0.67	2.2	6	30.6	0.64	3.3	5	19.7
12	0.57	2.3	5	24.6	0.55	3.2	5	16.9
13	3.10	5.3	266	58.3	2.70	4.9	24	55.3
14	0.80	4.4	26	18.1	1.09	6.9	167	15.8
15	0.67	2.5	5	26.8	0.59	2.8	5	20.6
16	5.14	4.8	99	108.1	5.20	6.0	63	86.5
17	1.60	6.1	260	26.2	1.30	5.4	16	24.2
18	1.00	5.4	140	18.6	1.20	7.1	188	16.9
19	0.96	4.2	28	22.8	1.00	4.6	8	21.9
20	3.80	4.7	298	80.4	4.35	5.9	91	73.2
10%	3.05	6.2	5	66.7	3.15	7.4	5	55.0
50%	1.32	3.9	37	33.5	1.35	4.8	25	28.1
90%	0.57	2.5	301	18.2	0.57	3.1	127	14.3
β	0.65	0.35	1.63	0.48	0.66	0.34	1.27	0.52

Table 3-5: Definition of damage states for IDA-based method

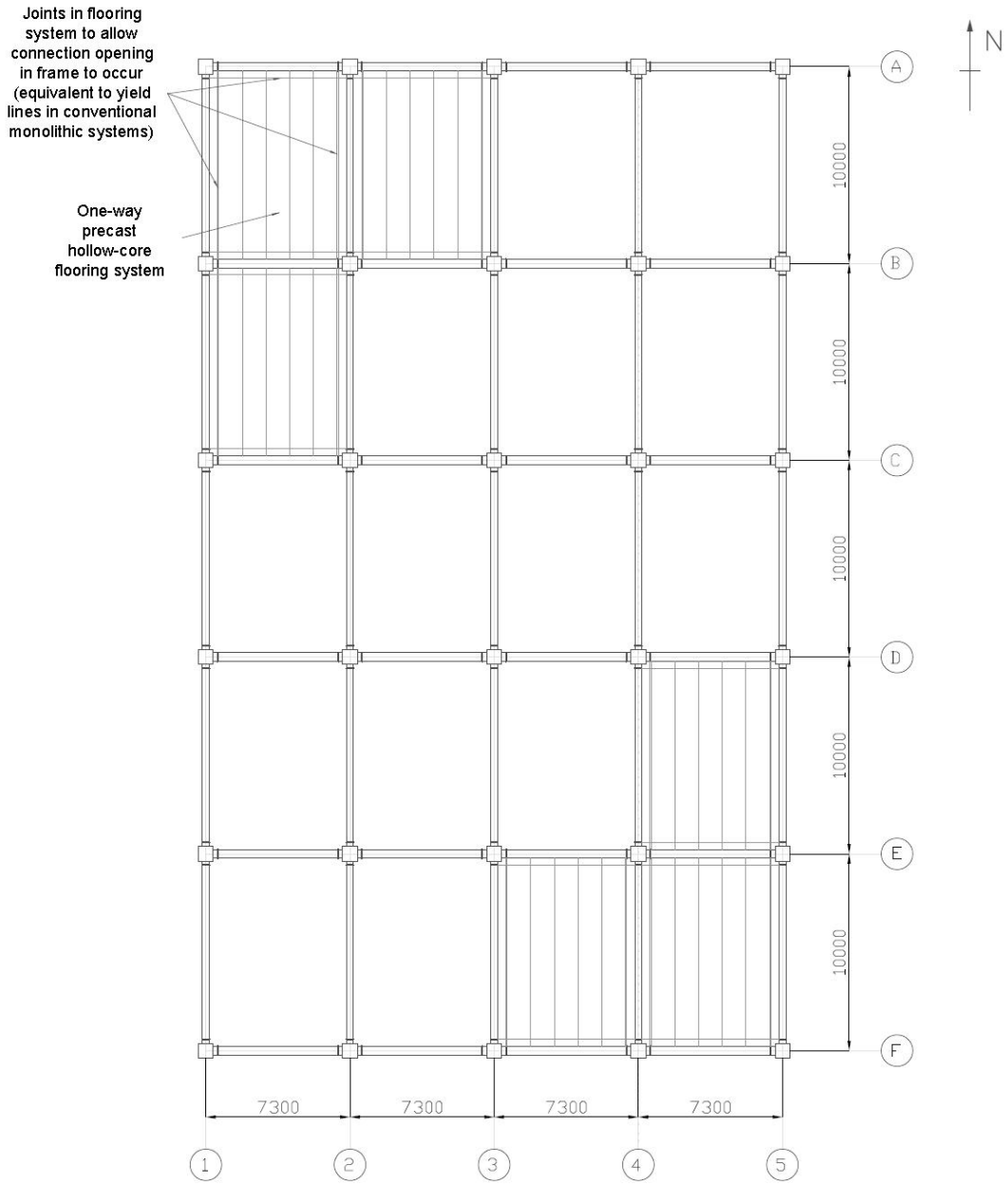
Damage State		Joint Rotation Range	E-W gravity frame max. drifts	N-S seismic frame max. drifts	Damage Ratio
DS1	Elastic Performance	$< \theta_d$	$< 1.9\%$	$< 1.1\%$	0%
DS2	Replace Energy Dissipators	$\theta_d - \theta_{PS\ yield}$	1.9 – 3.6%	1.1 – 4.0%	1%
DS3	Yield of Tendons	$\theta_{PS\ yield} - \theta_c$	3.6 – 3.9%	4.0 – 5.9%	2%
DS4	Irreparable Damage				
DS5	Complete Damage	$> \theta_c$	$> 3.9\%$	$> 5.9\%$	100%

Table 3-6: Sensitivity parameters for rapid-IDA evaluation

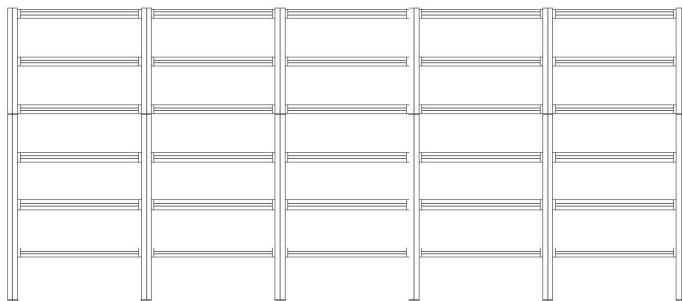
Parameter	E-W gravity frame	N-S seismic frame
$S_A(T = 475)$	3.03	3.03
q	1.43	1.48
M_b	-1.83	-0.49
η	-0.64	-0.62
β	2.53	2.82
$\theta_{j\ DS2}$	-0.32	-0.20
$\theta_{j\ DS3}$	-0.01	-0.02
$\theta_{j\ DS5}$	-0.88	-2.26
θ_{yield}	0.04	0.05
DR2	0.04	0.09
DR3	0.01	0.02
DR5	0.95	0.89

Table 3-7: Parameters defining resilience curves

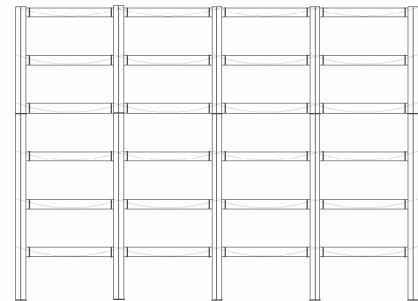
	E-W gravity frame		N-S seismic frame	
	Rapid	IDA	Rapid	IDA
$\tilde{p}_{a,DS2}$	2.7×10^{-4}	1.6×10^{-4}	4.9×10^{-4}	3.5×10^{-4}
$\tilde{p}_{a,DS3}$	4.4×10^{-5}	2.3×10^{-5}	4.0×10^{-5}	2.0×10^{-5}
$\tilde{p}_{a,DS4}$	2.7×10^{-5}	1.7×10^{-5}	2.0×10^{-5}	1.6×10^{-5}
$\beta_{p_{a,DSi}}$	1.80	1.77	1.80	1.88



(a) Plan



b) Seismic Frame (N-S) elevation



(c) Gravity Frame (E-W) elevation

Figure 3-1: Plan and elevation of proposed apartment building

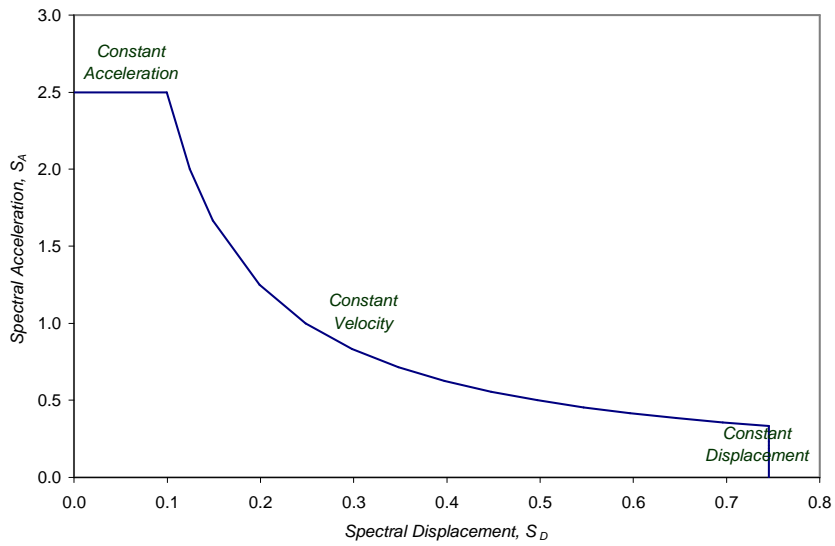


Figure 3-2: Elastic 5% damped ADRS for design

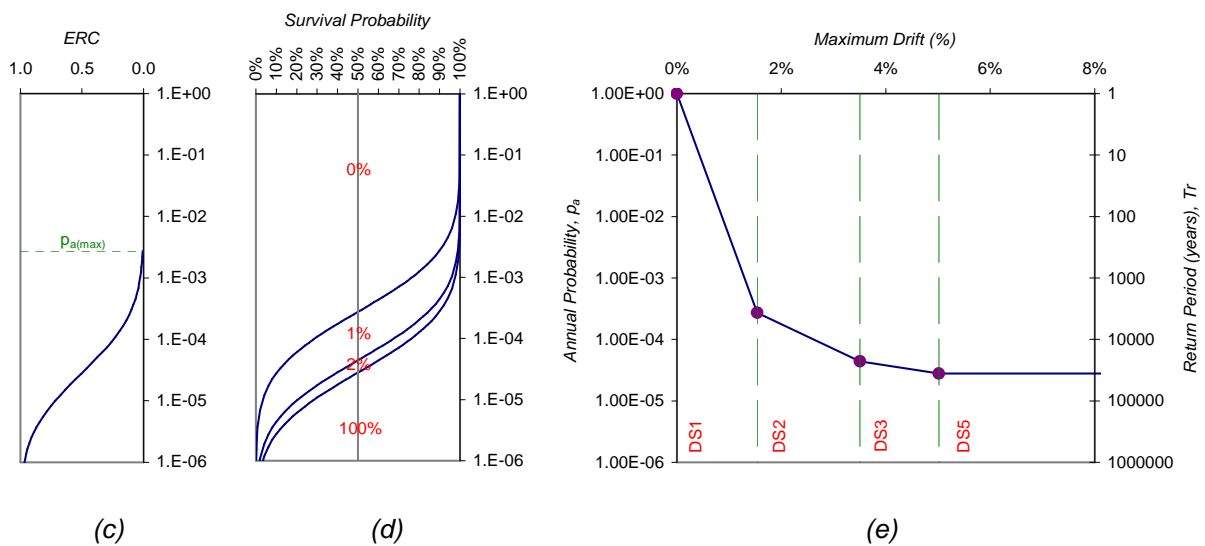
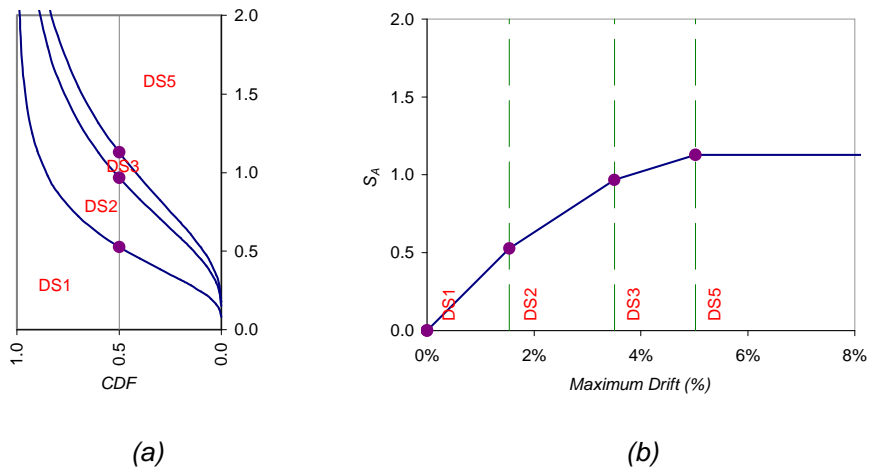
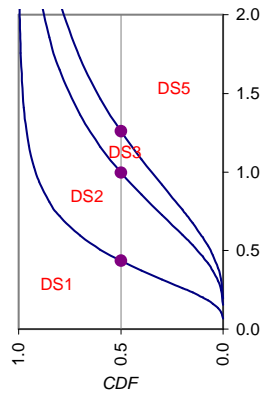
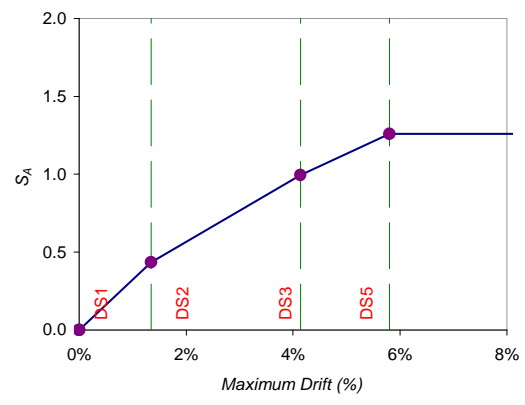


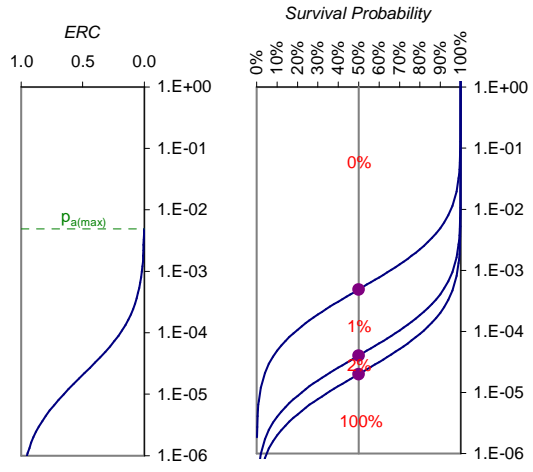
Figure 3-3: Summary of rapid-IDA to EAL method applied to E-W gravity frame



(a)

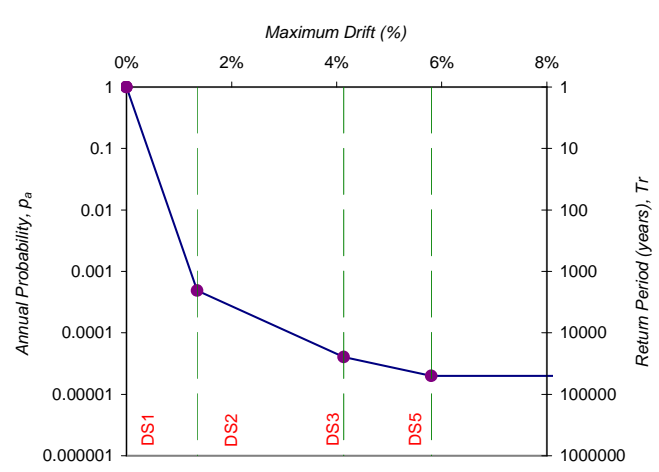


(b)



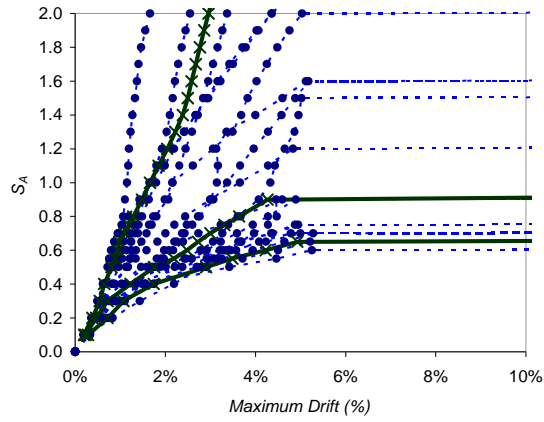
(c)

(d)

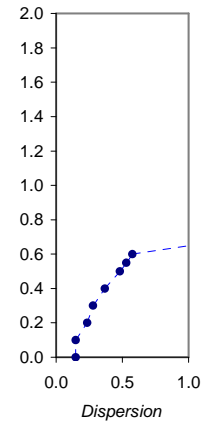


(e)

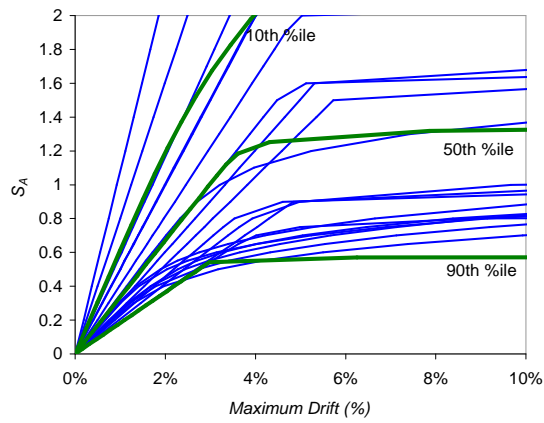
Figure 3-4: Summary of rapid-IDA to EAL method applied to the N-S seismic frame



(a) IDA curves for all earthquakes



(b) Dispersion β



(c) R-O curves fitted to data and summarised by 10th, 50th and 90th percentile curves

Figure 3-5: Incremental dynamic analysis output for E-W gravity frame

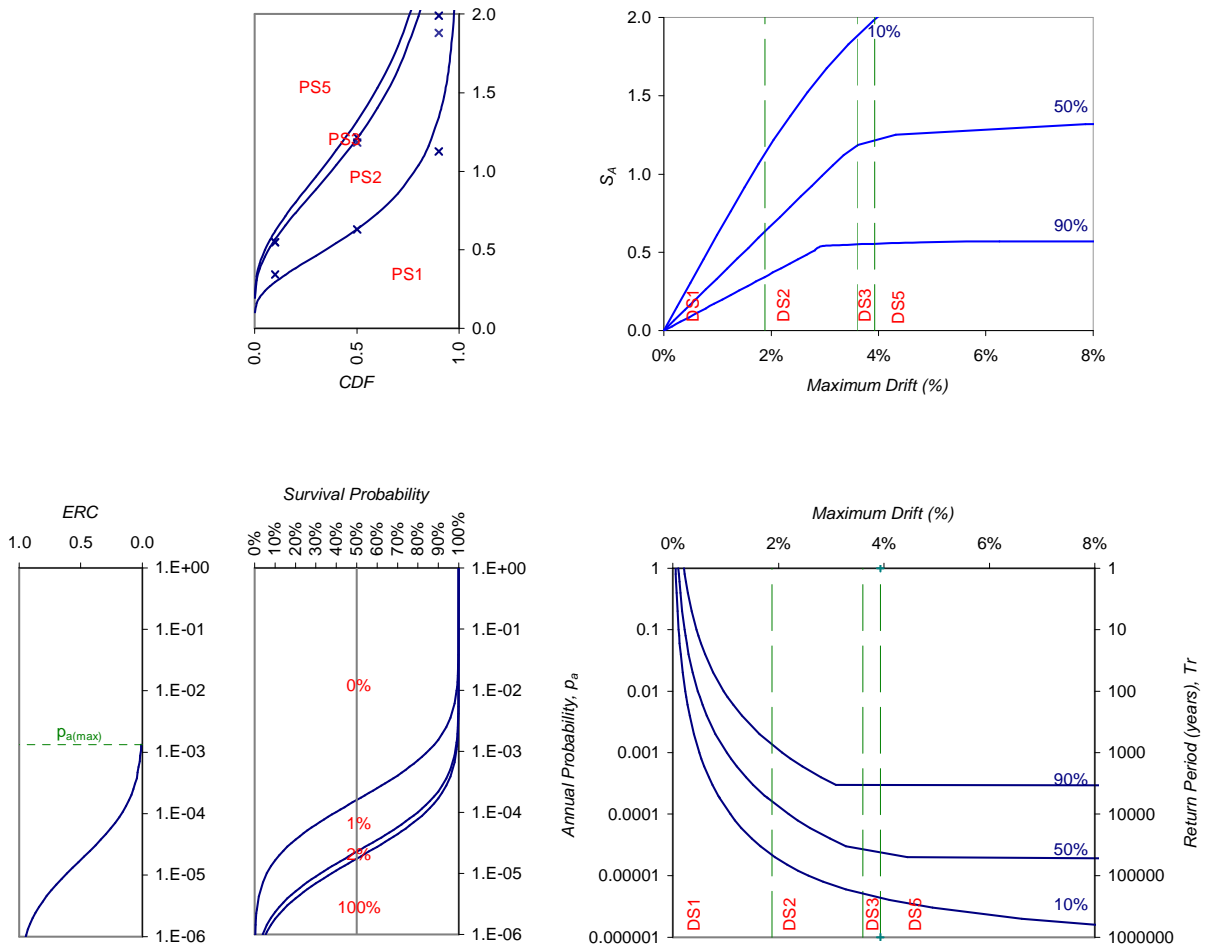
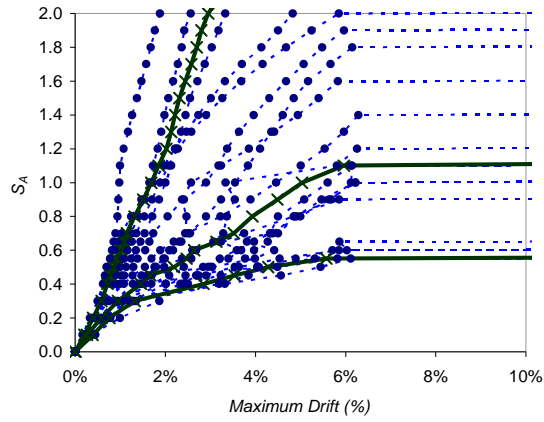
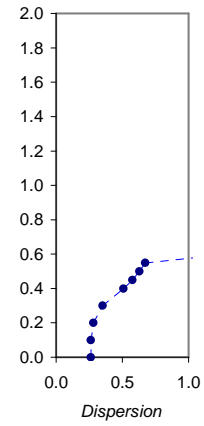


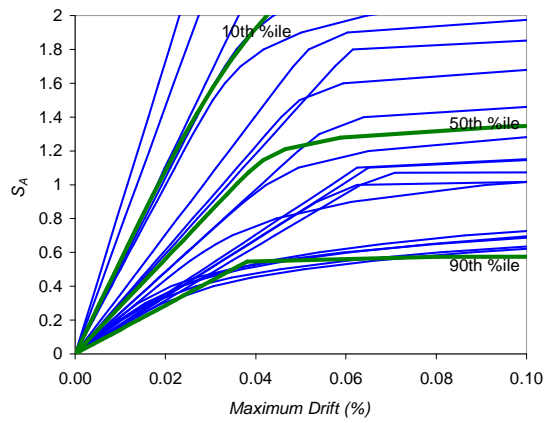
Figure 3-6: Summary of IDA-based probabilistic seismic vulnerability assessment of E-W Gravity Frame



(a) IDA curves for all earthquakes



(b) Dispersion β



(c) R-O curves fitted to data and summarised by 10th, 50th and 90th percentile curves

Figure 3-7: Incremental dynamic analysis output for N-S seismic frame

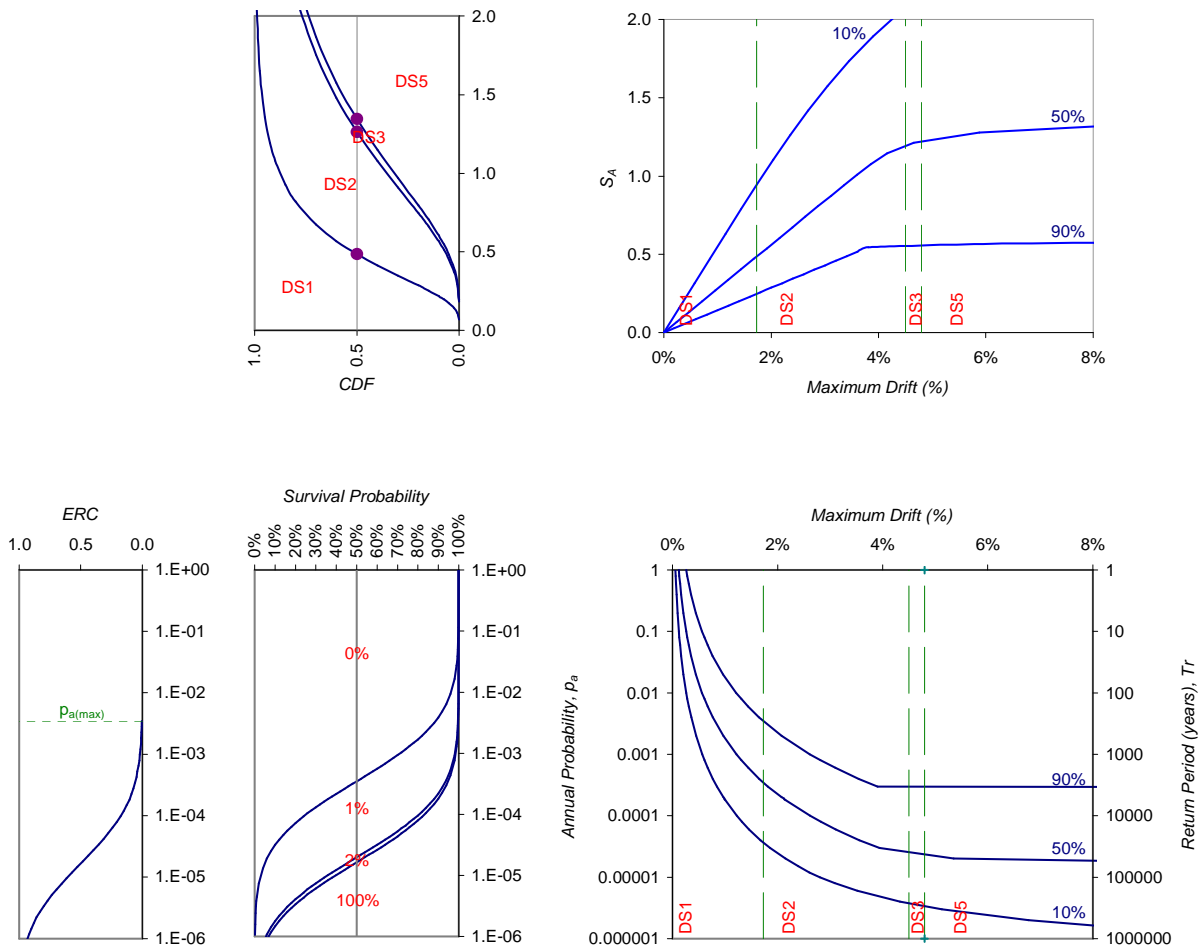
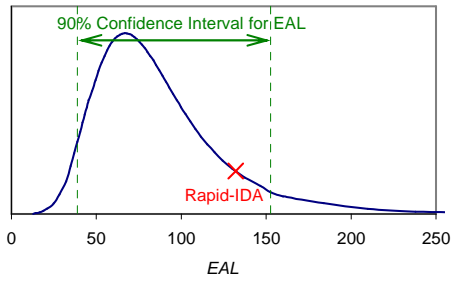
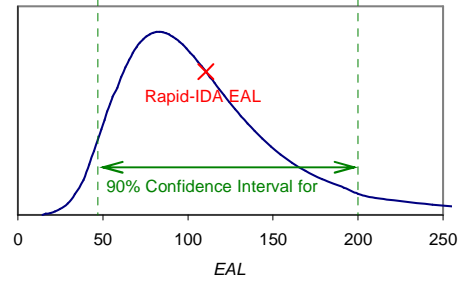


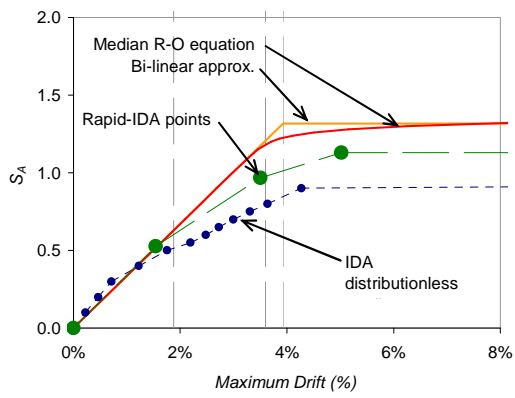
Figure 3-8: Summary of IDA-based probabilistic seismic vulnerability assessment of N-S Seismic Frame



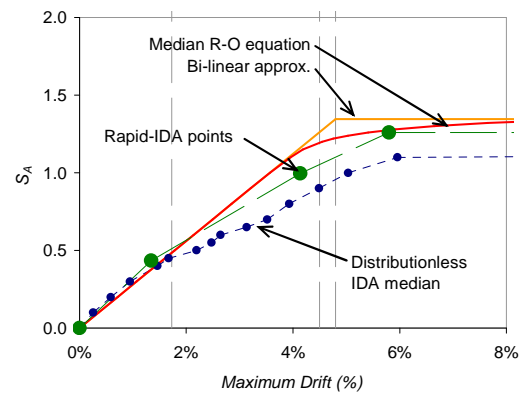
(a)



(b)



(c)



(d)

Figure 3-9: Observed differences between probabilistic seismic vulnerability methodology and rapid-IDA methodology

CLOSURE

Thesis Summary

The aim of this research was to develop and validate a design and assessment methodology for the next generation of damage avoidance design (DAD) frames. Improvements were made to the design methodologies proposed by Arnold (2004) and Davies (2003) to remove some of the inconsistencies observed between the design of the gravity and non-gravity load carrying frames. Assessment of the design is carried out by a probabilistic seismic vulnerability assessment methodology, which clearly illustrates all steps in the process of determining the expected annualised seismic loss (EAL). A large number of non-linear time-history analyses were carried out which indicate the displaced shape of the frame observed during the analyses is the same as the design displacement profile.

Two variations of the seismic vulnerability methodology were presented. The first method is based in incremental dynamic analysis (IDA). IDA was found to be time-consuming since it requires a large number of non-linear time-history analyses. The second method is a rapid-IDA approach which was developed from a static pushover analysis of the structure. Rapid-IDA implementation is a straightforward hand analysis.

Four DAD frames were successfully analysed during this research. The first two DAD frames were existing ten storey frames designed by Arnold (2004) and Davies (2003) in the gravity and non-gravity load carrying directions respectively. EAL for these frames calculated via the IDA-based methodology were found to be \$63 and \$110 per million dollars building value respectively. For comparison with state-of-practice ductile monolithic reinforced concrete construction, a ten storey conventional reinforced concrete frame was analysed, for which EAL was found to be \$2900 per million dollars building

value. Comparison of the EAL between the DAD and state-of-practice buildings clearly shows superior performance of the DAD frames.

The latter two DAD frames analysed were orthogonal frames from a proposed six storey apartment building, and EAL was estimated by the IDA based method and the rapid-IDA method. EAL for these frames was found to be \$77 and \$97 per million dollars building value via the IDA-based methodology, respectively, and \$132 and \$111 per million dollars building value via the rapid-IDA methodology, respectively. It was observed that the rapid-IDA estimates of EAL both fall within the 90% confidence interval for the EAL obtained via the IDA-based methodology. This result justifies the two proposed methodologies.

Recommendations for Further Research

Based on the research presented in this thesis, further research should be undertaken in the following areas:

Relating to the seismic vulnerability methodologies:

- Formal sensitivity analysis found the seismic hazard parameter significantly contributes to overall uncertainty of EAL. For these analyses the spectral acceleration at a period of 1 second obtained from the New Zealand Loadings Code (NZS 4203:1992) was used to define the seismic hazard at a return period of 475 years. This parameter is determined based on the structure location and one of three soil types. To improve the accuracy of EAL, the seismic hazard needs to be more carefully evaluated.
- The seismic hazard recurrence relationship, from which resilience curves can easily be determined, is a power-law curve extrapolated well beyond the range of

data given in NZS 4203:1992. Further research into the seismic hazard for low magnitude, highly frequent events and large magnitude, low frequency events is required to improve this relationship. Alternatively, the arrival of earthquake events could be considered as a Poisson process.

- Repetition of IDA with different suites of earthquakes that reflect a combination of near and far field effects as well as different levels of Richter magnitude (energy levels). Such analyses could be further used to validate the rapid-IDA methodology.

Relating to the design and behaviour of the DAD frames:

- The return periods for which there is a 90% survival probability of toppling of the DAD frames are significantly larger than the currently accepted maximum considered earthquake (MCE). This indicates taking $\phi = 0.7$, as suggested by Shama and Mander (2003), tends to suggest undue conservatism. Further consideration of desirable performance targets and analysis for the calibration of this factor is suggested.
- Non-linear time-history analysis of the DAD frames was carried out by approximating the rocking joint behaviour with a number of moment-rotation springs in parallel to obtain the theoretical hysteretic response, and neglecting beam-elongation effects. It is suggested that these analyses are repeated using a more highly refined rocking joint model that considers beam-elongation effects. Incorporation of other effects such as loss of prestress which occurs following yield of the tendons and low-cycle fatigue and fracture of energy dissipators, which were neglected in these analyses could also be considered.

- All non-linear time-history analyses presented in this thesis were carried out in two dimensions. Three dimensional non-linear time-history analysis of a complete building system is recommended to investigate possible torsional effects.
- Further research into the topology and behaviour of the beams in the upper levels of the structure is required, to determine the cause of, and prevent excessive beam moments developing in the upper levels when the lower beam joints open.

REFERENCES

- Abul Hamid, N.Y. (2006) ?. PhD Thesis, Department of Civil Engineering, University of Canterbury, Christchurch, New Zealand. *in preparation*.
- Arnold, D.M. (2004) Development and Experimental Testing of a Seismic Damage Avoidance Designed Beam to Column Connection Utilising Draped Unbonded Post-Tensioning. ME Thesis, Department of Civil Engineering, University of Canterbury, Christchurch, New Zealand.
- Bendimerad, F. (2001) Loss estimation: a powerful tool for risk assessment and mitigation. *Soil Dynamics and Earthquake Engineering*, **21**(5), 467-472.
- Bertero, V.V. (1980) 'Strength and Deformation Capacities of Buildings Under Extreme Environments'. In: *Structural Engineering and Structural Mechanics: A Volume Honouring Egor P. Popov*. Ed: K.S. Pister. Prentice Hall, Englewood Cliffs, NJ. pp 188-237.
- Carr, A.J. (2005) *Ruaumoko Computer Programme Manual*. Department of Civil Engineering, University of Canterbury, Christchurch, New Zealand.
- Cement and Concrete Association of New Zealand (CCANZ) (1998) *Examples of Concrete Structural Design to NZS 3101:1995 – "Red Book"*. Cement and Concrete Association of New Zealand, Wellington.
- Chopra, A.K. (1995) *Dynamics of Structures: Theory and Applications to Earthquake Engineering*. Prentice-Hall, New Jersey.
- Christopoulos, C., Filiatrault, A. and Folz, B. (2002) Seismic response of self-centring hysteretic SDOF systems. *Earthquake Engineering and Structural Dynamics*, **31**(5), 1131-1150.
- Christopoulos, C., Filiatrault, A., Uang, C.-M. and Folz, B. (2002) Post-tensioned Energy Dissipating Connections for Moment-Resisting Steel Frames. *Journal of Structural Engineering*, **128**(9), 1111-1120.

- Christopoulos, C., Pampanin, S. and Priestley, M.J.N. (2003) Performance-Based Seismic Response of Frame Structures Including Residual Deformations. Part I: Single-Degree of Freedom Systems. *Journal of Earthquake Engineering*, **7**(1), 97-118.
- Davies, M.N. (2003) Seismic Damage Avoidance Design on Beam-Column Joints Using Unbonded Post-Tensioning: Theory, Experiments and Design Example. ME Thesis, Department of Civil Engineering, University of Canterbury, Christchurch, New Zealand.
- Dhakal, R.P. and Mander, J.B. (2005) Probabilistic Risk Assessment Methodology Framework for Natural Hazards. Final Report submitted to Institute of Geological and Nuclear Science.
- Dutta A. and Mander J. B. (1998) “*Capacity design and fatigue analysis of confined concrete columns*”. Tech. Rep. MCEER-98-0007, Multidisciplinary Center for Earthquake Engineering. State University of New York at Buffalo, Buffalo, NY.
- Dutta, A. (1999) On Energy-Based Seismic Analysis and Design on Highway Bridges. PhD Dissertation, Department of Civil, Structural and Environmental Engineering, State University of New York at Buffalo, Buffalo, NY, USA.
- Elms, D.G. (1985) ‘The Principle of Consistent Crudeness’. In: *Proceedings of NSF Workshop on Civil Engineering Applications of Fuzzy Sets*. Eds: C.B. Brown, J.-L. Chameau, R.N. Palmer and J.T.P. Yao. Purdue University, West Lafayette, IN. pp 35-44.
- Elms, D.G. (2004) Structural safety – issues and progress. *Progress in Structural Engineering and Materials*, **6**(2), 116-126.
- El-Sheikh, M.T., Sause, R., Pessiki, S. and Lu, L.-W. (1999) Seismic Behaviour and Design of unbonded Post-Tensioned Precast Concrete Frames. *PCI Journal*, **44**(3), 54-71.
- Englekirk, R.E. (2002) Design-Construction of The Paramount – A 39-Story Precast Prestressed Concrete Apartment Building. *PCI Journal*, **47**(4), 56-71.

- Erberik, M.A. and Elnashai, A.S. (2004) Fragility analysis of flat-slab structures. *Engineering Structures*, **26**(7), 937-948.
- Eschenbach, T.G. (1992) Spiderplots versus Tornado Diagrams for Sensitivity Analysis. *Interfaces*, **22**(6) 40-46.
- Federal Emergency Management Agency (FEMA) (2003) HAZUS-MH MR1 Advanced Engineering Building Module: Technical and User's Manual. FEMA.
- FEMA 273 (1997) NEHRP Guidelines for the Seismic Rehabilitation of Buildings. Federal Emergency Management Agency, Washington.
- Fülöp, L.A., and Dubina, D. (2004) Performance of wall-stud cold-formed shear panels under monotonic and cyclic loading. Part II: Numerical modelling and performance analysis. *Thin-Walled Structures*, **42**(2), 339-349.
- Garlock, M.M., Ricles, J.M. and Sause, R. (2005) Experimental Studies of Full-Scale Posttensioned Steel Connections. *Journal of Structural Engineering*, **131**(3), 438-448.
- Karim, K.R. and Yamazaki, F. (2001) Effect of earthquake ground motions on fragility curves of highway bridge piers based on numerical simulation. *Earthquake Engineering and Structural Dynamics*, **30**(12), 1839-1856.
- Kennedy, R.P., Cornell, C.A., Campbell, R.D., Kaplan, S. and Perla, H.F. (1980) Probabilistic Seismic Safety Study of an Existing Nuclear Power Plant. *Nuclear Engineering and Design*, **59**(2), 315-338.
- Kircher, C.A., Nassar, A.A., Kustu, O. and Holmes, W.T. (1997) Development of Building Damage Functions for Earthquake Loss Estimation. *Earthquake Spectra*, **13**(4), 663-682
- Kiremidjian, A.A. and Basöz, N. (1997) Evaluation of Bridge Damage Data from Recent Earthquakes. *NCEER Bulletin*, **11**(2), 1-7.
- Krawinkler, H. and Miranda, E. (2004) 'Performance-Based Earthquake Engineering'. In: *Earthquake Engineering: From Engineering Seismology to Performance-Based*

Engineering. Eds: Y. Bozorgnia and V.V Bertero. CRC Press, Boca Raton, FL. Chapter 9.

- Krawinkler, H., Medina, R. and Alavi, B. (2003) Seismic drift and ductility demands and their dependence on ground motions. *Engineering Structures*, **25**(5), 637-653.
- Lang, K. and Bachmann, H. (2004) On the Seismic Vulnerability of Existing Buildings: A Case Study of the City of Basel. *Earthquake Spectra*, **20**(1), 43-66.
- Lin, Y.-Y. and Chang, K.-C. (2004) Effects of Site Classes on Damping Reduction Factors. *Journal of Structural Engineering*, **130**(11), 1667-1675.
- Lin, Y.-Y., Miranda, E. and Chang, K.-C. (2005) Evaluation of damping reduction factors for estimating elastic response of structures with high damping. *Earthquake Engineering and Structural Dynamics*, **34**(11), 1427-1443.
- Luco, N. and Cornell, C.A. (1998) Effects of Random Connection Fractures on the Demands and Reliability for a 3-Story Pre-Northridge SMRF Structure. Proceedings 6th US Conference on Earthquake Engineering. 31 May – 4 June. Seattle, WA. Paper 224.
- Mander J.B., and Basöz N. (1999) ‘Seismic Fragility Curve Theory for Highway Bridges in Transportation Lifeline Loss Estimation’. In: *Optimizing Post-Earthquake Lifeline System Reliability*, Eds: Elliot and McDonough. TCLEE Monograph No. 16, ASCE. pp 31-40.
- Mander, J.B. (2004) Beyond Ductility: The Quest Goes On. *Bulletin of the New Zealand Society of Earthquake Engineering*, **37**(1), 35-44.
- Mander, J.B. and Cheng, C.-T. (1997) *Seismic Resistance of Bridge Piers Based on Damage Avoidance Design*. Technical Report NCEER-97-0014, Department of Civil, Structural and Environmental Engineering, State University of New York at Buffalo, Buffalo, NY, USA.
- Martínez, M.E. (2002) Performance-Based Seismic Design and Probabilistic Assessment of Reinforced Concrete Moment Resisting Frame Structures. ME Thesis,

Department of Civil Engineering, University of Canterbury, Christchurch, New Zealand.

- Murahidy, A.G. (2004) Design, Construction, Dynamic Testing and Computer Modelling of a Precast Prestressed Reinforced Concrete Frame Building with Rocking Beam-Column Connections and ADAS Elements. ME Thesis, Department of Civil Engineering, University of Canterbury, Christchurch, New Zealand.
- Mwafy, A.M., and Elnashai, A.S. (2001) Static pushover versus dynamic collapse analysis of RC buildings. *Engineering Structures*, **23**(5), 407-424.
- Newmark, N.M. and Hall, W.J. (1982) Earthquake Spectra and Design. EERI Monograph Series. Earthquake Engineering Research Institute, Oakland, CA.
- Pampanin, S., Priestley, M.J.N. and Sritharan, S. (2001) Analytical Modelling of the Seismic Behavior of Precast Concrete Frames Designed with Ductile Connections. *Journal of Earthquake Engineering*, **5**(3), 329-367.
- Pekcan, G., Mander, J.B. and Chen, S.S. (1999) Fundamental considerations for the design of non-linear viscous dampers. *Earthquake Engineering and Structural Dynamics*, **28**(11), 1405-1425.
- Pekcan, G. (1998) Design of Seismic Energy Dissipation Systems for Reinforced Concrete and Steel Structures. PhD Dissertation, Department of Civil, Structural and Environmental Engineering, State University of New York at Buffalo, Buffalo, NY, USA.
- Porter, K.A. (2003) 'Seismic Vulnerability'. In: *Earthquake Engineering Handbook*. Eds: W.-F. Chen and C. Scawthorn. CRC Press, Boca Raton, FL. Chapter 21.
- Porter, K.A., Beck, J.L and Shaikhutdinov, R.V. (2004) Simplified Estimation of Economic Seismic Risk for Buildings. *Earthquake Spectra*, **20**(4), 1239-1263.
- Porter, K.A., Beck, J.L. and Shaikhutdinov, R.V. (2002) Sensitivity of Building Loss Estimates to Major Uncertain Variables. *Earthquake Spectra*, **18**(4), 719-743.

- Porter, K.A., Kiremidjian, A.S. and LeGrue, J.S. (2001) Assembly-Based Vulnerability of Buildings and Its Use in Performance Evaluation. *Earthquake Spectra*, **17**(2), 291-312.
- Prakash, V., Powell, G. and Campbell, S. (1993) *DRAIN-2DX Base Program Description and User Guide; Version 1.10*. Report No. UCB/SEMM-93/17 & 18, Structural Engineering Mechanics and Materials, Department of Civil Engineering, University of California, Berkeley, CA.
- Priestley, M.J.N. and MacRae, G.A. (1996) Seismic Tests of Precast Beam-to-Column Connections With Unbonded Tendons. *PCI Journal*, **41**(1), 64-81.
- Priestley, M.J.N. and Tao, J.R. (1993) Seismic Response of Precast Prestressed Concrete Frames With Partially Unbonded Tendons. *PCI Journal*, **38**(1), 58-69.
- Priestley, M.J.N., Sritharan, S., Conley, J.R. and Pampanin, S. (1999) Preliminary Results and Conclusions from the PRESSS Five-Story Precast Concrete Test Building. *PCI Journal*, **44**(6), 42-67.
- Rahardjo, T. (2004) Experiments and stochastic modelling of New Zealand grown *Pinus radiata* timber and timber piles under seismic loading. ME Thesis, Department of Civil Engineering, University of Canterbury, Christchurch, New Zealand.
- Reinhorn, A. (1997) 'Inelastic analysis techniques in seismic evaluations'. In: *Seismic Design Methodologies for the next generation of codes*, Proceeding of International Conference in Bled, Slovenia. Balkema Publishers, Rotterdam. 277-297.
- Ricles, J.M., Sause, R., Garlock, M.M. and Zhao, C. (2001) Posttensioned Seismic-Resistant Connections for Steel Frames. *Journal of Structural Engineering*, **127**(2), 113-121.
- Rojas, P., Garlock, M.M., Ricles, J.M. and Sause, R. (2002) Reducing Seismic Damage in Steel Frames Using Post-Tensioning. Proceedings Seventh U.S. National Conference on Earthquake Engineering (Boston, MA), 21-25 July. pp 4115-4124.

- Rosowsky, D.V. and Ellingwood, B.R. (2002) Performance-Based Engineering of Wood Frame Housing: Fragility Analysis Methodology. *Journal of Structural Engineering*, **128**(1), 32-38.
- Shama, A.A. and Mander, J.B. (2003) The seismic performance of braced timber pile bents. *Earthquake Engineering and Structural Dynamics*, **32**(3), 463-482.
- Shinozuka, M., Feng, M.Q., Lee, J. and Naganuma, T. (2000) Statistical Analysis of Fragility Curves. *Journal of Engineering Mechanics*, **126**(12), 1224-1231.
- Shome, N., Cornell, C.A., Bazzurro, P. and Carballo, J.E. (1998) Earthquakes, Records, and Nonlinear Responses. *Earthquake Spectra*, **14**(3), 469-500.
- Singhal, A. and Kiremidjian, A.S. (1996) Method for Probabilistic Evaluation of Seismic Structural Damage. *Journal of Structural Engineering*, **122**(12), 1459-1467.
- Smyth, A.W., Altay, G., Deodatis, G., Erdik, M., Franco, G., Gülkan, P., Kunreuther, H., Luş, H., Mete, E., Seeber, N. and Yüzügüllü, Ö. (2004) Probabilistic Benefit-Cost Analysis for Earthquake Damage Mitigation: Evaluating Measures for Apartment Houses in Turkey. *Earthquake Spectra*, **20**(1), 171-203.
- Solberg, K. (2006) ?. ME Thesis, Department of Civil Engineering, University of Canterbury, Christchurch, New Zealand. *in preparation*.
- Spieth, H.A., Arnold, D., Davies, M., Mander, J.B. and Carr, A.J. (2004a) Seismic Performance of Post-Tensioned Precast Concrete Beam to Column Connections with Supplementary Energy Dissipation. Proceedings New Zealand Society for Earthquake Engineering Conference (Rotorua), 19-21 March. Paper 15.
- Spieth, H.A., Carr, A.J., Murahidy, A.G., Arnold, D., Davies, M. and Mander, J.B. (2004b) Modelling of Post-Tensioned Precast Reinforced Concrete Frame Structures with Rocking Beam-Column Connections. Proceedings New Zealand Society for Earthquake Engineering Conference (Rotorua), 19-21 March. Paper 32.
- Standards New Zealand (1992) *Code of Practice for General Structural Design and Design Loadings for Buildings, known as the Loadings Code*, NZS 4203:1992, Volumes 1 and 2. Standards New Zealand, Wellington, New Zealand.

- Standards New Zealand (1995) *Concrete Structures Standard*, known as the Concrete Code, NZS 3101:1995, Volumes 1 and 2. Standards New Zealand, Wellington, New Zealand.
- Stanton, J., Stone, W.C. and Cheok, G.S. (1997) A Hybrid Reinforced Precast Frame for Seismic Regions. *PCI Journal*, **42**(2), 20-32.
- Vamvatsikos, D. (2002) Seismic Performance, Capacity and Reliability of Structures as seen through Incremental Dynamic Analysis. PhD Dissertation, Department of Civil and Environmental Engineering, Stanford University, CA.
- Vamvatsikos, D. and Cornell, C.A. (2002) Incremental dynamic analysis. *Earthquake Engineering and Structural Dynamics*, **31**(3), 491-514.
- Vamvatsikos, D. and Cornell, C.A. (2004) Applied Incremental Dynamic Analysis. *Earthquake Spectra*, **20**(2), 523-553.
- Vamvatsikos, D. and Cornell, C.A. (2005) Direct Estimation of Seismic Demand and Capacity of Multidegree-of-Freedom Systems through Incremental Dynamic Analysis of Single Degree of Freedom Approximation. *Journal of Structural Engineering*, **131**(4), 589-599.
- Whitman, R.V., Anagnos, T., Kircher, C.A., Lagorio, H.J., Lawson, R.C. and Schneider, P. (1997) Development of a National Earthquake Loss Estimation Methodology. *Earthquake Spectra*, **13**(4), 643-661.
- Yamazaki, F., Motomura, H. and Hamada, T. (2000) Damage Assessment of Expressway Networks in Japan based on Seismic Monitoring. Proceedings 12th World Conference on Earthquake Engineering (Auckland, New Zealand), 30 January – 4 February. Paper 0551.

APPENDIX A

MATHEMATICAL DERIVATION OF FRAGILITY AND RESILIENCE CURVES

It can be seen in Figure 1-3(b), repeated as Figure A-1 below, that as the r parameter of the R-O equation increases, the R-O curve tends towards a bi-linear curve. This property of the R-O curves shall be utilised to derive the mathematical basis of the fragility and resilience curves.

The bi-linear approximation to the R-O function can be expressed as:

$$EDP = \begin{cases} IM/K & 0 \leq IM \leq IM_c \\ \infty & IM > IM_c \end{cases} \quad (A-1)$$

It can be shown the bi-linear approximation to the R-O curve is a very good approximation, as the only significant deviation from the bi-linear curve occur when IM is close to IM_c .

Well known work by Kennedy et al (1980), has demonstrated that if independent lognormal distributed random variables are combined as:

$$d = \frac{a^r b^s}{c^t} q \quad (A-2)$$

in which a , b and c are random variables and r , s and t are constants, it is possible to define, by applying the central limit theorem, a new lognormal function with median given by:

$$\tilde{d} = \frac{\tilde{a}^r \tilde{b}^s}{\tilde{c}^t} \tilde{q} \quad (A-3)$$

and logarithmic standard deviation given by:

$$\beta_d = \sqrt{r^2 \beta_a^2 + s^2 \beta_b^2 + t^2 \beta_c^2} \quad (A-4)$$

where β_i = logarithmic standard deviations of the variables a, b and c.

Fragility Curves

Equation (A-1) can be rearranged to obtain the median IM for each damage state (DS), \tilde{IM}_{DSi} associated with reaching a given EDP:

$$\tilde{IM}_{DSi} = \tilde{EDP}_{DSi} \tilde{K} \quad (A-5)$$

where \tilde{EDP}_{DSi} would typically denote the median threshold EDP for its corresponding damage state. This approach can be used to determine the median IM for DS2, DS3 and DS4 on a fragility curve. The dispersion associated with IM_{DSi} , $\beta_{IM_{DSi}}$, can be expressed as

$$\beta_{IM_{DSi}} = \sqrt{\beta_{EDP_{DSi}}^2 + \beta_K^2} \quad (A-6)$$

where $\beta_{EDP_{DSi}}$ accounts for the randomness and uncertainty in the threshold EDP value between adjacent damage states; and β_K is the dispersion associated with parameter K , obtained from the preceding IDA analysis.

The onset of DS5 is conventionally assigned as the boundary between irreparable damage and partial or total collapse of the structure. Conveniently this is defined by onset of the flatline portion of the bi-linear curve. The height of the flatline of the curve occurs at:

$$\tilde{IM}_{DS5} = IM_C \quad (A-7)$$

Therefore, the median IM of collapse of the structure can be found with equation (A-1), and the threshold EDP for DS5 is determined as \tilde{EDP}_C from the preceding IDA analysis.

The dispersion associated with $\tilde{IM}_{collapse}$, $\beta_{IM_{collapse}}$, is given by

$$\beta_{IM_{DS5}} = \sqrt{\beta_{IM_C}^2} = \beta_{IM_C} \quad (A-8)$$

To avoid overlapping of the fragility curves at high and low confidence levels, β_{IM} is taken as the larger of $\beta_{IM_{DSi}}$ and $\beta_{IM_{DS5}}$ for all curves. This method has been used to plot the fragility curves in Figure 1-4(a).

Resilience Curves

The seismic hazard curve, relating the annual frequency of an event to its corresponding IM is defined as:

$$\lambda_T = \frac{IM(T = Tr)}{IM(T = 475)} = \left(\frac{Tr}{475}\right)^q = (475 p_a)^{-q} \quad (A-9)$$

where equation (A-9) is equation (1-2) repeated. By combining this equation with equation (A-1) the median annual frequency of reaching a given inter-storey drift can be obtained:

$$\tilde{P}_{a(DSi)} = \frac{1}{475} \left[\frac{IM(Tr = 475)}{EDP_{DSi} \tilde{K}} \right]^{1/q} \quad (A-10)$$

This approach can be used to determine the median probability of exceeding DS1, DS2 and DS3. The dispersion associated with $p_{a(DSi)}$, $\beta_{p_{a(DSi)}}$, can be expressed as

$$\beta_{p_{a(DSi)}} = \sqrt{\left(\frac{1}{q}\right)^2 \beta_{EDP_{DSi}}^2 + \left(\frac{1}{q}\right)^2 \beta_K^2} \quad (A-11)$$

The median annual probability of collapse of the structure (exceeding DS4) can be found by substituting equation (A-9) into equation (A-7) to give:

$$\tilde{p}_{a(DS5)} = \frac{1}{475} \left[\frac{IM(Tr = 475)}{\tilde{M}_c} \right]^{1/q} \quad (A-12)$$

and the dispersion associated with $\tilde{p}_{a(collapse)}$, $\beta_{p_{a(collapse)}}$, is given by

$$\beta_{p_{a(DS5)}} = \sqrt{\left(\frac{1}{q}\right)^2 \beta_{IM_c}^2} = \frac{\beta_{IM_c}}{q} \quad (A-13)$$

To avoid overlapping of the resilience curves at high and low confidence levels, β_{p_a} is taken as the maximum of $\beta_{p_{a(DS4)}}$ and $\beta_{p_{a(DS5)}}$ for all curves. This method has been used to plot the resilience curves in Figure 1-4(c).

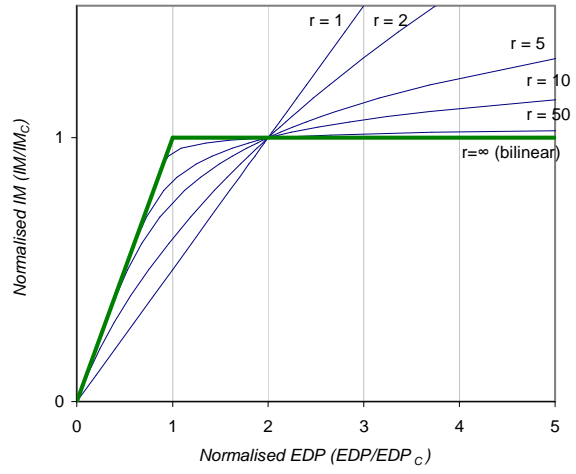


Figure A-1: Ramberg-Osgood curve parameters

APPENDIX B

DETAILS OF RAPID PUSHOVER METHOD

Figure B-1 shows the general plastic mechanism for a ten storey frame, being a combination of a column and beam sidesway mechanism. The general mechanism for a structure of N_s storeys is defined by the number of storeys participating in the plastic mechanism, n_{sp} . The correct number of storeys participating in the plastic mechanism, n_{sp} is found by energy minimisation.

External Work Done

The external lateral force vector is assumed to be proportional to the displaced shape of the structure, as illustrated in Figure B-1. The external work done due to the assumed lateral force vector is given the summation of the lateral forces multiplied by the lateral displacements:

$$EWD = \sum_{i=1}^{N_s} H_i \Delta_i \quad (B-1)$$

where H_i and Δ_i are the lateral force and displacement respectively at level i of the structure, and N_s is the number of storeys in the frame. Note that the base shear, V_{base} is calculated as:

$$V_{base} = \sum_{i=1}^{N_s} H_i \quad (B-2)$$

The lateral displacement at each level of the mechanism can be defined in terms of the column rotation, thus the external work is given by:

$$EWD = V_{base} \theta_c h_s \frac{\sum_{i=1}^{n_{sp}} i^2 + n_{sp}^2 (N_s - n_{sp})}{\sum i + N_s n_{sp} - n_{sp}^2} \quad (B-3)$$

where θ_c is the column rotation and h_s is the interstorey height of the frame.

Internal Work Done

The internal work done for the frame is given by the summation of the plastic hinge moments multiplied by the hinge rotations:

$$IWD = \sum M_{pc} \theta_c + \sum M_{pb} \theta_b \quad (B-4)$$

where M_{pc} and θ_c are the plastic moment capacity of the column and rotation of the columns, respectively, and M_{pb} and θ_b are the plastic moment capacity of the column and rotation of the beams, respectively.

The beam hinge rotation can be related to the column rotation through the geometry of the system, giving:

$$\theta_b = \frac{L}{L_{beam}} \theta_c \quad (B-5)$$

where L is the beam span measured between column centrelines and L_{beam} is the distance between the beam plastic hinges. For the damage avoidance design frames, L_{beam} is the distance between the rocking interfaces ('drop-in' beam length).

Assuming the same beam moment capacity is provided at each storey level, a column overstrength factor, relating the moment capacity of the columns to the moment capacity of the beams, can be defined as:

$$\lambda_{col} = \frac{M_{pc}}{M_{pb}} \quad (B-6)$$

Therefore, by combining equations (B-4), (B-5) and (B-6), the internal work can be expressed as:

$$IWD = 2\lambda_{col}(n_b + 1)M_{pb} \theta_c + 2n_b(n_{sp} - 1)\frac{L}{L_{beam}}M_{pb} \theta_c \quad (B-7)$$

Equate Expressions for Internal Work and External Work

By equating equations (B-3) and (B-7), and rearranging, the base shear can be expressed as a function of beam moment capacity:

$$V_{base} = \frac{\sum_{i=1}^{n_{sp}} i + N_s n_{sp} - n_{sp}^2}{\sum_{i=1}^{n_{sp}} i^2 + n_{sp}^2 (N_s - n_{sp})} \frac{\left[2\lambda(n_b + 1) + 2n_b(n_{sp} - 1)\frac{L}{L_{beam}} \right]}{h_s} M_{pb} \quad (B-8)$$

This expression can be simplified by introducing a factor, κ , relating the base shear to the beam moment capacity defined as:

$$\kappa = \frac{V_{base}}{M_{pb}} = \frac{\sum_{i=1}^{n_{sp}} i + N_s n_{sp} - n_{sp}^2}{\sum_{i=1}^{n_{sp}} i^2 + n_{sp}^2 (N_s - n_{sp})} \frac{\left[2\lambda(n_b + 1) + 2n_b(n_{sp} - 1)\frac{L}{L_{beam}} \right]}{h_s} \quad (B-9)$$

Therefore κ can be evaluated for all possible n_{sp} , as illustrated in as illustrated in Figure B-2, for the seismic only frame presented by Davies (2003). The correct number of storeys participating in the mechanism is identified from the minimum value of κ , thus the base shear can be expressed as:

$$V_{base} = \kappa M_{pb} \quad (B-10)$$

Transformation Factors for Equivalent SDOF System

The acceleration capacity and displacement of an equivalent single degree of freedom system (SDOF) are given by the following equations:

$$C_c^* = \frac{C_c}{\alpha_A} = \frac{V_{base}}{W \alpha_A} = \frac{\kappa M_{pb}}{W \alpha_A} \quad (B-11)$$

$$\Delta^* = \frac{\Delta_{top}}{\alpha_D} \quad (B-12)$$

in which C_c^* and Δ^* are the acceleration capacity and displacement of an equivalent SDOF system, C_c is the acceleration capacity of the structure, W is the total seismic weight of the structure, Δ_{top} is the top storey displacement of the mechanism, and α_A and α_D are the acceleration and displacement transformation factors, respectively.

The acceleration and displacement transformation factors can be evaluated as:

$$\alpha_A = \frac{m_i \left[(N_s - n_{sp}) + \sum_{i=1}^{n_{sp}} \frac{i}{n_{sp}} \right]^2}{\sum_{i=1}^{N_s} m_i (N_s - n_{sp}) + \sum_{i=1}^{n_{sp}} \left(\frac{i}{n_{sp}} \right)^2} \quad (B-13)$$

$$\alpha_D = \frac{(N_s - n_{sp}) + \sum_{i=1}^{n_{sp}} \frac{i}{n_{sp}}}{(N_s - n_{sp}) + \sum_{i=1}^{n_{sp}} \left(\frac{i}{n_{sp}}\right)^2} \quad (B-14)$$

in which m_i is the mass associated with level i . These equations were derived in this form by Martínez (2002) for elasto-plastic structural systems, and are based on well known work presented by Chopra (1995) and Reinhorn (1997) and incorporated in FEMA 273 (1997).

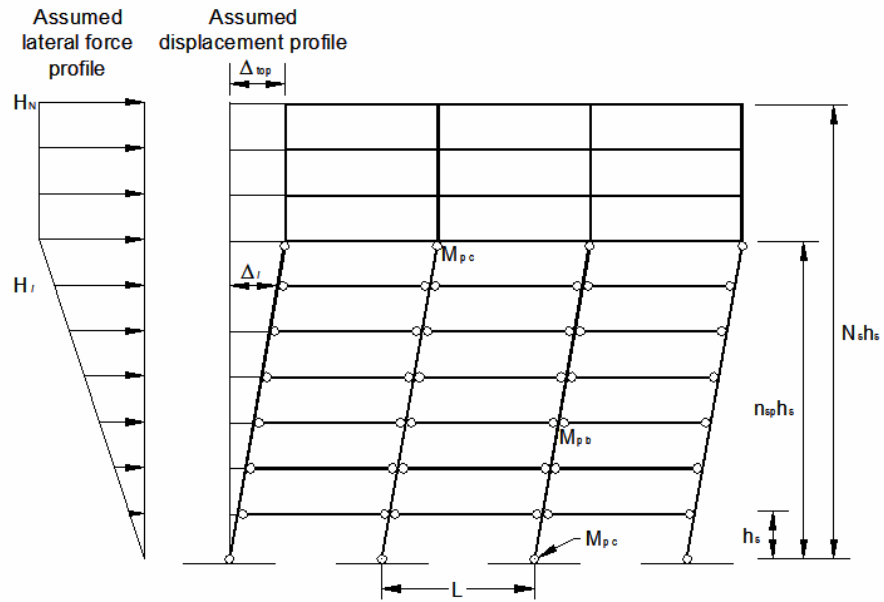


Figure B-1: General collapse mechanism of lateral resisting frame (adapted from Davies, 2003)

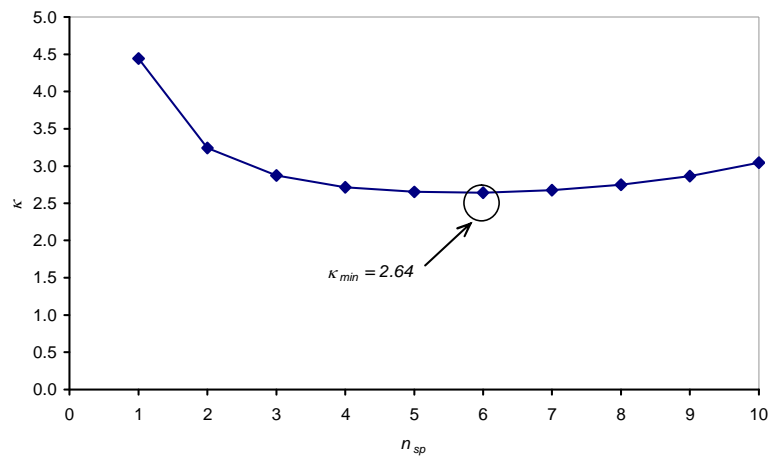


Figure B-2: Base shear force evaluation from plastic mechanism analysis (adapted from Davies, 2003)

APPENDIX C

SOME OBSERVATIONS OF THE DYNAMIC BEHAVIOUR OF THE TEN STOREY CONVENTIONAL AND DAMAGE AVOIDANCE DESIGN FRAMES

C.1 MODE SHAPES AND PERIODS OF VIBRATION

The first three mode shapes for each of the three frames analysed in Chapter Two, obtained from a modal analysis carried out by *RUAUMOKO-2D*, are presented in Figure C-1. The mode shapes and periods of vibration are presented for both the DAD frames with both rocking beam and column joints closed (ie. the elastically responding structure) and open. The mode shapes for all three elastically responding structures are very similar, also, the mode shapes for the DAD frames, once the joints have opened are similar.

Previous non-linear time-history studies of conventional ductile reinforced concrete frames have shown it is uncommon to observe beam plastic hinges forming throughout the frame at the same time. Rather it is observed that plastic hinges form progressively up the frame as the base shear developed from strong ground shaking travels up the frame. However, during the non-linear time-history analysis of the DAD frames, it was observed that the beam and column joints often opened and closed in very quick succession. Therefore, for reasonable lengths of the earthquake duration, when all the joints were open, the DAD frames had rather different modal properties, and hence the mode shapes and periods of vibration for the DAD frames when the joints are open were investigated.

It is observed the first mode shape when the joints are open is very close to the shape of the mixed mechanism from the rapid pushover analysis. This observation is favourable, and it indicates the validity of the proposed design methodology.

C.2 IDENTIFICATION OF CRITICAL EARTHQUAKE GROUND MOTIONS

When carrying out a detailed examination of structural behaviour from non-linear time-history analysis using actual earthquake records, one is faced with the dilemma of choosing which ‘*critical*’ earthquake ground motion(s) should be selected from a suite of eligible candidate records. Incremental dynamic analysis (IDA) results are a useful basis for choosing appropriate earthquakes.

For further examination of the behaviour of the three frames presented in Chapter Two, earthquake ground motions are selected from the IDA curves corresponding to:

- 50th percentile response for DBE (intensity $S_A = 0.4 g$)
- 90th percentile response for DBE
- 50th percentile response for MCE (intensity $S_A = 0.7 g$)

By using such criteria for selection of earthquake ground motions for detailed analysis one can identify the probability of surviving certain damage states.

C.3 TIME-HISTORY DISPLACEMENT PROFILES

A selection of lateral displacement earthquake time-history analysis results are presented in Figures C-2 to C-10 for each of the three frames analysed in Chapter Two. The results presented correspond to the 50th percentile response and 90th percentile responses for DBE,

and the 50th percentile response for MCE. Some of the observations that can be drawn from these time-history analyses are listed below:

- Residual deformations are observed for the Red Book frame however the DAD frames display no residual deformation once the frame comes to rest.
- The displaced shape of the Red Book frame tends to be close to the six storey mixed mechanism obtained from the rapid pushover analysis, which indicates the validity of the rapid pushover method when applied to this particular frame.
- The displaced shape of the DAD frames is very close to the design mechanism at large displacements. Again, this result can be used to validate the applicability of the rapid pushover design method for these frames. At smaller displacements, higher mode effects are observed (eg. Figure C-8(a)), however as they only tend to occur at small displacements, they are reasonably insignificant.

The median and 90th percentile drifts for each level are plotted in Figure C-11 for each of the three frames analysed in Chapter Two. This figure shows that there is reduced drift in the upper levels of the DAD frames when compared to the Red Book frame. An advantage of this is that the structure will not sustain the same level of damage throughout its height. This phenomenon would also reduce non-structural damage in the upper levels of the structure, and could be exploited by keeping expensive or essential equipment on these levels.

C.4 VALIDITY OF MODELLING ASSUMPTIONS

For convenience it was assumed the beams in the upper levels of the DAD frames had the same properties, owing to the same reinforcing and prestress configuration, as those beams participating in the mechanism. This assumption can be soundly reasoned based on

construction simplicity, as all beams having the same reinforcing and prestress configuration simplifies the construction process and reduces the possibility for error.

The maximum beam joint moments, for both the upper and lower levels of the structure, along with the joint capacities are indicated in Figure C-12. This figure indicates that the maximum moments imposed on the upper level joints certainly cause the joints to open, and even exceed the joint capacity corresponding to yield of the prestress tendons. This result is problematic as it indicates damage would occur to the upper levels of the frames. Further examination of selected time-history analysis results indicates the moments in the upper levels of the structure exceed those of the lower levels of the structure when joint opening occurs.

Currently, no research has been conducted into the behaviour of the upper levels of the proposed DAD frames. While approximations in the modelling of the rocking beam and column joints may be exacerbating the observed maximum moments, these time-history results indicate further research is required to improve the behaviour of the storeys of the frame not participating in the mechanism. One suggestion is to construct the upper levels of the building in a similar fashion to the lower levels (however, joint armouring is not needed), but then use full prestress to the yield level. This would roughly double the joint moment opening capacity.

Throughout the analyses, beam-elongation effects have been neglected. It has been shown (Murahidy, 2004) that beam-elongation caused the opening of the joints causes strange effects to occur in the columns. As the base of the columns are restrained, excessive column shears will exist, particularly in the ground floor. Furthermore, lower prestress forces are expected in the upper levels when the beam-column joints open at lower levels. Further investigation, incorporating beam-elongation effects are required.

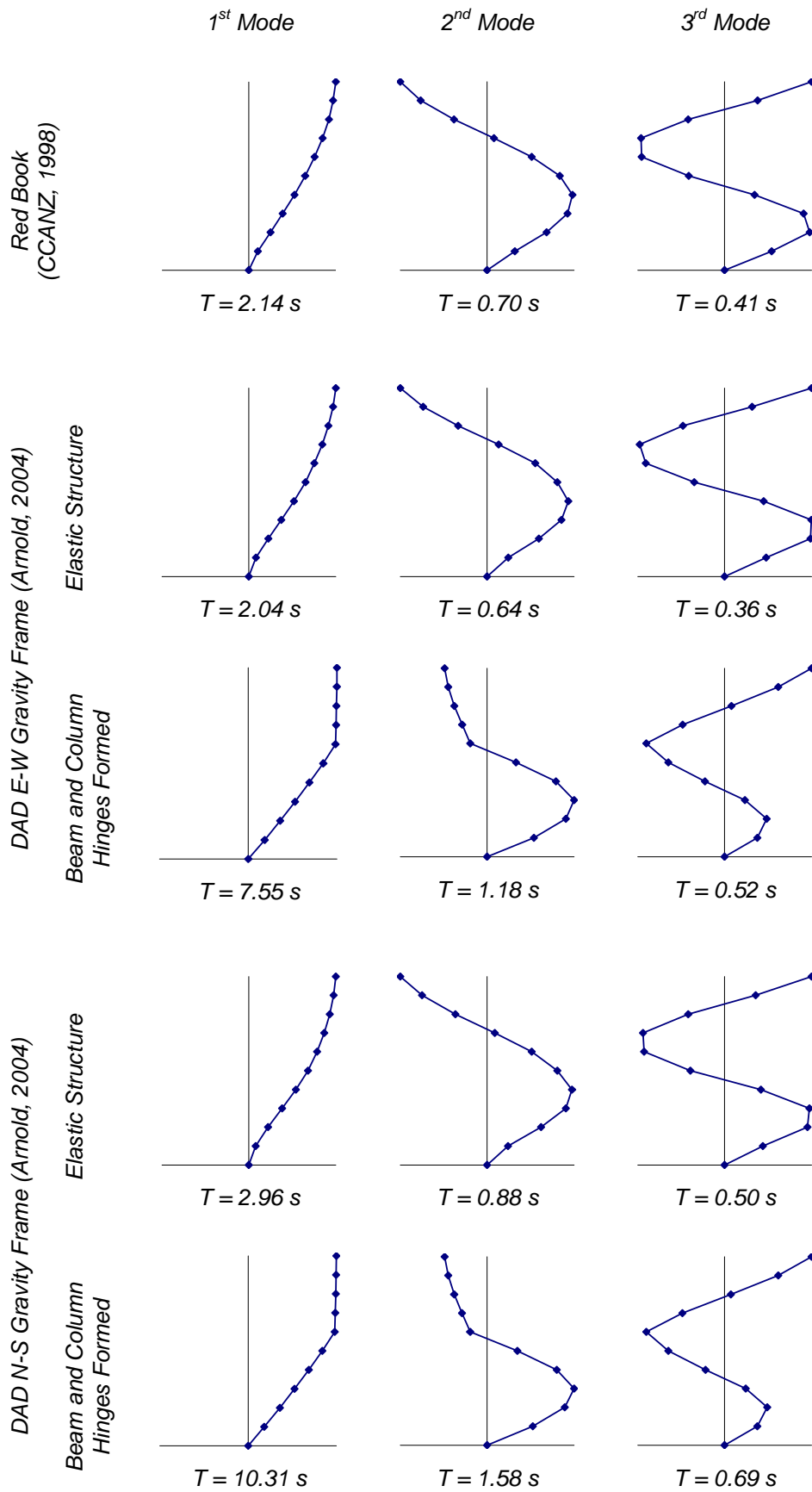
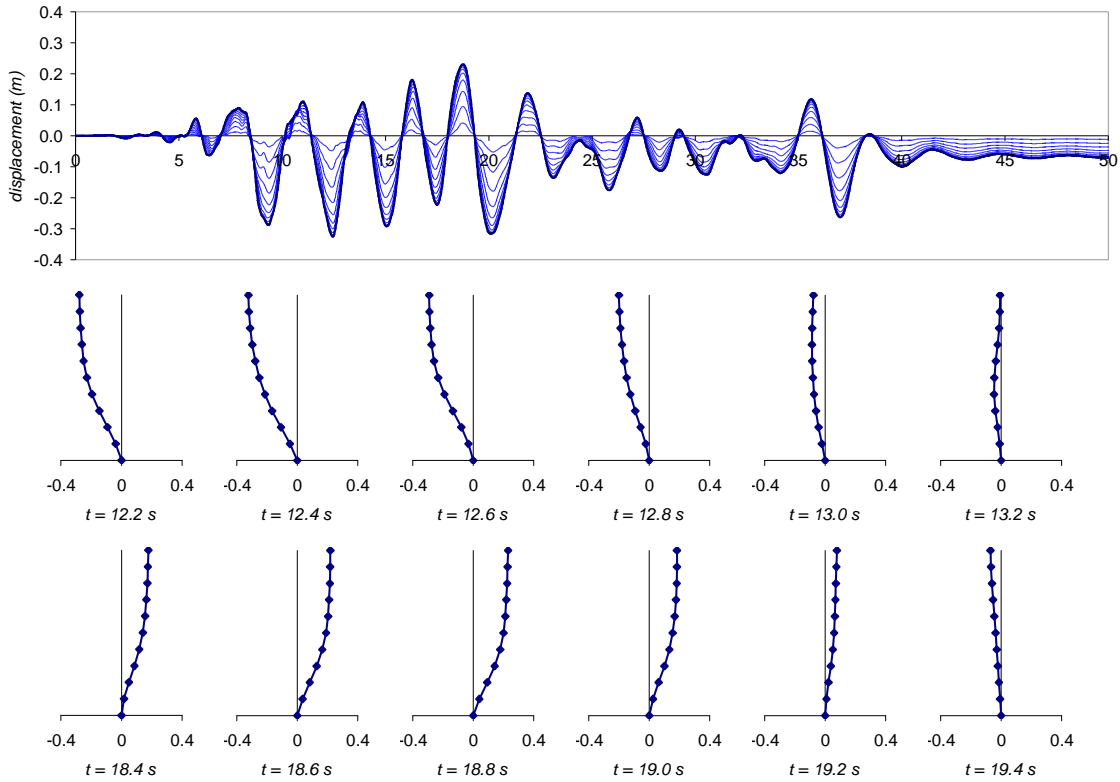
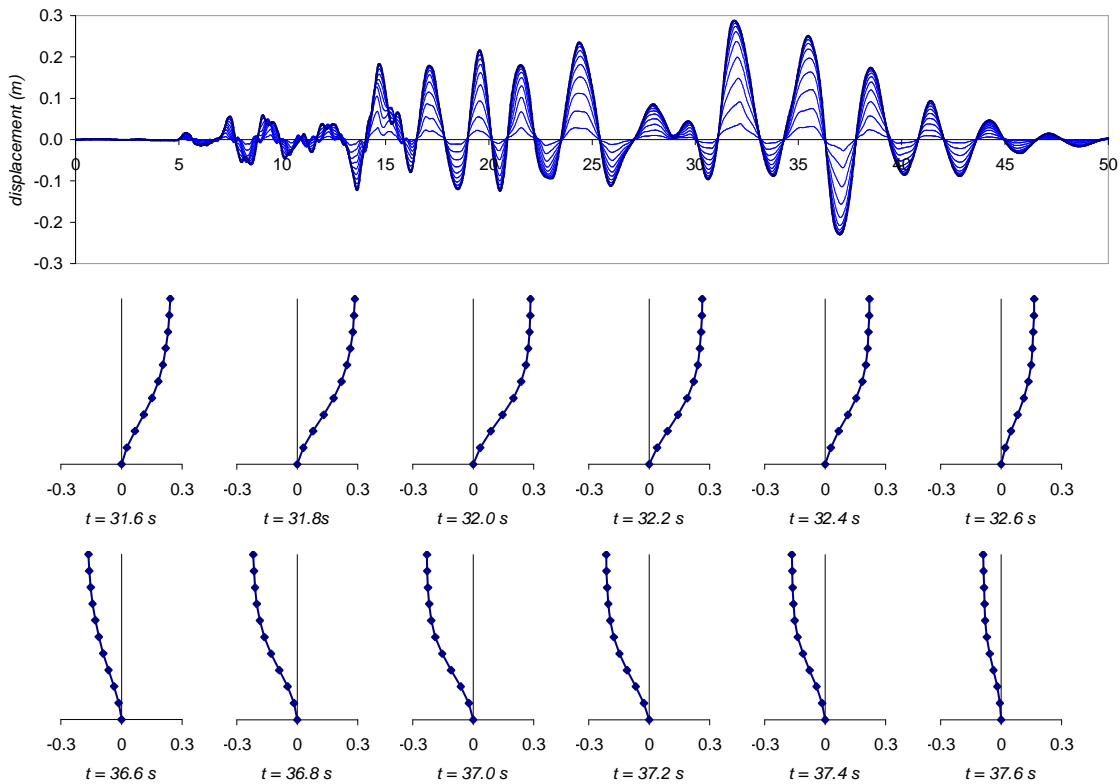


Figure C-1: Mode shapes and periods of vibration for the ten storey frames

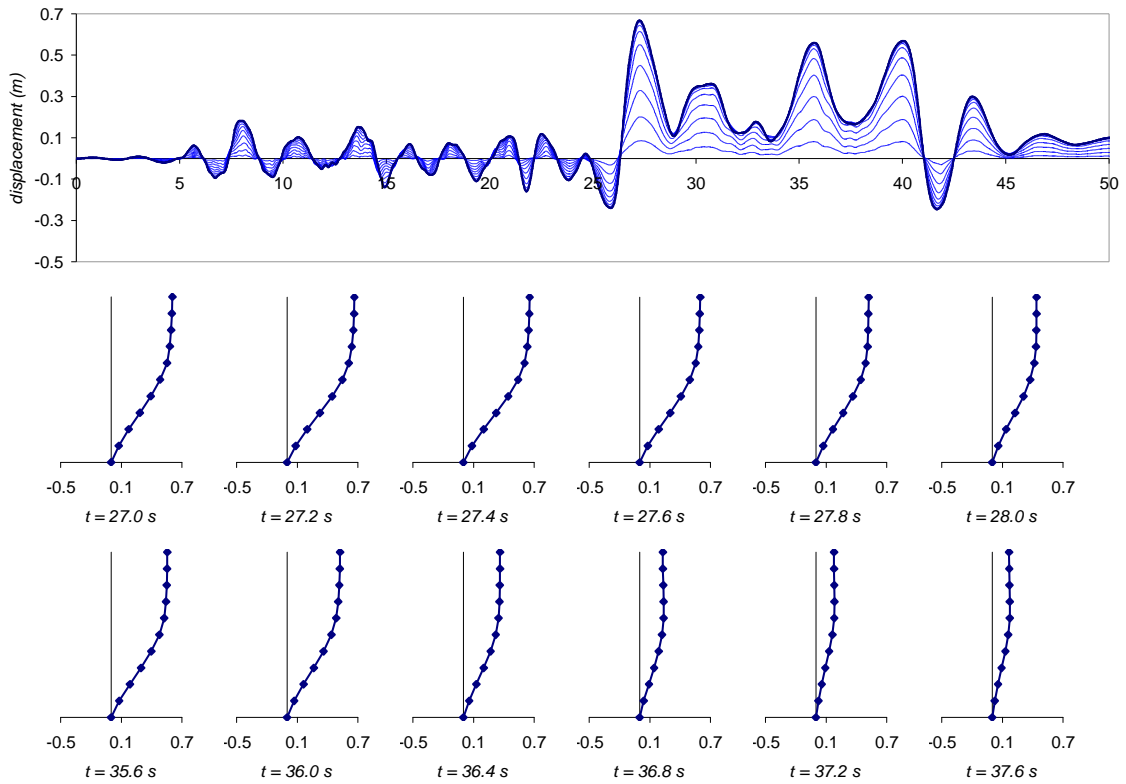


(a) Earthquake 1 – 1989 Loma Prieta at Agnews State Hospital

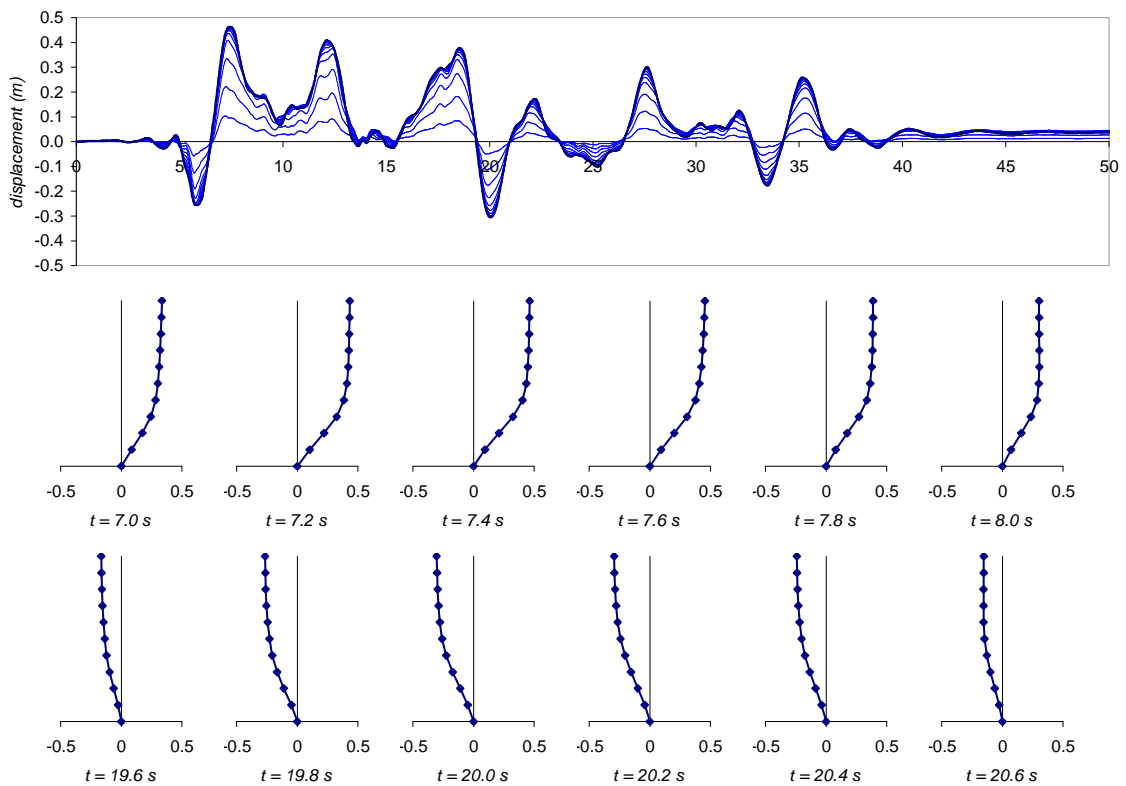


(b) Earthquake 17 – 1987 Superstition Hills at Wildlife Liquefaction Array, N-S component

Figure C-2: Red Book (CCANZ, 1998) displacement time histories and selected vertical snapshots for earthquakes representative of the 50th percentile DBE

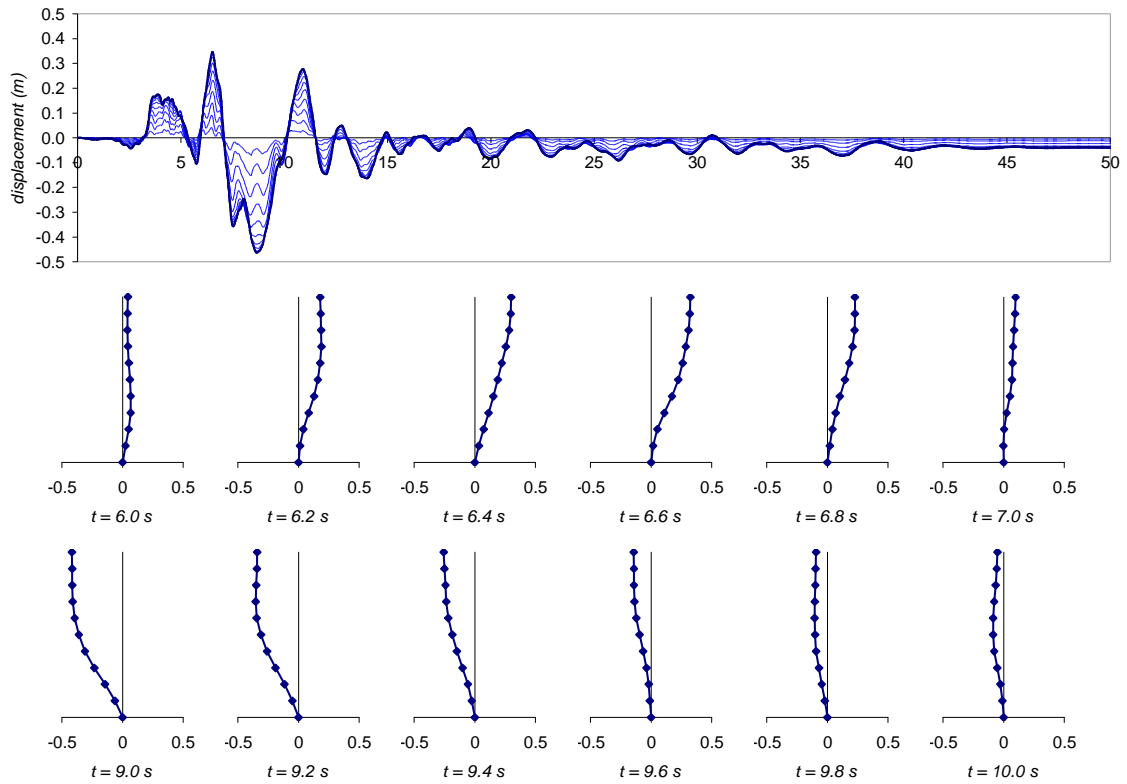


(a) Earthquake 12 – 1987 Superstition Hills at Wildlife Liquefaction Array, E-W component

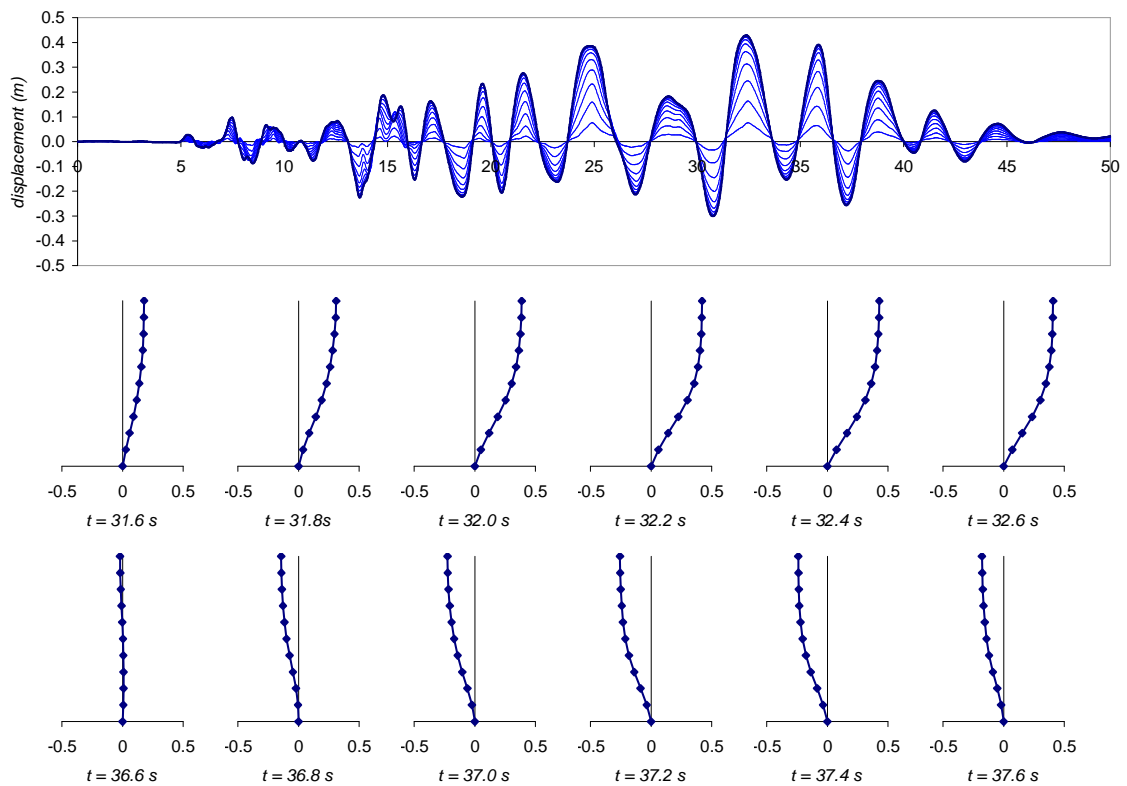


(b) Earthquake 15 – 1979 Imperial Valley at Westmoreland Fire Station, N-S component

Figure C-3: Red Book (CCANZ, 1998) displacement time histories and selected vertical snapshots for earthquakes representative of the 90th percentile DBE

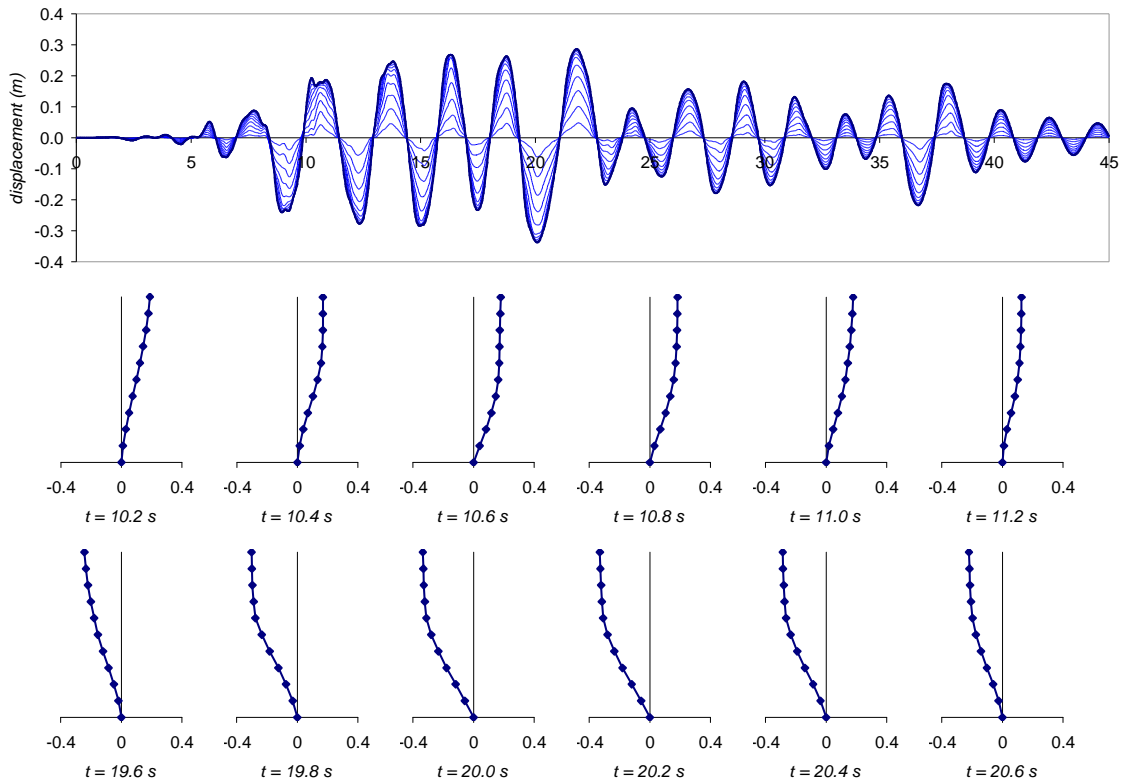


(a) Earthquake 5 – 1979 Imperial Valley at Coyote Lake Dam

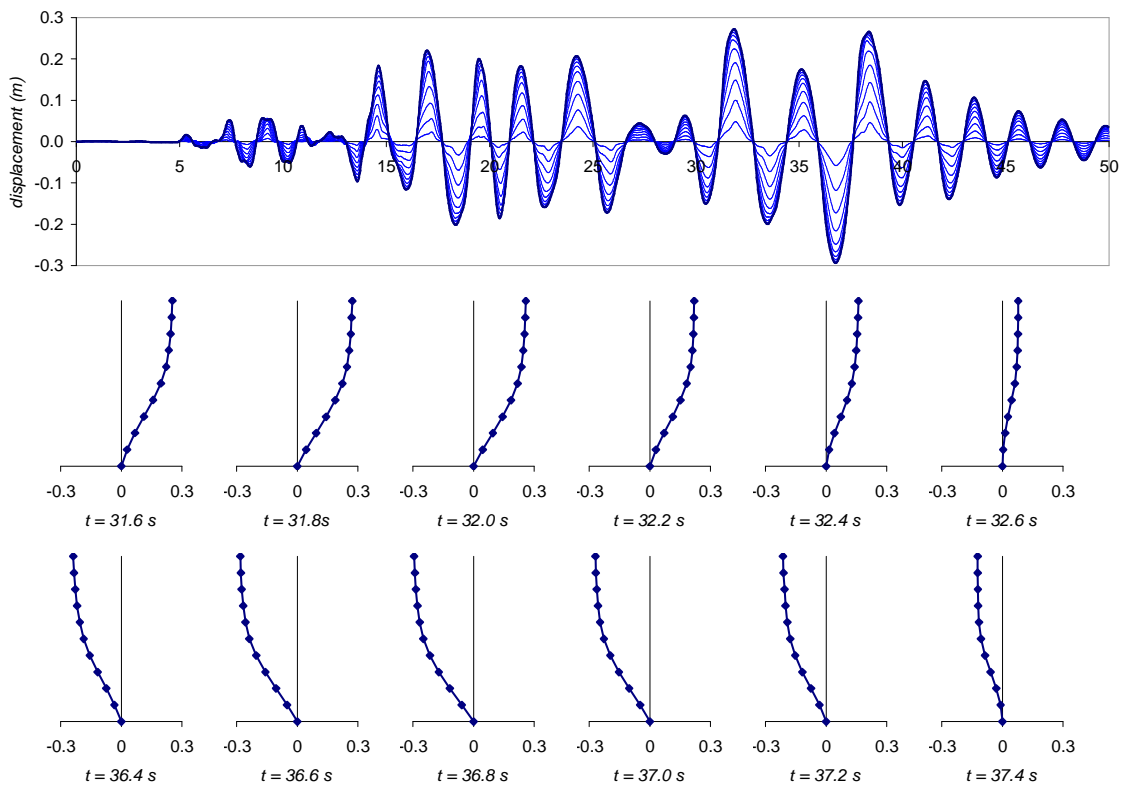


(b) Earthquake 17 – 1987 Superstition Hills at Wildlife Liquefaction Array, N-S component

Figure C-4: Red Book (CCANZ, 1998) displacement time histories and selected vertical snapshots for earthquakes representative of the 50th percentile MCE

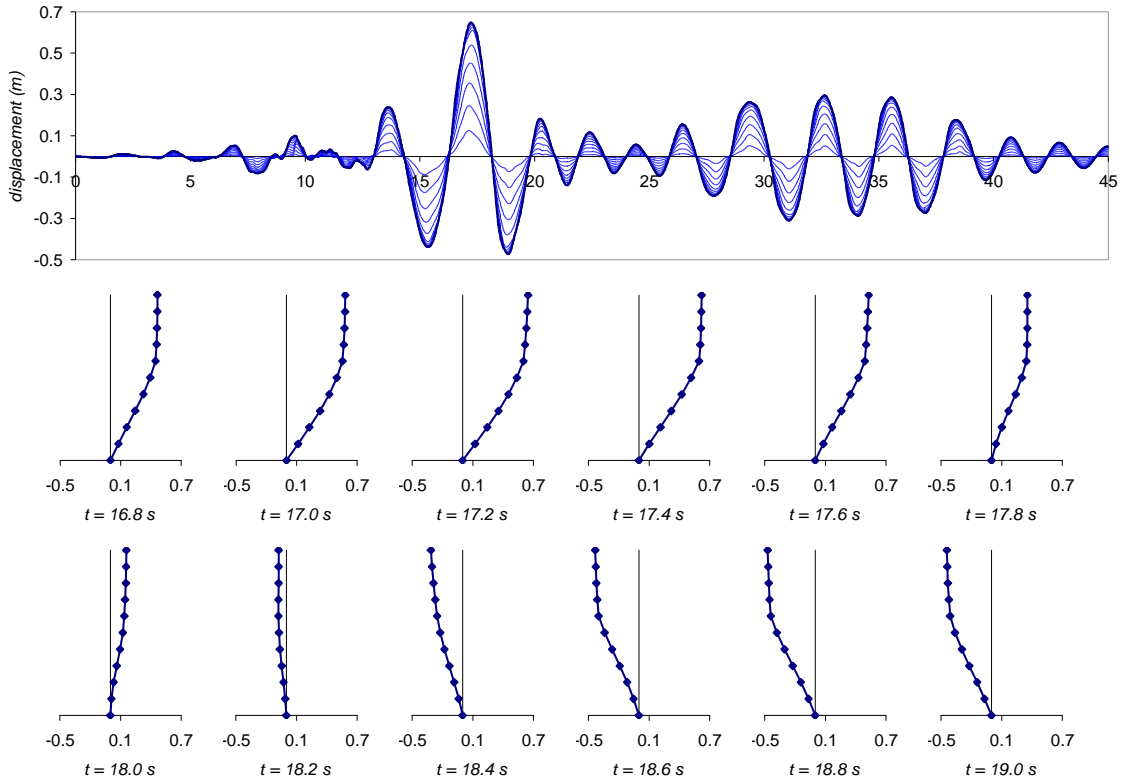


(a) Earthquake 1 – 1989 Loma Prieta at Agnews State Hospital

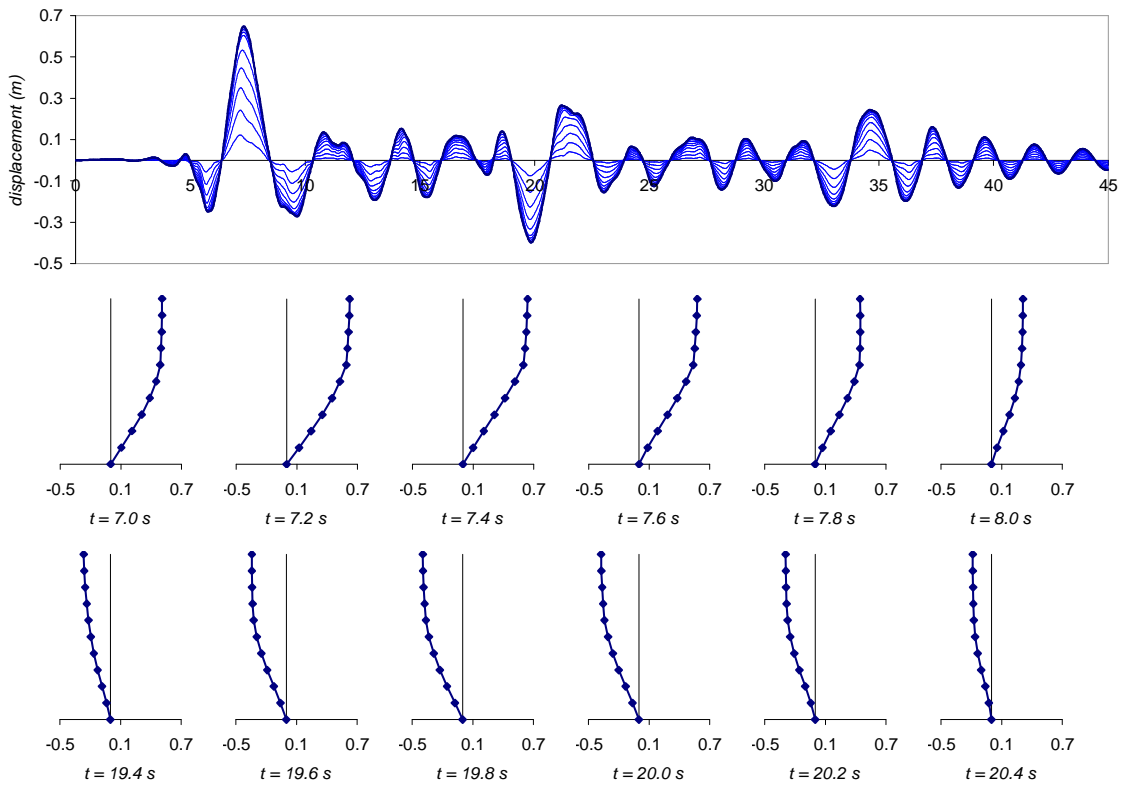


(b) Earthquake 17 – 1987 Superstition Hills at Wildlife Liquefaction Array, N-S component

Figure C-5: DAD E-W gravity frame (Arnold, 2004) displacement time histories and vertical snapshots for earthquakes representative of the 50th percentile DBE

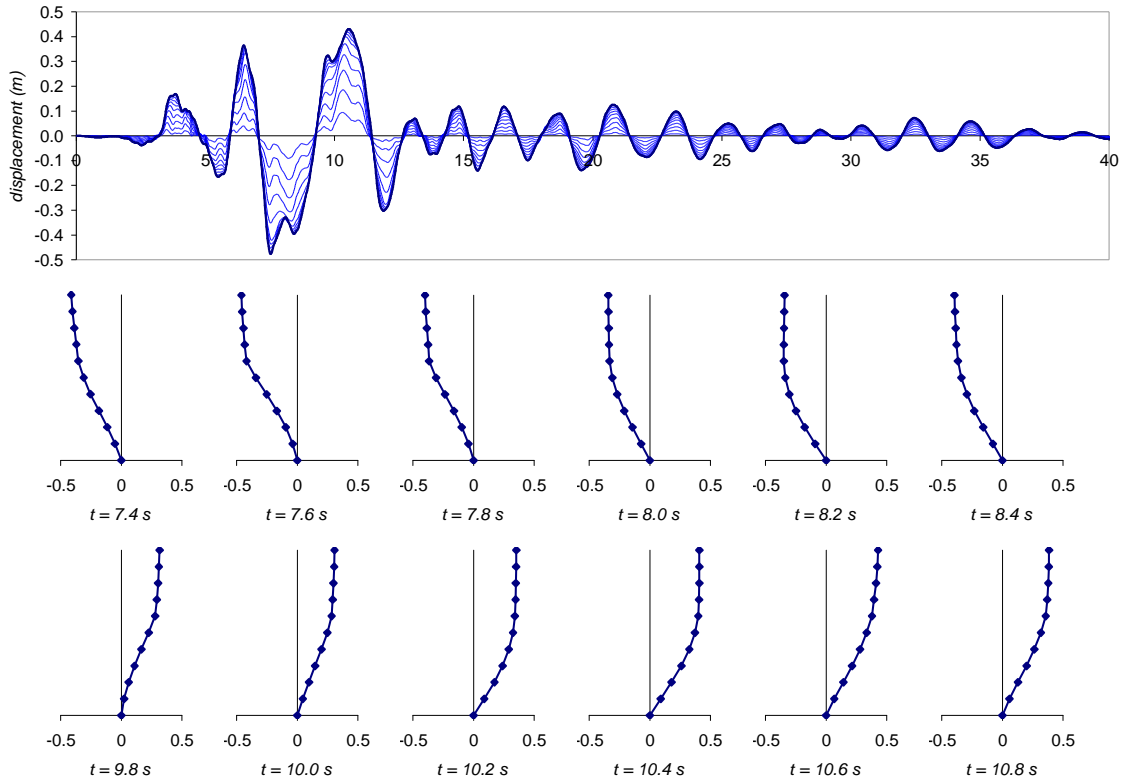


(a) Earthquake 11 – 1989 Loma Prieta at Sunnyvale Colton Ave, N-S component

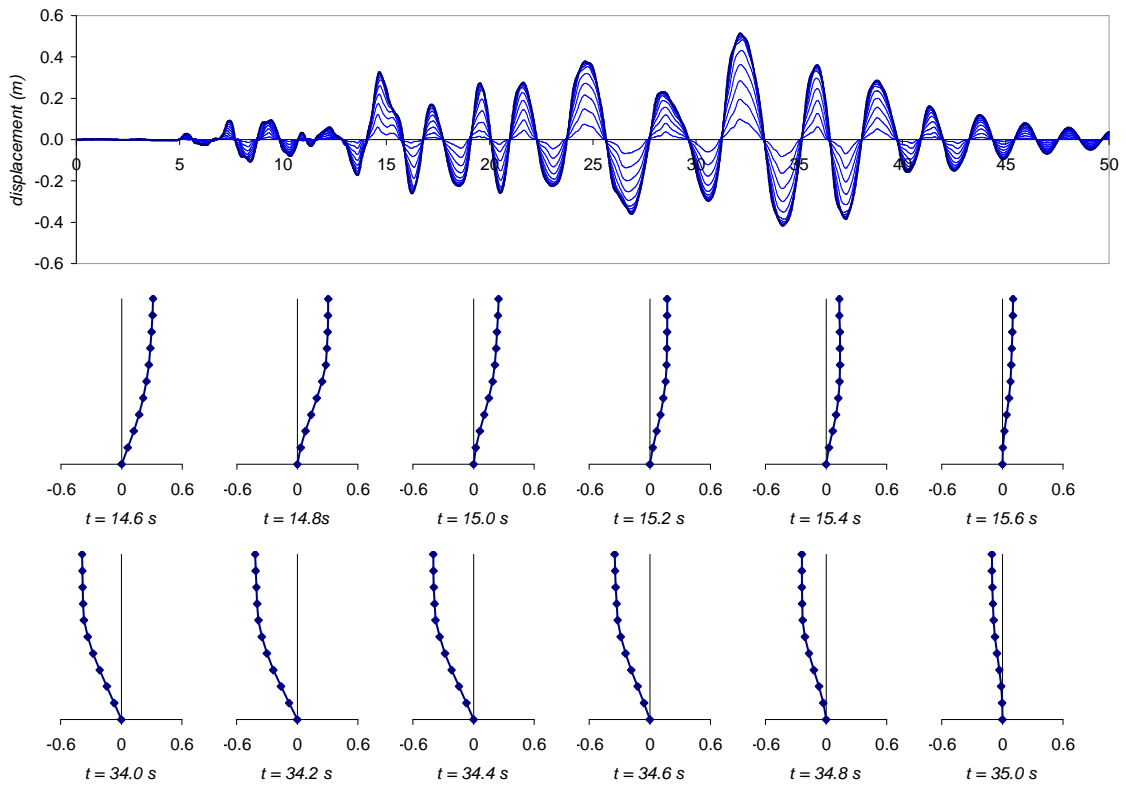


(b) Earthquake 15 – 1987 Superstition Hills at Westmoreland Fire Station, N-S component

Figure C-6: DAD E-W gravity frame (Arnold, 2004) displacement time histories and vertical snapshots for earthquakes representative of the 90th percentile DBE

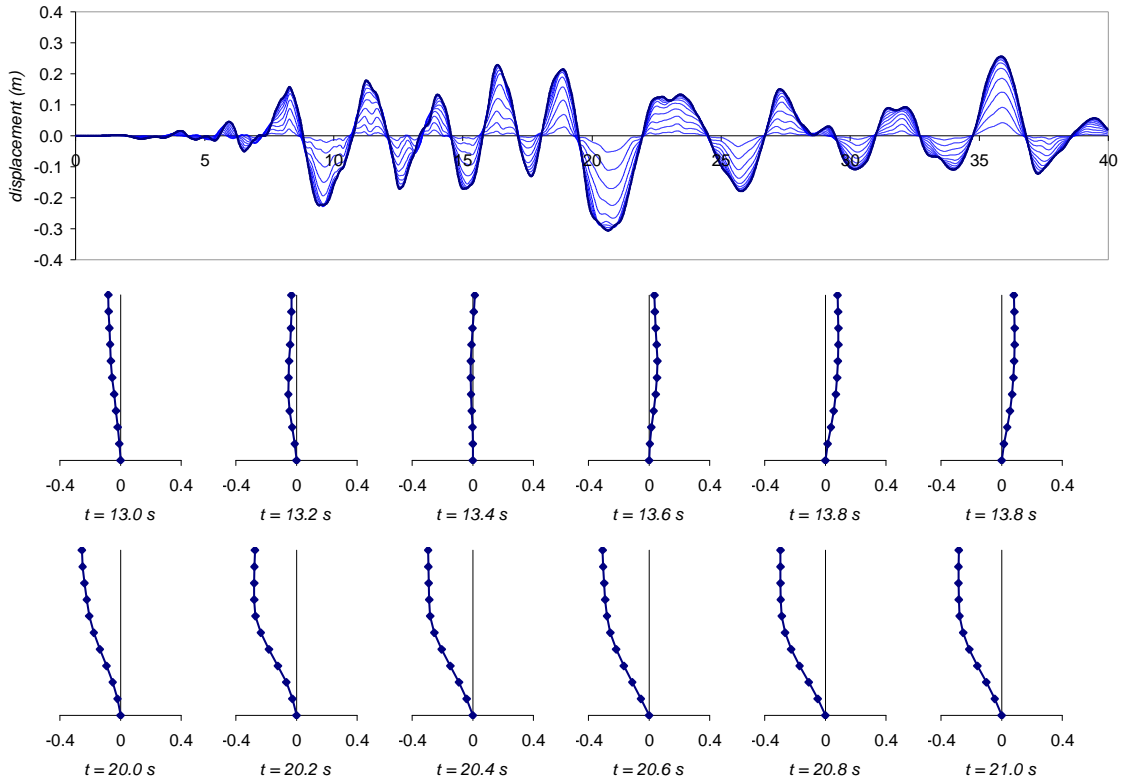


(a) Earthquake 5 – 1979 Imperial Valley at Coyote Lake Dam

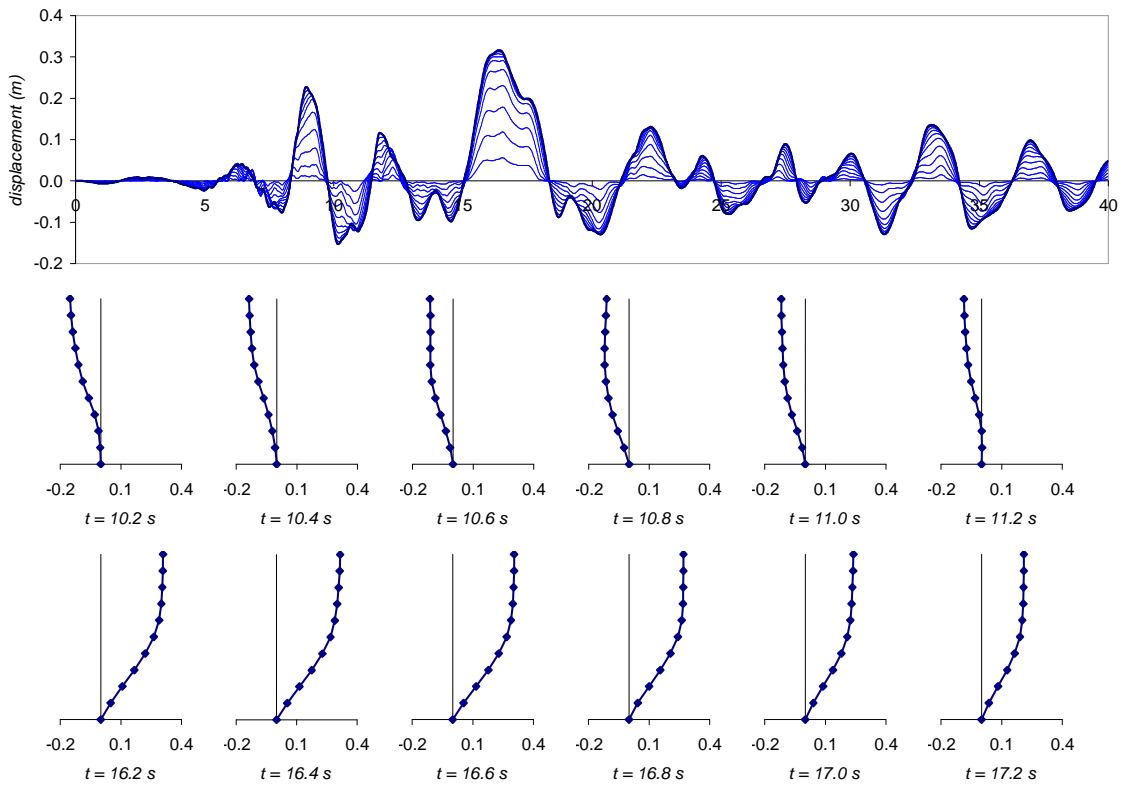


(b) Earthquake 17 – 1987 Superstition Hills at Wildlife Liquefaction Array, N-S component

Figure C-7: DAD E-W gravity frame (Arnold, 2004) displacement time histories and vertical snapshots for earthquakes representative of the 50th percentile MCE

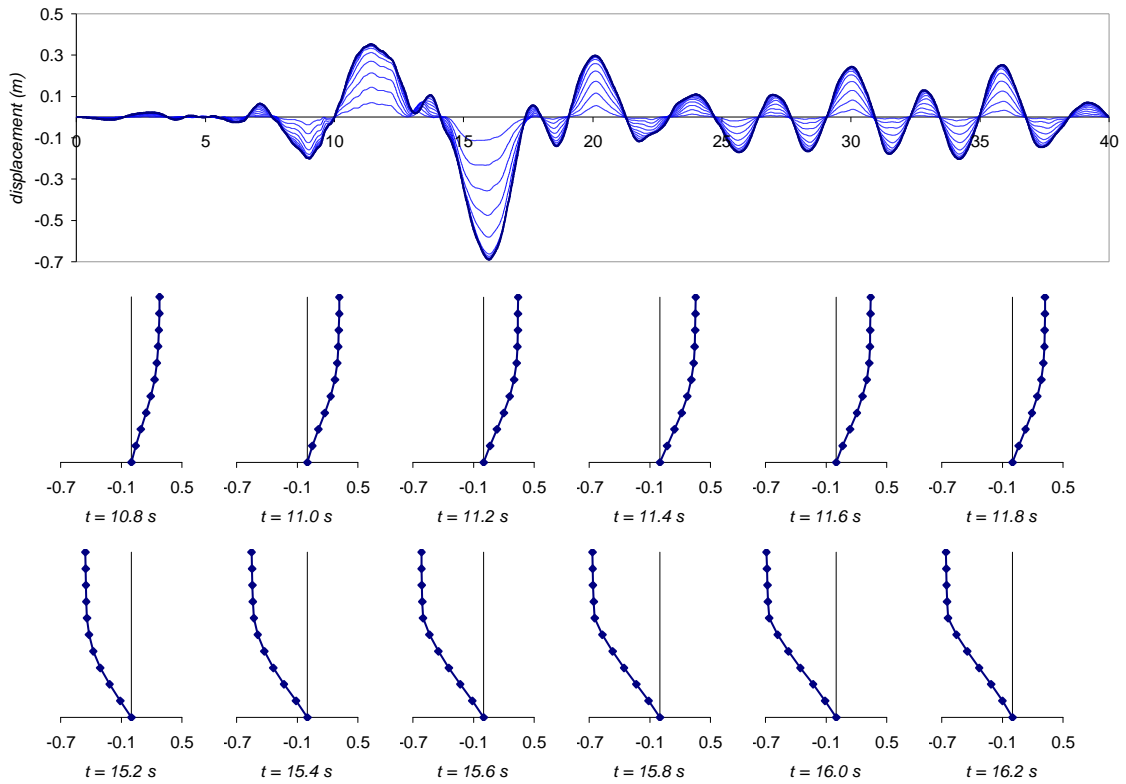


(a) Earthquake 1 – 1989 Loma Prieta at Agnews State Hospital

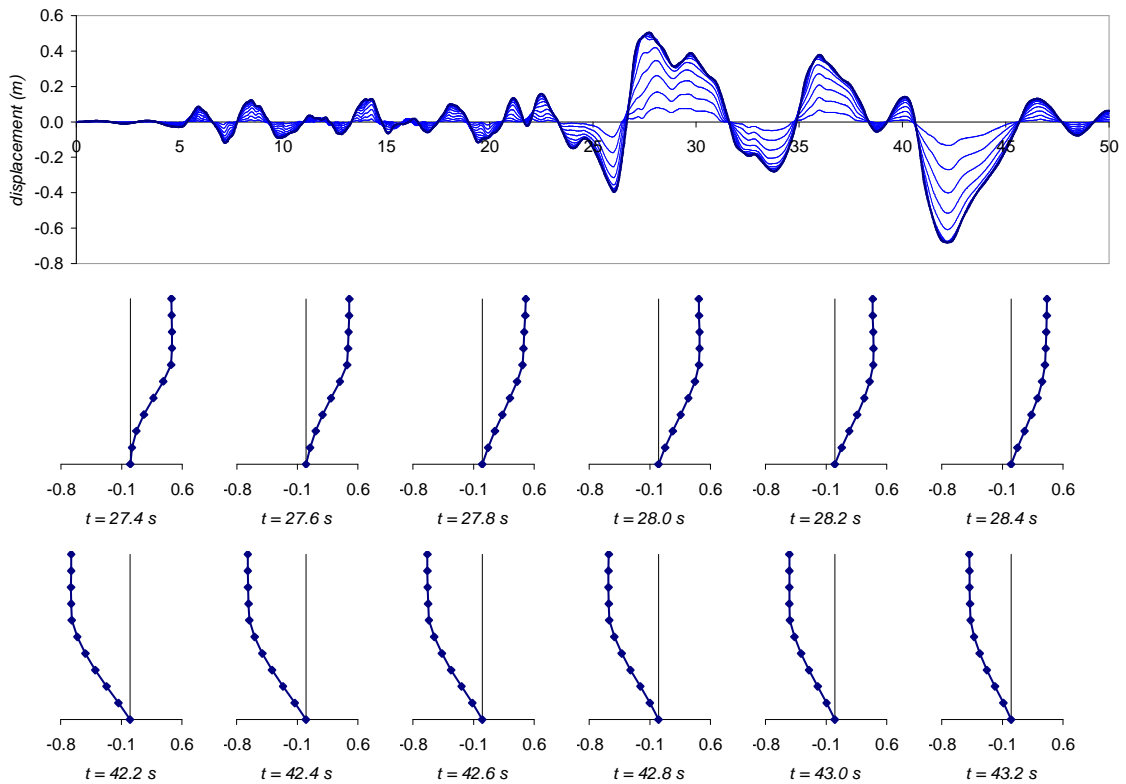


(b) Earthquake 8 – 1979 Imperial Valley at El Centro Array #13, S40E component

Figure C-8: DAD N-S seismic frame (Davies, 2003) displacement time histories and vertical snapshots for earthquakes representative of the 50th percentile DBE

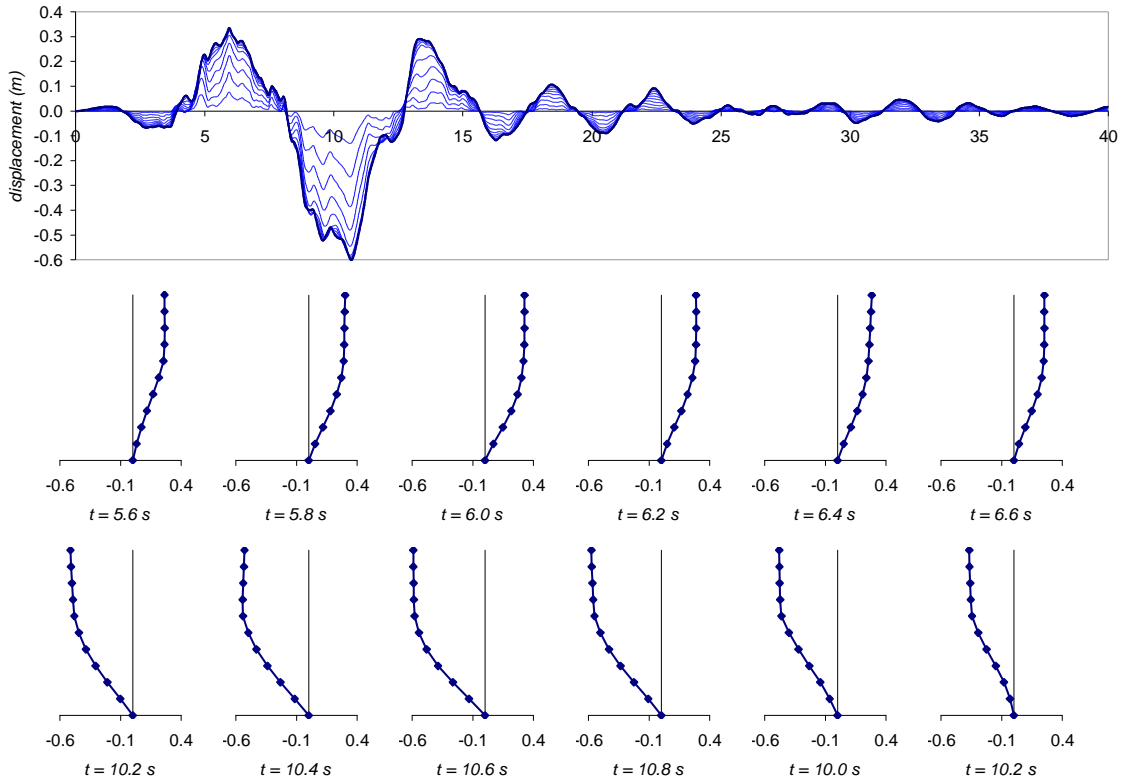


(a) Earthquake 11 – 1989 Loma Prieta at Sunnyvale Colton Ave, N-S component

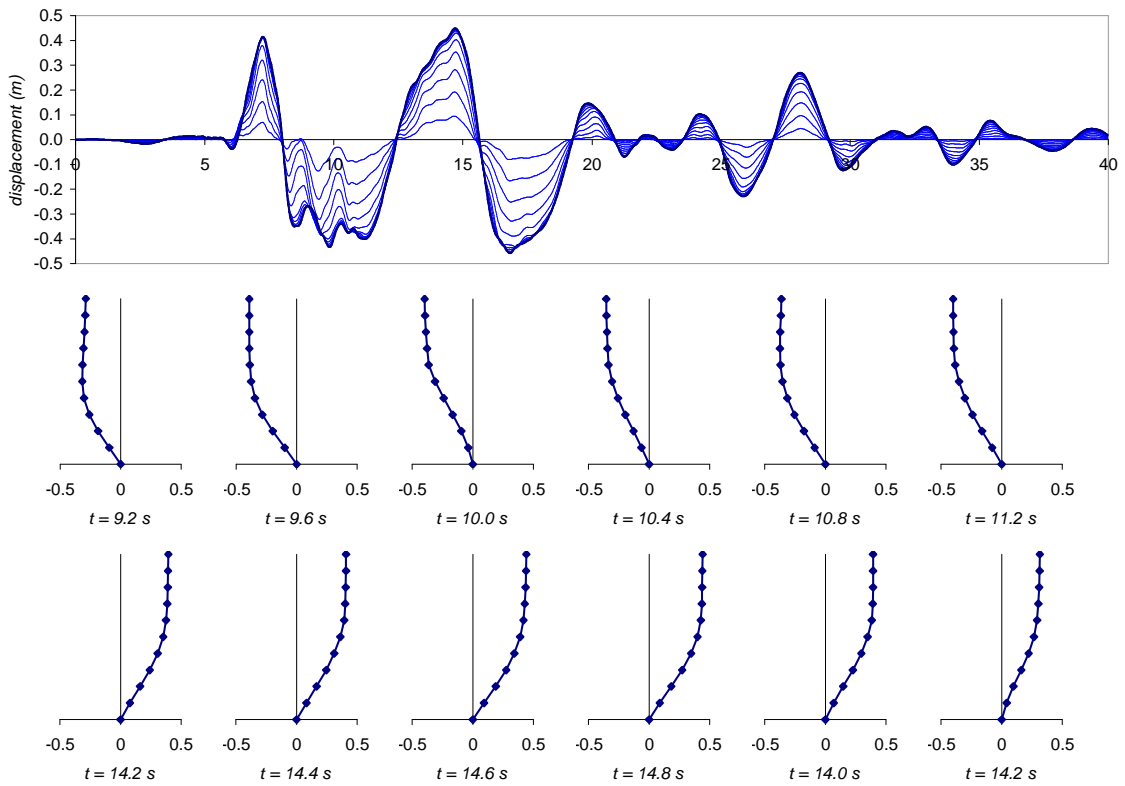


(b) Earthquake 12 – 1987 Superstition Hills at Wildlife Liquefaction Array, E-W component

Figure C-9: DAD N-S seismic frame (Davies, 2003) displacement time histories and vertical snapshots for earthquakes representative of the 90th percentile DBE

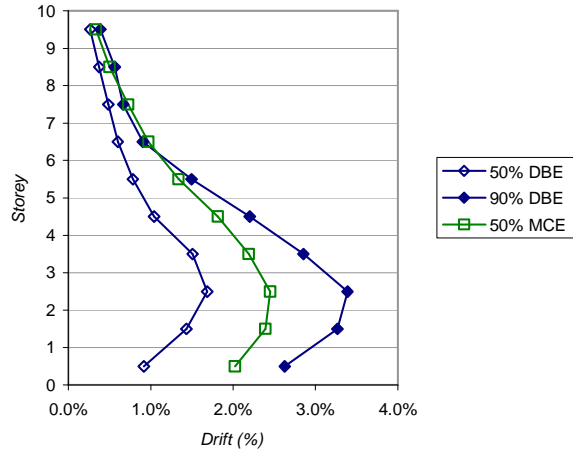


(a) Earthquake 4 – 1989 Loma Prieta at Anderson Dam

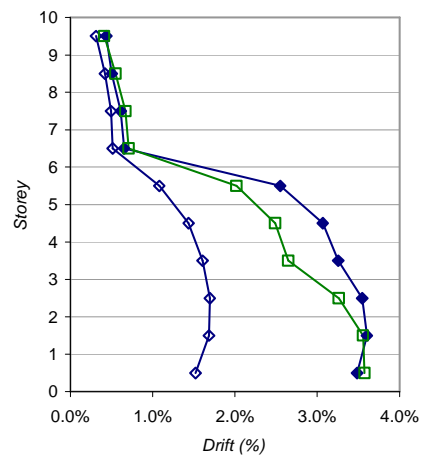
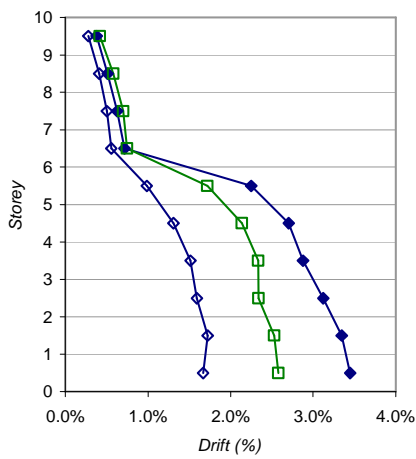


(b) Earthquake 19 – 1989 Loma Prieta at Hollister Diff. Array, S15E component

Figure C-10: DAD N-S seismic frame (Davies, 2003) displacement time histories and vertical snapshots for earthquakes representative of the 50th percentile MCE



(a) Red Book (CCANZ, 1998)



(b) DAD E-W gravity frame (Arnold, 2004) (c) DAD N-S seismic frame (Davies, 2003)

Figure C-11: Vertical drift profiles at DBE and MCE

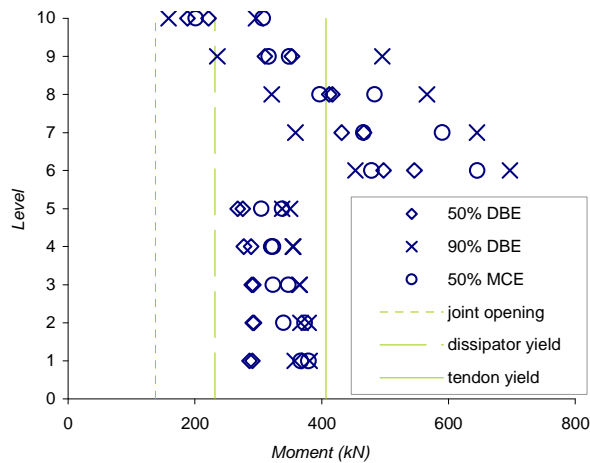


Figure C-12: Maximum beam moments occurring during selected analyses

APPENDIX D

DESIGN OF A SIX STOREY DAMAGE AVOIDANCE DESIGN APARTMENT BUILDING

The design calculations for a proposed apartment building utilising a damage avoidance design philosophy are presented in this appendix. The design methodology is derived from the methodologies proposed by Arnold (2004) and Davies (2003). It was observed that there were a number of inconsistent assumptions in these two methods, and an attempt to remove some of these inconsistencies was made. In the following sections, the structural loadings, design of the gravity frames, seismic frames and columns are presented. Shear across the rocking interfaces is considered in Section D.5.

D.1 LOADINGS

The proposed building, illustrated in Figure D-1 (for sake of completeness, this is Figure 3-2 repeated) is five bays, of 10 *m*, long by four bays, of 7.3 *m*, wide. 300 *mm* deep hollowcore units, with 75 *mm* in-situ topping, span 10 *m* west-east along the building, supported by gravity beams. The gravity beams, spanning north-south, with draped tendons, are 450 *mm* wide by 700 *mm* deep on grids B to E and 450 *mm* wide by 600 *mm* deep on grids A and F. In the orthogonal west-east direction, 350 *mm* wide by 700 *mm* deep beams with straight tendons form a frame that predominantly resists lateral loading. The column dimensions are 750 *mm* by 750 *mm* throughout the building. The seismic weight is calculated using these dimensions assuming $\gamma_{conc} = 23.5 \text{ kN/m}^3$, and allowing 0.8 *kPa* superimposed dead load. The design live load is 3.0 *kPa* for apartment buildings (NZS 4203:1992).

The proposed building is located on intermediate soil in Christchurch. The spectral acceleration $F_v S_1$ is obtained from the acceleration response spectra given by the New Zealand loadings code (NZS 4203:1992) as 0.4 g. (This is calculated from the basic seismic hazard coefficient of $C_h(\mu = 1, T = 1) = 0.5 g$, multiplied by a zone factor of $Z = 0.8$). Therefore the design basis earthquake (DBE) spectral acceleration demand is expressed as:

$$(F_v S_1)_{DBE}^* = 0.4 g \quad (D-1)$$

The corresponding design drift is 2%.

D.2 DESIGN OF GRAVITY FRAMES

The design of the gravity frames is carried out in a similar fashion to the method presented by Arnold (2004). The calculations for the frames on grids B to E are different to those for those frames on grids A and F. This difference is due to the difference in gravity load applied to the beams. The design procedure is set out step by step. In the first part of the process, the frame is designed for gravity loads, while in the later steps the seismic load of the frame is evaluated. Calculations are presented first for the internal frames on grids B to E, then for the external frames on grids A and F.

D.2.1 INTERNAL GRAVITY FRAMES (GRIDS B TO E)

Step One: Balance Gravity Loads

The initial prestress force, after losses, is set such that the gravity load applied to the frame beams is balanced by the prestress force. For a parabolic prestress profile, the required initial prestress is calculated:

$$P_{PSi} = \frac{w_G L^2}{8e_c} \quad (D-2)$$

where w_G is the gravity load applied to the beam, L is the length of the beam, between column centrelines, and e_c is the overall drape of the prestress tendons, measured from the top of the beam (ie. the overall beam depth minus cover to the tendons).

For the interior spans, where $w_G = 62 \text{ kN-m}$ and $e_c = 640 \text{ mm}$ (assuming cover of 60 mm from the bottom of the beam to the centreline of the tendon), the initial prestress required is:

$$P_{PSi} = \frac{62 \times 7.3^2}{8 \times 0.64} = 645 \text{ kN} \quad (D-3)$$

Step Two: Service Load Stress Evaluation

The stresses in the beams need to be checked under service load conditions of $G + Q$, (where G = dead load and Q = design live load) to ensure that under these conditions the beam remains in an elastic stress state. Since the gravity loads are balanced by the prestress, the moment induced by the live load Q need to be checked and compared with the elastic flexural capacity, ie.

$$M_Q < M_{elastic} \quad (D-4)$$

where M_Q is the moment induced by the live load and $M_{elastic}$ is the elastic flexural capacity of the beam. The elastic flexural capacity is given by the lessor of:

$$M_{elastic} = \left(\alpha \sqrt{f'_c} + \frac{P_{PSi}}{A_g} \right) S_x \quad (D-5)$$

$$M_{elastic} = \left(\beta f'_c - \frac{P_{PSi}}{A_g} \right) S_x \quad (D-6)$$

where $\alpha\sqrt{f'_c}$ is the maximum elastic concrete tension stress, where $\alpha = 0.7$ (f'_c in MPa units) for partial reinforcing, $\beta f'_c$ is the maximum elastic concrete compression stress equations, where $\beta = 0.5$ typically, A_g is the gross cross-sectional area and S_x the elastic section modulus. Equations (D-5) and (D-6) refer to the tension and compression limits respectively. If equation (D-4) does not hold, the section dimensions need to be increased.

Assuming $f'_c = 30$ MPa, the elastic flexural moment capacities are given as:

$$M_{elastic} = \left(0.7\sqrt{30} + \frac{645 \times 10^3}{315 \times 10^3} \right) 36.75 \times 10^6 = 216 \text{ kN-m} \quad (D-7)$$

$$M_{elastic} = \left(0.5 \times 30 - \frac{645 \times 10^3}{315 \times 10^3} \right) 36.75 \times 10^6 = 476 \text{ kN-m} \quad (D-8)$$

The tension limit governs, giving $M_{elastic} = 216 \text{ kN-m}$.

The live load on the beam, w_Q , is 30 kN/m. Conservatively assuming the beam is simply supported, M_Q can be calculated as:

$$M_Q = \frac{w_Q L^2}{8} = \frac{30 \times 7.3^2}{8} = 200 \text{ kN-m} \quad (D-9)$$

hence equation (D-4) holds, and the beams should experience minimal stress over the lifetime of the structure.

Step Three: Preliminary Prestress Design

The column rotation at yield of the beam tendons is selected from the design criteria. From this, the minimum area of prestressing steel in the beams, $A_{PS \min}$ can be selected from:

$$A_{PS \min} = \frac{P_{PS i}}{1 - \theta_{RBR(PS \text{ yield})} \frac{L}{L_{beam}} \frac{d_b}{L_{PS}} \frac{E_{PS}}{f_{PS}}} \quad (D-10)$$

where $\theta_{RBR (PS \text{ yield})}$ is the rigid body rotation capacity of the frame when yield of the tendons occurs, L_{beam} is the length of the drop-in beam. For this case, $\theta_{RBR (PS \text{ yield})}$ is selected as 3%, $L_{beam} = 6.1 \text{ m}$, $d_b = 0.7 \text{ m}$, $f_{PS} = 950 \text{ MPa}$ and $E_{PS} = 205 \text{ GPa}$, so $A_{PS \text{ min}}$ is calculated as:

$$A_{PS \text{ min}} = \frac{645}{\left(1 - 0.03 \times \frac{7.3}{6.1} \times \frac{0.7}{8.23} \times \frac{205 \times 10^3}{950}\right)} = 1890 \text{ mm}^2 \quad (D-11)$$

Two 36 mm diameter *dywidag* bars are chosen, giving $A_{PS} = 2040 \text{ mm}^2$.

Step Four: Mechanism Assessment

The base shear capacity of the structure is established by performing a plastic mechanism analysis described in Appendix B. The resulting base shear can be and expressed as:

$$V_{base} = \kappa M_b \quad (D-12)$$

where κ relates the beam plastic hinge capacity to the base shear capacity of the structure, evaluated for the number of storeys participating in the mechanism which satisfies energy minimisation, and M_b is the beam hinge moment. For this frame four storeys are found to be participating in the mechanism and $\kappa = 4.25$, so the base shear capacity can be expressed as:

$$V_{base} = 4.25 M_b \quad (D-13)$$

The acceleration and displacement transformation factors are evaluated from equations (B-13) and (B-14) as $\alpha_A = 0.871$ and $\alpha_D = 1.161$.

Step Five: Assessment of Seismic Capacity

The spectral acceleration capacity of the frame can be evaluated from:

$$(F_v S_1)_{cap} = 2\pi B \sqrt{\frac{C_c^* \Delta^*}{g}} \quad (D-14)$$

where B is the reduction factor to allow for system damping, and C_c^* and Δ^* are the acceleration capacity and displacement of an equivalent SDOF system, described in Appendix B.

The total effective damping, ξ_{eff} , is evaluated by adding the contributions of any intrinsic damping ξ_{int} ; radiation damping due to rocking, ξ_{rad} ; and hysteretic damping, ξ_{hyst} :

$$\xi_{eff} = \xi_{int} + \xi_{rad} + \xi_{hyst} \quad (D-15)$$

It is assumed that ξ_{rad} is small compared with ξ_{int} and ξ_{hyst} , so shall be ignored. Typically ξ_{int} is taken as 5% for reinforced concrete structures, and ξ_{hyst} can be approximated by (Pekcan et al., 1999):

$$\xi_{hyst} = \frac{2}{\pi} \eta \left[1 - \frac{1}{\mu} \right] \quad (D-16)$$

where η is an experimentally calibrated energy efficiency absorption factor and μ is the ductility. The reduction factor to account for damping is approximated by:

$$B = \left(\frac{\xi_{eff}}{0.05} \right)^{0.3} \quad (D-17)$$

which was proposed by Pekcan et al. (1999) and was used by both Arnold (2004) and Davies (2003). It is acknowledged that further research has been carried out into damping reduction factors and equation (D-17) has been superseded by alternative formulations.

The base shear capacity is expressed as a function of the beam moment in equation (D-12). The total beam connection moment is calculated as the sum of the contributions from the prestress tendons and energy dissipators, expressed as:

$$M_b = M_{PS} + M_d \quad (D-18)$$

where M_{PS} is the moment contribution provided by the prestress and M_d is the moment contribution provided by the dissipators.

In order to evaluate the beam moment, it is necessary to evaluate the prestress force at the design drift from:

$$P_{PS} = P_{PSi} + \frac{E_{PS} A_{PS}}{L_{PS}} d_b \theta_j \quad (D-19)$$

where θ_j is the rotation of the beam-column connection, evaluated as:

$$\theta_j = (\theta - \theta_{ce}) \frac{L}{L_{beam}} \quad (D-20)$$

where θ is the design drift, and θ_{ce} is the column drift due to elastic flexure of the frame elements. Conservatively estimating θ_{ce} as 0.5%, equation (D-19) can be evaluated as:

$$P_{PS} = 645 \times 10^3 + \frac{205\,000 \times 2040}{8.23} \times 0.7 \times (0.02 - 0.005) \times \frac{7.3}{6.1} = 1280 \text{ kN} \quad (D-21)$$

The average moment contribution from the prestress is evaluated as:

$$M_{PS\,ave} = \frac{M_{PS}^+ + M_{PS}^-}{2} = \frac{P_{PS} d_b}{2} = \frac{1280 \times 0.7}{2} = 449 \text{ kN-m} \quad (D-22)$$

Thus the base shear capacity can be evaluated using equation (D-13) as 1910 kN.

Initially assuming there are no additional energy dissipators, the acceleration capacity and displacement of an equivalent single degree of freedom system (SDOF) can now be evaluated from equations (B-11) and (B-12) of Appendix B, respectively, where:

$$C_c^* = \frac{V_{base}}{W \alpha_A} = \frac{1910}{13450 \times 0.871} = 0.163 \quad (D-23)$$

$$\Delta^* = \frac{h_s n_{sp} \theta}{\alpha_D} = \frac{3.6 \times 4 \times 0.02}{1.161} = 0.248 \text{ m} \quad (D-24)$$

and the spectral acceleration capacity is:

$$(F_v S_1)_{DBE}^{cap} = 2\pi \sqrt{\frac{0.163 \times 0.248}{9.81}} = 0.40 \quad (D-25)$$

Step Six: Compare Spectral Acceleration Capacity with Spectral Acceleration Demand

The spectral acceleration capacity is compared with the spectral acceleration demand:

$$(F_v S_1)^* \leq \phi (F_v S_1)^{cap} \quad (D-26)$$

where the earthquake spectral acceleration demand is given by equation (D-1) and $\phi = 0.7$ (Shama and Mander, 2003), therefore:

$$0.4 > 0.7 \times 0.4 = 0.28 \quad \therefore \text{Insufficient capacity}$$

Since the spectral acceleration capacity at the design drift is less than the code spectral acceleration demand, supplemental energy dissipators should be included in the design, and the procedure needs to be re-evaluated from Step Five.

Step Seven: Supplemental Energy Dissipators

Supplemental energy dissipators will increase the connection moment. To ensure re-centring of the connection, the connection moment provided by the dissipators should satisfy:

$$\lambda_d M_d \leq \phi_{PS} M_{PS} \quad (D-27)$$

where λ_d is an overstrength factor to account for strain-hardening of the dissipator material, ϕ_{PS} is a prestress undercapacity factor, and M_d and M_{PS} are the moment

contributions of the dissipators and prestress, respectively. Assuming tension-compression ‘dog-bone’ dissipators mounted on either side of the beam at the depth of the prestress, similar to those designed by Arnold (2004), the maximum force in the dissipators is calculated as:

$$P_d = \frac{\phi_{PS}}{\lambda_d} P_{PSi} = \frac{0.8}{1.34} \times 645 = 387 \text{ kN} \quad (D-28)$$

where ϕ_{PS} is taken as 0.8 and λ_d is taken as 1.34, since probable rather than nominal strength values are being used.

Assuming the dissipators are constructed from 20 mm thick mild steel plate, with characteristic strength of 336 MPa, the width of the dissipator is calculated as:

$$w_d = \frac{P_d}{f_d t_d} = \frac{387 \times 10^3}{336 \times 20} = 29 \text{ mm} \quad (D-29)$$

The additional moment contribution due to the presence of the dissipators is determined from:

$$M_{d \text{ ave}} = \frac{M_d^+ + M_d^-}{2} = \frac{P_d d_b}{2} = \frac{387 \times 0.7}{2} = 135 \text{ kN-m} \quad (D-30)$$

The total connection moment, found by adding prestress and dissipator contributions is found to be 585 kN-m, from which the base shear capacity of the frame is re-evaluated from equation (D-13) as 2490 kN. The equivalent SDOF acceleration capacity is recalculated as:

$$C_c^* = \frac{V_{base}}{W \alpha_A} = \frac{2490}{13450 \times 0.871} = 0.212 \quad (D-31)$$

To evaluate the spectral acceleration capacity, consideration of the total effective damping must be made. Assuming $\eta = 0.15$ (Arnold, 2004), and conservatively assuming

opening of the rocking joints occurs at an elastic column drift of $\theta_{ce} = 0.5\%$, the additional hysteretic damping provided by supplemental energy dissipators, is calculated as:

$$\xi_{hyst} = \frac{2}{\pi} \times 0.15 \times \left[1 - \frac{1}{4} \right] = 0.072 \quad (D-32)$$

Therefore the total effective damping is 0.122. Thus the factor to account for damping may be evaluated as:

$$B = \left(\frac{0.122}{0.05} \right)^{0.3} = 1.31 \quad (D-33)$$

Therefore the spectral acceleration capacity may be re-evaluated as:

$$(F_v S_1)_{DBE}^{cap} = 2\pi \times 1.31 \times \sqrt{\frac{0.212 \times 0.248}{9.81}} = 0.60 \quad (D-34)$$

The spectral acceleration capacity can again be compared with the spectral acceleration demand according to equation (D-26):

$$0.4 < 0.7 \times 0.6 = 0.42 \quad \therefore \text{Sufficient capacity}$$

Step Eight: Maximum Drift Capacity

To ensure adequate performance of the structure at earthquake demands greater than DBE, the drift capacity of the structure is determined when yield of the prestress tendons occurs.

This drift, $\theta_{c(Ps\ yield)}$, is calculated by adding the elastic, θ_{ce} , and rigid body rotation,

$\theta_{RBR(Ps\ yield)}$, components of the drift:

$$\theta_{c(Ps\ yield)} = \theta_{ce} + \theta_{RBR(Ps\ yield)} \quad (D-35)$$

The elastic contribution to the storey drift has been determined using the moment-area theorem, assuming rigid beam-column joint panel zones as (Davies, 2003):

$$\theta_{ce} = \frac{H}{12 h_s} \left[\frac{(h_s - d_b)^3}{EI_{col}^*} + \frac{h_s^2 (L - d_c)^3}{L^2 EI_{beam}^*} \right] \quad (D-36)$$

where H is the column lateral force, evaluated as:

$$H = \frac{2M_b}{h_s} \frac{L}{L_{beam}} \quad (D-37)$$

The rigid body rotation is determined as:

$$\theta_{RBR} = \theta_j \frac{L_{beam}}{L} \quad (D-38)$$

where θ_j is the connection rotation. The connection rotation, corresponding to yield of the prestress occurs is:

$$\theta_{j(Ps\ yield)} = \left(1 - \frac{f_i}{f_{PS}}\right) \frac{f_{PS}}{E_{PS}} \frac{L_{PS}}{d_b} \quad (D-39)$$

where (f_i / f_{PS}) is the initial prestress ratio, and L_{PS} is the length of the prestress tendon, measured between anchorages.

Once yield of the prestress tendons occurs, the prestress force is 1940 kN, so the elastic drift, $\theta_{ce} = 0.7\%$, and the rigid body rotation drift $\theta_{RBR(Ps\ yield)} = 3.0\%$, giving a drift capacity of 3.7% before yield of the tendons occurs. This is considered acceptable.

D.2.2 EXTERNAL GRAVITY FRAMES (GRIDS A AND F)

Step One: Balance Gravity Loads

The initial prestress force, after losses, is calculated as:

$$P_{PS\ i} = \frac{31 \times 7.3^2}{8 \times 0.54} = 382 \text{ kN} \quad (D-40)$$

where $w_G = 31 \text{ kN/m}$ and $e_c = 540 \text{ mm}$ (assuming cover of 60 mm from the bottom of the beam to the centreline of the tendon), for the exterior frame.

Step Two: Service Load Stress Evaluation

The elastic flexural moment capacities for the exterior frames, assuming $f'_c = 30 \text{ MPa}$, are given as:

$$M_{elastic} = \left(0.7\sqrt{30} + \frac{382 \times 10^3}{270 \times 10^3} \right) 27 \times 10^6 = 142 \text{ kN-m} \quad (D-41)$$

$$M_{elastic} = \left(0.5 \times 30 - \frac{382 \times 10^3}{270 \times 10^3} \right) 27 \times 10^6 = 367 \text{ kN-m} \quad (D-42)$$

The tension limit governs, giving $M_{elastic} = 142 \text{ kN-m}$.

The live load on the beam, w_Q , is 15 kN/m . Again assuming the beam is simply supported, M_Q can be calculated as:

$$M_Q = \frac{w_Q L^2}{8} = \frac{15 \times 7.3^2}{8} = 100 \text{ kN-m} \quad (D-43)$$

hence equation (D-4) holds, and the beams should experience minimal stress over the lifetime of the structure.

Step Three: Preliminary Prestress Design

The minimum area of prestressing steel in the beams, $A_{PS \min}$, for the exterior frames is determined as:

$$A_{PS \min} = \frac{382}{\left(1 - 0.03 \times \frac{7.3}{6.1} \times \frac{0.6}{8.19} \times \frac{205 \times 10^3}{950} \right)} = 884 \text{ mm}^2 \quad (D-44)$$

from which two 32 mm diameter *dywidag* tendons are chosen, giving $A_{PS} = 1608 \text{ mm}^2$. It is observed that one 36 mm diameter tendon would have provided sufficient prestress area, however it is desirable to have more than one tendon to resist torsional effects, and added reliability.

Step Four: Mechanism Assessment

The only difference in the geometry of the this frame, when compared to the interior frames, is the depth of the beam. This does not affect the capacity of the mechanism that forms, therefore the base shear capacity can again be expressed as:

$$V_{base} = 4.25 M_b \quad (D-45)$$

where four storeys found to be participating in the mechanism. The acceleration and displacement factors are evaluated as $\alpha_A = 0.871$ and $\alpha_D = 1.161$, the same as for the interior gravity frames.

Step Five: Assessment of Seismic Capacity

The base shear capacity is expressed as a function of the beam moment in equation (D-45). The joint moment capacity has contributions from both the prestress and energy dissipators. The prestress force for the DBE is evaluated as:

$$P_{PS} = 382 \times 10^3 + \frac{205\,000 \times 1608}{8.19} \times 0.6 \times (0.02 - 0.005) \times \frac{7.3}{6.1} = 816 \text{ kN} \quad (D-46)$$

where θ_{ce} is again conservatively estimated as 0.5%.

Since energy dissipators were required for the frames on grids B to E, similar tension-compression ‘dog-bone’ dissipators mounted on either side of the connection at the depth of the prestress shall also be provided for these frames. To ensure recentring of the connections, the maximum force in the dissipators is:

$$P_d = \frac{\phi}{\lambda_d} P_{PSi} = \frac{0.9}{1.5} \times 382 = 229 \text{ kN} \quad (D-47)$$

The average moment, considering contributions from both the prestress and dissipators is determined as:

$$M_{con\ ave} = \frac{M_{con}^+ + M_{con}^-}{2} = \frac{(P_{PS} + P_d)d_b}{2} = \frac{(816 + 229)0.6}{2} = 314\ kN \quad (D-48)$$

from which the base shear capacity is determined from equation (D-45) as 1330 kN.

The acceleration capacity and displacement of an equivalent single degree of freedom system (SDOF) is now calculated from equations (B-11) and (B-12) of Appendix B, respectively, where:

$$C_c^* = \frac{V_{base}}{W \alpha_A} = \frac{1330}{6720 \times 0.871} = 0.228 \quad (D-49)$$

$$\Delta^* = \frac{h_s n_{sp} \theta}{\alpha_D} = \frac{3.6 \times 4 \times 0.02}{1.161} = 0.248\ m \quad (D-50)$$

The hysteretic damping provided by supplemental energy dissipators, again assuming $\eta = 0.15$, is calculated as:

$$\xi_{hyst} = \frac{2}{\pi} \times 0.15 \times \left[1 - \frac{1}{4} \right] = 0.072 \quad (D-51)$$

Therefore the total effective damping is 0.122 so the factor to account for damping is evaluated as:

$$B = \left(\frac{0.122}{0.05} \right)^{0.3} = 1.31 \quad (D-52)$$

Therefore the spectral acceleration capacity is:

$$(F_v S_1)_{DBE}^{cap} = 2\pi \times 1.31 \times \sqrt{\frac{0.228 \times 0.248}{9.81}} = 0.62 \quad (D-53)$$

Step 6: Compare Spectral Acceleration Capacity with Spectral Acceleration Demand

The spectral acceleration capacity is compared with the spectral acceleration demand according to (D-26), where the earthquake spectral acceleration demand is given by equation (D-1) for DBE, and $\phi = 0.7$. Therefore:

$$(F_v S_1)_{DBE}^* \leq \phi (F_v S_1)_{DBE}^{cap} \quad (D-54)$$

$$0.4 > 0.7 \times 0.62 = 0.44 \quad \therefore \text{Sufficient DBE capacity}$$

Step 7: Maximum Drift Capacity

The drift capacity when yield of the prestressed tendons occurs is determined by adding the elastic and rigid body components of the drift. The yield force of the prestress tendons is 1530 kN, so the elastic drift θ_{ce} is 0.7%, and the rigid body rotation drift $\theta_{RBR(PS\ yield)}$ is 4.0%, giving a drift capacity of 4.7% before yield of the tendons occurs. This is considered acceptable.

D.3 DESIGN OF SEISMIC FRAME

The design of the non-gravity load carrying frames which resist only seismic loads is carried out using a similar method to that presented by Davies (2003). The biggest change is that a capacity reduction factor is incorporated in the design process. The design calculations for this frame are presented step by step.

Step One: Mechanism Assessment

The base shear capacity of the structure is established by performing a plastic mechanism analysis described by Appendix B, and expressed as a function of M_b by equation (D-12). Four storeys were found to be participating in the mechanism, and $\kappa = 5.06$, so the base shear capacity can be expressed as:

$$V_{base} = 5.06 M_b \quad (D-55)$$

Step Two: Evaluation of Required Beam Moment Capacity

The spectral acceleration capacity of the frame can be evaluated from equation (D-14), however this requires evaluation of the damping reduction factor. This can be approximated by equation (D-17), where the total effective damping is found from equation (D-15). Davies (2003) assumes $\xi_{hyst} = 0.11$ for preliminary calculations and $\xi_{int} = 0.02$; using these assumptions the damping reduction factor can be calculated as:

$$B = \left(\frac{0.13}{0.05} \right)^{0.3} = 1.33 \quad (D-56)$$

The required beam connection capacity can be evaluated by substituting equations (B-11), (B-12) and (D-55) into equation (D-14) and rearranging:

$$M_{b\ des} = \frac{W\alpha_A\alpha_D g}{h_s n_{sp} \kappa \theta_c} \left(\frac{F_v S_1}{2\pi\phi B} \right)^2 \quad (D-57)$$

This is evaluated as:

$$M_{b\ des} = \frac{13450 \times 0.871 \times 1.161 \times 9.81}{3.6 \times 4 \times 5.06 \times 0.02} \left(\frac{0.4}{2\pi \times 0.7 \times 1.33} \right)^2 = 427 \text{ kN-m} \quad (D-58)$$

Step Three: Prestress Design

The methodology used for the design of the connection, given that the required moment at 2% drift is known, now proceeds closely to the method used by Davies (2003). The remainder of this process shall be described for completeness.

To ensure closing of the connection after it opens during a seismic event, the dissipator moment must satisfy equation (D-27). To prevent yielding of the tendons during small earthquakes, it is desirable to ensure the tendon strain at connection rotation corresponding to design drift is less than the yield strain:

$$\varepsilon_{PS\ \alpha} < \varepsilon_{PS\ yield} \quad (D-59)$$

in which α denotes the connection rotation at 2% column drift. This requirement is analogous to determining the minimum area of prestressing steel based on the rigid body rotation capacity of the frame when the prestress tendons yield for the gravity frame.

The required prestress moment at the design drift is evaluated from:

$$M_{PS\alpha} = \frac{M_{b\ des}}{1 + \frac{\phi_{PS}}{\lambda_d} \left(1 - \frac{\alpha d_b}{\varepsilon_{PS\alpha} L_{PS}} \right)} \quad (D-60)$$

however in order to evaluate equation (D-60), the connection rotation at the design drift α must be determined. The total drift is determined using equation (D-35). Once the elastic contribution to the total drift is evaluated using equation (D-36) the connection rotation at the design rotation can be found from equation (D-38).

The allowable design prestress strain is selected as $\varepsilon_{PS\alpha} = 0.75 \times \varepsilon_{PS\ yield}$, and the design connection rotation is calculated to be $\alpha = 1.85\%$, thus the required prestress moment at the design drift is evaluated as:

$$M_{PS\alpha} = \frac{427}{1 + \frac{0.8}{1.34} \left(1 - \frac{0.0185 \times 0.7}{0.00348 \times 8.9} \right)} = 317 \text{ kN-m} \quad (D-61)$$

where $\varepsilon_{PS\alpha}$ is 0.00463 and the length of the prestress tendons between anchorages, L_{PS} is 8.9 m (taken as $L_{beam} + 50 \text{ mm}$ to allow for the additional thickness of the armour plates).

Now the prestress moment is known, the tendon force and required prestress area can be found from the tendon strain at the design drift:

$$P_{PS\alpha} = \frac{2 M_{PS\alpha}}{d_b} = \frac{2 \times 317}{0.7} = 905 \text{ kN} \quad (D-62)$$

$$A_{PS\ min} = \frac{P_{PS\alpha}}{\varepsilon_{PS\alpha} E_{PS}} = \frac{905}{0.00348 \times 205 \times 10^6} = 1270 \text{ mm}^2 \quad (D-63)$$

Two 32 mm diameter prestressing threadbars are chosen, giving a total area of 1608 mm². The required initial prestress force based on the connection rotation at the design drift is given by:

$$P_{PS\ i} = \frac{\lambda_d}{\lambda_d + \phi_{PS}} \left[\frac{2 M_{des\ \alpha}}{d_b} - \alpha d_b \frac{A_{PS\ prov} E_{PS}}{L_{PS}} \right] \quad (D-64)$$

which for this frame is given by:

$$P_{PS\ i} = \frac{1.34}{1.34 + 0.8} \left[\frac{2 \times 427 \times 10^3}{0.7} - 0.0185 \times 0.7 \times \frac{1608 \times 205 \times 10^3}{8.9} \right] = 463\ kN \quad (D-65)$$

For simplicity, it was decided to take the initial prestress force as 32% of the yield prestress force. The initial prestress moment is therefore defined as:

$$M_{PS\ i} = \frac{0.32 P_{PS\ yield} d_b}{2} = \frac{0.32 \times 950 \times 1608 \times 700}{2} = 171\ kN\cdot m \quad (D-66)$$

in which $P_{PS\ yield} = f_{PS} A_{PS}$.

Step Four: Dissipator Design

Similar to Davies (2003), tension-compression dog-bone energy dissipators are to be mounted on the top and bottom of the connection. The dissipator moment can be evaluated by rearranging equation (D-27) to obtain:

$$M_d = \frac{\phi_{PS}}{\lambda_d} M_{PS\ i} = \frac{0.8}{1.34} \times 171 = 103\ kN\cdot m \quad (D-67)$$

Assuming the dissipators are constructed from 20 mm thick mild steel plate, with characteristic strength of 336 MPa, the width of the dissipator can be calculated as:

$$w_d = \frac{M_d}{d_b f_d t_d} = \frac{103 \times 10^3}{700 \times 336 \times 20} = 22\ mm \quad (D-68)$$

The length of the yielding portion of the dissipator is dependent on the allowable strain (Davies, 2003). To prevent fracture of the dissipator, the strain at the design rotation is limited so that the dissipator still has strain capacity when the design rotation is exceeded. Fracture in mild steel typically occurs at a strain of 0.2, hence if the strain is limited to 50% of this value at the design rotation, extra capacity is provided to prevent fracture. The yielding length of the dog-bone can then be calculated as:

$$L_d = \frac{\alpha d_b}{\varepsilon_{d \text{ allow}}} = \frac{0.0185 \times 700}{0.5 \times 0.2} = 130 \text{ mm} \quad (D-69)$$

The yield displacement of the dissipator is found by multiplying the yielding length by the yield strain of the dissipator material:

$$\Delta_{d \text{ yield}} = \varepsilon_{d \text{ yield}} L_d = \frac{336}{200\,000} \times 130 = 0.22 \text{ mm} \quad (D-70)$$

from which the connection rotation to first cause yield of the dissipators is:

$$\theta_{d \text{ yield}} = \frac{\Delta_{d \text{ yield}}}{d_b} = \frac{0.22}{700} = 0.03 \% \quad (D-71)$$

D.4 DESIGN OF COLUMNS

The column dimensions were selected as 750 mm by 750 mm, with four ducts for 36 mm post-tensioned tendons running the full height of the column. Additionally, the columns are reinforced with 12 D25 reinforcing bars. This section briefly describes how the prestressing was determined for the columns.

While carrying out the mechanism assessment for each of the frames, the column moment overstrength factor, λ_{col} , was assumed to be 2.4. Therefore, the column rocking connections, located at the base of the columns, and at the underside of level four, are required to be designed with a capacity of $2.4 \times M_b$. However, to add to the complexity of

the column design, the orthogonal frames have different beam moments at DBE, so once the prestress area had been selected, the average required post-tensioning was assumed to be applied to the columns. The following calculations are proposed for design of the columns, with numerical examples given for the typical internal columns. The details for other columns are presented in Table D-1.

Firstly, the required column moments, in both directions for DBE, and the column axial loads are obtained from the preceding design. The required moments are $M_{col\ NS}^* = 1070\ kN-m$ and $M_{col\ WE}^* = 1120\ kN-m$, and axial loads are $N_{top} = 208\ kN$ at the underside of level four, $N_{bottom} = 512\ kN$ at the base of the columns, and $N_{average} = 360\ kN$.

The required initial prestress force, $P_{PS\ i}$, is determined, assuming $N_{average}$ is already applied at both the top and bottom column rocking joint, as follows:

$$P_{PS\ i} = \frac{2M^*}{d_c} - \frac{\theta_{RBR} d_c A_{PS} E_{PS}}{L_{PS}} - N_{average} \quad (D-72)$$

where θ_{RBR} is the rigid body rotation required by the columns at DBE, calculated by considering the elastic deformations at DBE. In the seismic only direction, $P_{PS\ i}$ is determined as:

$$P_{PS\ i} = \frac{2 \times 1070}{0.75} - \frac{0.0164 \times 0.75 \times 4080 \times 205}{21.6} - 360 = 2010\ kN \quad (D-73)$$

and in the gravity + seismic direction:

$$P_{PS\ i} = \frac{2 \times 1120}{0.75} - \frac{0.0152 \times 0.75 \times 4080 \times 205}{21.6} - 360 = 2190\ kN \quad (D-74)$$

The required initial prestressing is determined as a percentage of the yield prestress force, calculated to be $3880\ kN-m$. An average of the values calculated by equations (D-73) and (D-74) is determined to be $2100\ kN$, therefore the initial prestress

force for the columns is taken as 55% of the yield force (rounding up rather than rounding down).

The moment-rotation response is given by a tri-linear curve, where joint opening is characterised by:

$$M_{open} = \frac{(P_{PS\ i} + N)d_c}{2} \quad (D-75)$$

where N is the axial load at the connection, and yield of the prestress is characterised by:

$$M_{PS\ yield} = \frac{(P_{PS\ yield} + N)d_c}{2} \quad (D-76)$$

$$\theta_{j\ (PS\ yield)} = \left(1 - \frac{f_i}{f_{PS}}\right) \frac{f_{PS}}{E_{PS}} \frac{L_{PS}}{d_c} \quad (D-77)$$

D.5 SHEAR DESIGN

Although friction between the post-tensioned rocking interfaces carries shear forces while the joints are closed, this mechanism can not be relied on to carry shear forces when the joints open under lateral displacement. Arnold (2004) and Davies (2003) provided shear keys to prevent shear and torsional failure in their experimental investigations. Similar keys, to prevent a shear or torsional failure need to be included in the rocking beam-column connections and in the rocking column joints.

Since a shear failure is undesirable, the shear keys need be designed to carry the shear force that will develop in the beam when the prestress is yielding. Thus, the design beam joint shear, $V_{j\ des}$, can be calculated as:

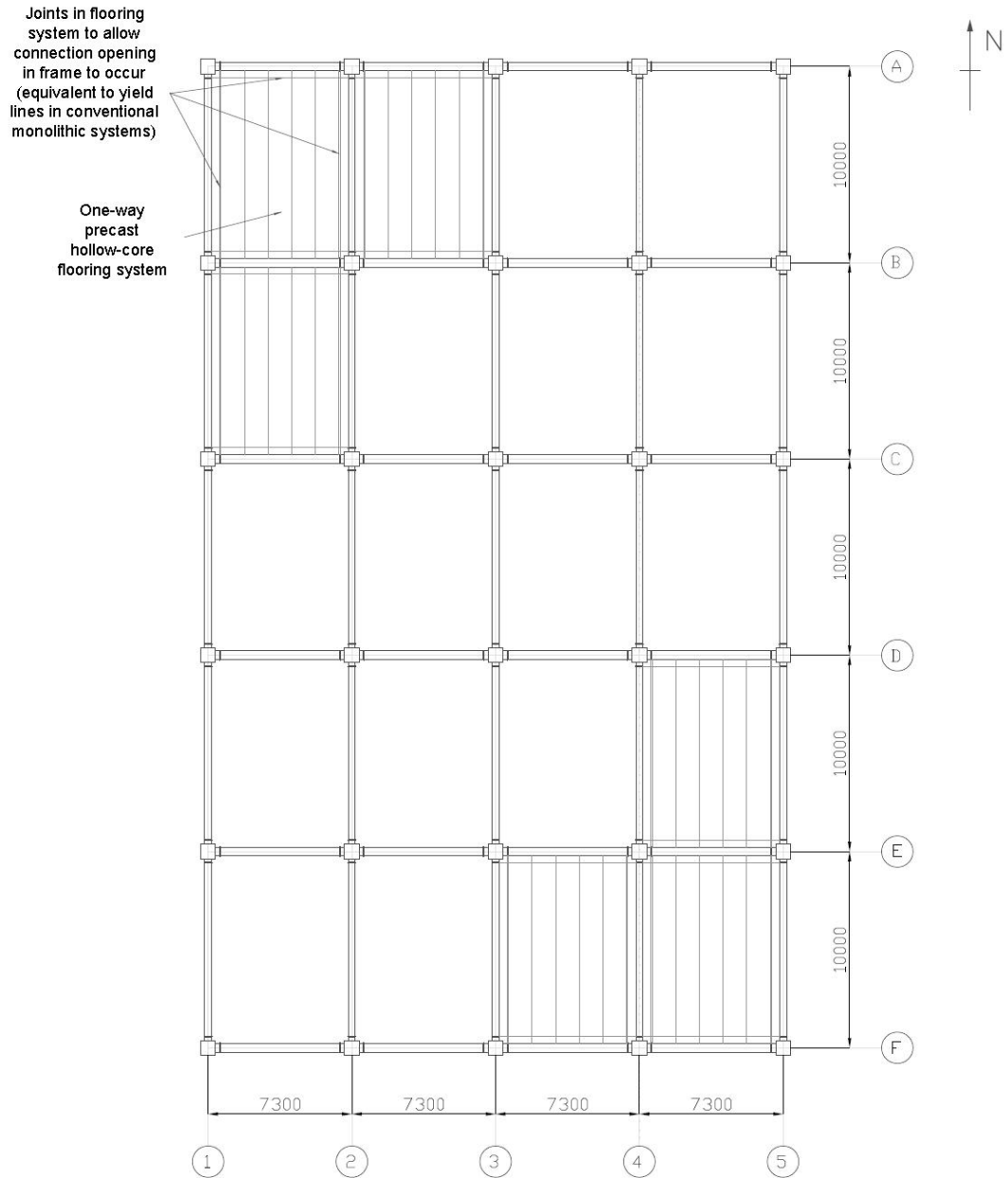
$$V_{j\ des} = \frac{2 M_{PS\ yield}}{L_{beam}} \quad (D-78)$$

where $M_{PS\ yield}$ is the moment capacity of the beam joint (including any contribution from energy dissipation devices) when yield of the prestress tendons occurs. $V_{j\ des}$ is calculated as 267 kN, 173 kN and 152 kN for the internal gravity frames, external gravity frames and seismic frames, respectively.

Similarly, the shear resistance required by the base of the column hinges can be determined by proportionally distributing the total base shear which occurs when the prestress in the beams is yielding amongst the columns. By assuming each of the columns resists equal shear, the shear forces at the column hinge bases are determined as 691 kN, 448 kN and 567 kN for the internal gravity frames, external gravity frames and seismic frames, respectively. Thus, it follows that shear keys at the base of the columns should be designed to resist lateral forces of 700 kN in both the N-S and E-W directions.

Table D-1: Column hinge design and properties

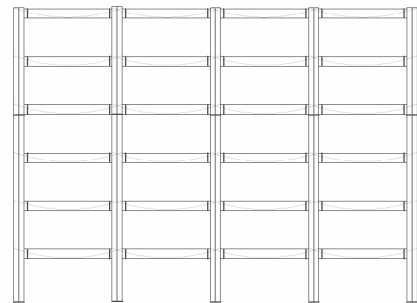
	A	B	C	D
M_{NS}^*	1070	1070	1070	1070
M_{WE}^*	610	1120	610	1120
N_{top}	120	150	150	210
N_{bottom}	340	400	400	510
$N_{average}$	230	275	275	360
$P_{PS\ i(NS)}^*$	2140	210	2100	2010
$P_{PS\ i(WE)}^*$	930	2280	890	2190
$P_{PS\ i}$	1550	2210	1510	2130
top hinge analysis				
M_{open}	630	890	620	880
$M_{PS\ yield}$	1500	1510	1510	1530
$\theta_j (PS\ yield)$	8.0	5.7	8.1	6.0
bottom hinge analysis				
M_{open}	710	980	720	990
$M_{PS\ yield}$	1580	1600	1600	1650
$\theta_j (PS\ yield)$	8.0	5.7	8.1	6.0



(a) Plan



b) Seismic frame (N-S) elevation



(c) Gravity frame (E-W) elevation

Figure D-1: Plan and elevation of proposed building

APPENDIX E

SOME OBSERVATIONS ON THE DYNAMIC BEHAVIOUR OF THE PROPOSED SIX STOREY DAMAGE AVOIDANCE DESIGN APARTMENT BUILDING

E.1 MODE SHAPES AND PERIODS OF VIBRATION

The first three mode shapes obtained from modal analyses carried out by *RUAUMOKO-2D*, for the orthogonal frames are presented in Figure E-1. The mode shapes observed in both directions are very similar. Mode shapes for both the elastic structure and once the joints have opened are presented.

Similar to the results observed for the ten storey frames, the first mode shape when the joints are open is very close to the shape of the mixed mechanism from the rapid pushover analysis. This observation is favourable, as it indicates the validity of the proposed design methodology.

E.2 TIME-HISTORY DISPLACEMENT PROFILES

A selection of lateral displacement earthquake time-history analysis results are presented in Figures E-2 to E-7 for the orthogonal frames analysed by incremental dynamic analysis in Chapter Three. The results presented correspond to the 50th percentile and 90th percentile responses for DBE, and the 50th percentile response for MCE.

The displaced shape of the DAD frames is again very close to the design mechanism at large displacements. This result can be used to validate the applicability of the rapid pushover design method for these frames. At smaller displacements, higher

mode effects are observed however as they only tend to occur at small displacements, they are reasonably insignificant.

The median and 90th percentile drifts for each level are plotted in Figure E-8 for each of the three frames analysed in Chapter Two. This figure is comparable to figure C-11 for the ten storey frames and again shows that there is reduced drift in the upper levels of the DAD frames.

E.3 VALIDITY OF MODELLING ASSUMPTIONS

For convenience it was assumed the beams in the upper levels of the DAD frames had the same properties, owing to the same reinforcing and prestress configuration, as those beams participating in the mechanism. This assumption can be soundly reasoned based on construction simplicity, as all beams having the same reinforcing and prestress configuration simplifies the construction process and reduces the possibility for error.

The maximum beam joint moments, for both the upper and lower levels of the structure, along with the joint capacities are indicated in Figure E-9. This figure indicates that the maximum moments imposed on the upper level joints certainly cause the joints to open, and even exceed the joint capacity corresponding to yield of the prestress tendons. This result is problematic as it indicates damage would occur to the upper levels of the frames. Again, further examination of selected time-history analysis results indicates the moments in the upper levels of the structure exceed those of the lower levels of the structure when joint opening occurs.

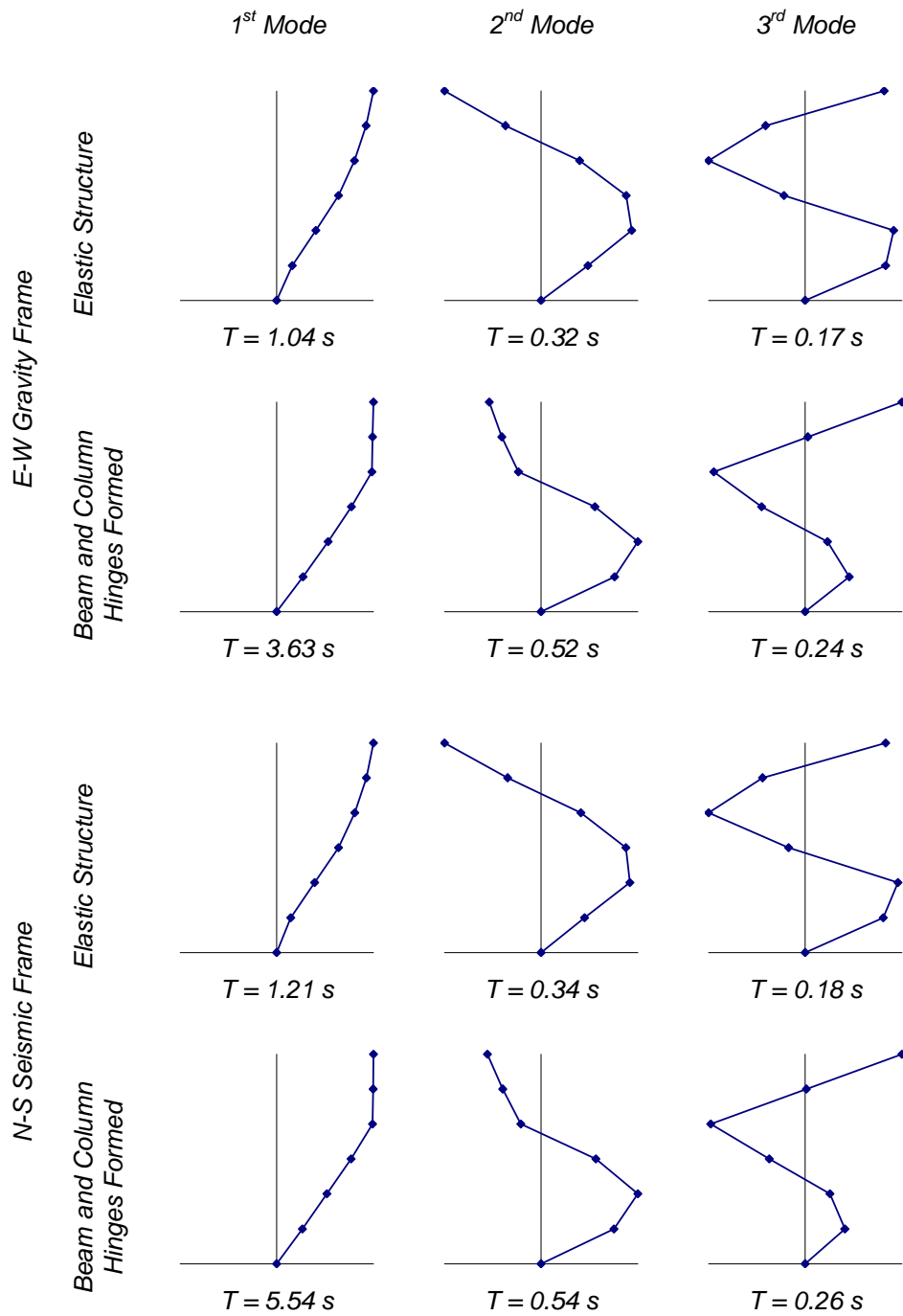
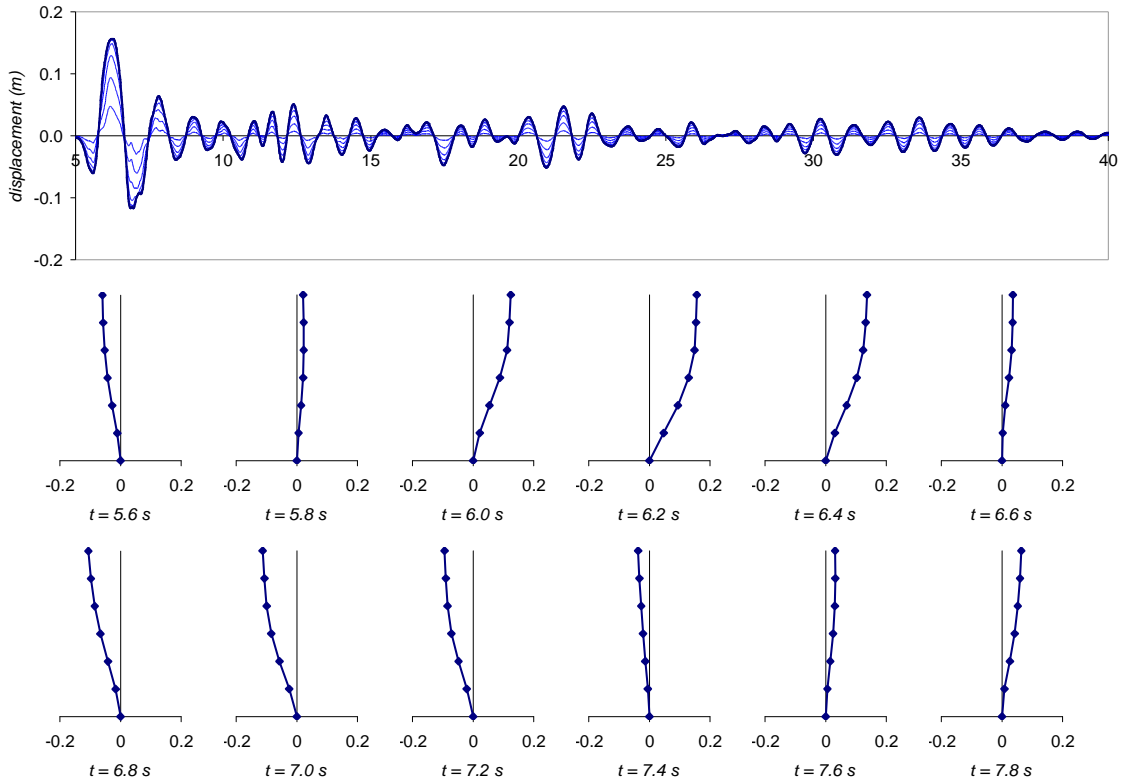
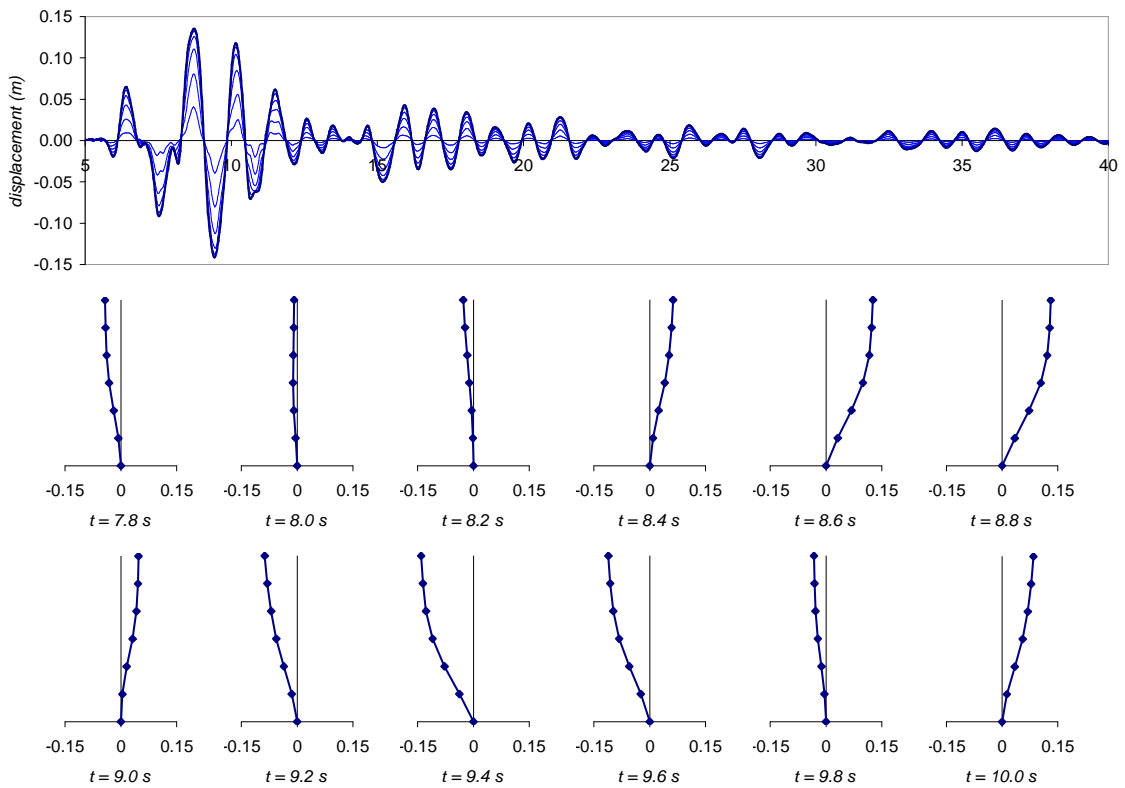


Figure E-1: Mode shapes and periods of vibration for the proposed six storey apartment building

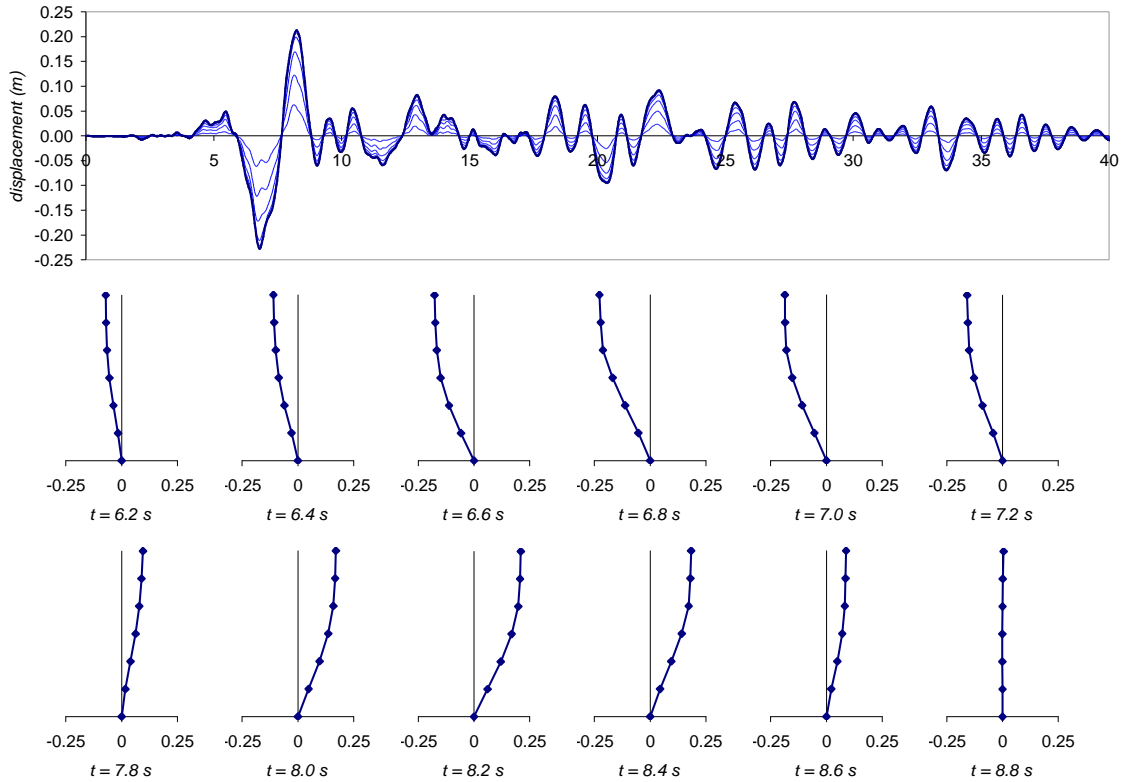


(a) Earthquake 6 – 1979 Imperial Valley at Cucapah

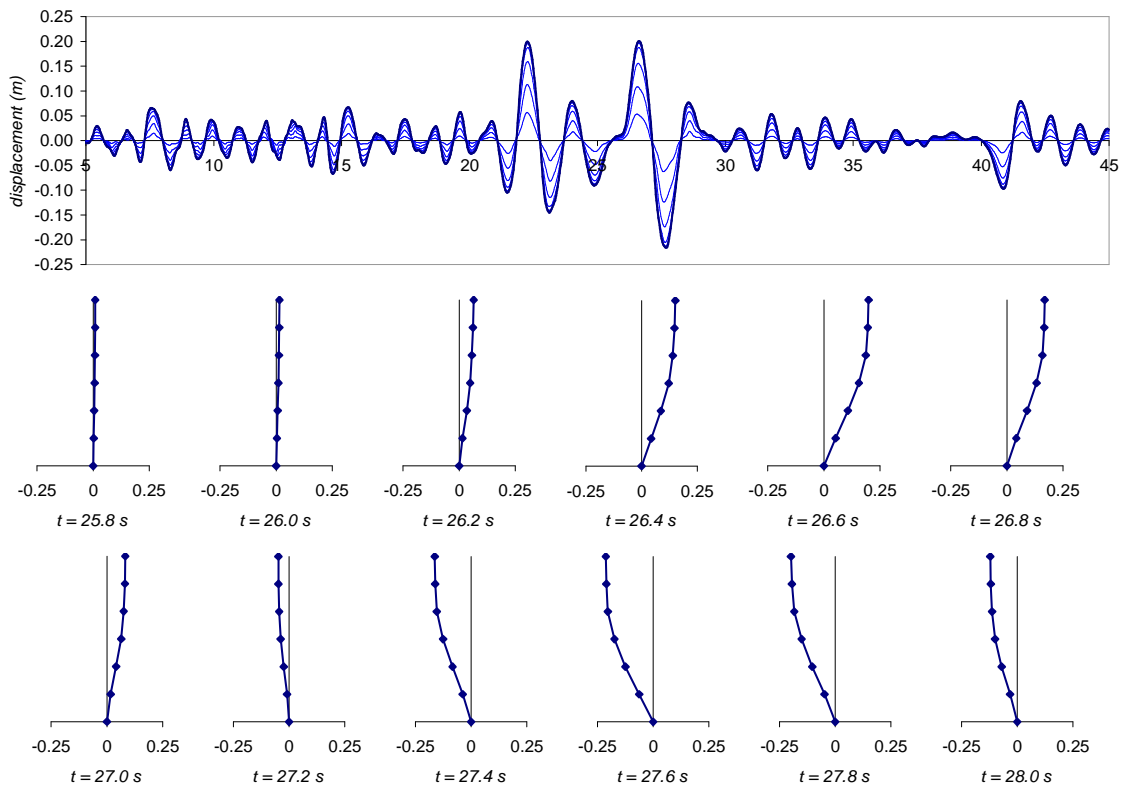


(b) Earthquake 19 – 1989 Loma Prieta at Hollister Diff. Array, S15E component

Figure E-2: E-W gravity DAD frame displacement time histories and selected vertical snapshots for earthquakes representative of the 50th percentile DBE

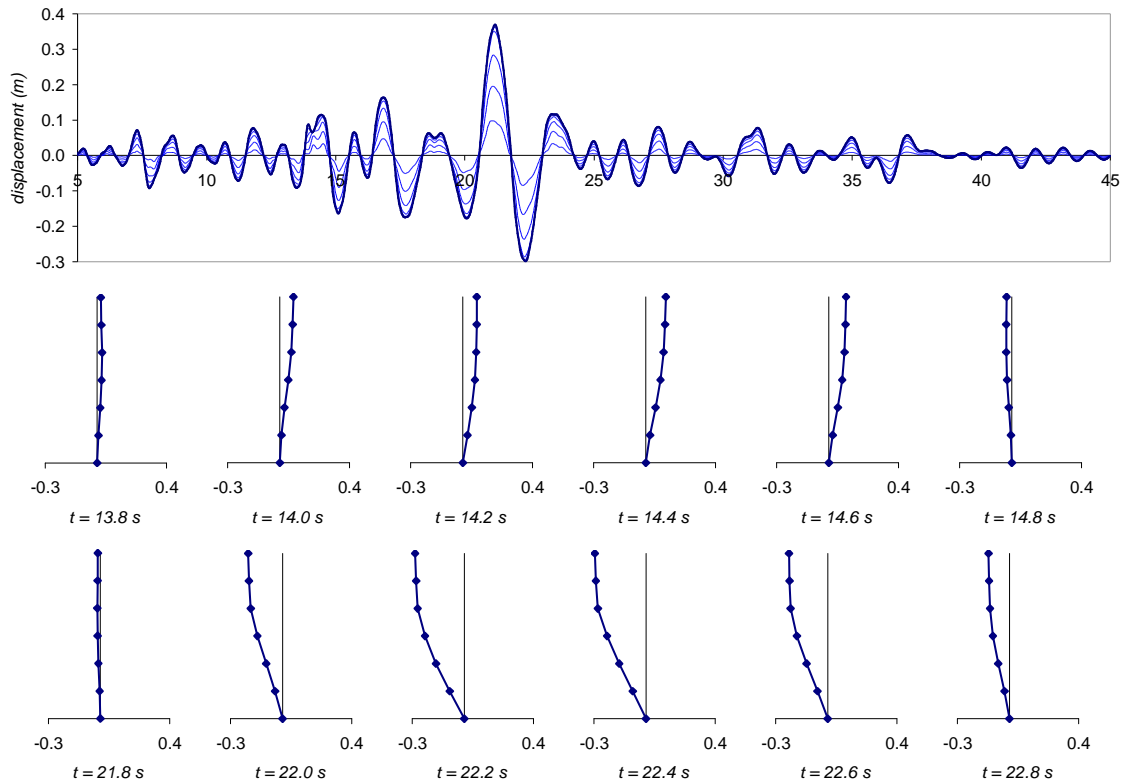


(a) Earthquake 9 – 1979 Imperial Valley at Westmoreland Fire Station, E-W component

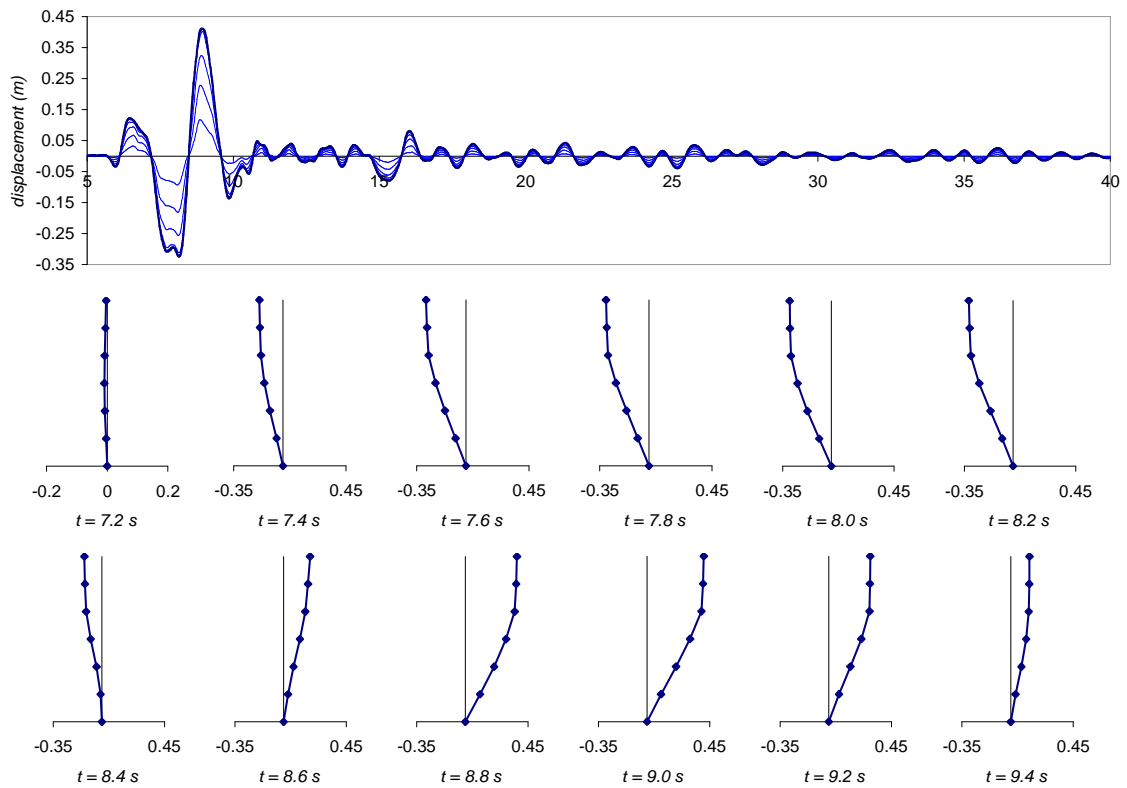


(b) Earthquake 12 – 1987 Superstition Hills at Wildlife Liquefaction Array, E-W component

Figure E-3: E-W gravity DAD frame displacement time histories and selected vertical snapshots for earthquakes representative of the 90th percentile DBE

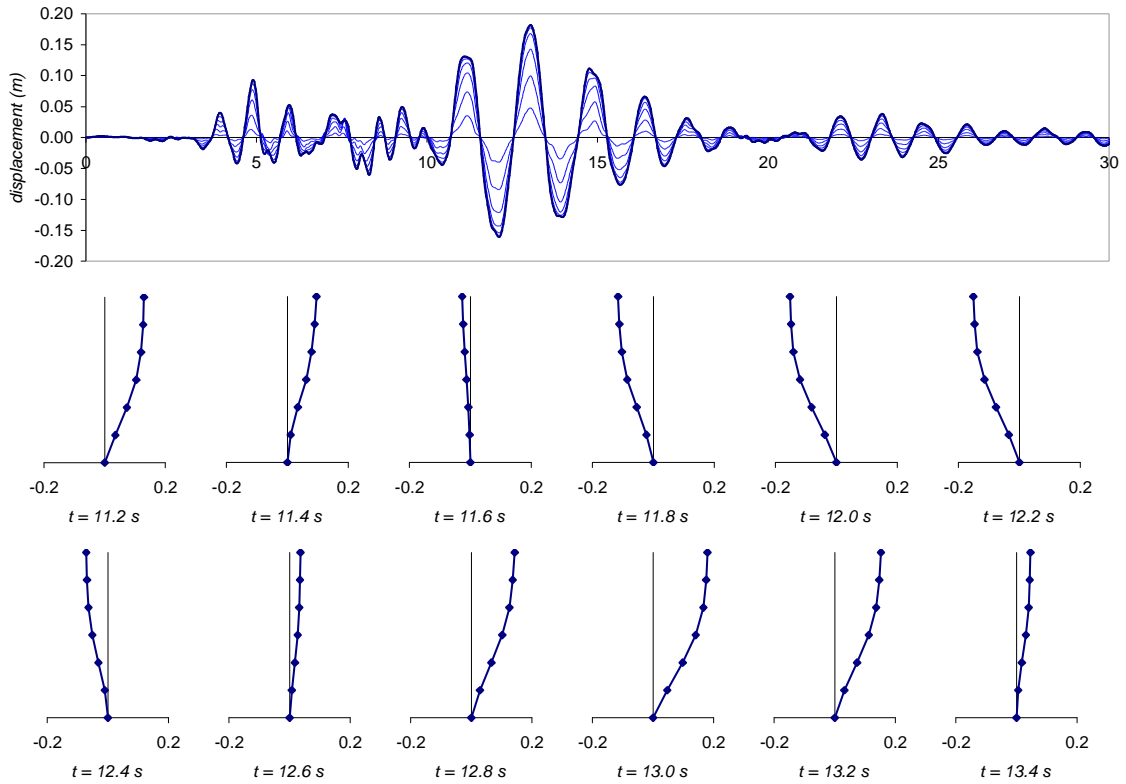


(a) Earthquake 17 – 1987 Superstition Hills at Wildlife Liquefaction Array, N-S component

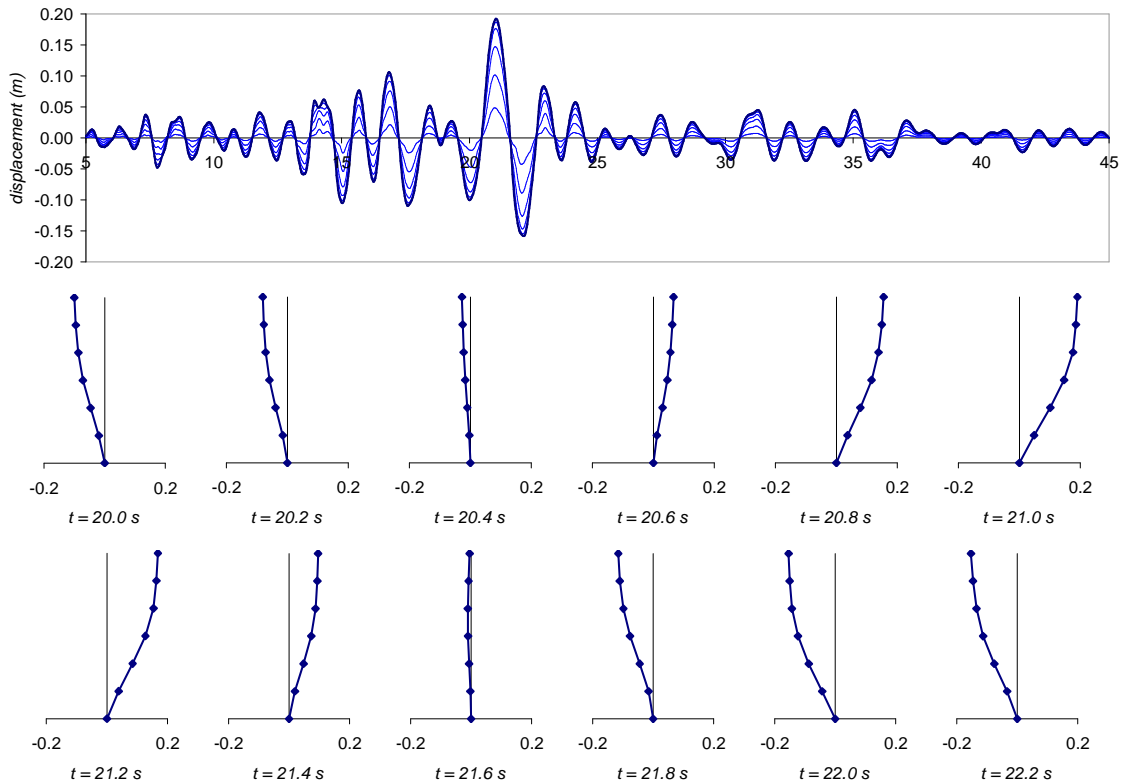


(b) Earthquake 19 – 1989 Loma Prieta at Hollister Diff. Array, S15E component

Figure E-4: E-W gravity DAD frame displacement time histories and selected vertical snapshots for earthquakes representative of the 50th percentile MCE

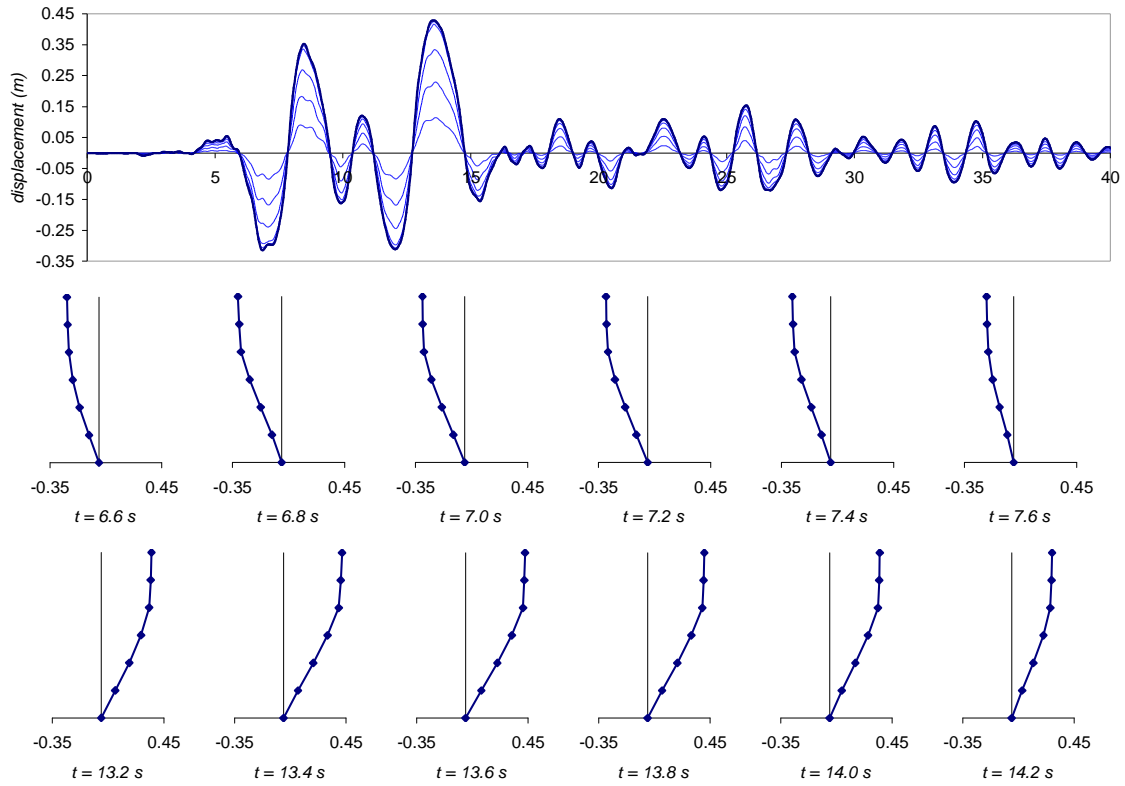


(a) Earthquake 4 – 1989 Loma Prieta at Anderson Dam

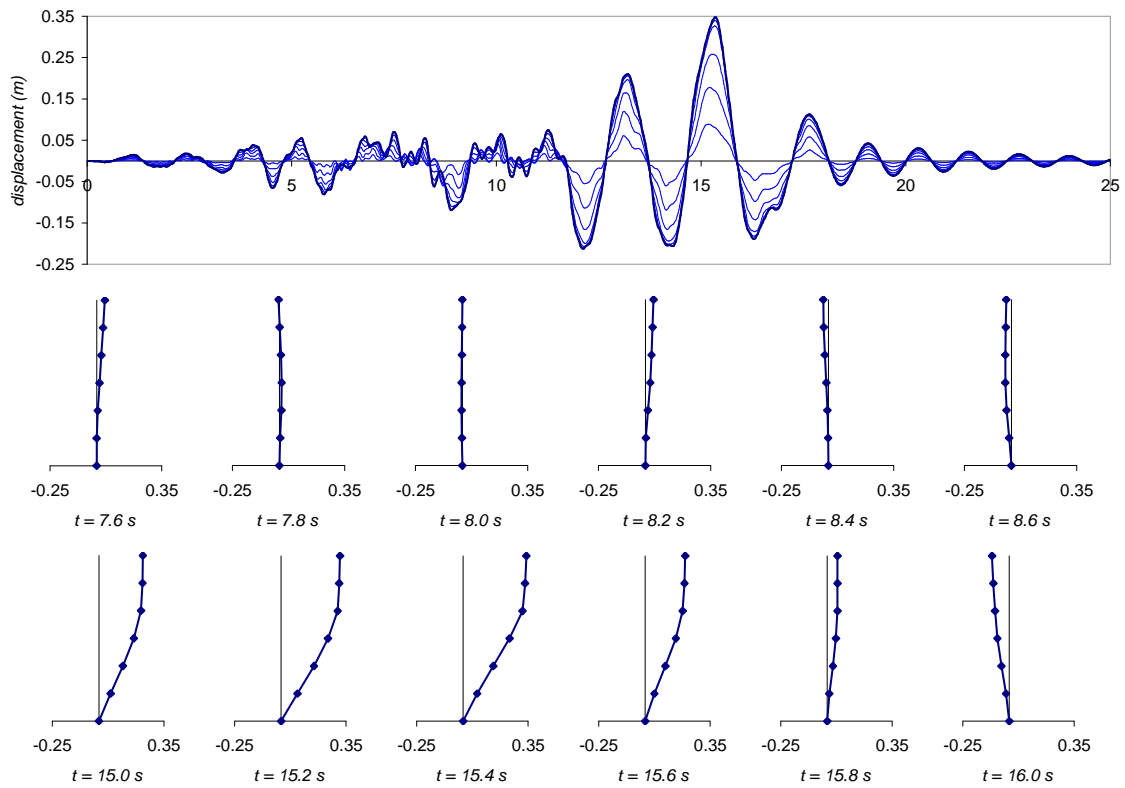


(b) Earthquake 17 – 1987 Superstition Hills at Wildlife Liquefaction Array, N-S component

Figure E-5: N-S seismic DAD frame displacement time histories and vertical snapshots for earthquakes representative of the 50th percentile DBE

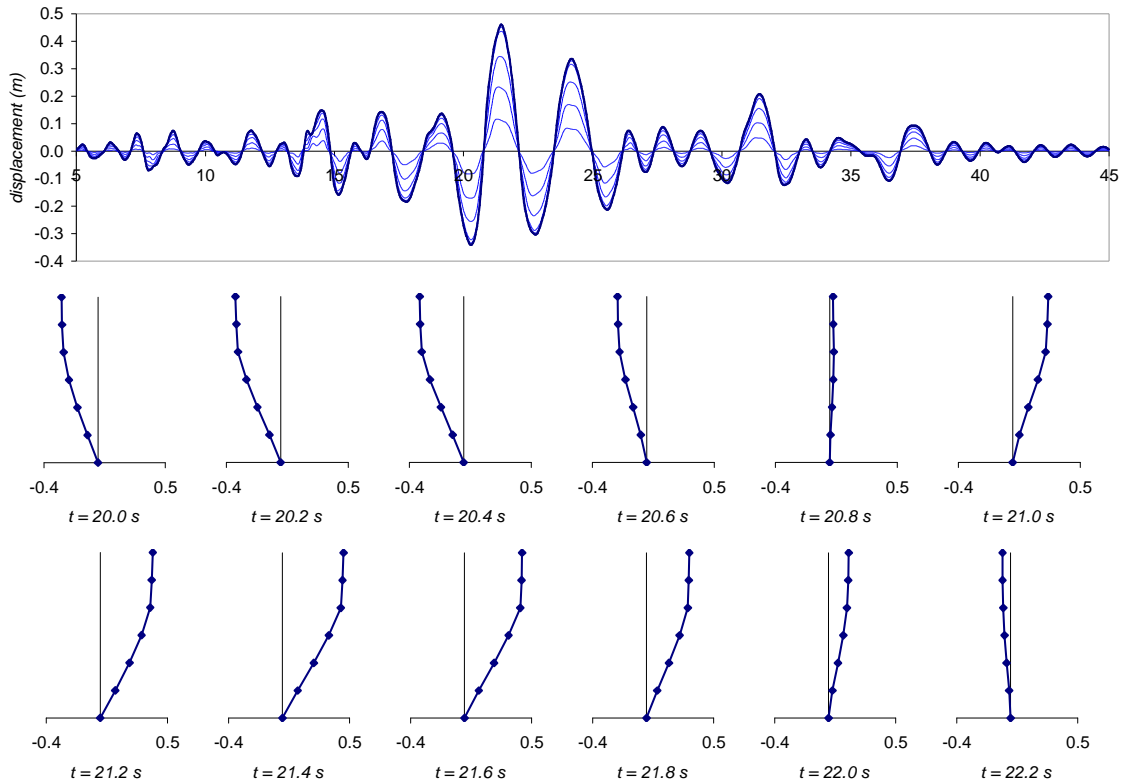


(a) Earthquake 9 – 1979 Imperial Valley at Westmoreland Fire Station, E-W component

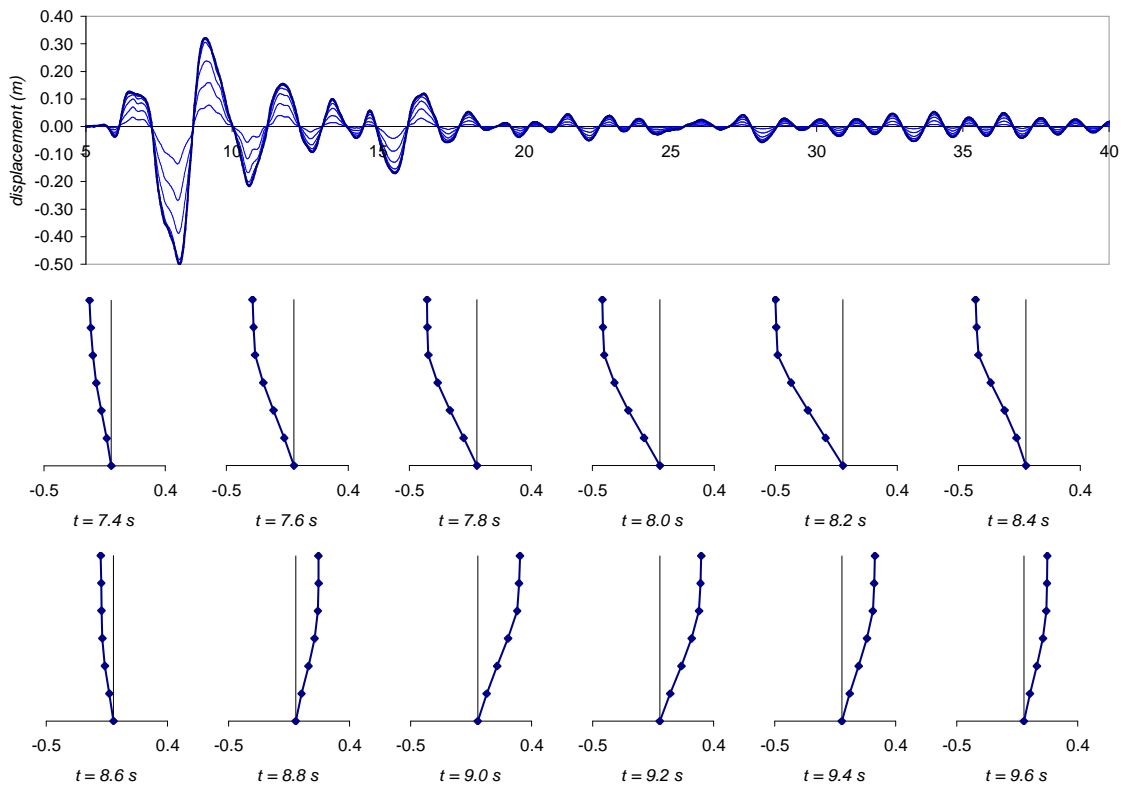


(b) Earthquake 18 – 1979 Imperial Valley at Plaster City, N45E component

Figure E-6: N-S seismic DAD frame displacement time histories and vertical snapshots for earthquakes representative of the 90th percentile DBE



(a) Earthquake 17 – 1987 Superstition Hills at Wildlife Liquefaction Array, N-S component



(b) Earthquake 19 – 1989 Loma Prieta at Hollister Diff. Array, S15E component

Figure E-7: N-S seismic DAD frame displacement time histories and vertical snapshots for earthquakes representative of the 50th percentile MCE

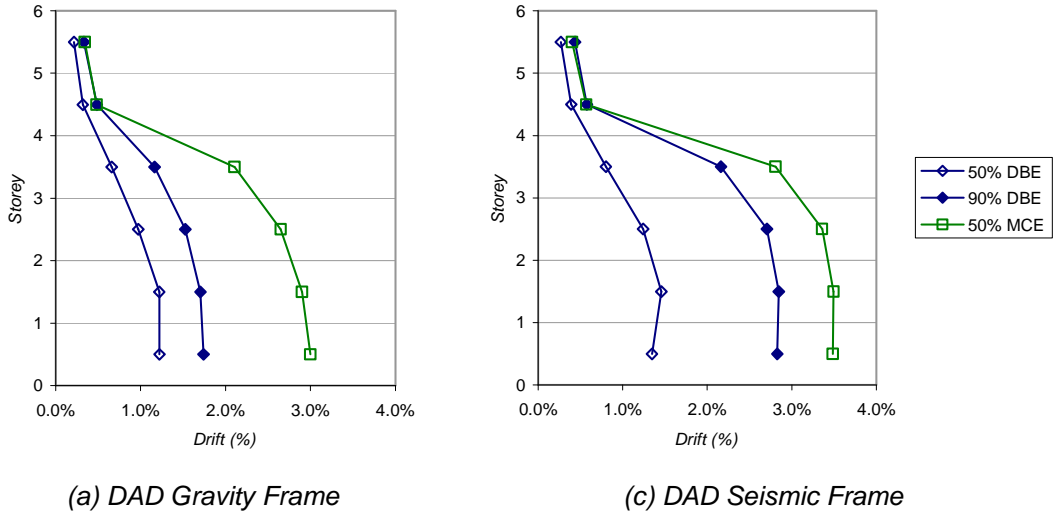


Figure E-8: Vertical drift profiles at DBE and MCE

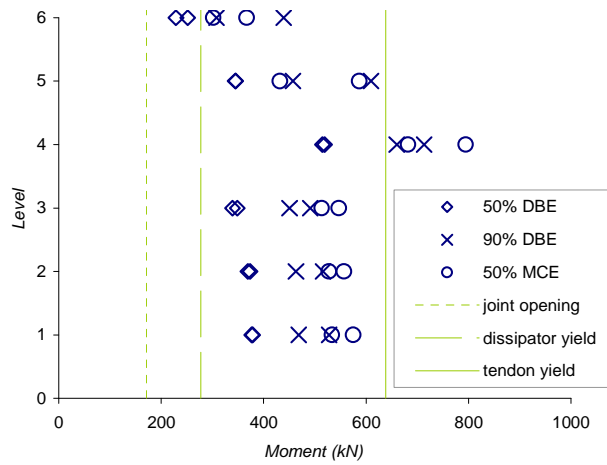


Figure E-9: Maximum beam moments occurring during selected analyses